ULPGC
Universidad de Las Palmas de Gran Canaria

Doctorando en Ingenierías Química, mecánica y fabricación

TESIS DOCTORAL

ESPECTROSCOPIA DE IMPEDANCIA ELECTROQUIMICA: MODELACION DEL COMPORTAMIENTO EN SERVICIO DE LOS BIOMATERIALES

Las Palmas de Gran Canaria, junio de 2022

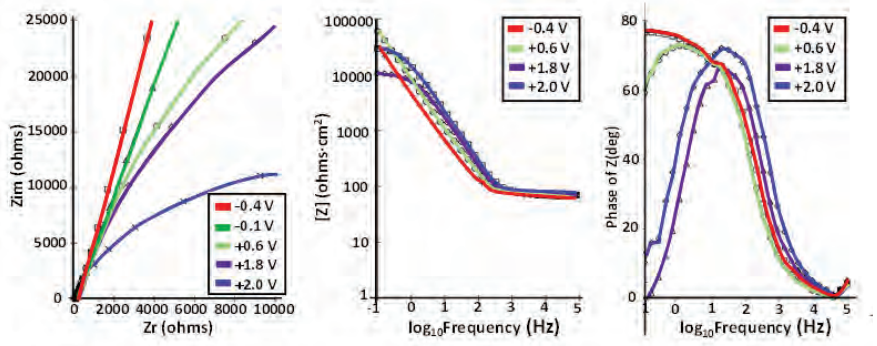

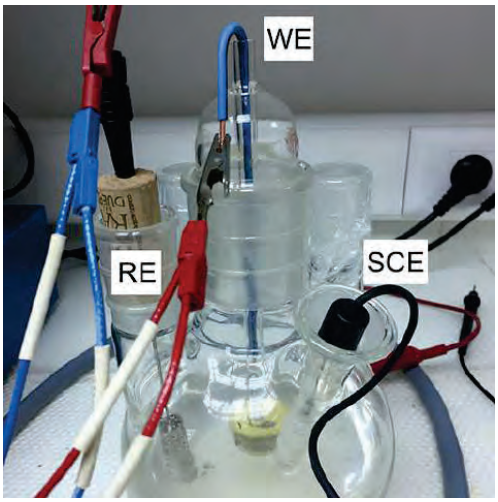

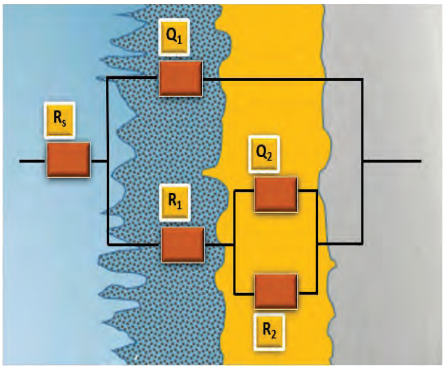

Autor:

Pedro P. Socorro Perdomo

Directores:

Dra. Julia Claudia Mirza Rosca

Dr. Néstor R. Florido Suárez

D. José Miguel Doña Rodríguez, COORDINADOR DEL PROGRAMA DE DOCTORADO en Ingenierías Química, Mecánica y de Fabricación de la UNIVERSIDAD DE LAS PALMAS DE GRAN CANARIA

INFORMA,

De que la Comisión Académica del Programa de Doctorado, en su sesión de fecha ..... tomó el acuerdo de dar el consentimiento para su tramitación, a la tesis doctoral titulada: "ESPECTROSCOPIA DE IMPEDANCIA ELECTROQUIMICA: MODELACION DEL COMPORTAMIENTO EN SERVICIO DE LOS BIOMATERIALES" presentada por el doctorando D. Pedro Socorro Perdomo y dirigida por los Doctores Dña. Julia Mirza Rosca y D. Néstor Rubén Florido Suárez.

Y para que así conste, y a efectos de lo previsto en el Art. 11 del Reglamento de Estudios de Doctorado (BOULPGC 04/03/2019) de la Universidad de Las Palmas de Gran Canaria, firmo la presente en Las Palmas de Gran Canaria, a ..... de.....de dos mil veintidós.

UNIVERSIDAD DE LAS PALMAS DE GRAN CANARIA

ESCUELA DE DOCTORADO

Programa de doctorado en Ingenierías Química, Mecánica y de Fabricación

Departamento de Ingeniería Mecánica

Título de Tesis

ESPECTROSCOPIA DE IMPEDANCIA ELECTROQUIMICA: MODELACION DEL COMPORTAMIENTO EN SERVICIO DE LOS BIOMATERIALES

Directores: Dña Julia Mirza Rosca y D. Néstor Rubén Florido Suárez

Las Palmas de Gran Canaria, a 25 de abril de 2022

Los Directores,

MIRZA ROSCA JULIANA CLAUDIA - 45360672A

Firmado digitalmente por MIRZA ROSCA JULIANA CLAUDIA - 45360672A
Fecha: 2022.05.09 19:13:46 +01'00'

FLORIDO SUAREZ NESTOR RUBEN - 43752800S

Firmado digitalmente por FLORIDO SUAREZ NESTOR RUBEN - 43752800S
Fecha: 2022.05.09 19:10:33 +01'00'

El Doctorando,

SOCORRO PERDOMO PEDRO - 42789076Z

Firmado digitalmente por SOCORRO PERDOMO PEDRO - 42789076Z
Fecha: 2022.05.09 19:10:58 +01'00'

AGRADECIMENTOS

El agradecimiento es un reconocimiento hacia las personas que han participado de forma activa ó pasiva en el proyecto de interés para el que lo suscribe, de forma que, contempla ese sentir de gratitud que llega a satisfacer a los que se sienten involucrados.

Agradecido a la vida por darme siempre lo que es bueno para mí, a pesar de que a priori no entendiere a corto plaza las señales que me muestra.

Efectivamente, más que nunca tengo que reconocer y agradecer a mi equipo de vida académica investigadora, campeones en mostrar siempre los sentimientos positivos que definen con ello, su calidad de persona y de buena gente, me refiero a Julia, Néstor y Santiago. Sin ellos no estaríamos leyendo este documento tan importante para mí.

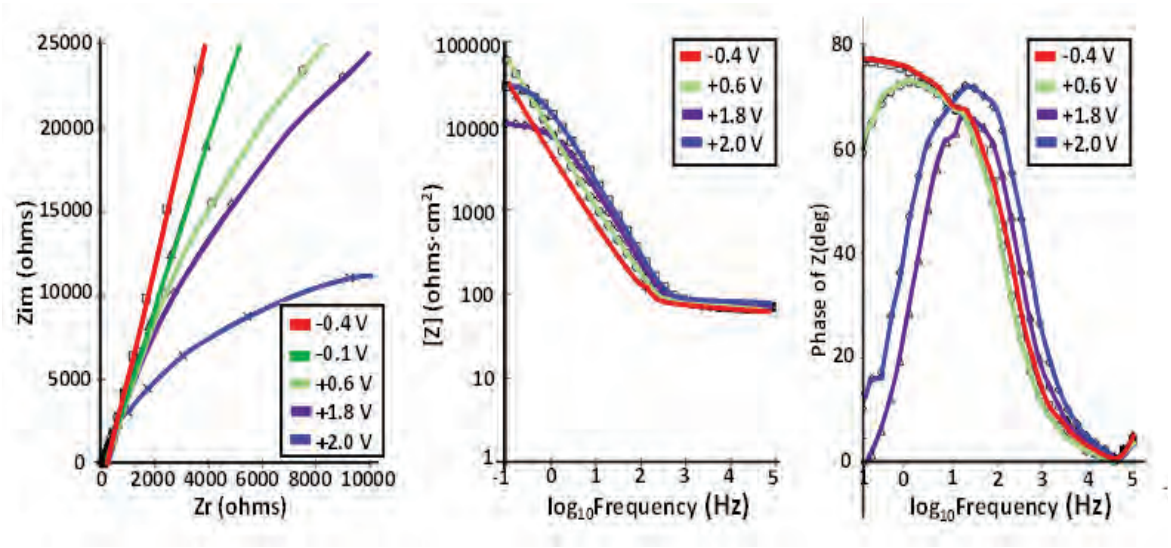
Zim (ohms)
Zr (ohms)
-0.4 V
-0.1 V
+0.6 V
+1.8 V
+2.0 V
[Z] (ohms·cm²)
log10Frequency (Hz)
Phase of Z(deg)

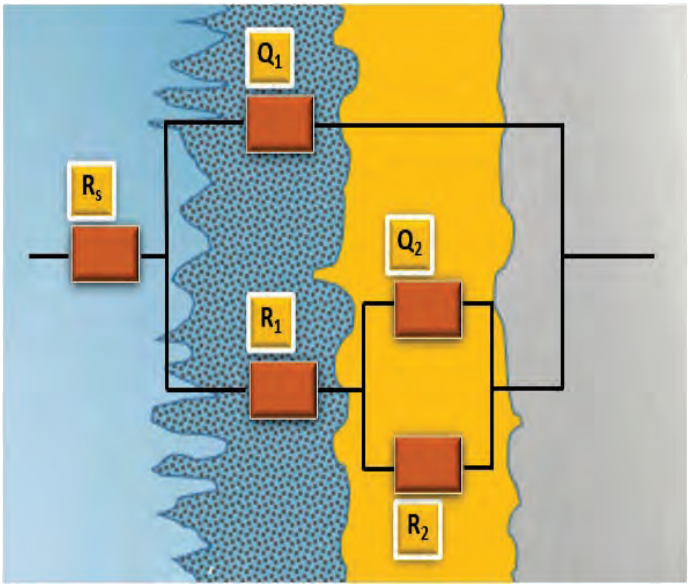
Q1
Rs
Q2
R1
R2

Resumen

Resumen

El **objetivo principal** de este trabajo de tesis es la aplicación de la técnica de Espectroscopia de Impedancia Electroquímica (EIS) en el estudio del mecanismo del proceso que tiene lugar al estar en contacto una aleación con un medio determinado.

Este objetivo general se aborda a través de los siguientes **objetivos específicos**:

1. Analizar la influencia de las adiciones de Tantalio en las aleaciones de titanio-tantalio para poder utilizarlos como posibles dispositivos biomédicos teniendo en cuenta que los materiales utilizados actualmente como implantes generan problemas de salud a larga plazo.

2. Modelar y simular con circuitos eléctricos equivalentes el comportamiento en HCl 20% de tres materiales, Ti, Ti-15Mo y Ti-15Mo-5Al fabricados mediante el proceso de fusión por láser para sus utilizaciones como materiales resistentes a la corrosión en diversos elementos mecánicos como: los intercambiadores de calor, turbinas bombas, válvulas, etc.

3. Conocer el impacto del contenido del aluminio en la película pasiva formada sobre una aleación de alta entropía (HEA) para su posible uso en la fabricación de instrumentos médicos utilizados en condiciones especiales como infecciones, hematomas, alergias, etc.

El tema de tesis propuesto se encuentra relacionado con las siguientes **líneas de investigación** del programa de doctorado en Ingenierías Química, Mecánica y de Fabricación (QUIMEFA):

- Nanomateriales
- Corrosión de los metales
- Biomateriales para aplicaciones de ingeniería medica

La tesis trata del estudio de la corrosión de varios materiales metálicos para su posible uso en el sector sanitario. Por lo tanto, se puede observar que el tema de la tesis es totalmente coherente con las líneas de investigación seleccionadas.

La **Espectroscopia de Impedancia Electroquímica (EIS)** se aplica para caracterizar el comportamiento de diferentes metales y aleaciones en diversos entornos y para proporcionar nueva información que antes no podía obtenerse con las técnicas clásicas de corriente continua. Aunque se ha llevado a cabo una cantidad significativa de investigaciones utilizando la EIS para caracterizar los biomateriales, se ha realizado poca investigación sobre las mediciones de EIS de las aleaciones de Ti-Ta, Ti-Mo y otras. Se observa que es esencial para todos los sistemas considerar modelos de impedancia adecuados que puedan utilizarse para ajustar los resultados experimentales y proporcionar los datos relevantes que caracterizan el proceso de corrosión.

Las **aleaciones de alta entropía (HEAs**) pueden proporcionar alternativas y cambios en las limitaciones de las propiedades de los materiales clásicos, de forma que su particular disposición espacial de los elementos que componen la misma, hacen que estas adopten el concepto de entropía, dando así la definición de dichas aleaciones.

Las **aleaciones de titanio** en su estructura cristalina se suelen establecer en tres fases alotrópicas: aleaciones α y casi α, aleaciones α + β y aleaciones β. Las aleaciones β de Ti contienen una mayor presencia de estabilizadores de la fase β y un menor contenido de alfágenos que las aleaciones α + β.

En el artículo "**Comparative EIS study of titanium-based materials in high corrosive environments**" se analiza el comportamiento en HCl 20% de tres materiales, Ti, Ti-

15 Mo y Ti-15Mo-5Al fabricados mediante el proceso de fusión por rayo láser, utilizando para simulación y modelación la espectroscopia de impedancia electroquímica (EIS).

En el artículo "**Compartive EIS Study of AlxCoCrFeNi Alloys in Ringer´s Solution for Medical Instruments**". Se estudia y aclara cómo el contenido de Al impacta en las películas pasivas formadas en estas aleaciones. Además, se examina la relación entre las características de la película de óxido y la concentración de Al variando el potencial entre -0,7 y 0,7 V frente al electrodo de referencia de calomelano saturado (SCE). La corrosión en el medio fisiológico se debe principalmente a los iones de cloro que contiene, al pH y a las condiciones especiales de uso como infecciones, hematomas, alergias, etc. En este trabajo se simuló un ambiente fisiológico infeccioso añadiendo HCl a la solución Ringer hasta alcanzar un pH = 3 a 37ºC.

En el artículo "**EIS Characterization of Ti Alloys in Relation to Alloying Additions of Ta**" se caracterizaron varias aleaciones de Ti-xTa (con x=5, 15, 25, 30) utilizando espectroscopia de impedancia electroquímica (EIS) y diferentes otras técnicas para confirmar los resultados obtenidos. Se generaron mapas de alta resolución de la superficie de los materiales mediante microscopía de barrido en túnel (STM) y se obtuvo información sobre los mapas de distribución de átomos mediante espectroscopia de rayos X por dispersión de energía (EDS). La composición química y, por tanto, la estructura cristalográfica de las aleaciones se identificó mediante difracción de rayos X (XRD). Además, se investigó el comportamiento electroquímico de estas aleaciones Ti-xTa en líquido corporal simulado (SBF) a diferentes potenciales

ULPGC

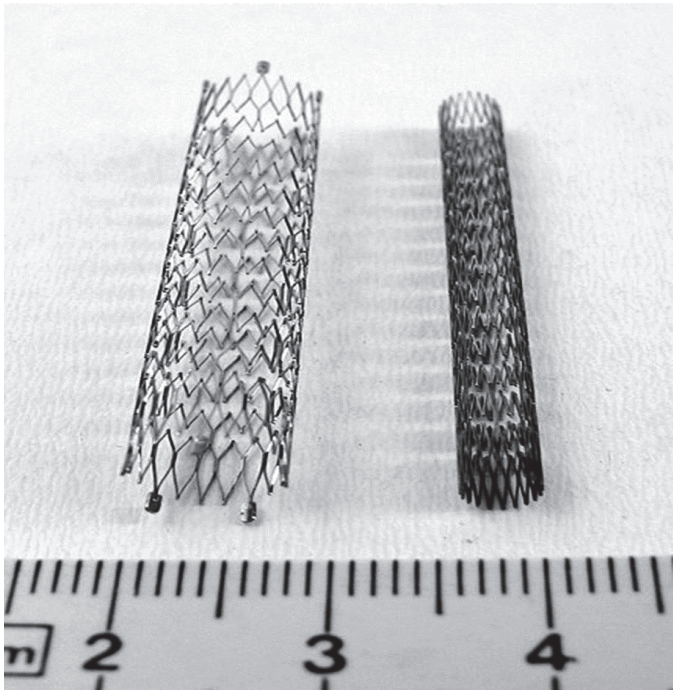

Indice

Indice

ULPGC

TITANIUM

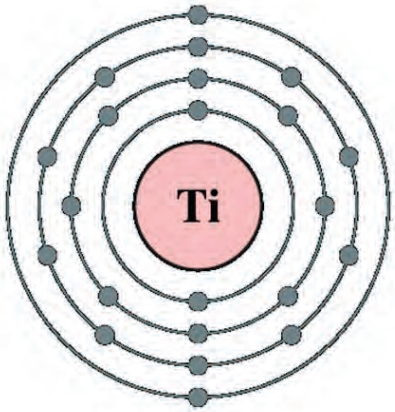

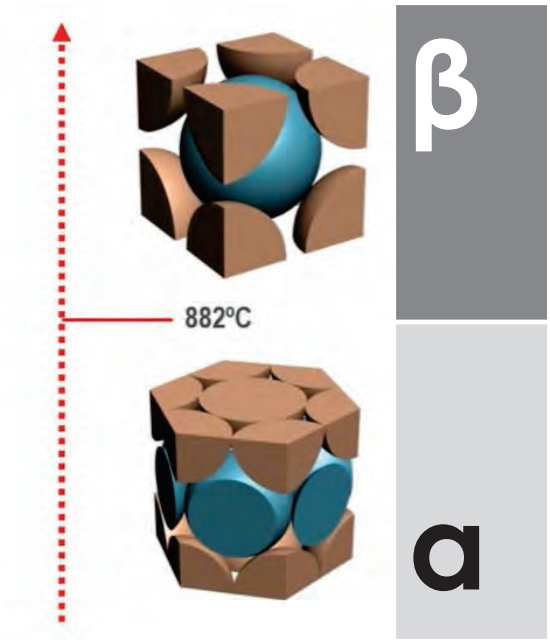

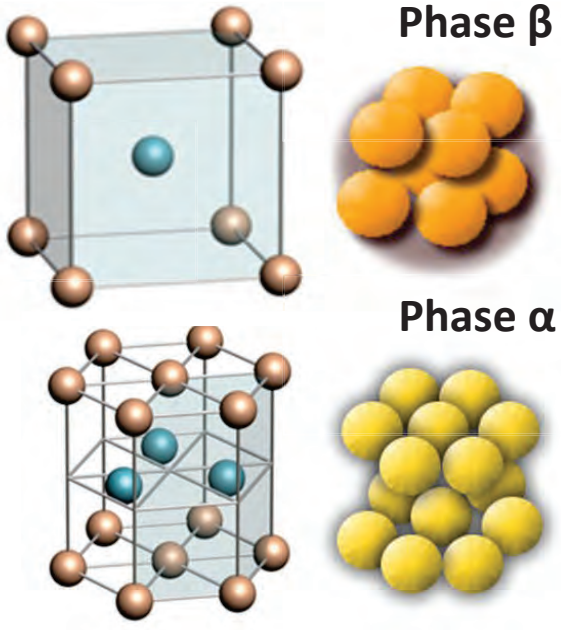

Introducción 1

1. Introducción

Los metales resultan ser los materiales más adecuados en la reparación o reemplazo de tejido óseo dañado para aquellas aplicaciones que impliquen esfuerzo o carga, ya que combinan una elevada resistencia mecánica y a la fractura [1]. A pesar de esto, el uso de materiales metálicos en medios acuosos, como es el cuerpo humano, da lugar a la aparición de fenómenos corrosivos en dicho medio, denominados procesos electroquímicos [2]. La liberación de productos de corrosión y de iones metálicos producida por la corrosión electroquímica y, en especial, por la retirada mecánica de la capa de pasivación y la corrosión galvánica, son causa de preocupación en las aplicaciones de los metales como biomateriales debido a sus posibles efectos citotóxicos [3-5].

Las técnicas electroquímicas convencionales, tales como la voltametría cíclica, la polarización anódica o los pulsos de potencial y/o de corriente permiten hacer caracterizaciones sobre velocidades y mecanismos de reacción, la estructura de la doble capa, características difusivas, morfología del material o la estructura de la interfaz. No obstante, estas técnicas, generalmente desplazan el sistema lejos del equilibrio, por lo que las velocidades de reacción y los parámetros interfaciales pueden ser alterados por el propio método de medición.

El **objetivo principal** de este trabajo de tesis es la aplicación de la técnica de Espectroscopia de Impedancia Electroquímica (EIS) en el estudio del mecanismo del proceso que tiene lugar al estar en contacto una aleación con un medio determinado.

Este objetivo general se aborda a través de los siguientes **objetivos específicos**:

- Evaluación de la técnica de espectroscopía de impedancias electroquímicas, cuyo ámbito de aplicación en el campo de los biomateriales se encuentra en desarrollo.

- Estudio desde el punto de vista de la resistencia a la corrosión de varias aleaciones para su empleo como implante en el cuerpo humano o para instrumental médico. Dicho estudio se efectuará a partir de medidas del potencial a circuito abierto (OCP), barridos potenciodinámicos, ensayos potenciostáticos y de la aplicación de la técnica de espectroscopía de impedancia electroquímica.

Por ellos se ha llevado a cabo:

1. Analizar la influencia de las adiciones de Tantalio en las aleaciones de titanio-tantalio para poder utilizarlos como potenciales productos biomédicos teniendo en cuenta que los materiales utilizados actualmente como implantes generan problemas de salud a larga plazo,

2. Modelar y simular con circuitos eléctricos equivalentes el comportamiento en HCl 20% de tres materiales, Ti, Ti-15Mo y Ti-15Mo-5Al fabricados mediante fusión por láser para sus utilizaciones como materiales resistentes a la corrosión en los intercambiadores de calor, turbinas bombas, válvulas, etc.

3. Conocer el impacto del contenido del aluminio en la película pasiva formada sobre una aleación de alta entropía (HEA) para su posible uso en la fabricación de instrumentos médicos utilizados en condiciones especiales como infecciones, hematomas, alergias, etc.

La impedancia es uno de los valores más importantes que puede ser medido en electroquímica y ciencia de la corrosión. Si se efectúa un muestreo con un ancho de banda infinito, éste contendrá toda la información que puede ser obtenida del sistema mediante medios

puramente eléctricos. El trabajo a realizar se basa en las siguientes características de la técnica de espectroscopia de impedancia electroquímica:

- Las mediciones pueden llevarse a cabo en estado estacionario u otra condición específica.
- El sistema puede ser tratado como lineal. Es una medición eléctrica relativamente sencilla que puede ser automatizada.
- Se pueden caracterizar las propiedades del medio y de la interfaz en todo tipo de materiales (conductores, semiconductores, dieléctricos, cerámicos, composites, etc.).
- Es posible verificar los modelos de reacción.
- Pueden realizarse mediciones en electrolitos de baja conductividad.
- Se trata de una medición de elevada precisión.
- Es una técnica no destructiva cuando se aplica bajo condiciones de equilibrio.

Las publicaciones científicas derivadas de esta tesis doctoral cubren las estrategias mencionadas, proponiendo mecanismos y circuitos eléctricos equivalentes que permitan apreciar la adecuada utilización y el comportamiento de nuevos materiales en determinadas condiciones de uso. En total, se presentan 3 artículos publicados como primer autor, varios artículos como coautor y comunicaciones orales y en poster a varias conferencias internacionales. Todas estas publicaciones suponen el núcleo central del trabajo desarrollado, justificando la unidad temática y permitiendo la presentación de la presente tesis bajo la modalidad de **tesis por compendio de publicaciones.**

El tema de tesis propuesto se encuentra relacionado con las siguientes líneas de investigación del programa de doctorado en Ingenierías Química, Mecánica y de Fabricación (QUIMEFA):

- Nanomateriales
- Corrosión de los metales
- Biomateriales para aplicaciones de ingeniería medica

La tesis trata del estudio de la corrosión de varios materiales metálicos para su posible uso en el sector sanitario. Por lo tanto, se puede observar que el tema de la tesis es totalmente coherente con las líneas de investigación seleccionadas.

TANTALIUM

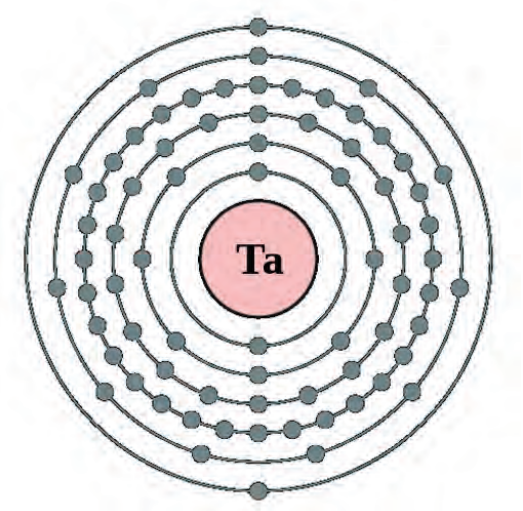

Justificación del compendio

2

2. Justificación del compendio

Las publicaciones científicas básicas derivadas de esta tesis doctoral son 3 artículos publicados como primer autor. He participado en 8 artículos indexados JCR como co-autor, 2 artículos sin índice de impacto de los cuales 1 como primer autor y 5 capítulos de libros como co-autor. También he sido autor principal o co-autor en 31 presentaciones en eventos cientificos (poster o comunicación oral). Un resumen de cada publicación básica se presenta a continuación:

TÍTULO :	**"EIS Characterization of Ti Alloys in Relation to Alloying Additions of Ta"**
AUTORES:	**Socorro-Perdomo, P.P.; Florido-Suárez, N.R.; Mirza-Rosca, J.C.; Saceleanu, M.V.**
REVISTA:	**Materials**
ÍNDICE DE IMPACTO:	**3.623**
CUARTIL:	**Q1**
DOI:	**10.3390/ma15020476.**
ISSN:	**1996-1944**
EDITORIAL:	**MDPI**
MES Y AÑO:	**01/2022**
VOLUMEN:	**15**
PÁGINAS:	**15**

La creciente popularidad del Ti y sus aleaciones como importantes biomateriales está impulsada por su bajo módulo, su mayor biocompatibilidad y su mejor resistencia a la corrosión en comparación con los biomateriales tradicionales, como el acero inoxidable y las aleaciones de Co-Cr. Las aleaciones de Ti se utilizan con éxito en situaciones de estrés severo, como el Ti-6Al-4V, pero esta aleación está relacionada con problemas de salud a largo plazo y, en respuesta, se han desarrollado diferentes aleaciones de Ti compuestas por elementos no tóxicos y no alérgicos, como Nb, Zr, Mo y Ta, para aplicaciones biomédicas. En este contexto, se han desarrollado aleaciones binarias de titanio y tantalio que se prevé que sean posibles materiales para fines médicos.

Además, hoy en día, se han desarrollado nuevas aleaciones, como las aleaciones de alta entropía con Ti y Ta, para aplicaciones biomédicas, por lo que es necesario aclarar la influencia del tántalo en el comportamiento de la aleación. En este estudio, se caracterizaron varias aleaciones Ti-xTa (con x = 5, 15, 25 y 30) utilizando diferentes técnicas. Se generaron mapas de alta resolución de las superficies de los materiales mediante microscopía de barrido en túnel (STM) y se obtuvieron mapas de distribución de átomos mediante espectroscopia de dispersión de energía de rayos X (EDS). La difracción de rayos X (XRD) permitió identificar la composición química y, además, la estructura cristalográfica de las aleaciones.

Se investigó el comportamiento electroquímico de estas aleaciones de Ti-Ta mediante EIS en fluido corporal simulado a diferentes potenciales. La resistencia de la capa pasiva aumenta con el potencial debido a la formación de la capa pasiva de $TiO_2 \cdot Ta_2O_5$ luego disminuye debido a los procesos de disolución a través de la película pasiva. Dentro de las aleaciones Ti-xTa, Ti-25Ta demuestra excelentes propiedades de resistencia a la capa pasiva y

a la corrosión, por lo que parece ser un producto prometedor para dispositivos médicos metálicos.

TÍTULO :	**“Comparative EIS study of titanium-based materials in high corrosive environments”**
AUTORES:	**Socorro-Perdomo, P.P.; Florido-Suárez, N.R.; Verdú-Vázquez, A.; Mirza-Rosca, J.C**
REVISTA:	**International Journal Surface Science and Engineering**
ÍNDICE DE IMPACTO:	**1.178**
CITESCORE 2020	**2.2**
DOI:	**10.1504/IJSURFSE.2021.116333**
ISSN:	**1794-785X**
EDITORIAL:	**Inderscience Publishers**
AÑO:	**2021**
VOLUMEN:	**15**
PÁGINAS:	**152–164**

La espectroscopia de impedancia electroquímica (EIS) es una técnica relativamente compleja y moderna que debe su existencia a la aparición de los circuitos electrónicos. En este trabajo se ha analizado mediante EIS el comportamiento en ácido clorhídrico de tres aleaciones, Ti, Ti-15 Mo y Ti-15Mo-5Al, fabricados mediante fusión por rayo láser.

Los espectros de impedancia se han obtenido a varios potenciales, desde el potencial de circuito abierto hasta +2,0 V frente al potencial del electrodo de referencia. Una vez analizados los perfiles de los espectros de impedancia, los datos experimentales se ajustaron a un modelo

eléctrico equivalente. Se presentaron dos modelos de circuitos equivalentes: en el potencial de corrosión E_{corr} se utiliza un circuito simple mientras que en el rango de potencial pasivo se utilizó un circuito equivalente con 2 constantes de tiempo para ajustar los datos experimentales. Se concluyó que el titanio y las aleaciones de titanio estudiadas sufren una pasivación espontánea debido a la película de óxido que se forma en la superficie en contacto con la solución ácida reductora y por lo tanto, le confiere una alta resistencia en este entorno muy agresivo.

TÍTULO :	**"Comparative EIS study of $Al_xCoCrFeNi$ alloys in ringer's solution for medical instruments"**
AUTORES:	**Socorro-Perdomo, P.P.; Florido-Suárez, N.R.; Voiculescu, I.; Mirza-Rosca, J.C.**
REVISTA:	**Metals**
ÍNDICE DE IMPACTO:	**2.351**
CUARTIL:	**Q2**
DOI:	**10.3390/met11060928**
ISSN:	**2075-4701**
EDITORIAL:	**MDPI**
MES Y AÑO:	**07/2021**
VOLUMEN:	**11**
PÁGINAS:	**14**

En función de las propiedades requeridas para el instrumental médico, en comparación con los materiales clásicos, las aleaciones de alta entropía (HEA´s) son una opción versátil. Se han realizado medidas de Espectroscopia de Impedancia Electroquímica (EIS) en aleaciones de alta entropía tipo $Al_xCoCrFeNi$ con distintas concentraciones de contenido de Al (x = 0,6, 0,8 y 1,0) para caracterizar su película pasiva y su resistencia a la corrosión a 37ºC bajo condiciones fisiológicas infecciosas simuladas (solución de Ringer acidulada con HCl) a pH = 3. Los espectros de impedancia se obtuvieron a diferentes valores de potencial entre -0,7 y +0,7 V frente a la referencia de calomelano saturado (SCE). El análisis de los espectros de impedancia se llevó a cabo ajustando diferentes circuitos equivalentes a los datos experimentales. Para el ajuste de los espectros se pueden utilizar satisfactoriamente dos circuitos equivalentes, con una y dos constantes de tiempo respectivamente: una constante de tiempo representa las características de la película pasiva compacta y la segunda es para la película pasiva porosa.

Con la disminución del contenido de Al, los resultados EIS obtenidos se correlacionan con la evolución de la microdureza y la microestructura, que se caracteriza por Microscopía Óptica (OM), Microscopía Electrónica de Barrido (SEM) y Espectroscopía de Rayos X de Energía Dispersa (EDAX). Se observa para todas las aleaciones que la resistencia de la película pasiva es muy alta y disminuye con el potencial: la muy alta resistencia de la película pasiva implica una alta resistencia a la corrosión, que puede ser asignada a la formación de la capa de óxido protector y demuestra que las aleaciones analizadas cumplen los prerrequisitos para su uso como nuevos materiales para la fabricación de instrumentos médicos.

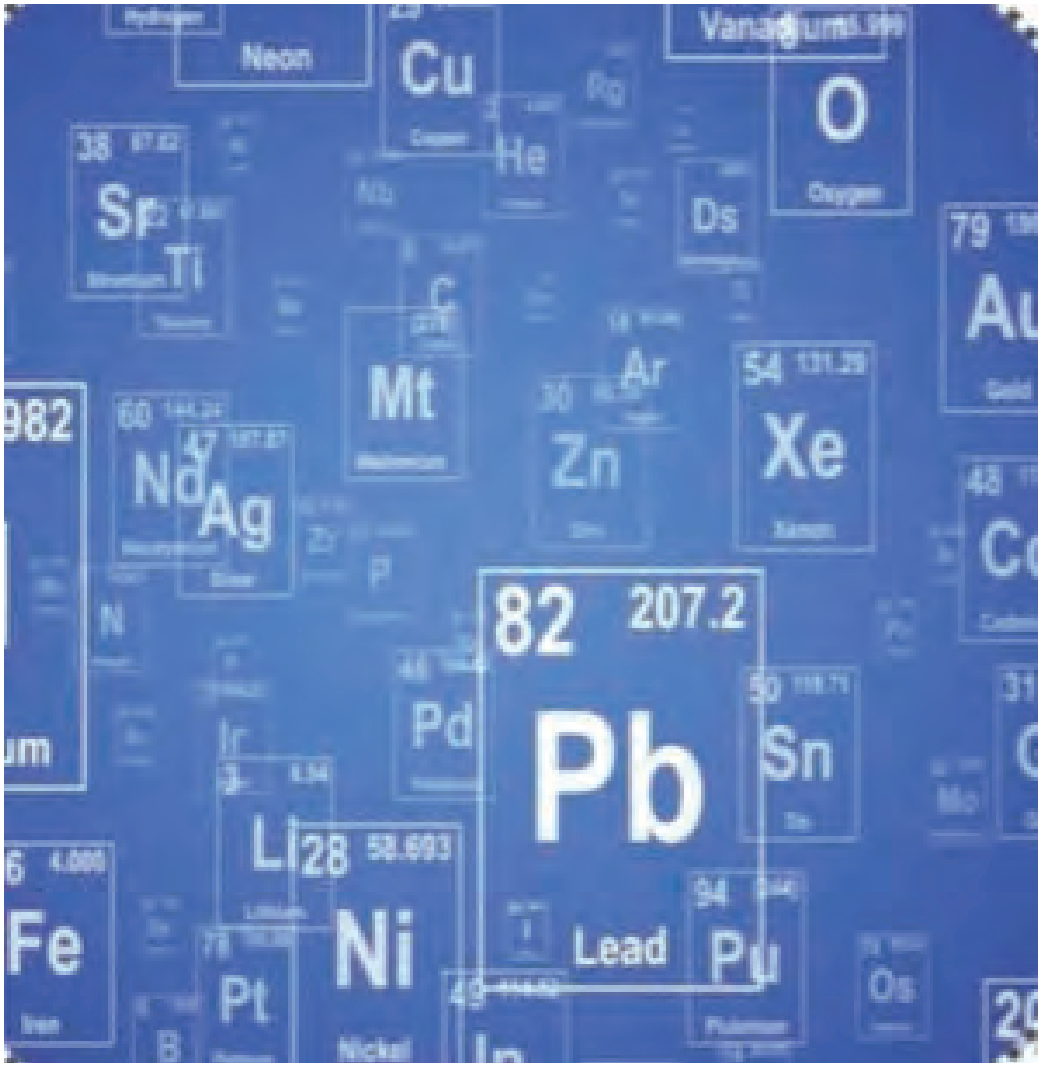

Publicaciones

3

3. Publicaciones

3.1 EIS Characterization of Ti Alloys in Relation to Alloying Additions of Ta

TÍTULO :	**"EIS Characterization of Ti Alloys in Relation to Alloying Additions of Ta"**
AUTORES:	**Socorro-Perdomo, P.P.; Florido-Suárez, N.R.; Mirza-Rosca, J.C.; Saceleanu, M.V.**
REVISTA:	**Materials**
ÍNDICE DE IMPACTO:	**3.623**
CUARTIL:	**Q1**
DOI:	**10.3390/ma15020476.**
ISSN:	**1996-1944**
EDITORIAL:	**MDPI**
MES Y AÑO:	**01/2022**
VOLUMEN:	**15**
PÁGINAS:	**15**

materials

MDPI

Article

EIS Characterization of Ti Alloys in Relation to Alloying Additions of Ta

Pedro P. Socorro-Perdomo [1], Néstor R. Florido-Suárez [1], Julia C. Mirza-Rosca [1,*] and Mircea Vicentiu Saceleanu [2]

[1] Mechanical Engineering Department, Las Palmas de Gran Canaria University, 35017 Las Palmas de Gran Canaria, Spain; pedro.socorro@ulpgc.es (P.P.S.-P.); nestor.florido@ulpgc.es (N.R.F.-S.)
[2] Neurosurgery Department, Faculty of Medicine, "Lucian Blaga" University, 550024 Sibiu, Romania; vicentiu.saceleanu@gmail.com
* Correspondence: julia.mirza@ulpgc.es

Abstract: The increased popularity of Ti and its alloys as important biomaterials is driven by their low modulus, greater biocompatibility, and better corrosion resistance in comparison to traditional biomaterials, such as stainless steel and Co–Cr alloys. Ti alloys are successfully used in severe stress situations, such as Ti–6Al–4V, but this alloy is related to long-term health problems and, in response, different Ti alloys composed of non-toxic and non-allergic elements such as Nb, Zr, Mo, and Ta have been developed for biomedical applications. In this context, binary alloys of titanium and tantalum have been developed and are predicted to be potential products for medical purposes. More than this, today, novel biocompatible alloys such as high entropy alloys with Ti and Ta are considered for biomedical applications and therefore it is necessary to clarify the influence of tantalum on the behavior of the alloy. In this study, various Ti–xTa alloys (with x = 5, 15, 25, and 30) were characterized using different techniques. High-resolution maps of the materials' surfaces were generated by scanning tunneling microscopy (STM), and atom distribution maps were obtained by energy dispersive X-ray spectroscopy (EDS). A thorough output of chemical composition, and hence the crystallographic structure of the alloys, was identified by X-ray diffraction (XRD). Additionally, the electrochemical behavior of these Ti–Ta alloys was investigated by EIS in simulated body fluid at different potentials. The passive layer resistance increases with the potential due to the formation of the passive layer of TiO_2 and Ta_2O_5 and then decreases due to the dissolution processes through the passive film. Within the Ti–xTa alloys, Ti–25Ta demonstrates excellent passive layer and corrosion resistance properties, so it seems to be a promising product for metallic medical devices.

Keywords: Ti–Ta alloys; corrosion; electrochemical impedance spectroscopy

Citation: Socorro-Perdomo, P.P.; Florido-Suárez, N.R.; Mirza-Rosca, J.C.; Saceleanu, M.V. EIS Characterization of Ti Alloys in Relation to Alloying Additions of Ta. *Materials* **2022**, *15*, 476. https://doi.org/10.3390/ma15020476

Academic Editors: Jun Liang and Shengqiang Ma

Received: 21 October 2021
Accepted: 5 January 2022
Published: 8 January 2022

1. Introduction

Titanium achieves its excellent corrosion protection because of the high stability of the passive layer that develops on its surface [1], which can be re-formed at body temperature and in physiological fluid if it is damaged. The increased popularity of Ti and its alloys as important biomaterials is driven by their low modulus [2–4], greater biocompatibility, and better corrosion resistance in comparison to traditional biomaterials, such as stainless steel and Co–Cr alloys [5].

These desirable qualities were the motivating force for the early insertion of Ti as an implantable material. Ti has low mechanical strength [6,7], and when aluminum and vanadium are incorporated in low amounts, the resistance of the alloy is greatly improved over that of titanium and the alloy could be successfully used in severe stress situations, such as Ti–6Al–4V, which has been predominantly employed.

However, Ti–6Al–4V has significant toxicity; harmful tissue reactions are caused by vanadium and the release of both V and Al ions are related to long-term health disorders such as peripheral neuropathy and Alzheimer's and Parkinson's diseases [8,9].

In response to these health problems, different Ti alloys composed of non-toxic and non-allergic elements such as Nb, Zr, Mo, Ta, etc., have been developed for biomedical applications [4,10–12]. However, the non-toxicity of alloying elements is only the first of the three criteria for metallic materials to be used for medical applications. The second important criterion for biomaterials is their resistance to corrosion, which also dictates the tissue compatibility and eventual osseointegration of the implant—critical aspects to consider for implant alloy design. The last important criterion is the Young's modulus of the implant in comparation with that of the bone. A mismatch between these modules can lead to a reallocation of loads surrounding the implant, causing implant loosening [13].

In this context, binary alloys of titanium and tantalum have been developed and analyzed [14–23] and are predicted to be potential products for medical purposes; as tantalum is a non-toxic element [24], they have better compatibility with bone tissue compared with cp–Ti and Ti–6Al–4V alloys [21], and Ti–Ta alloys exhibit reduced modulus of elasticity and increased relative strength (at equivalent stiffness) compared with commercially pure titanium (cp-Ti) [25]. More than this, today novel biocompatible alloys such as high entropy alloys with Ti and Ta are considered for biomedical applications and, therefore, it is necessary to clarify the influence of tantalum in the behavior of the alloy.

Electrochemical impedance spectroscopy (EIS) is applied to characterize the behavior of different metals and alloys in various environments and to provide new information that previously could not be obtained with classical dc techniques [26,27]. Although a significant amount of research has been performed using EIS to characterize the biomaterials, little research has been conducted on EIS measurements of Ti–Ta alloys [17,28]. It is observed that it is essential for all systems to consider suitable impedance models that can be used to fit the experimental results and to provide the relevant data that characterize the corrosion process.

In this study, various Ti–xTa alloys (with x = 5, 15, 25, and 30) were characterized using different techniques. High-resolution maps of the materials´ surface were generated using scanning tunneling microscopy (STM), and information about atom distribution maps was obtained using energy dispersive X-ray spectroscopy (EDS). A thorough output of chemical composition and hence the crystallographic structure of the alloys were identified by X-ray diffraction (XRD). Additionally, the electrochemical behavior of these Ti–xTa alloys was investigated in simulated body fluid (SBF) at different potentials.

2. Materials and Methods

2.1. Material and Sample Preparation

The studied titanium tantalum alloys were Ti–5Ta, Ti–15Ta, Ti–25Ta, and Ti–30Ta from R&D CS (Research & Development Consulting and Services), Bucharest, Romania. The Ti–Ta ingots (diameter = 20 mm, length = 30 mm) were produced by levitation fusion in a high-frequency induction furnace operating with a cold copper crucible followed by a homogenization heat treatment (heating rate 5 °C/min, homogenized at 1000 °C for 8 h followed by natural cooling) in order to eliminate the segregation. The chemical composition of the alloys was determined by the supplier; for Ti and Ta content, the XRF technique was applied, while for the impurities (e.g., O, N, and C), the inert gas fusion technique was employed. The detailed chemical composition of the alloys is presented in Table 1.

Table 1. Chemical composition of Ti–xTa alloys.

Alloy	Ti (wt. %)	Ta (wt. %)	O (wt. ppm)	N (wt. ppm)	C (wt. ppm)
Ti–5Ta	94.20 ± 0.06	4.92 ± 0.05	180 ± 14	80 ± 7	110 ± 8
Ti–15Ta	84.41 ± 0.06	14.82 ± 0.07	162 ± 11	75 ± 5	101 ± 6
Ti–25Ta	74.52 ± 0.05	24.89 ± 0.09	158 ± 12	82 ± 6	103 ± 5
Ti–30Ta	69.61 ± 0.07	29.67 ± 0.05	172 ± 11	78 ± 5	111 ± 4

The elastic modulus E and tensile strength σ_t of the obtained alloys are Ti–5Ta (E = 142 GPa, σ_t = 381 MPa), Ti–15Ta (E = 101 GPa, σt = 402 MPa), Ti–25Ta (E = 65 GPa, σt = 464 MPa), and Ti–30Ta (E = 94 GPa, σ_t = 445 MPa). The experimental methods followed the ASTM E3-11 (2017) standard for metallo-graphic sample preparation [29]. The ingots were cut with minimal deformation using the Buehler IsoMet 4000 Precision Saw, (Chicago, IL, USA) and one-micron positioning allows for precise sectioning. Then, the specimens were mounted with acrylic (compression hot mounting) in order to protect edges during the polishing process. The next operation involves the grinding up to 2500 grit with SiC paper and then polishing with 0.1 μm alpha-alumina until a mirror finish is obtained in a Struers TegraPol-11 (Copenhague, Denmark) polishing machine. The samples were ultrasonically cleaned using deionized water and rinsed thoroughly with distilled water and ethanol.

2.2. Microstructural Characterization

EDS measurements were carried out with an environmental scanning electron microscope model FEI XL30 ESEM with an LaB6 cathode attached to an energy dispersive X-ray electron sample analyzer, model EDAX Sapphire.

The structures of the Ti–Ta alloys were investigated by high-resolution scanning tunneling microscopy (STM). All determinations were performed in air with a Hitachi TM3030 microscope that had been transversely calibrated by imaging atomically accurate oriented pyrolytic graphite. The tips were obtained by chopping a 0.20 mm Pt0.8Ir0.2 wire. The data were acquired in constant current operation with specific tunneling currents of 0.13–0.3 nA and a specimen polarization of 0.4–1.0 V. No tip-induced shifts were noted.

X-ray diffraction (XRD) determinations were made using an Empyrean diffractometer (Malvern-Panalytical). The device worked with a Cu Kα anode (1.5406 Å) in the range of 2θ = 0–64° with a step size of 0.04° at a power of 45 kV and 40 mA in Bragg–Brentano geometry. The samples have been rotated while collecting data in order to achieve better data capture. The obtained patterns were simulated in order to determine the presence of the crystalline phase, the lattice parameter, and the diameter of the grain with the assistance of Malvern-Panalytical's HighScore Plus software.

2.3. Electrochemical Measurements

Electrochemical measurements were carried out with a PAR 263 A potentiostat coupled with a PAR 5210 (AMETEK, Berwyn, PA, USA) lock-in amplifier. A standard three-electrode electrochemical cell with a Pt grid as a counter electrode and a saturated calomel electrode (SCE) as a reference electrode was used. The mounted, grinded, and polished samples of Ti–xTa alloys were employed as working electrode for the electrochemical measurements. All the measurements were performed in simulated body fluid (SBF) prepared in our laboratory with the pH = 7.8 measured with a multiparameters analyzer CONSORT 831C and the composition is presented in Table 2.

The open circuit potential was recorded for 24 h with the samples immersed in SBF solution. The potentiodynamic polarization curves were obtained with a scanning rate of 0.166 mV/s in the potential range −800 to +2000 mV vs. SCE. The polarization resistance R_p was calculated from traces of the polarization curve at ±10 mV versus open circuit potential.

Table 2. Composition of simulated body fluid (SBF).

Compound	Composition [g/L]
NaCl	6.80
KCl	0.40
$CaCl_2$	0.20
$MgSO_4 \cdot 7H_2O$	0.20
$NaH_2PO_4 \cdot H_2O$	0.14
$NaHCO_3$	2.20
Glucose	1.00

The effect of the potential on the passive film of Ti–Ta alloys operating in a simulated physiological environment was evaluated by electrochemical impedance spectroscopy (EIS). The AC potential amplitude was set at 10 mV, and single sine wave recordings were performed at frequencies in the range of 10^{-1} and 10^5 Hz for all specimens. To characterize the oxide layer, impedance spectra were registered in the range of −400 to 2000 mV with a step of 100 mV by continuously polarizing the electrodes and letting the system equilibrate for 600 s at every potential. For the numerical fit of the measured impedance data, the software program ZSimWin was used.

All the electrochemical tests were normally repeated three or four times to ensure that they presented reasonable reproducibility.

3. Results and Discussions

The EDS analysis has been performed on micro-zones of the same square area, and the elemental distribution maps (see Figure 1) and chemical composition for the four alloys (see Table 3) are presented. It can be observed that there are no impurities in the metallic mass and titanium and tantalum were the only identified elements.

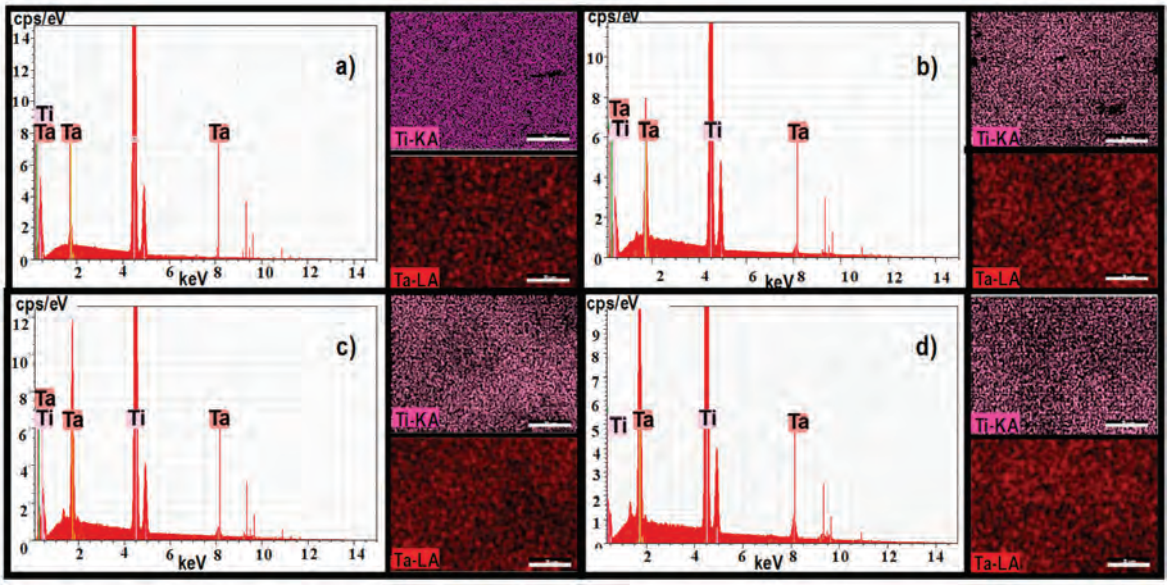

Figure 1. Atoms distribution of Ti and Ta in the studied alloys: (**a**) Ti5Ta, (**b**) Ti15Ta, (**c**) Ti25Ta, and (**d**) Ti30Ta.

In Figure 2, we can observe the surface topography acquired by scanning tunneling microscopy (STM). A three-dimensional analysis of the surface topography reveals nanoscale deviations within an overall homogeneous nanoscale architecture found on the surface of the Ti–Ta alloy.

Table 3. EDS global analysis on micro-areas for Ti–xTa alloys.

Alloy	Ti			Ta		
	at.%	wt.%	Error, %	at.%	wt.%	Error, %
Ti–5Ta	99.01	94.95	1.22	0.88	4.38	3.67
Ti–15Ta	95.62	83.95	1.95	4.38	14.87	2.24
Ti–25Ta	91.76	74.63	2.03	8.23	24.83	2.15
Ti–30Ta	90.06	69.74	1.81	9.95	29.72	1.98

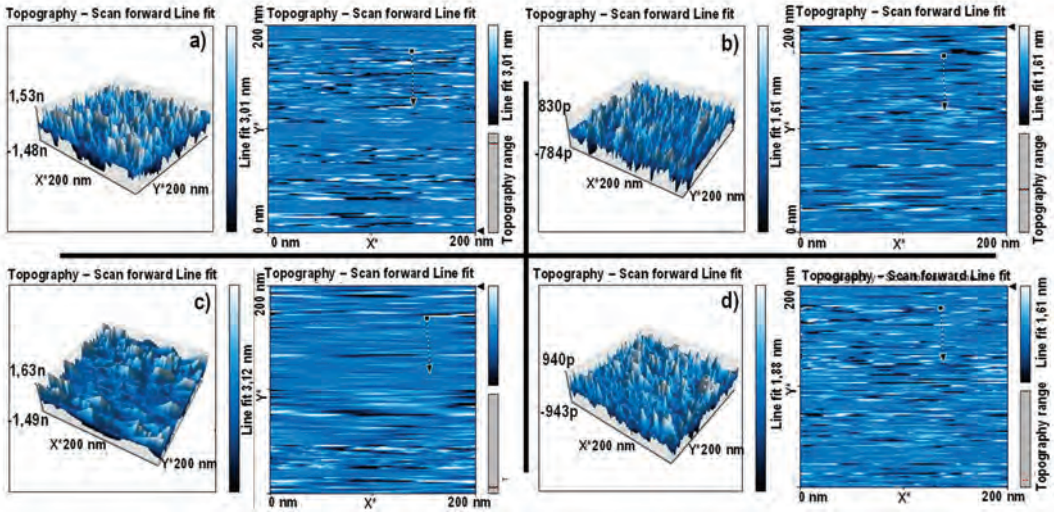

Figure 2. Representative scanning tunneling microscopy (STM) images of surface topographies for (**a**) Ti5Ta, (**b**) Ti15Ta, (**c**) Ti25Ta, and (**d**) Ti30Ta.

Nanoscale deviations, suggestive of the topography present in natural tissue, have been repetitively demonstrated to enhance the protein-specific adsorption, thus further driving cellular activity and cell–cell relationships [30]. Thus, these features enable a very promising interface to enhance cellular interaction because of increased nanoscale roughness of the material interface.

Pure titanium has a closed hexagonal structure (HCP), i.e., an α-phase at room temperature. At temperatures above 883 °C, there is a body-centered cubic (BCC) structure, i.e., a β-phase. The β-phase is stable at temperatures below 883 °C with the addition of β-stabilizers, and its stability depends on the amount of β-alloying elements. The quantity of β-stabilizer required to retain the pure β-phase at room temperature depends on the molybdenum equivalence, a rule derived from the analysis of binary titanium alloys. Molybdenum equivalence is given by [31]:

$$Mo_{eq} = 1.0\ Mo + 0.67\ V + 0.44\ W + 0.28\ Nb + 0.22\ Ta + 1.6\ Cr + \ldots\ \ldots\ -1.0\ Al$$

In general, a molybdenum equivalency of approximately 10 is necessary to stabilize the β-phase while quenching [14], and the critical value to reach a complete β-phase is ap-proximately 25. As we can see for the studied Ti–Ta alloys, the Moeq is below the mini-mum value needed for a fully stable β phase, and the microstructure is made up of α″ grains within β grains. Figure 3 presents the XRD patterns taken from the Ti–xTa alloys.

Because the Ta element is a β phase former in the Ti-based alloys and Moeq is low, the microstructures of all studied samples are clearly a mixture of α″ phase (orthorhombic structure) and β phase. However, the intensity of α″ phase decreased as the concentration of Ta increased, and this is attributed to the variation of the volume fraction of α″ phase in the matrix.

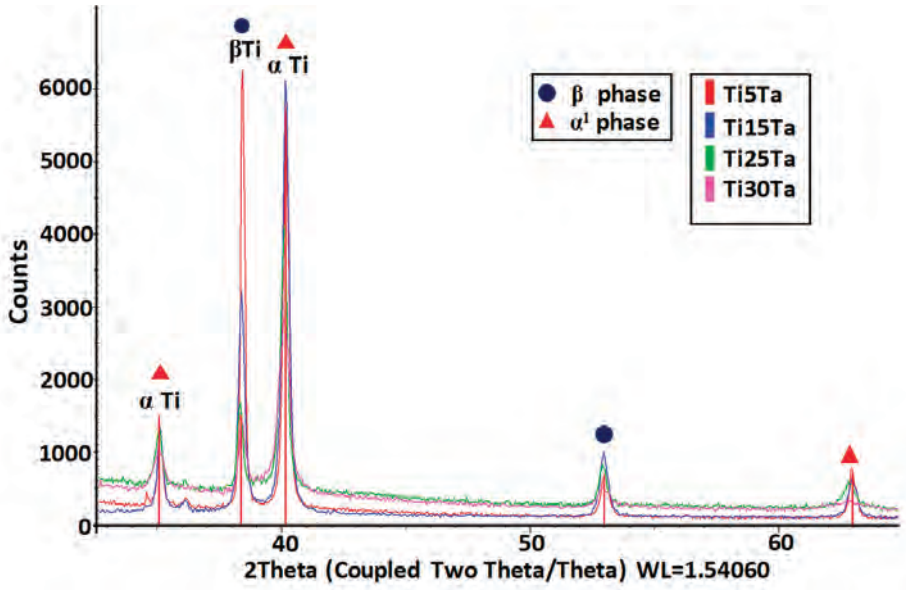

Figure 3. XRD pattern for TixTa alloys.

3.1. Electrochemical Impedance Spectroscopy

Figure 4 shows the open circuit potential curves for all four Ti–xTa alloys immersed for 24 h in simulated body fluid. It can be observed that following the immersion, an abrupt displacement of the potential has taken place towards positive values during a pe-riod of 2–6 h. Afterwards, the open circuit potential continued to increase slowly, suggesting the growth of a passive layer on the metallic surface. The linear polarization curves, in semilogarithmic coordinates for the tested Ti–xTa alloys in simulated body fluid, are displayed in Figure 5, and Table 4 shows the instantaneous corrosion parameters in this physiological environment. All samples are characterized by high values of the polarization resistance R_p (10^5 Ω·cm^2).

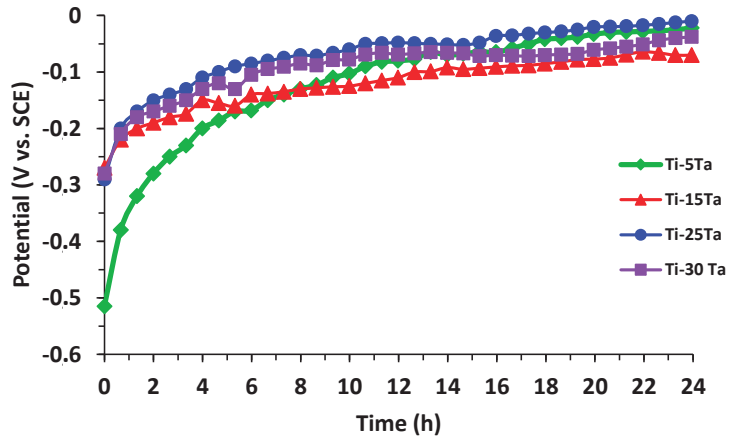

Figure 4. Open circuit potential curves for Ti–xTa alloys during 24 h immersion in SBF.

The electric potential difference between the reference electrode and metal interface is a relevant factor directly related to the surface conditions. EIS tests have been carried out at various potentials in three areas: cathodic–anodic transition, passive transition, and quasi-transpassive transition. The impedance results will be used to compare the effect of the potential on the properties of the passive layer.

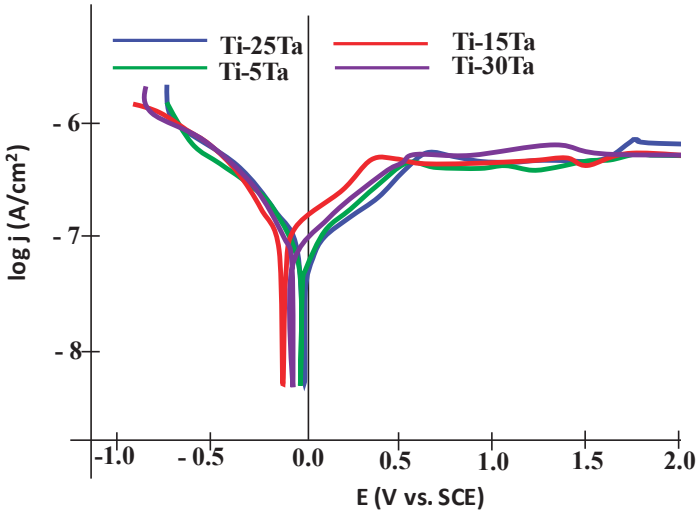

Figure 5. Polarization curves for Ti–xTa alloys.

Table 4. Corrosion parameters from polarization curves (mean ± SD).

Alloy	E_{corr} (mV vs. SCE)	i_{corr} (μA/cm²)	i_{pass} (μA/cm²)	R_p (kΩ·cm²)
Ti–5Ta	−22 ± 4	0.67 ± 0.06	0.61 ± 0.11	522 ± 16
Ti–15Ta	−70 ± 3	0.52 ± 0.12	0.58 ± 0.05	501 ± 23
Ti–25Ta	−10 ± 3	0.43 ± 0.04	0.51 ± 0.16	598 ± 28
Ti–30Ta	−38 ± 4	0.58 ± 0.21	0.57 ± 0.18	495 ± 12

3.1.1. Plots Interpretation

The Nyquist plots correspond to the impedance of Ti–5Ta, Ti–15Ta, Ti–25Ta, and Ti–30Ta at different potential values. Even the EIS data were recorded within the $-0.4\ V \leq E \leq 2.0\ V$ potential range with a step of 100 mV; not all the obtained curves are shown in Figures 6–9.

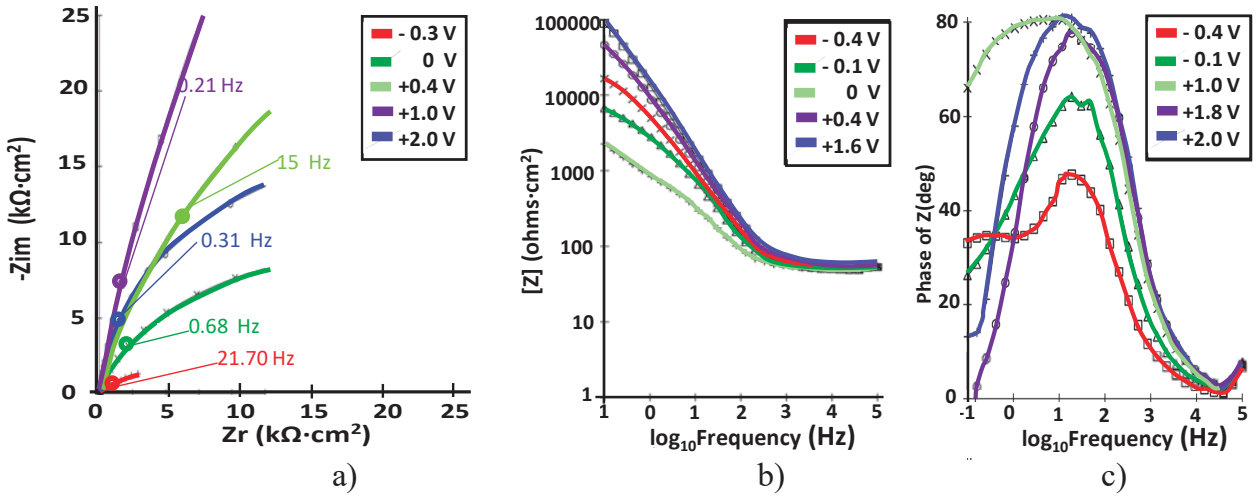

Figure 6. (**a**) Nyquist; (**b**) Bode –IZI and (**c**) Bode-phase spectra at different potentials for Ti–5Ta in simulated body fluid at pH = 7.8.

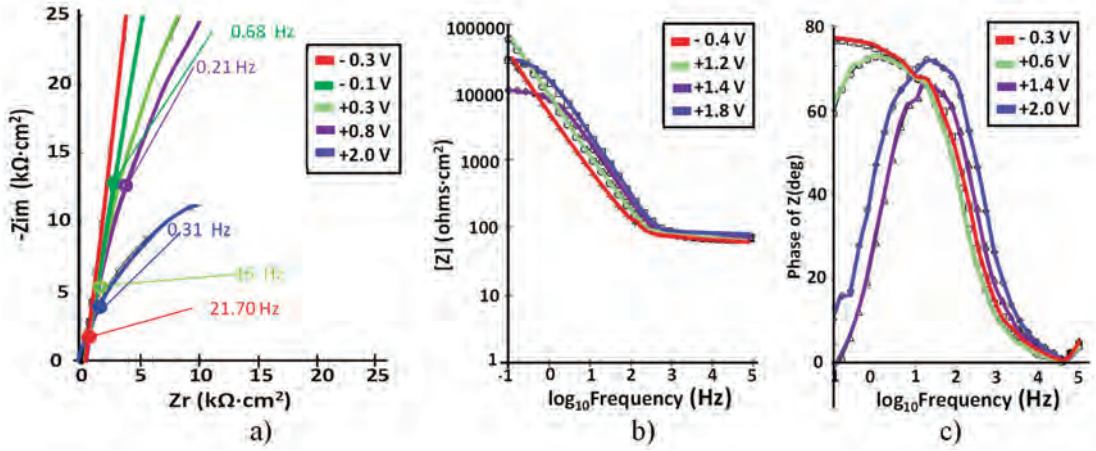

Figure 7. (**a**) Nyquist; (**b**) Bode –IZI and (**c**) Bode-phase spectra at different potentials for Ti–15Ta in simulated body fluid at pH = 7.8.

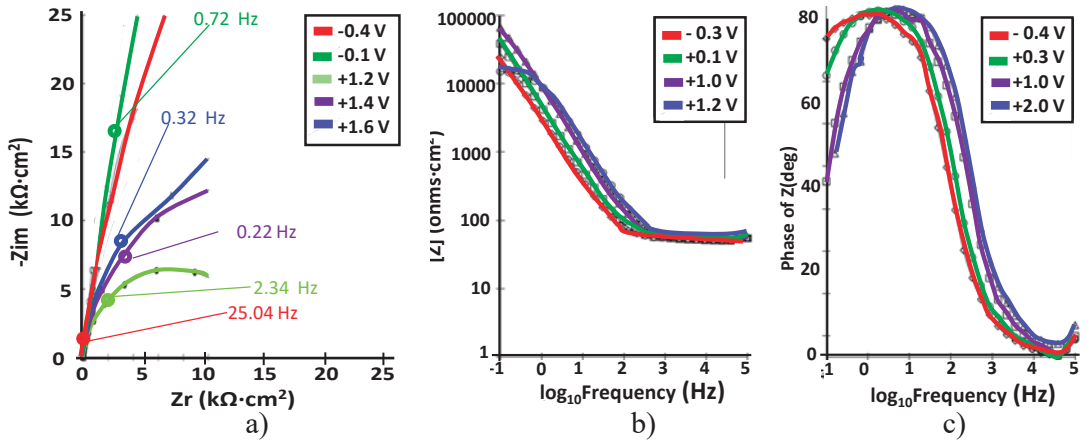

Figure 8. (**a**) Nyquist; (**b**) Bode –IZI and (**c**) Bode-phase spectra at different potentials for Ti–25Ta in simulated body fluid at pH = 7.8.

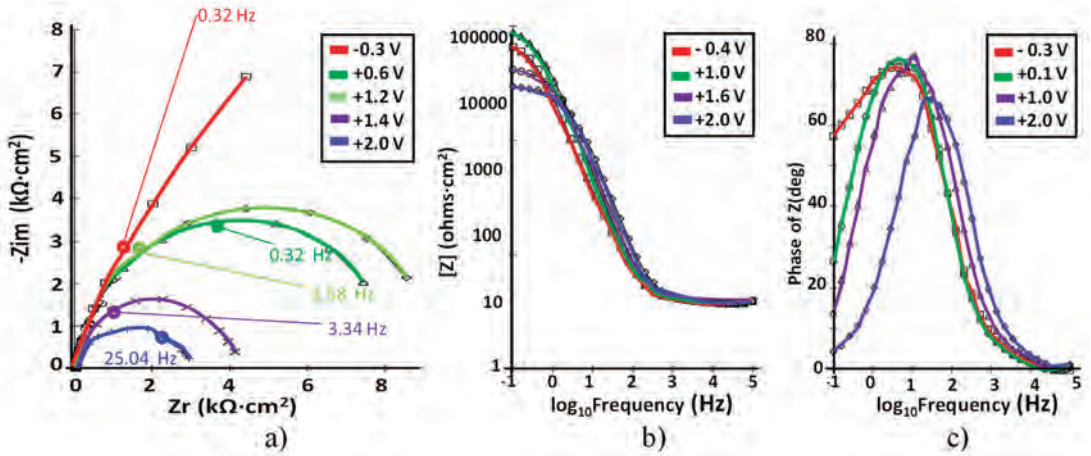

Figure 9. (**a**) Nyquist; (**b**) Bode –IZI and (**c**) Bode-phase spectra at different potentials for Ti–30Ta in simulated body fluid at pH = 7.8.

3.1.2. Ti–5Ta

The corresponding EIS plots are presented in Figure 6.

At all potentials, a near capacitive response was detected, characterized in Nyquist plots (see Figure 6a) by incomplete semicircles. In the higher frequency band (1–100 kHz),

the Bode plot (Figure 6b) shows constant values (horizontal line) of log |Z| versus log(f) with a phase angle approaching 0°. From 0 to 1 V, in the wide range of low and medium frequencies, the spectra show a linear slope of approximately –1 in log |Z| as the frequency decreases, while the phase angle values are close to 80°. This is the typical response of a compact passive film capacitor. The acquired values for passive film resistance are high until 1.8 V, after which they decrease with the potential. In Figure 6c, it can be observed that the phase angle observed for Ti–5Ta was encountered in the range of about −65° to −80°, suggesting a highly stable film on Ti–5Ta [19]. At a potential value higher than 0 V, a unique peak is noted in the phase angle graphs, which indicates the engagement of one relaxation time.

3.1.3. Ti–15Ta

The corresponding EIS plots are presented in Figure 7.

For this alloy, the shape of the impedance data is similar to that of Ti–5Ta but the response of the compact passive oxide can be observed until 1.2 V, with no modifications of the value of the electrolytic solution resistance (see Figure 7b). Bode-|Z| spectra displayed a linear slope of about −1 and high impedance values (order of 10^5 Ω·cm^2) in the low and middle frequency ranges, which represent the characteristic response of a capacitive behavior of the passive film [32]; after a potential value of 1.2 V, the impedance values slightly decreased over time as result of the low dissolution of the passive layer [10].

3.1.4. Ti–25Ta

The corresponding EIS plots are presented in Figure 8.

For this alloy, we can also observe a strong change in the shapes of the impedance data, but at lower potential than for Ti–5Ta and Ti–15Ta. This change takes place between 0.8 and 1.0 V. The Nyquist plots illustrate, at all applied potentials, one depressed semicircle, suggesting non-ideal capacitive behavior (high corrosion resistance) for Ti–25Ta. When the semicircles deformed and their diameters decreased over time, it shows some dissolution processes through the passive film. During the potential scan, the electrolytic resistance is constant (60 Ω·cm^2), and the passive layer capacitance slowly decreases with the potential. With the Ti–25Ta alloy, the best results in EIS spectra were obtained, completing the lowest elastic modulus and the highest ratio of strength to modulus among Ti–Ta alloys [33]. It can be observed that Bode-|Z| impedance plots showed linear portions with the slope amounting to −1 (from −0.96 to −0.99) over a large frequency range (from 100 mHz to 100 kHz). At all analyzed potential values, a single peak is observed in phase angle plots, which indicates the involvement of one relaxation time.

3.1.5. Ti–30Ta

The corresponding EIS plots are presented in Figure 9.

It can be observed that the Nyquist plots revealed the same capacitive loops but with the lowest impedance values compared with the other alloys. It can be seen that the Bode-|Z| impedance plots exhibited linear parts with a slope around −1 only at intermediate frequencies. It was found that the maximum phase angle observed for Ti–30Ta was the lowest among all the values obtained for the Ti–Ta alloys. It can be observed that the electrolytic resistance was constant during the experiments (27 Ω·cm^2).

3.2. Equivalent Circuits

The obtained impedance data were matched by employing a nonlinear regression approach using the Randles equivalent circuit (see Figure 10a) [34–36]. This widely used electrical equivalent circuit involves an ohmic solution resistance (R_s) in series with the parallel arrangement of a CPE (Q_l) and a resistor (R_l). R_l is a numerical indicator that provides a value for the corrosion resistance of the passive layer that acts as a damper to the flux of electrons (resistance) across the metallic material/electrolyte interface and gives a measure of the level of protection provided by the passive layer that forms at the

inter-face [10,37]. The employment of a constant phase element (Q_l) in place of an "ideal" capacitor was required due to the inhomogeneous nature of the passive layer formed on the alloy surface and because of the differences between the flat surface of an ideal capacitor. From the obtained data, it was found that the value of R_s does not change significantly during the test due to the fact that the controlling factors that affect its magnitude, as the stability of the exhibited surface and the number of ions in the simulated body fluid solution do not change.

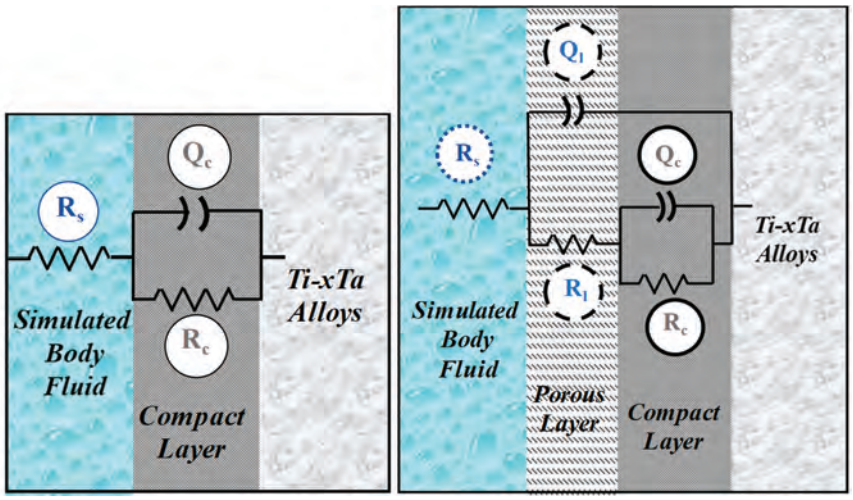

Figure 10. Equivalent circuits used for fitting the experimental data with: (**a**) one time-constant; (**b**) two time-constants.

In the corrosion process, a passive layer is developed on the metallic surface and the charge transfer reaction that occurs can be disregarded and the resulting measured impedance could be assigned to the impedance of the passive film. The components of the equivalent circuit are:

R_s—ohmic resistance of the physiological solution

R_l—resistance of the passive layer

C_l—capacitance of the passive layer

The analysis of the impedance plots was carried out by fitting these data with ZSimp-Win software. The performance of the fit to the equivalent circuit was assessed in the first place by the chi-square value and in the second place by comparing experimental data with simulated data.

In place of capacitance, a constant phase element (CPE), representing the shift from the real capacitive performance, was employed. The impedance of a CPE is characterized by [27]:

$$Z_{CPE} = \frac{1}{Y^0(j\omega)^n} \quad (1)$$

where:

– Z is the impedance of the constant phase element CPE
– j is the imaginary number ($j^2 = -1$)
– ω is the angular frequency ($rad \cdot s^{-1}$)
– $n\pi/2$ is the constant phase angle of the constant phase element (rad)
– Y^0 is the constant of the constant phase element [$S(s \cdot rad^{-1})^n$]

According to all Bode plots and our previous work [10], only one time constant can be clearly distinguished; however, at low frequencies, no clear definition of the second time constant can be observed so only the high–medium frequencies' data have been analyzed in this work and only the simple circuit was used. Different studies [38,39] have proven that data at low potentials have indicated the growth of a single layer of oxide on titanium

characterized by one-time constant equivalent circuit; the same circuit was reported by others who studied the corrosion of tantalum either in its pure form or as a coating [40–43].

When the impedance spectra were fitted to the equivalent circuits presented in Figure 10, a CPE element was used because, generally, a distributed relaxation feature is presented for TiO_2 films.

In order to obtain the total impedance of the equivalent circuit, we determine the admittance of the parallel arrangement (R_lQ_l):

$$\frac{1}{Z_l} = \frac{1}{Z_{R_l}} + \frac{1}{Z_{Q_l}} \tag{2}$$

Because the roughness factor "n" is > 0.85, near to 1, the resulting Y^0 value of Q_l is assumed to be C_l in the following discussion:

$$\frac{1}{Z_l} = \frac{1}{R_l} + j\,w\,C_l \tag{3}$$

The diagnostic considerations for the selection of equivalent circuits for modeling the impedance data can be resumed by visual observations of the shifts in the experimental Bode diagrams with the change of potential and concentration of the alloying metal. It appears that, in the passive zone potentials (mostly strictly capacitive impedance), the Bode graphs provide a good fit if the total impedance is modeled following the circuit in Figure 10a. The obtained results of C_l and R_l are presented in Figures 11 and 12, respectively.

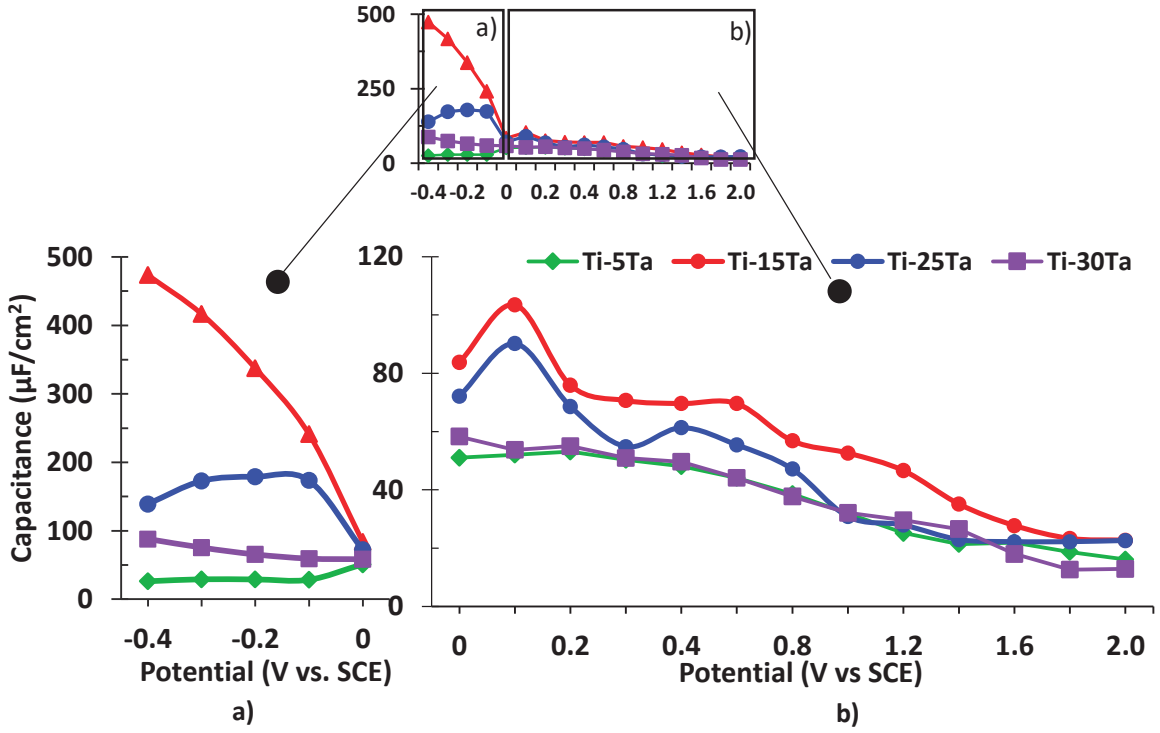

Figure 11. Capacitance of the passive films for Ti–Ta alloys in simulated body fluid: (**a**) at negative potentials; (**b**) at positive potentials.

Figure 11 points to the fast decreasing of the passive film capacitance. A high initial C_l is compatible with a high initial active surface and a high roughness factor. The evolution of C_l with the potential is also compatible with the decreasing of the active surface due to the increasing of the passive layer thickness, with all the alloys eventually reaching the same order of film thickness.

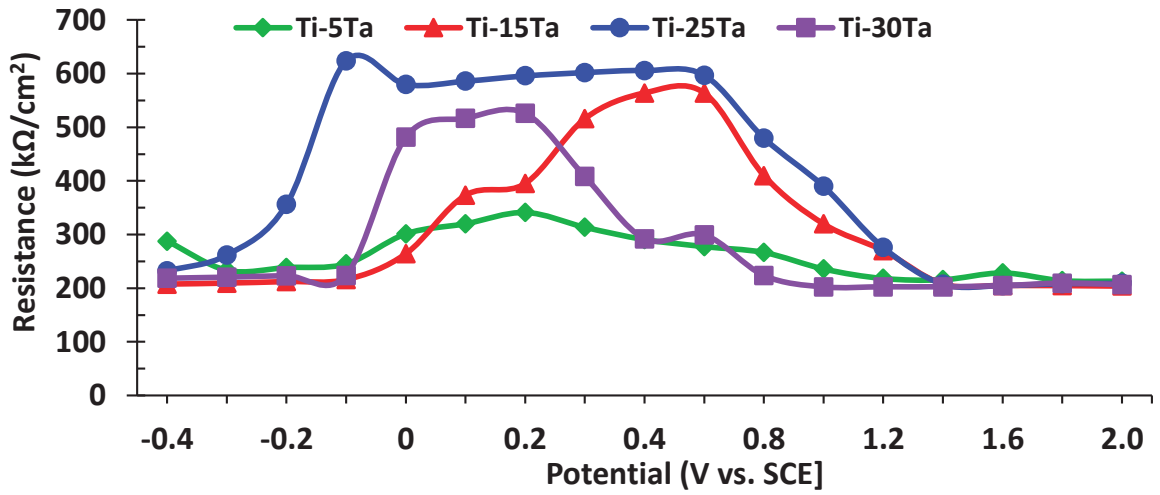

Figure 12. Resistance of the passive films for Ti–Ta alloys in Ringer's solution.

In Figure 12, the resistance of the passive film ($k\Omega \cdot cm^{-2}$) as a function of potential is presented. It can be observed that the value obtained for Ti–25Ta is higher than that of the other alloys, which depicts its highest corrosion resistance in simulated body fluid. This is due to the chemical composition of this alloy, which is closed to the compositional boundary between the α' and α'' phase and has the lowest elastic modulus and the highest ratio of strength to modulus among Ti–Ta alloys [9].

The shape of the potentiodynamic polarization curves indicated that all the Ti–xTa alloys are passivating immediately at immersion in simulated body fluid, a behavior that can be termed stable passivity. In these conditions, after 24 h of immersion, the passive film is thicker and the EIS data can be fitted with good results (chi^2 of 10^{-4} order) by the two-time equivalent electrical circuit presented in Figure 10b. In Table 5, the main parameters of the proposed circuit for all the studied alloys are presented. Polarization resistance R_p is represented by the sum of the resistance of the porous passive film and the compact barrier layer ($R_l + R_c$) [44]. The value of the "n" parameter corresponds to the extent of dispersion and is attributed to the surface inhomogeneity. The values of n_c are almost 1, and Q_c is similar with a pure capacitor. The values of n_p are lower than those of n_c, and this may be due to the higher roughness and diffusion through the outer layer. The simulated data are in good agreement with the experimental data, and chi-square values of 10^{-4} were obtained.

Table 5. Circuit parameters calculated from the fitting of the EIS spectra at corrosion potential to the equivalent circuit from Figure 10b.

Alloy	R_s ($\Omega \cdot cm^2$)	$Y^0_p \cdot 10^5$ ($S \cdot s^n/cm^2$) $0 < n < 1$	n_o	R_l ($\Omega \cdot cm^2$)	$Y^0_c \cdot 10^5$ ($S \cdot s^n/cm^2$) $0 < n < 1$	n_c	R_c ($k\Omega \cdot cm^2$)	$\chi^2 \cdot 10^4$
Ti–5Ta	34.2	1.72	0.59	500.6	2.71	0.89	153.1	7.24
Ti–15Ta	59.0	9.90	0.78	887.5	17.6	0.91	322.4	4.37
Ti–25Ta	11.5	1.74	0.72	14.5	4.31	0.94	577.3	4.89
Ti–30Ta	27.1	6.13	0.79	28.1	1.10	0.90	485.9	1.88

The corrosion resistance of an alloy could be characterized by the polarization resistance at the corrosion potential. This parameter can be calculated in two ways: (1) taking the slope of the E vs. I relationship in the range of ± 10 mV vs. open circuit potential; (2) from the fitting results of EIS spectra with all the implicated resistances [45]. Comparing the values obtained by the two techniques, it is observed that, for low concentrations of tantalum (Ti–5Ta and Ti–15Ta), the values of corrosion resistance obtained by EIS are lower than those of the DC experiments. This is probably due to the fact that with the shift of the

potential towards more positive values vs Ecorr, titanium forms a more compact oxide layer than it does at the corrosion potential. At higher Ta concentrations (Ti–25Ta and Ti–30Ta), Ta_2O_5 plays a more important role in the compactness of the passive film and the corrosion resistance values from EIS and polarization curves are approximately the same. It can be observed that the highest corrosion resistance of Ti–xTa alloys was obtained for Ti–25Ta.

Titanium is not a noble metal, and if this metal generally exerts a high electrode potential, it is because a passivating film of oxide is formed on its surface; the stability of this layer protects the metal from further deterioration.

During the anodic polarization, a film of TiO_2 is formed:

$$Ti + 2H_2O \rightarrow TiO_2 + 4H^+ + 4e^- \quad (4)$$

For Ti, the Porbaix diagram of Ti–H_2O indicates that the substantial decrease in the passive film resistance at potentials close to 1 V can be attributed to the development of TiO_3–H_2O on the surface of the alloys.

The Pourbaix Ta–H_2O diagram [46] shows that the high strength of tantalum is attributed to the development of a protective film of tantalum pentoxide (Ta_2O_5). Tantalum, during the anodic polarization, tends to cover itself with this layer of Ta_2O_5, which has good qualities (compactness, continuity, etc.). The reaction that takes place is:

$$2Ta + 5H_2O \rightarrow Ta_2O_5 + 10H^+ + 10e^- \quad (5)$$

Tantalum pentoxide can exist in the hydrated state; it has a variable percentage of water of crystallization and is attributed the formula $Ta_2O_5 \cdot H_2O$ or $HTaO_3$.

4. Conclusions

1. The Nyquist plots for all the Ti–Ta alloys show the same incomplete semicircles with large diameters increasing with the potential (up until a critical value for each alloy) due to the improvement of the protective properties of the passive film formed on the surface of the alloy.
2. For all Ti–Ta alloys, the Bode phase plots exhibited one phase angle—typical for a capacitive barrier passive layer formed on the surface of an alloy.
3. Impedance spectra are fitted with a one-time constant equivalent circuit, common for a compact oxide layer, for all Ti–Ta alloys in extra-cellular fluids. After a long immersion period in simulated body fluid, the passive film is thicker and develops a bi-layer structure: an outer porous layer and an inner compact layer. Tantalum addition increases the stability of the passive film due to the development of Ta_2O_5.
4. Of the Ti–Ta alloys, Ti–25Ta demonstrates excellent passive layer and corrosion resistance properties, and thus it seems to be a promising product for metallic medical devices.

Author Contributions: conceptualization, P.P.S.-P. and J.C.M.-R.; methodology, J.C.M.-R.; software, N.R.F.-S.; validation, M.V.S., N.R.F.-S., and J.C.M.-R.; formal analysis, N.R.F.-S.; investigation, P.P.S.-P.; resources, M.V.S.; data curation, P.P.S.-P.; writing—original draft preparation, J.C.M.-R.; writing—review and editing, P.P.S.-P., M.V.S., and N.R.F.-S.; visualization, N.R.F.-S.; supervision, J.C.M.-R.; project administration, N.R.F.-S.; funding acquisition, M.V.S. All authors have read and agreed to the published version of the manuscript.

Funding: This research was funded by Asociatia Neurochirurgie Sibiu and Gran Canaria Cabildo, project number CABINFR2019-07.

Acknowledgments: We are grateful for the company's support and generosity of R&D CS (Research & Development Consulting and Services) from Bucharest, Romania, in the absence of which this study could not have been carried out.

Conflicts of Interest: The authors declare no conflict of interest.

References

1. Rack, H.J.; Qazi, J.I. Titanium alloys for biomedical applications. *Mater. Sci. Eng. C* **2006**, *26*, 1269–1277. [CrossRef]
2. Lee, T.; Lee, S.; Kim, I.S.; Moon, Y.H.; Kim, H.S.; Park, C.H. Breaking the limit of Young's modulus in low-cost Ti–Nb–Zr alloy for biomedical implant applications. *J. Alloys Compd.* **2020**, *828*, 154401. [CrossRef]
3. Zhou, Y.L.; Niinomi, M.; Akahori, T. Effects of Ta content on Young's modulus and tensile properties of binary Ti-Ta alloys for biomedical applications. *Mater. Sci. Eng. A* **2004**, *371*, 283–290. [CrossRef]
4. Verestiuc, L.; Spataru, M.-C.; Baltatu, M.S.; Butnaru, M.; Solcan, C.; Sandu, A.V.; Voiculescu, I.; Geanta, V.; Vizureanu, P. New Ti–Mo–Si materials for bone prosthesis applications. *J. Mech. Behav. Biomed. Mater.* **2021**, *113*, 104198. [CrossRef] [PubMed]
5. Zhang, L.C.; Chen, L.Y. A Review on Biomedical Titanium Alloys: Recent Progress and Prospect. *Adv. Eng. Mater.* **2019**, *21*, 1–29. [CrossRef]
6. Souto, B.M.; Burstein, G.T. A preliminary investigation into the microscopic depassivation of passive titanium implant materials in vitro. *J. Mater. Sci. Mater. Med.* **1996**, *7*, 337–343. [CrossRef]
7. Kokubo, T.; Kim, H.-M.; Kawashita, M.; Nakamura, T. REVIEW Bioactive metals: Preparation and properties. *J. Mater. Sci. Mater. Med.* **2004**, *15*, 99–107. [CrossRef]
8. Khadija, G.; Saleem, A.; Akhtar, Z.; Naqvi, Z.; Gull, M.; Masood, M.; Mukhtar, S.; Batool, M.; Saleem, N.; Rasheed, T.; et al. Short term exposure to titanium, aluminum and vanadium (Ti 6Al 4V) alloy powder drastically affects behavior and antioxidant metabolites in vital organs of male albino mice. *Toxicol. Rep.* **2018**, *5*, 765–770. [CrossRef]
9. Kim, T.I.; Han, J.H.; Lee, I.S.; Lee, K.H.; Shin, M.C.; Choi, B.B. New titanium alloys for biomaterials: A study of mechanical and corrosion properties and cytotoxicity. *Biomed. Mater. Eng.* **1997**, *7*, 253–263. [CrossRef]
10. Perdomo-Socorro, P.P.; Florido-Suárez, N.R.; Verdú-Vázquez, A.; Mirza-Rosca, J.C. Comparative EIS study of titanium-based materials in high corrosive environments. *Int. J. Surf. Sci. Eng.* **2021**, *15*, 152–164. [CrossRef]
11. Florido-Suarez, N.R.; Verdu-Vazquez, A.; Socorro-Perdomo, P.P.; Mirza-Rosca, J.C. Past Advances and Future Perspective of Ti-Ta Alloys. *Glob. J. Eng. Sci.* **2021**, *7*, 20–22. [CrossRef]
12. Geanta, V.; Voiculescu, I.; Vizureanu, P.; Victor Sandu, A. High Entropy Alloys for Medical Applications. In *Engineering Steels and High Entropy-Alloys*; IntechOpen: London, UK, 2020; pp. 4–12. [CrossRef]
13. Manivasagam, G.; Dhinasekaran, D.; Rajamanickam, A. Biomedical Implants: Corrosion and its Prevention—A Review. *Recent Patents Corros. Sci.* **2010**, *2*, 40–54. [CrossRef]
14. Song, T.; Tang, H.P.; Li, Y.; Qian, M. Liquid metal dealloying of titanium-tantalum (Ti-Ta) alloy to fabricate ultrafine Ta ligament structures: A comparative study in molten copper (Cu) and Cu-based alloys. *Corros. Sci.* **2020**, *169*. [CrossRef]
15. Huang, S.; Sing, S.L.; de Looze, G.; Wilson, R.; Yeong, W.Y. Laser powder bed fusion of titanium-tantalum alloys: Compositions and designs for biomedical applications. *J. Mech. Behav. Biomed. Mater.* **2020**, *108*, 103775. [CrossRef]
16. Wu, C.; Peng, P.; Chou, H.; Ou, K. Microstructural, mechanical and biological characterizations of the promising titanium-tantalum alloy for biomedical applications. *J. Alloys Compd.* **2018**, *735*, 2604–2610. [CrossRef]
17. Mendis, S.; Xu, W.; Tang, H.P.; Jones, L.A.; Liang, D.; Thompson, R.; Choong, P.; Brandt, M. Characteristics of oxide films on Ti-(10–75) Ta alloys and their corrosion performance in an aerated Hank' s balanced salt solution. *Appl. Surface Sci.* **2020**, *506*, 145013. [CrossRef]
18. Chen, G.; Yin, J.; Zhao, S.; Tang, H.; Qu, X. Microstructure and tensile properties of a Ti-28Ta alloy studied by transmission electron microscopy and digital image correlation. *Int. J. Refract. Met. Hard Mater.* **2019**, *81*, 71–77. [CrossRef]
19. Zhao, S.; Yin, J.; Shen, L.; Ge, Y.; Chen, G. Ti-60Ta Powders Produced by PREP and Their Properties. *Xiyou Jinshu Cailiao Yu Gongcheng/Rare Met. Mater. Eng.* **2017**, *46*, 1679–1683.
20. Capellato, P.; Sachs, D.; Vasconcelos, L.V.B.; Melo, M.M.; Silva, G.; Ranieri, M.G.A.; Zavaglia, C.A.d.C.; Nakazato, R.Z.; Alves Claro, A.P.R. Optimization of anodization parameters in Ti-30Ta alloy. *Metals (Basel)* **2020**, *10*, 1–11. [CrossRef]
21. Soro, N.; Attar, H.; Brodie, E.; Veidt, M.; Molotnikov, A.; Dargusch, M.S. Evaluation of the mechanical compatibility of additively manufactured porous Ti–25Ta alloy for load-bearing implant applications. *J. Mech. Behav. Biomed. Mater.* **2019**, *97*, 149–158. [CrossRef]
22. Traxel, K.D.; Bandyopadhyay, A. Modeling and experimental validation of additively manufactured tantalum-titanium bimetallic interfaces. *Mater. Des.* **2021**, *207*, 109793. [CrossRef]
23. Zhao, D.; Liang, H.; Han, C.; Li, J.; Liu, J.; Zhou, K.; Yang, C.; Wei, Q. 3D printing of a titanium-tantalum Gyroid scaffold with superb elastic admissible strain, bioactivity and in-situ bone regeneration capability. *Addit. Manuf.* **2021**, *47*, 102223. [CrossRef]
24. Niinomi, M. Mechanical biocompatibilities of titanium alloys for biomedical applications. *J. Mech. Behav. Biomed. Mater.* **2008**, *1*, 30–42. [CrossRef]
25. Zhou, Y.L.; Niinomi, M.; Akahori, T. Changes in mechanical properties of Ti alloys in relation to alloying additions of Ta and Hf. *Mater. Sci. Eng. A* **2008**, *483–484*, 153–156. [CrossRef]
26. Al-Muhanna, K.; Habib, K. Corrosion behavior of different alloys exposed to continuous flowing seawater by electrochemical impedance spectroscopy (EIS). *Desalination* **2010**, *250*, 404–407. [CrossRef]
27. Escobar Claros, C.A.; Contri Campanelli, L.; Moreira Jorge, A.; Leprêtre, J.C.; Bolfarini, C.; Roche, V. Corrosion behaviour of biomedical β-titanium alloys with the surface-modified by chemical etching and electrochemical methods. *Corros. Sci.* **2021**, *188*. [CrossRef]

28. Mareci, D.; Chelariu, R.; Gordin, D.M.; Ungureanu, G.; Gloriant, T. Comparative corrosion study of Ti-Ta alloys for dental applications. *Acta Biomater.* **2009**, *5*, 3625–3639. [CrossRef]
29. ASTM International. ASTM E3-11(2017), Standard Guide for Preparation of Metallographic Specimens. ASTM International: West Conshohocken, PA, USA, 2017.
30. Smith, B.S.; Capellato, P.; Kelley, S.; Gonzalez-Juarrero, M.; Popat, K.C. Reduced in vitro immune response on titania nanotube arrays compared to titanium surface. *Biomater. Sci.* **2013**, *1*, 322–332. [CrossRef]
31. Welsch, G.; Boyer, R.; Collings, E.W. (Eds.) *Materials Properties Handbook: Titanium Alloys*, 4th ed.; ASM International: Geauga County, OH, USA, 1993.
32. Vaswani-Reboso, J.; Florido-Suarez, N.; Socorro-Perdomo, P.; Mirza-Rosca, J. Study of Biocompatibility, Mechanical Properties and Microstructural Analysis af Ag-Pd Alloy. *Microsc. Microanal.* **2021**, *27*, 550–552. [CrossRef]
33. Zhou, Y.L.; Niinomi, M. Ti-25Ta alloy with the best mechanical compatibility in Ti-Ta alloys for biomedical applications. *Mater. Sci. Eng. C* **2009**. [CrossRef]
34. Garcia-Falcon, C.M.; Gil-Lopez, T.; Verdu-Vazquez, A.; Mirza-Rosca, J.C. Electrochemical characterization of some cobalt base alloys in Ringer solution. *Mater. Chem. Phys.* **2021**, *260*, 124164. [CrossRef]
35. Garcia-Falcon, C.M.; Gil-Lopez, T.; Verdu-Vazquez, A.; Mirza-Rosca, J.C. Corrosion behavior in Ringer solution of several commercially used metal alloys. *Anti-Corrosion Methods Mater.* **2021**, *68*, 324–330. [CrossRef]
36. Li, X.; Wang, L.; Fan, L.; Zhong, M.; Cheng, L.; Cui, Z. Understanding the effect of fluoride on corrosion behavior of pure titanium in different acids. *Corros. Sci.* **2021**, *192*, 109812. [CrossRef]
37. López Ríos, M.; Socorro Perdomo, P.P.; Voiculescu, I.; Geanta, V.; Crăciun, V.; Boerasu, I.; Mirza Rosca, J.C. Effects of nickel content on the microstructure, microhardness and corrosion behavior of high-entropy AlCoCrFeNix alloys. *Sci. Rep.* **2020**, *10*, 1–11. [CrossRef]
38. Yu, X.Y.; Zhu, W.Q.; Chen, W.; Chen, W.Q.; Zhang, S.M.; Qiu, J. Osteoclast-mediated biocorrosion of pure titanium in an inflammatory microenvironment. *Mater. Sci. Eng. C* **2021**, *119*, 111610. [CrossRef] [PubMed]
39. Bojinov, M.; Betova, I.; Karastoyanov, V. Modeling barrier film growth and dissolution on titanium based on EIS, XPS and photocurrent data. *Electrochim. Acta* **2020**, *344*, 136137. [CrossRef]
40. Huo, W.T.; Zhao, L.Z.; Yu, S.; Yu, Z.T.; Zhang, P.X.; Zhang, Y.S. Significantly enhanced osteoblast response to nano-grained pure tantalum. *Sci. Rep.* **2017**, *7*, 40868. [CrossRef] [PubMed]
41. Fattah-alhosseini, A.; Elmkhah, H.; Ansari, G.; Attarzadeh, F.; Imantalab, O. A comparison of electrochemical behavior of coated nanostructured Ta on Ti substrate with pure uncoated Ta in Ringer's physiological solution. *J. Alloys Compd.* **2018**, *739*, 918–925. [CrossRef]
42. Hee, A.C.; Martin, P.J.; Bendavid, A.; Jamali, S.S.; Zhao, Y. Tribo-corrosion performance of filtered-arc-deposited tantalum coatings on Ti-13Nb-13Zr alloy for bio-implants applications. *Wear* **2018**, *400*, 31–42. [CrossRef]
43. Fattah-alhosseini, A.; Pourmahmoud, M. Passive and Semiconducting Properties Assessment of Commercially Pure Tantalum in Hank's Physiological Solution. *J. Mater. Eng. Perform.* **2018**, *27*, 116–123. [CrossRef]
44. Moreto, J.A.; Marino, C.E.B.; Bose Filho, W.W.; Rocha, L.A.; Fernandes, J.C.S. SVET, SKP and EIS study of the corrosion behaviour of high strength Al and Al-Li alloys used in aircraft fabrication. *Corros. Sci.* **2014**, *84*, 30–41. [CrossRef]
45. Sowa, M.; Simka, W. Electrochemical impedance and polarization corrosion studies of tantalum surface modified by DC Plasma electrolytic oxidation. *Materials (Basel)* **2018**, *11*, 545. [CrossRef]
46. Pourbaix, M.; Zhang, H.; Pourbaix, A. Presentation of an Atlas of chemical and electrochemical equilibria in the presence of a gaseous phase. *Mater. Sci. Forum* **1997**, *251–254*, 143–148. [CrossRef]

3.2 Comparative EIS study of titanium-based materials in high corrosive environments

TÍTULO :	**“Comparative EIS study of titanium-based materials in high corrosive environments”**
AUTORES:	**Socorro-Perdomo, P.P.; Florido-Suárez, N.R.; Verdú-Vázquez, A.; Mirza-Rosca, J.C**
REVISTA:	**International Journal Surface Science and Engineering**
ÍNDICE DE IMPACTO:	**1.178**
CITESCORE 2020	**2.2**
DOI:	**10.1504/IJSURFSE.2021.116333**
ISSN:	**1794-785X**
EDITORIAL:	**Inderscience Publishers**
AÑO:	**2021**
VOLUMEN:	**15**
PÁGINAS:	**152–164**

Comparative EIS study of titanium-based materials in high corrosive environments

Pedro P. Socorro Perdomo

Department of Mechanical Engineering,
University of Las Palmas de Gran Canaria, Spain
Email: pedro-socorro@ulpgc.es

Comparative EIS study of titanium-based materials in high corrosive environments

Pedro P. Socorro Perdomo

Department of Mechanical Engineering,
University of Las Palmas de Gran Canaria, Spain
Email: pedro-socorro@ulpgc.es

Néstor R. Florido Suárez*

Department of Processing Engineering,
University of Las Palmas de Gran Canaria, Spain
Email: nestor.florido@ulpgc.es
*Corresponding author

Amparo Verdú-Vázquez

Department of Building Technology,
Universidad Politécnica de Madrid, Spain
Email: amparo.verdu@upm.es

Julia C. Mirza Rosca

Department of Mechanical Engineering,
University of Las Palmas de Gran Canaria, Spain
Email: julia.mirza@ulpgc.es

Abstract: Electrochemical impedance spectroscopy (EIS) is a technique relatively complex and modern that owes its existence to the emergence of electronic circuits. In this work, the behaviour in HCl 20% of three materials, Ti, Ti-15 Mo and Ti-15Mo-5Al fabricated by laser beam melting, was analysed using EIS. Impedance spectra have been obtained at various potentials, from open circuit potential to +2.0 V vs. Ref. Once the profiles of the impedance spectra were analysed, the experimental data were adjusted to an equivalent electrical model. Two models of equivalent circuits were presented: at Ecorr simple circuit is used while in the passive potential range an equivalent circuit with 2-time constants was used for fit the experimental data. It was concluded that titanium and studied titanium alloys undergo spontaneous passivation due to the oxide film formed on their surface in the reducing acid solution.

Keywords: titanium; titanium alloys; equivalent circuit; electrochemical impedance spectroscopy; EIS; HCl; corrosion.

Reference to this paper should be made as follows: Socorro Perdomo, P.P., Florido Suárez, N.R., Verdú-Vázquez, A. and Mirza Rosca, J.C. (2021) 'Comparative EIS study of titanium-based materials in high corrosive environments', *Int. J. Surface Science and Engineering*, Vol. 15, No. 2, pp.152–164.

Biographical notes: Pedro P. Socorro Perdomo received his first degree in Mechanical Engineering from the University of León, Spain. He is an Assistant Professor at the University of Las Palmas de Gran Canaria, Spain. He is a member of Nanomaterials and Corrosion Research group (NanCorr). He is working in the Department of Mechanical Engineering. His scientific interests mainly cover the field of industrial materials, biomaterials and nanomaterials.

Néstor R. Florido Suárez received his first degree in Industrial Engineering from the University of Las Palmas de Gran Canaria, Spain. He is a part-time Lecturer at the University of Las Palmas de Gran Canaria, Spain. He is a member of Nanomaterials and Corrosion Research group (NanCorr). He is working in the Department of Process Engineering. His scientific interests mainly cover the field of biomedicine, biotechnology, industrial materials, and nanomaterials.

Amparo Verdú-Vázquez is an Associate Professor at the Polytechnic University of Madrid. She is working in the Department of Building Technology at the Higher Technical School of Building. Her scientific interests mainly cover technology transfer projects. She has devoted her time to research in materials and their applications in industry and education.

Julia C. Mirza Rosca is a Professor at the University of Las Palmas de Gran Canaria, Spain. She is working in the Department of Mechanical Engineering. She is the Head of Nanomaterials and Corrosion Research group (NanCorr). Her scientific interests mainly cover the field of electrochemical processes, corrosion, biomaterials and nanomaterials.

1 Introduction

Titanium has a great resistance to corrosion (Peters and Leyens, 2003) and this explains the great influence that titanium is acquiring in the chemical, biomedical and power generation industries. The price of titanium is high but due to the intrinsic nature of these industries, it is profitable because it lowers the maintenance costs.

Titanium is normally used in those areas where stainless steel does not provide sufficient resistance to corrosion; titanium and titanium alloys have high tensile strength, high strength-to-weight ratio and excellent corrosion resistance due to a native oxide film formed on the surface. Therefore, it is found in facilities exposed to strong inorganic acids but unfortunately, this protective passive film is susceptible to failure in HCl environment industries. In these industries, less mechanical resistance is required than in others, but greater resistance to corrosion, which is why titanium and titanium alloys are used. Their uses are many, among which are: condensers, heat exchangers, turbines, purifiers, storage tanks, pipes, pumps, valves, etc.

Pure titanium undergoes an allotropic phase transformation at 882°C, changing from a body-centred cubic crystalline structure (phase α) above the transformation temperature, to a compact hexagonal structure (phase β) below this temperature (Vasylyev et al., 2020). The exact temperature at which the transformation takes place strongly depends on the interstitial and substitutional elements found in this metal. It depends, ultimately, on the purity of the material.

The existence of two different crystalline structures makes possible to carry out thermal treatments with total transformation, since allotropic forms present a different behaviour against deformation: the phase α, little deformable and resistant to room temperature and the phase β, easily deformable (Kaur and Singh, 2019).

The alloy elements that change the allotropic transformation temperature can be divided into three groups, α-stabilisers (Al, O, N, C), β-stabilisers (V, Mo, Nb, Ta, Fe, Mn, Cr, Ni, Cu, Si) and neutralisers (Zr, Sn).

It is common to divide titanium alloys into three groups, depending on the phases present: alloys α and almost-α; alloys α-β and alloys β. The titanium β alloys have a higher content of β phase stabilising elements and a lower content of alphagenes than the alloys α-β. They are characterised by their high hardening capacity, since, for example, in small thicknesses they reach air hardening and completely retain the β phase (Kolli and Devaraj, 2018). They are titanium alloys with better aptitude for conformation by plastic deformation, being able to deform in cold much better than the α or α-β alloys (Noori Banu and Devaki Rani, 2019).

Ti-Mo alloys are shown as one of the large families of alloys within β-Ti alloys. Molybdenum is a β phase stabilising element, so it decreases the transition temperature from β structure to α structure and stabilises the β phase. This temperature is directly increased by the presence of β phase stabilising alloy elements and in many cases, this temperature is below room temperature, so alloys with this characteristic have β structure in use at room temperature.

There are many studies regarding the properties of titanium alloys with different concentrations of molybdenum starting at 3% Mo till 20% Mo, generally for biomedical applications. These alloys were most of them obtained by arc melting in an ultra-pure argon atmosphere (Oliveira and Guastaldi, 2008, 2009; Oliveira et al., 2007, 2009; Ho et al., 1999; Cardoso et al., 2014), but some of them were synthetised by laser-assisted (Almeida et al., 2012), using a DC magnetron sputtering method (Habazaki et al., 2003) or direct energy deposition – laser additive manufacturing (Bhardwaj et al., 2019).

There are many techniques used in additive manufacturing, depending on the process used or the types of materials are needed to use. On some occasions, for example in the industrial environment, it is necessary to manufacture metal parts, and it is then when such innovative techniques as fusion or sintering of metal powder by electron beam namely electron beam melting come into play. This is a technology that makes possible to build geometrically complex parts and is very similar to selective laser sintering, but in which the energy source is more powerful.

In this work, the behaviour in HCl 20% of three materials, Ti, Ti-15 Mo and Ti-15Mo-5Al fabricated by laser beam melting, was analysed using electrochemical impedance spectroscopy (EIS).

2 Experimental

Titanium and the following titanium alloys were studied: Ti-15Mo and Ti-15Mo-5Al (the numbers signify the wt. %) with the composition given in Table 1 and obtained by Electron Beam Melting (Arcam AB, Sweden) from high purity metallic gas atomised powders. The samples were built layer-by-layer on a titanium commercially pure grade 2 as substrate and selectively melted at a voltage of 60 kV and electron beam size of

200 μm. Due to the high reactivity of titanium, the process was carried out in a controlled atmosphere under high purity argon gas. The samples obtained are in the form of flat discs (approx. 0.5 cm in diameter) and the impedance tests have been carried out in a 20% HCl solution. The samples were initially polished on a Struers Tegrapol-11 polishing machine with emery discs of various sizes (800 to 2,500) and then with diamond paste (0.1 μm) on a polishing cloth. The surface of each sample has been left as a mirror surface to ensure reproducibility of results. Subsequently, the polished samples have been washed with acetone and then in an ultrasonic cleaner for ten minutes. Finally, they have been rinsed with bi-distilled water and air dried at room temperature.

The electrochemical tests have been done at 25ºC using a cell containing 100 ml of electrolyte. The flat surface of each sample was brought into contact with the solution by means of a hanging meniscus assembly. To measure the potential of the analysed samples at all times, a saturated calomelane reference electrode (SCE) was used; a cylindrical, high-surface platinum mesh was used as a counter electrode.

Impedance spectra have been obtained at various potentials, from open circuit potential to +2.0 V and therefore a set of potentiostat and blocking amplifier PARC 263 A and PARC 5210 respectively have been used. At each potential, single sine wave recordings were made at frequencies between 100 mHz and 100 kHz.

3 Results and discussion

EIS is a technique relatively complex and modern that owes its existence to the emergence of electronic circuits fast enough and sensible enough to create and evaluate a variable frequency and phase signal (Ciucci, 2019; Gabrielli, 2020; Mareci et al., 2007; Niaz, 2020). It is a non-destructive technique (in case of tests in equilibrium conditions), particularly sensible to small modifications in the system, which permits the characterisation of the properties of the materials and the mechanism of electrochemical processes (Goulart et al., 2007; Oliveira and Guastaldi, 2009; Mareci et al., 2010). For many materials and electrochemical processes, the impedance varies with the frequency and the applied potential and therefore we relate it to the properties of these materials. This is due to the physical characteristics of the material, to the electrochemical processes that take place on the surface or a combination of both. Therefore, if we carry out impedance measurements in a suitable range of frequencies, the spectra obtained relate the physical and chemical properties of the samples to the mechanism of the electrochemical process that takes place.

The interpretation of the impedance spectrum requires the selection of an appropriate electrical system that fits the experimental data (González and Mirza-Rosca, 1999). Through the model, the obtained measurements using this technique provide information related to the dissolution resistance, polarisation resistance and double-layer capacitance of Helmholtz. The dissolution resistance is obtained at high frequencies and the data acquired at low frequencies give information on the kinetics of the reaction. According to the model that is proposed and the way to propose it, information of the characteristic parameters of the process can be obtained.

Firstly, the obtained results for the studied alloys at various applied passivation potentials will be commented analysing the most significant graphs (Nyquist and Bode graphs).

As can be seen in the Nyquist diagrams (see Figure 1), at the corrosion potential the radius of the semicircle is very small, which indicates a low polarisation resistance or what is the same, a low resistance to corrosion because on the material begins to form a passive layer. As the potential increases, the resistance to polarisation and implicitly the resistance to corrosion increases.

Figure 1 Nyquist plots at Ecorr, 0.1V vs. SCE, 0.2V vs. SCE and 2.0V vs. SCE for (a) Ti, (b) Ti-15Mo and (c) Ti-15Mo-5Al (see online version for colours)

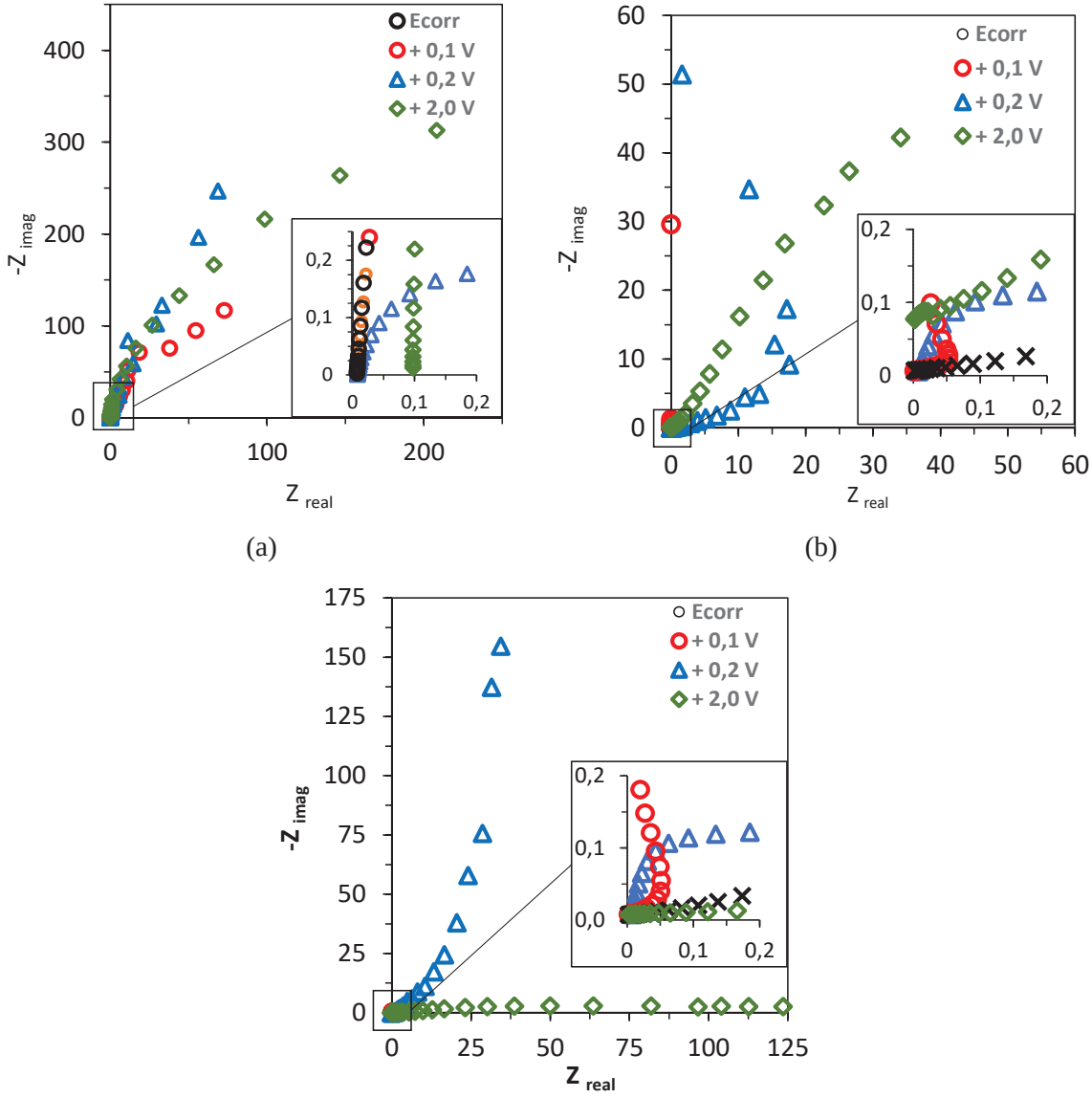

It can be observed the beginning of another semicircle at 100 mV which translates into the beginning of a new stage of the process of passivation. At 200 mV the passive layer increases in thickness and the resistance to corrosion is also greatly increased. As potential increases the materials are still very stable in HCl 20% and the radius of the semi-circle in the Nyquist diagram undergoes a considerable increase which translates into an increase of the polarisation resistance (Rp) or, in other words, an increase of the resistance to corrosion.

In the Bode-IZI diagrams (see Figure 2) a strong displacement of the impedance module towards higher values is observed, clearly indicating an increase in corrosion resistance due to the formation of the passive layer on the surface of the three materials.

Figure 2 Bode-IZI plots at Ecorr, 0.1V vs. SCE, 0.2V vs SCE and 2.0V vs. SCE for (a) Ti, (b) Ti-15Mo and (c) Ti-15Mo-5Al (see online version for colours)

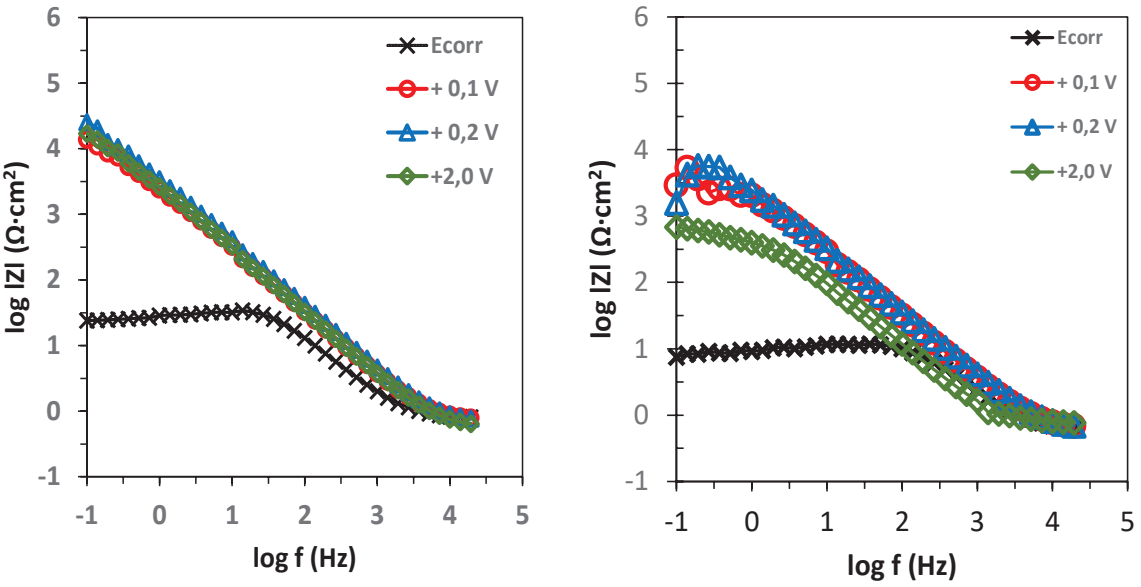

(a) (b)

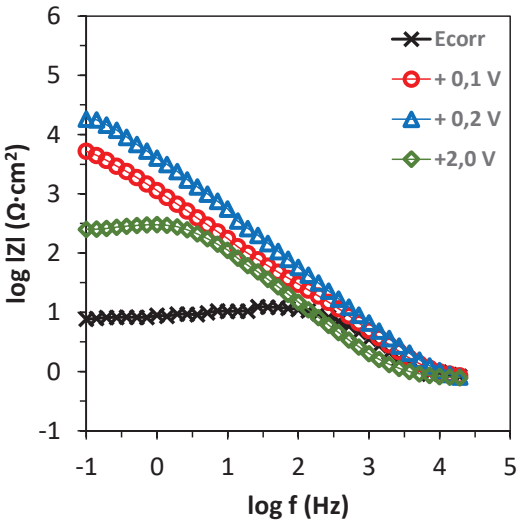

(c)

The profile of the results at 200 mV is very similar and a little higher than that obtained at 100 mV due to the increase in thickness of the passive layer with the increase in potential. The slopes of the graphs follow –1 at both 100 mV and 200 mV (including till 2 V) indicating the capacitive behaviour of the passive film formed.

In the Bode-phase diagrams (see Figure 3), a typical behaviour of the initial nucleation of a passive layer on the surface of the metal is observed in the corrosion potential.

Figure 3 Bode – phase plots at Ecorr, 0.1V vs. SCE, 0.2V vs SCE and 2.0V vs SCE for (a) Ti, (b) Ti-15Mo and (c) Ti-15Mo-5Al (see online version for colours)

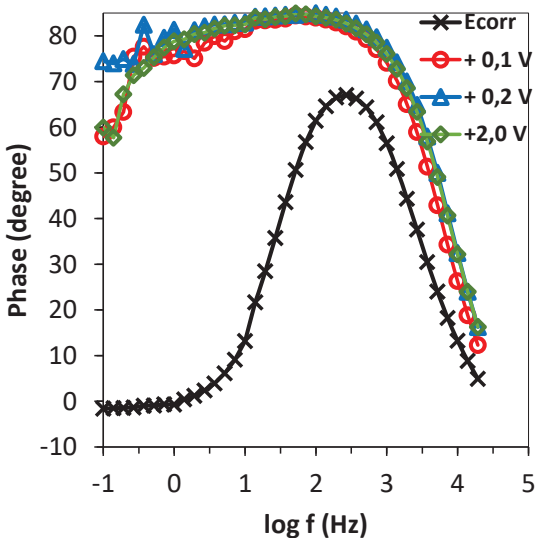

(a)

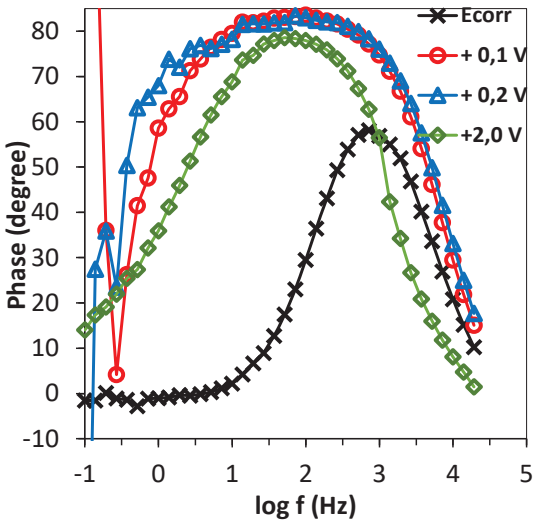

(b)

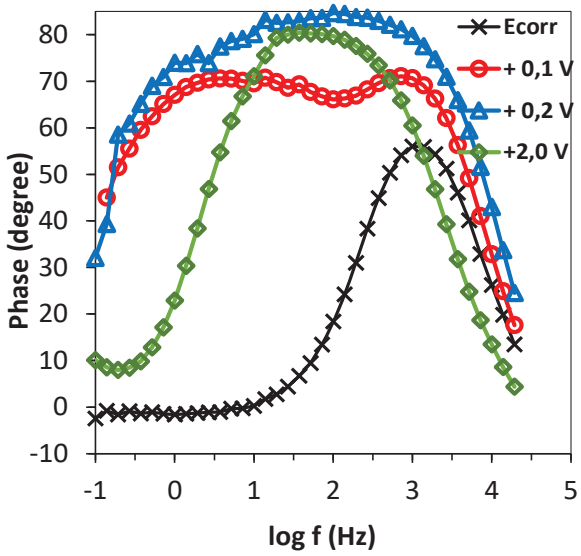

(c)

As the potential increases, the formed film increases in thickness and has a capacitive response illustrated by a phase angle close to 90º over a wide range of frequencies. This phenomenon is associated with an increase in the capacity (C), which is related to an increase in effective surface area.

Once the profiles of the impedance spectra are analysed, the obtained experimental data will be adjusted to an equivalent electrical model. An equivalent circuit is a combination of passive elements (resistances, capacitances, inductors and other forms of distributed impedance) that give a corrosion-like response in the frequency range under analysis.

When the EIS experimental data is analysed, it is compared with the response of an equivalent electrical circuit and the values of the different electrical parameters are

measured. In the case of corrosion processes, these values are used to obtain information on both the corrosion resistance of the material and the corrosion mechanism.

In the use of equivalent electrical circuits for EIS data analysis it is necessary to consider that there are, normally, a wide variety of circuit configurations that can reproduce, with high accuracy, the same response that is obtained experimentally from a real process.

The equivalent circuit represented in Figure 4 corresponds to the simplest one with is possible to adjust the experimental data, when only the load transfer is taking into account. This circuit has been used to fit the experimental data obtained at the corrosion potential. In this case, the theoretical transfer function, $Z(\omega)$, is represented by a parallel combination of a resistor R2 and a capacitance Q1, both in series with another resistor R1.

Figure 4 Equivalent circuit used for fit the experimental data at Ecorr

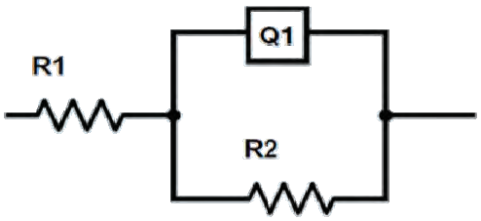

R1 represents the resistance of the electrolyte, whose value can be calculated by a sweep at high frequencies. R2 is the term for load transfer resistance, Rct.

The capacity of the double layer Cdl (Q1) is related to the interactions that have place at the electrode/electrolyte interface.

A constant phase element (CPE) has been chosen instead of an ideal capacitance (Ibriş and Mirza Rosca, 2002) in order to be able to take into account the heterogeneities of the passivated surface.

The impedance of a CPE is given by Boukamp (1986):

$$Q = Z_{CPE}(\omega) = \left[C(j\omega)^n\right]^{-1}$$

For this reason, one of the parameters obtained when modelling the system is the coefficient of ideality '*n*', so that the response of the real system is closer to the ideal as the value of n is closer to the unit and therefore the surface is more homogeneous. So, for $n = 1$, the CPE element reduces to a capacitor with a capacitance Y_0 and for $n = 0$ to a simple resistance.

The experimental data at corrosion potential fit the equation 4 and the fitting results are presented in Table 1.

R_2 represents the polarisation resistance at the interface metal/passive film so, represents the corrosion resistance of the metal. It can be observed that this resistance increases with the addition of the Mo which is well-known that improves the pitting and crevice corrosion resistance enhancing the passive film resistance by decreasing the number of defects points in the film. R_2 increases even more when Al is added due to the formation of a compact and protective Al_2O_3 film.

Table 1 Values of the fitted parameters of the experimental data with the equivalent circuit with one-time constant

Alloy	R_1 (Ωcm^2)	Y_0 (Fcm^{-2})	*N*	R_2 (Ωcm^2)
Ti	0.81	8.9×10^{-4}	0.62	14.7
Ti-15Mo	0.64	8.2×10^{-4}	0.64	16.9
Ti-15Mo-5Al	0.83	7.9×10^{-4}	0.70	17.2

For potentials higher than the corrosion potential, the single circuit has unacceptable setting errors and therefore a circuit with two time constants which takes into account the structure of the passive layer already formed on the surface of the materials has been used. It should be recalled that in this study the main objective is to check the validity of the EIS technique for this type of system, so it is not so important the selected equivalent circuit, but that it allows to reveal the existence or not of differences in the electrochemical behaviour of the material depending on the applied passivation potential or the composition of the employed material.

The circuit that best fits the experimental data in these cases is the one presented in Figure 5.

The component elements are:

R_1 dissolution resistance

Q_1 CPE of the porous external passive layer

R_2 resistance of the external porous layer

Q_2 CPE of the inner passive layer

R_3 polarisation resistance.

First, we calculate the admittance of the parallel combination (R_2Q_1):

$$\frac{1}{Z_{eq}} = \frac{1}{Z_{R_2}} + \frac{1}{Z_{Q_1}} \tag{1}$$

Even a CPE was used for experimental data fitting, the obtained value is taken as the capacitance in the forthcoming discussion:

$$\frac{1}{Z_{eq}} = \frac{1}{Z_{R_2}} + j\, w\, C_1 \tag{2}$$

And after multiplying by R_2:

$$Z_{eq} = \frac{R_2 - j\left(wC_1R_2^2\right)}{1+\left(wC_1R_2^2\right)} \tag{3}$$

We added the ohmic resistance of the electrolyte:

$$Z_{eq} = R_1 \frac{R_2 - j\left(wC_1R_2^2\right)}{1+\left(wC_1R_2^2\right)} \tag{4}$$

The total impedance is,

$$Z_{eq} = R_1 + \cfrac{1}{jwC_1 + \cfrac{1}{R_2 + \cfrac{1}{R_3 + jwC_2}}} \tag{5}$$

After standard calculations, the following equation was obtained:

$$Z_{eq} = R_1 + \frac{A - w^2AB + w^2CD}{(1 - w^2B)^2 + w^2C^2} + jw\frac{D - AC - w^2BD}{(1 - w^2B)^2 + w^2C^2} \tag{6}$$

where

$A = R_1 + R_2$

$B = \tau_1\tau_2$

$C = \tau_1 + \tau_2 + C_1R_3$

$D = \tau_2R_2$

$\tau_1 \equiv$ time constant of porous film [s]

$\tau_2 \equiv$ time constant of compact film [s]

The first coupled parameters R_2 and Q_1 describe the processes at the outer porous passive film/solution interface and the second coupled parameters R_3 and Q_2 represent the properties of the reactions at the inner barrier layer/metal interface. The results of the fitting are presented in Table 2 and in Figure 6 residual error plots are shown for fits using the first (see Figure 4) and the second equivalent circuit (see Figure 5). From the value of the chi-square and the distribution of errors versus frequency, it can be seen that when a model with two time constants is employed, the quality of the fit is improved, so this circuit had to be considered.

Table 2 Parameters obtained from fitting EIS data for Ti and Ti alloys at different potentials

Alloy	*Pot.vs OCP*	R_1 (Ωcm^2)	Y_0 (Fcm^{-2})	*n*	R_2 (Ωcm^2)	Y_0 (Fcm^{-2})	*n*	R_3 ($k\Omega cm^2$)
Ti	0.1	0.79	1.8×10^{-4}	0.82	660.2	6.2×10^{-3}	0.95	7.3
	0.2	0.77	1.6×10^{-4}	0.84	680.3	5.3×10^{-3}	0.96	8.2
	2.0	0.64	2.0×10^{-4}	0.87	522.4	6.8×10^{-3}	0.90	7.1
Ti-15Mo	0.1	0.69	2.1×10^{-4}	0.80	720.8	5.5×10^{-3}	0.96	9.6
	0.2	0.70	1.9×10^{-4}	0.82	786.4	5.2×10^{-3}	0.93	10.1
	2.0	0.77	2.3×10^{-4}	0.85	702.3	5.9×10^{-3}	0.89	9.2
Ti-15Mo-5Al	0.1	0.84	2.3×10^{-4}	0.79	782.8	5.2×10^{-3}	0.91	11.7
	0.2	0.81	2.0×10^{-4}	0.82	880.5	4.8×10^{-3}	0.94	12.2
	2.0	0.79	2.3×10^{-4}	0.88	723.4	5.2×10^{-3}	0.88	10.6

The parameter R_1 has a value from 0.64 to 0.84 Ω cm^2 and is ascribed to electrolyte resistance and during the experiments there is no appreciable variation of the values which mean that no ions released in the solution during the passive potential range.

Figure 5 Equivalent circuit used for fit the experimental data at passivation potentials

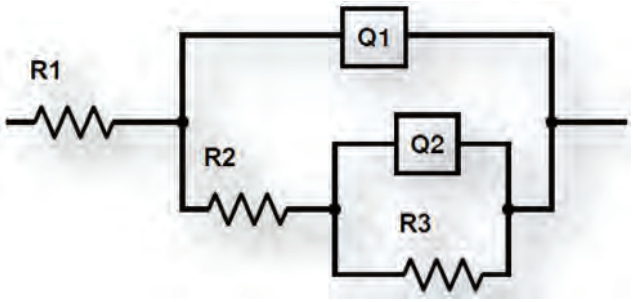

The values of R_2 are lower than R_3 values, reflecting that the outer porous film exhibits lower resistance than the inner barrier layer. High values of R_3 are observed at all potential and an increase with Mo concentration and Al addition, confirming the formation of a passive layer with high corrosion protection ability.

It can be observed that the fitted values of R_3 increase with potential while Y_0 decreases, indicating that the thickness and stability of the protective oxide film increased in passivation potential range.

The residual error plots using equivalent circuits with one and two-time constant are shown in Figures 6(a) and 6(b).

It can be observed that with the second equivalent circuit the fitting quality is very good (chi-square = $1.8 \cdot 10^{-5}$) better that with simple circuit.

Figure 6 Residual error plots for fits using (a) one and (b) two time constant

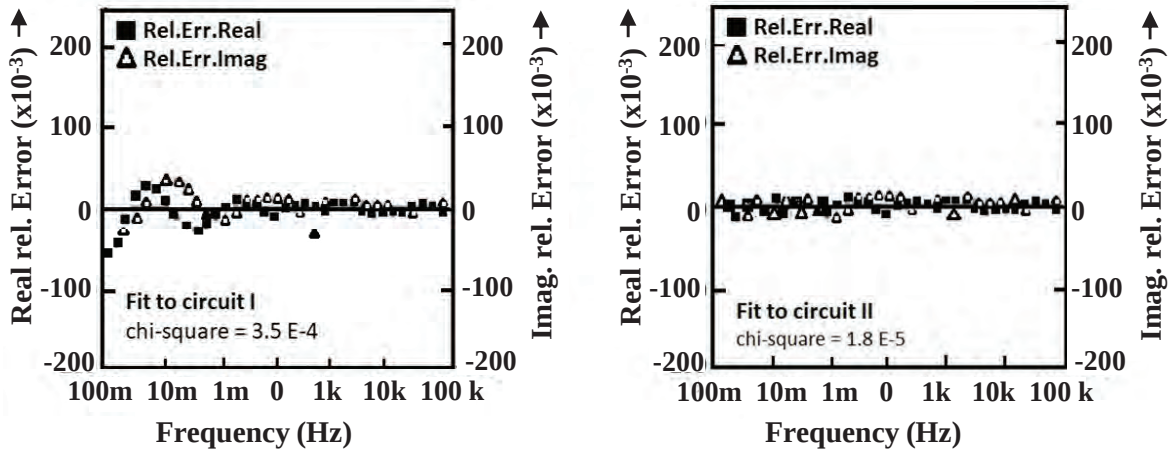

(a) (b)

4 Conclusions

1 Titanium and titanium alloys undergo spontaneous passivation due to the oxide film formed on their surface in the reducing acid solution.

2 The passive potential range is very large for the studied materials in HCl 20% (exceeding 2.0 V).

3 As the potential increases, the thickness of the passive film increases and it has a capacitive response (good stability) over a wide frequencies range.

4 Two models of equivalent circuits describing the spontaneous passivation of Ti, Ti-15Mo and Ti-15Mo-5Al in HCl 20% were presented. At E_{corr} simple Randles circuit is used while in the passive potential range an equivalent circuit with 2 time constants was used for fit the experimental data. Also a CPE was employed instead of the capacitive element.

5 For all the analysed materials there are no released ions in the solution during the passive potential range.

6 The addition of Mo and Al generates the formation of a passive layer with higher corrosion protection ability than for titanium.

7 In a HCl 20% solution, the oxide film on Ti and Ti studied alloys fabricated by laser beam melting exhibits a high corrosion resistance and a long-term stability, which recommends their use for the manufacture of metallic parts employed in aggressive industrial environments.

References

Almeida, A. et al. (2012) 'Laser-assisted synthesis of Ti-Mo alloys for biomedical applications', *Materials Science and Engineering C*, Vol. 32, No. 5, pp.1190–1195, DOI: 10.1016/j.msec.2012.03.007.

Bhardwaj, T. et al. (2019) 'Direct energy deposition – laser additive manufacturing of titanium-molybdenum alloy: parametric studies, microstructure and mechanical properties', *Journal of Alloys and Compounds*, Vol. 787, pp.1238–1248, DOI: 10.1016/j.jallcom.2019.02.121.

Boukamp, B.A. (1986) 'A nonlinear least squares fit procedure for analysis of' immitance data of electrochemical systems', *Solid State Ionics*, Vol. 20, pp.31–44, DOI: 10.1015/0167-2738(86)90031-7.

Cardoso, F.F. et al. (2014) 'Ti-Mo alloys employed as biomaterials: Effects of composition and aging heat treatment on microstructure and mechanical behavior', *Journal of the Mechanical Behavior of Biomedical Materials*, Vol. 32, pp.31–38, DOI: 10.1016/j.jmbbm.2013.11.021.

Ciucci, F. (2019) 'Modeling electrochemical impedance spectroscopy', *Current Opinion in Electrochemistry*, DOI: 10.1016/j.coelec.2018.12.003.

Gabrielli, C. (2020) 'Once upon a time there was EIS', *Electrochimica Acta*, Vol. 331, pp.1–20 DOI: 10.1016/j.electacta.2019.135324.

González, J.E.G. and Mirza-Rosca, J.C. (1999) 'Study of the corrosion behavior of titanium and some of its alloys for biomedical and dental implant applications', *Journal of Electroanalytical Chemistry*, Vol. 471, No. 2, pp.109–115, DOI: 10.1016/S0022-0728(99)00260-0.

Goulart, P.R. et al. (2007) 'Dendritic microstructure affecting mechanical properties and corrosion resistance of an Al-9 wt% Si alloy', *Materials and Manufacturing Processes*, Vol. 22, No. 3, pp.328–332, DOI: 10.1080/10426910701190345.

Habazaki, H. et al. (2003) 'Formation of barrier-type amorphous anodic films on Ti-Mo alloys', *Surface and Coatings Technology*, Vols. 169–170, pp.151–154, DOI: 10.1016/S0257-8972(03)00216-0.

Ho, W.F., Ju, C.P. and Chern Lin, J.H. (1999) 'Structure and properties of cast binary Ti-Mo alloys', *Biomaterials*, Vol. 20, No. 22, pp.2115–2122, DOI: 10.1016/S0142-9612(99)00114-3.

Ibriş, N. and Mirza Rosca, J.C. (2002) 'EIS study of Ti and its alloys in biological media', *Journal of Electroanalytical Chemistry*, Vol. 526, Nos. 1–2, DOI: 10.1016/S0022-0728(02)00814-8.

Kaur, M. and Singh, K. (2019) 'Review on titanium and titanium based alloys as biomaterials for orthopaedic applications', *Materials Science and Engineering C*, February, Vol. 102, pp.844–862, DOI: 10.1016/j.msec.2019.04.064.

Kolli, R.P. and Devaraj, A. (2018) 'A review of metastable beta titanium alloys', *Metals*, Vol. 8, No. 7, pp.1–41, DOI: 10.3390/met8070506.

Mareci, D. et al. (2010) 'The corrosion of dental amalgam in some commercial mouthwash solutions', *Revista de Chimie*, Vol. 61, No. 5, pp.443–448.

Mareci, D., Ungureanu, G., Aelenei, N., Chelariu, R. and Rosca, J.C.M. (2007) 'EIS diagnosis of some dental alloys in artificial saliva', *Environmental Engineering and Management Journal* Vol. 6, No. 4, pp.313–317.

Niaz, A. (2020) 'Corrosion and passive film study of cermet-coatings deposited by high-velocity oxygen fuel method in an acidic environment', *International Journal of Surface Science and Engineering*, DOI: 10.1504/IJSURFSE.2020.110533.

Noori Banu, P.S. and Devaki Rani, S. (2019) 'Microstructure evaluation and modelling the tensile strength and yield strength of titanium alloys', *International Journal of Microstructure and Materials Properties*, DOI: 10.1504/ijmmp.2019.10019610.

Oliveira, N.T.C. and Guastaldi, A.C. (2008) 'Electrochemical behavior of Ti-Mo alloys applied as biomaterial', *Corrosion Science*, Vol. 50, No. 4, pp.938–945, DOI: 10.1016/j.corsci. 2007.09.009.

Oliveira, N.T.C. and Guastaldi, A.C. (2009) 'Electrochemical stability and corrosion resistance of Ti-Mo alloys for biomedical applications', *Acta Biomaterialia*, Vol. 5, No. 1, pp.399–405, DOI: 10.1016/j.actbio.2008.07.010.

Oliveira, N.T.C. et al. (2007) 'Development of Ti-Mo alloys for biomedical applications: microstructure and electrochemical characterization', *Materials Science and Engineering A*, Nos. 452–453, pp.727–731, DOI: 10.1016/j.msea.2006.11.061.

Oliveira, N.T.C. et al. (2009) 'Photo-electrochemical investigation of anodic oxide films on cast Ti-Mo alloys. I. Anodic behaviour and effect of alloy composition', *Electrochimica Acta*, Vol. 54, No. 5, pp.1395–1402, DOI: 10.1016/j.electacta.2008.08.074.

Peters, M. and Leyens, C. (2003) *Titanium and Titanium Alloys: Fundamentals and Applications, Titanium and Titanium Alloys Fundamentals and Applications*, Wiley-VCH Verlag GmbH ~Co, Weinheim, Germany, ISBN 3-527-30534-3.

Vasylyev, M.A., Mordyuk, B.N., Bevz, V.P., Voloshko, S.M. and Mordiuk, O.B. (2020) 'Ultrasonically nanostructured electric-spark deposited Ti surface layer on Ti6Al4V alloy: enhanced hardness and corrosion resistance', *International Journal of Surface Science and Engineering*, DOI: 10.1504/IJSURFSE.2020.105874.

3.3 *Comparative EIS study of AlxCoCrFeNi alloys in ringer's solution for medical instruments*

TÍTULO :	**"Comparative EIS study of $Al_xCoCrFeNi$ alloys in ringer's solution for medical instruments"**
AUTORES:	**Socorro-Perdomo, P.P.; Florido-Suárez, N.R.; Voiculescu, I.; Mirza-Rosca, J.C.**
REVISTA:	**Metals**
ÍNDICE DE IMPACTO:	**2.351**
CUARTIL:	**Q2**
DOI:	**10.3390/met11060928**
ISSN:	**2075-4701**
EDITORIAL:	**MDPI**
MES Y AÑO:	**07/2021**
VOLUMEN:	**11**
PÁGINAS:	**14**

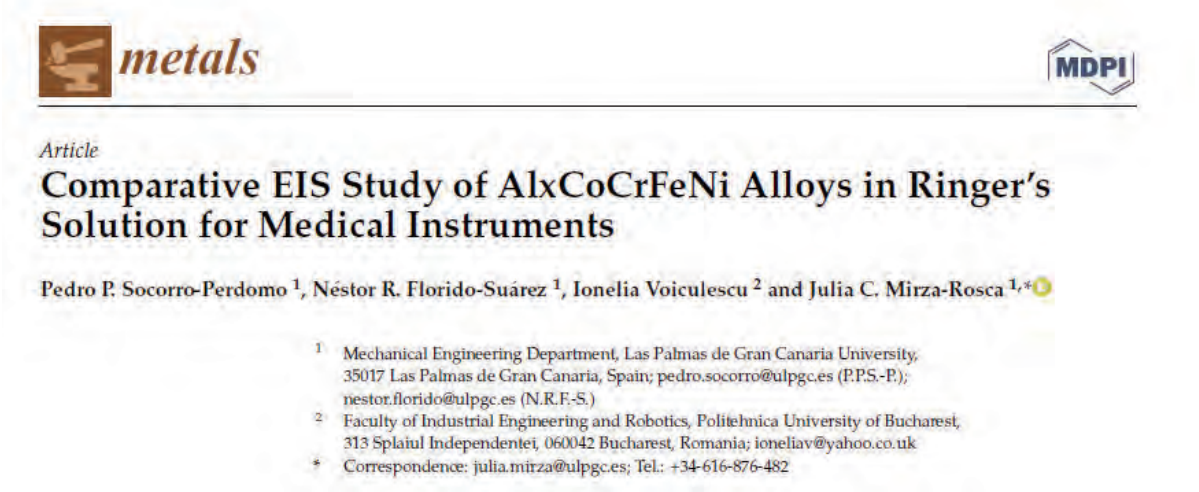

metals

MDPI

Article

Comparative EIS Study of AlxCoCrFeNi Alloys in Ringer's Solution for Medical Instruments

Pedro P. Socorro-Perdomo [1], Néstor R. Florido-Suárez [1], Ionelia Voiculescu [2] and Julia C. Mirza-Rosca [1,*]

[1] Mechanical Engineering Department, Las Palmas de Gran Canaria University, 35017 Las Palmas de Gran Canaria, Spain; pedro.socorro@ulpgc.es (P.P.S.-P.); nestor.florido@ulpgc.es (N.R.F.-S.)
[2] Faculty of Industrial Engineering and Robotics, Politehnica University of Bucharest, 313 Splaiul Independentei, 060042 Bucharest, Romania; ioneliav@yahoo.co.uk
* Correspondence: julia.mirza@ulpgc.es; Tel.: +34-616-876-482

metals

MDPI

Article

Comparative EIS Study of AlxCoCrFeNi Alloys in Ringer's Solution for Medical Instruments

Pedro P. Socorro-Perdomo [1], Néstor R. Florido-Suárez [1], Ionelia Voiculescu [2] and Julia C. Mirza-Rosca [1,*]

[1] Mechanical Engineering Department, Las Palmas de Gran Canaria University, 35017 Las Palmas de Gran Canaria, Spain; pedro.socorro@ulpgc.es (P.P.S.-P.); nestor.florido@ulpgc.es (N.R.F.-S.)
[2] Faculty of Industrial Engineering and Robotics, Politehnica University of Bucharest, 313 Splaiul Independentei, 060042 Bucharest, Romania; ioneliav@yahoo.co.uk
* Correspondence: julia.mirza@ulpgc.es; Tel.: +34-616-876-482

Abstract: Depending on the properties required for the medical instruments, compared with the classical materials, the high-entropy alloys (HEAs) are a versatile option. Electrochemical Impedance Spectroscopy (EIS) measurements have been performed on Al*x*CoCrFeNi-type high-entropy alloys with various concentrations of Al content (x = 0.6, 0.8, and 1.0) in order to characterize their passive film and corrosion resistance at 37 °C under infectious simulated physiological conditions (Ringer´s solution acidulated with HCl) at pH = 3. The impedance spectra were obtained at different potential values between −0.7 and +0.7 V vs. SCE. Analysis of the impedance spectra was carried out by fitting different equivalent circuits to the experimental data. Two equivalent circuits, with one time constant and two time constants respectively, can be satisfactorily used for fitting the spectra: one time constant represents the characteristics of the compact passive film, and the second one is for the porous passive film. With the decreasing of Al content, the obtained EIS results are correlated with the evolution of the microhardness and microstructure, which is characterized by Optical Microscopy (OM), Scanning Electron Microscopy (SEM), and Energy-Dispersive X-Ray Spectroscopy (EDAX). It can be observed for all alloys that the resistance of the passive film is very high and decreases with the potential: the very high resistance of the passive film implies a high corrosion resistance, which can be assigned to the formation of the protective oxide layer and demonstrates that the analyzed alloys fulfill the prerequisites for their use as new materials for the manufacturing of medical instruments.

Keywords: high-entropy alloys; aluminum; Electrochemical Impedance Spectroscopy (EIS); equivalent circuit; corrosion resistance; passivation; Ringer solution

Citation: Socorro-Perdomo, P.P.; Florido-Suárez, N.R.; Voiculescu, I.; Mirza-Rosca, J.C. Comparative EIS Study of AlxCoCrFeNi Alloys in Ringer's Solution for Medical Instruments. *Metals* **2021**, *11*, 928. https://doi.org/10.3390/met11060928

Academic Editor: Fahe Cao

Received: 17 May 2021
Accepted: 5 June 2021
Published: 7 June 2021

1. Introduction

The high-entropy alloys (HEAs), due to their particular composition, offer an alternative point of view for the new generation of materials that can possibly change the properties limitations of the classical materials. Two definitions of HEA are widely accepted: one based on the composition of the alloy and another based on the entropy concept. The first definition categorizes HEAs as materials containing five or more elements where every element has an atomic proportion between 5% and 35% [1]. According to the second definition, HEAs are considered to be alloys that have a conformational entropy larger than 1.61 R where R is the universal gas constant [2]. The high-entropy solid solutions are typically FCC alloys, BCC alloys, and also amorphous-structured alloys (high-entropy bulk metallic glass), but HCP-structured alloys were also reported [3]. Actually, there has been a great increase in the number of works that report on these novel microstructures with excellent properties [4–7].

The high-entropy solid solution AlCoCrFeNi was developed by Zhang's team at Beijing University of Science and Technology [8]. The microstructure, yield stress, compressive

strength, plastic strain, and fracture mechanism of this alloy were studied [8,9]. The modification of Al content to high-entropy alloys (HEA) with cubic face-centered structures (FCC) leads to significant modifications in its physical and structural characteristics [10]. These changes are due to Al's ability to introduce a grading tendency within the FCC matrix, as well as a network disturbance due to the increased atomic radius of Al (142 Å) in comparison with the remaining elements of HEAs (with an average of the atomic radius of Co, Fe, Ni = 125 Å) [11]. For these reasons, many studies on this HEA with different aluminum concentration were performed. For instance, the following properties were measured: Vickers hardness for $Al_{0.25}$ [12]; microstructure and tensile behaviors for $Al_{0.3}$ [13–15]; microstructure, hardness, and corrosion properties of $Al_{0.5}$ [16], tribological properties for $Al_{0.6}$ [17]; and compressive strength, Vickers, and Brinell Hardness for $Al_{0.8}$ [18].

Since the properties of the Al_xCoCrFeNi change significantly with aluminum concentration, comparative studies with x varying at different values from 0 to 3 were performed, and some characteristics were investigated: microstructure [19–21], hardness [16,22], electrochemical properties [23–25], electric, magnetic, and Hall properties [26]. Review articles and books were also written [3,8,27–29], and as a result, AlCoCrFeNi was found to exhibit high hardness, toughness, and stiffness, low modulus of electricity, and high thermal stability, which are properties that make it an option as a material for medical instruments such as cutters, saws, scissors, etc.

Despite the very good properties, AlCoCrFeNi alloy can produce metallic ions that can be diffused through passive oxide films. Some of these ions react with chlorine ions from the human body, forming complexes and precipitates; those that react with the water can form hydroxides and oxides, and in these conditions, the local change of pH is produced. Accordingly, pH gradients are produced along the different areas of the medical instruments, and this condition can produce and perpetuate crevice corrosion [30]. Consequently, local proliferation of the corrosion on some zones of HEA could appear.

However, the investigation of the degradation behavior of Al_xCoCrFeNi in simulated body fluid does not exist yet (for their use as medical instruments: cutting elements, tissue detachment sewing, etc.), so this study clarifies how the Al content impacts on the passive films formed on these alloys. In addition, the relationship between the characteristics of the oxide film and the Al concentration is examined by varying the potential between −0.7 and 0.7 V vs. SCE. The corrosion in the physiological environment is mainly due to the chlorine ions that it contains, to pH, and to the special conditions of use such as infections, hematomas, allergies, etc. In this paper, an infectious physiological environment was simulated by adding HCl to Ringer solution until it reached pH = 3 at 37 °C.

2. Materials and Methods

2.1. Materials and Samples Preparation

The VAR (Vacuum Arc Remelting) process was used for the manufacture of high-entropy Al_xCrFeCoNi alloys (see Table 1) by using the MRF ABJ 900 VAR (Allenstown, Merrimack, NH 03275, USA) at ERAMET Laboratory. High-purity granular base materials of Al, Cr, Fe, Co, and Ni (99.9%) were used and classified according to ASTM B214-16 [31]. Eventual losses of material by vaporization are to be expected in accordance with the theoretical chemical elements assimilations degree into the melt. Both conditions are taken into account for the charge. The obtained alloys were melted in a VAR unit up to six times, making use of argon as inert atmosphere, so that an adequate homogeneity could be achieved. The mini ingot was presented in the shape of a cylindrical rod of approximately 10 cm in length and 1.5 cm in diameter. For a microstructural quality examination, the first step is to cut the samples. A precision sectioning saw (BUEHLER USA, Lake Bluff, IL 60044, USA), IsoMet®4000 Buehler, is used to ensure cuts with minimal deformation. To simplify the manipulation of the samples and also to protect the edges of the samples, they have been pasted with an epoxy system. Then, with a Struers grinding-polishing machine (Struers Inc., Cleveland, OH 44145, USA), model TegraForce-1, the specimens were wet ground and polished with 260 to 3000 grain SiC papers and continued by a 0.1 µm alumina

suspension for final polishing. To remove traces of other substances, as we do with all materials [32], the specimens were ultrasonically cleansed in ethanol for 10 min followed by rinsing two times with deionized water. The experimental steps complied with the ASTM E3-11(2017) standard for the preparation of metallographic samples [33].

Table 1. Composition (wt %) for analyzed HEAs.

Composition (wt %)	Al	Cr	Fe	Co	Ni
$Al_{1.0}$CrFeCoNi ($Al_{1.0}$)	10.67	20.55	22.13	23.32	23.33
$Al_{0.8}$CrFeCoNi ($Al_{0.8}$)	8.72	21.00	22.61	23.82	23.85
$Al_{0.6}$CrFeCoNi ($Al_{0.6}$)	6.68	21.47	23.12	24.36	24.36

2.2. Test Environment

All data were obtained in Ringer Grifols solution (from Grifols Laboratories, Barcelona, Spain) with the corresponding contents in mmol/L: Na^+ 129.9; K^+ 5.4; Ca^{2+} 1.8; Cl^- 111.7; and $C_3H_5O_3$ 27.2 and acidified with HCl until reaching a pH = 3. The Ringer Grifols solution is a complex physiological mixture in which some of the chloride ions are substituted by lactate ions and some of the sodium ions are substituted by calcium and potassium ions. A thermostatic bath at 37 ± 0.1 °C was used to obtain the test data.

2.3. Microstructural Characterization

The microstructure of the samples was studied through optical microscopy. The surface of the samples was electrochemically etched with a 10% solution of oxalic acid where the samples were immersed for 10 s and 5 A current. The optical observations of the surface were made using a Zeiss AxioVert A1 microscope (Carl-Zeiss QEC GmbH, Ostfildern, Germany). The SEM and the EDAX observations were performed with an environmental scanning electron microscope model Fei XL30 ESEM (MTM, Leuven, Belgium) with LaB6 cathode coupled to an analyzer by energy-dispersive electron probe X-ray, model EDAX Sapphire. Finally, the samples were coated by spraying with gold for the analysis of the cross-section of the passive layer.

2.4. Microhardness

The microhardness of the samples was studied by performing an indentation test with a microhardness tester model Remet HX-1000 (NCS Lab., Carpi, Italy). The sample, which had been polished to a mirror finish as explained previously, was inspected with an optical microscope, and then, the microhardness determinations were conducted perpendicularly to the surface. The indentations were placed every 0.5 mm on the diameter of the sample. A load of 100 g and dwell time of 15 s were performed [32]. Finally, the average level for individual samples was calculated and reported as Vickers hardness (HV).

2.5. Electrochemical Measurements

The influence of potential on the passive film of HEAs under simulated physiological conditions was investigated by Electrochemical Impedance Spectroscopy (EIS). The equipment consists of a potentiostat PAR 263 A connected with a lock-in amplifier, model PAR 5210, to a conventional electrochemical cell. Three electrodes are needed to perform this technique: first, the working electrode (experimental sample); second, the electrode used as reference is the saturated calomel electrode (SCE); and third, as counter electrode, a platinum grid was used.

AC impedance measurements were recorded at open circuit potential, with an AC potential amplitude of 10 mV, and single sine wave measurements were conducted at frequencies between 10^{-1} and 10^5 Hz. To analyze the characteristics of the oxide film, the impedance spectra were recorded between −0.7 and +0.7 V with a 0.2 V step permitting the system to be stabilized for 10 min at each potential. Thus, the electrodes are polarized in a continuous way [33]. A personal computer was used for data acquisition and analysis using ZSimpWin software (AMETEC, Princeton, NJ, USA) to interpret the spectra.

3. Results and Discussion

3.1. Microstructural Characterization

Optical images can be seen in Figure 1a–c in which the general characteristic of the microstructure is dendritic. The individual concentration of the elements in the different alloys influences the morphology of the phases. Accordingly, in the case of $Al_{1.0}$ and $Al_{0.6}$, the aspect of the dendrites is almost rounded, while for $Al_{0.8}$, it presents acicular forms with different orientations. It was found that even for small changes in the chemical composition, there are changes in the phases and compounds in these alloys. The explanation is that at certain proportions of Al in this matrix, the crystal structures change from FCC to BCC + FCC or to BCC. The SEM microstructural aspects at higher magnifications shown in Figure 1d–f are comparable to those found by optical microscopy. At higher magnifications, the individual features of each alloy are emphasized. For instance, in the case of $Al_{1.0}$ (Figure 1d), the microstructure is constituted by phases disposed in an orderly manner in the metallic matrix, which is flanked by straight grain edges. The microstructure of $Al_{0.8}$ (Figure 1e) reveals the propensity of growth of acicular phases (Widmanstätten), resulting in significantly larger grain boundaries. In regard to the $Al_{0.6}$ sample (Figure 1f), the two phases are significantly different. Since the structure of the alloy with $x = 0.6$ is the one that presents in wide spaces the presence of two phases and therefore is the most representative, we have chosen it to show the EDAX results (see Figure 2 and Table 2).

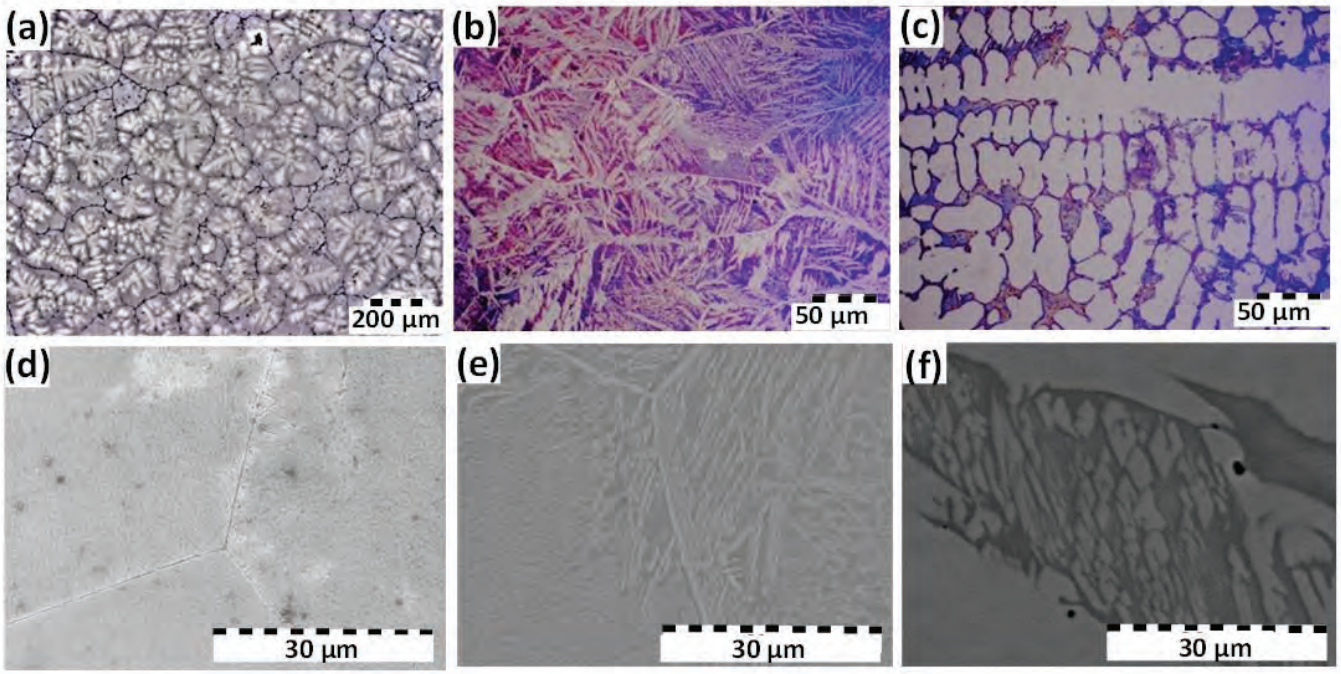

Figure 1. Metallographic microscopy and SEM images for $Al_{1.0}$CrFeCoNi (**a**,**d**), $Al_{0.8}$CrFeCoNi (**b**,**e**), and $Al_{0.6}$CrFeCoNi (**c**,**f**).

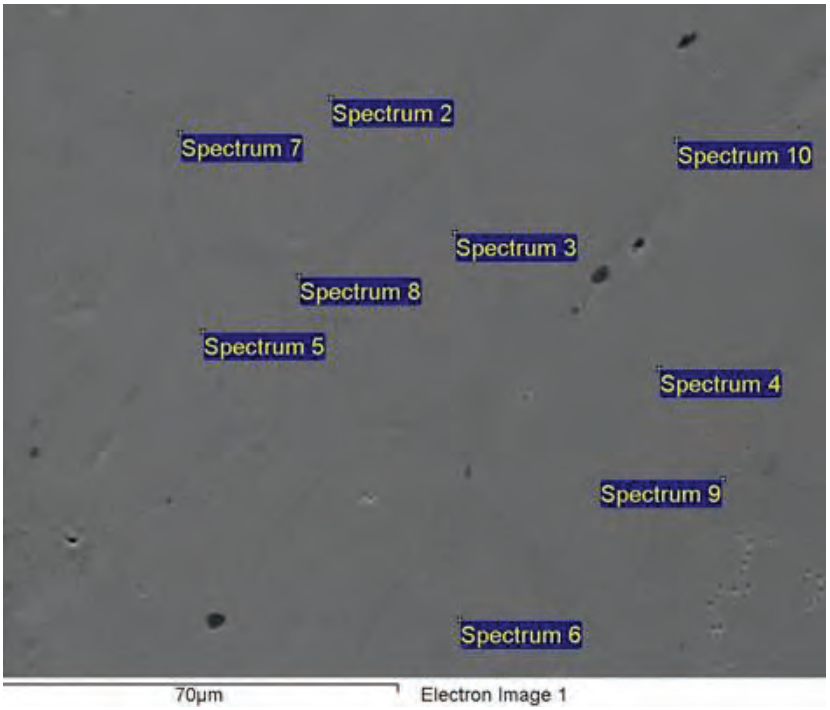

Figure 2. EDAX analysis on the surface of the alloy $Al_{0.6}CrFeCoNi$ (the point analysis of chemical composition was in the right upper corner of each rectangle).

Table 2. The results in weight percentage of EDAX analysis of the alloy$Al_{0.6}CrFeCoNi$.

Spectrum	Al	Cr	Fe	Co	Ni
Sum Spectrum	6.87	20.66	24.18	24.04	24.26
Spectrum 2	5.74	20.90	26.23	25.04	22.09
Spectrum 3	5.86	20.78	26.07	24.82	22.47
Spectrum 4	6.02	20.93	25.43	24.71	22.91
Spectrum 5	5.74	20.89	26.10	24.88	22.38
Spectrum 6	6.12	20.71	25.70	24.63	22.84
Spectrum 7	8.75	22.12	22.70	22.48	23.95
Spectrum 8	8.16	21.08	23.08	23.45	24.24
Spectrum 9	8.57	22.28	22.99	22.55	23.61
Spectrum 10	9.04	21.48	22.59	22.38	24.52
Mean	7.09	21.18	24.51	23.90	23.33
Standard deviation	1.38	0.58	1.55	1.09	0.89

On the surface of the HEA, there are two zones: a dendritic zone (*D*) and an interdendritic zone (*ID*) with significant compositional differences of the elements (see Table 3). A segregation factor [9], the segregation ratio (S_R), was used to calculate the level of element segregation, which is defined as:

$$S_R = \frac{element\ concentration\ in\ D\ area}{element\ concentration\ in\ ID\ area}. \quad (1)$$

Table 3. Composition analysis results in D and ID areas and S_R values for $Al_{0.6}CrFeCoNi$ and $Al_{0.8}CrFeCoNi$ alloys.

Alloy	Parameters	Al	Cr	Fe	Co	Ni
$Al_{0.6}CrFeCoNi$	D	5.74	20.9	26.23	25.04	22.09
	ID	9.04	21.48	22.59	22.38	24.52
	S_R	0.63	0.97	1.16	1.12	0.90
$Al_{0.8}CrFeCoNi$	D	7.98	26.63	23.32	22.15	19.92
	ID	10.85	20.99	20.63	22.39	25.15
	S_R	0.74	1.27	1.13	0.99	0.79

For $Al_{0.6}CrFeCoNi$, the nanoscale analysis revealed the dendritic region rich in Fe and Co but depleted in Ni and Al and the interdendritic region rich in Al and Ni but depleted in Co and Fe. Only chromium shows no significant difference in the two areas with a somewhat higher concentration in the interdendritic zone.

As the content of Al increments, the effect of chromium is more powerful, and Co shows no obvious difference in the two zones, which is in accordance with the results of other researchers [9].

Aluminum and chromium increase their segregation ratios, while nickel and cobalt decrease it. We would say that they form less intermetallic compounds (or that they "precipitate" less). Iron does not substantially vary its segregation ratio.

It could almost be said that the increase in aluminum reduces the solubility limit of the solid phase for nickel and cobalt, increases it for chromium, and iron is almost unaffected.

3.2. EIS Results

To evaluate the passive layer characteristic, the impedance data will be used. In Nyquist plots (Figure 3), it can be noted that all samples present three distinct region consisting of (i) an arc with a small ratio at high frequencies (low impedances); (ii) another arc at medium frequencies with the ratio bigger than that of high frequencies and (iii) a line at low frequencies (high impedances). This is clearly indicative of the feedback from at least two different frequency-dependent processes with their respective time constants.

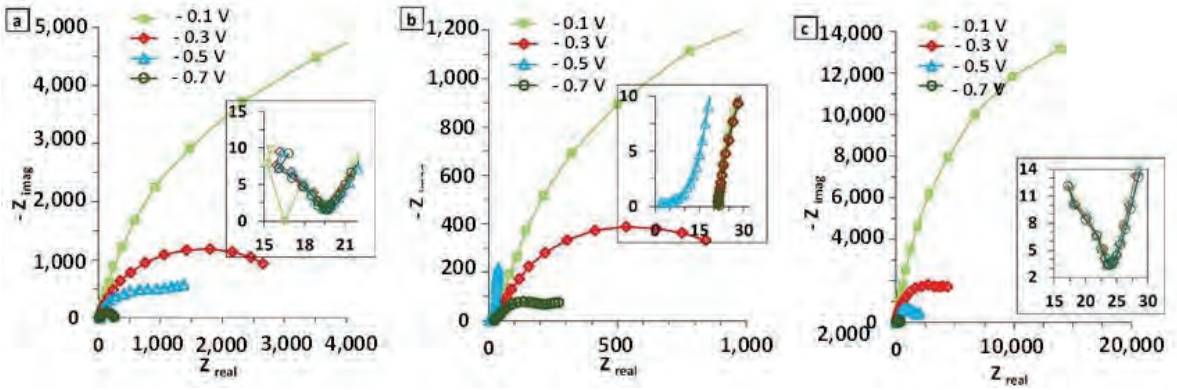

Figure 3. Nyquist diagrams evolution with the potential for (**a**) $Al_{1.0}$, (**b**) $Al_{0.8}$, and (**c**) $Al_{0.6}$.

From the Bode-phase spectra in the range −700 to −100 mV (Figure 4) for the three HEAs, the changing of a widely capacitive film to a resistive one can be observed, and this is a measure of the integrity of the film and therefore of the corrosion resistance.

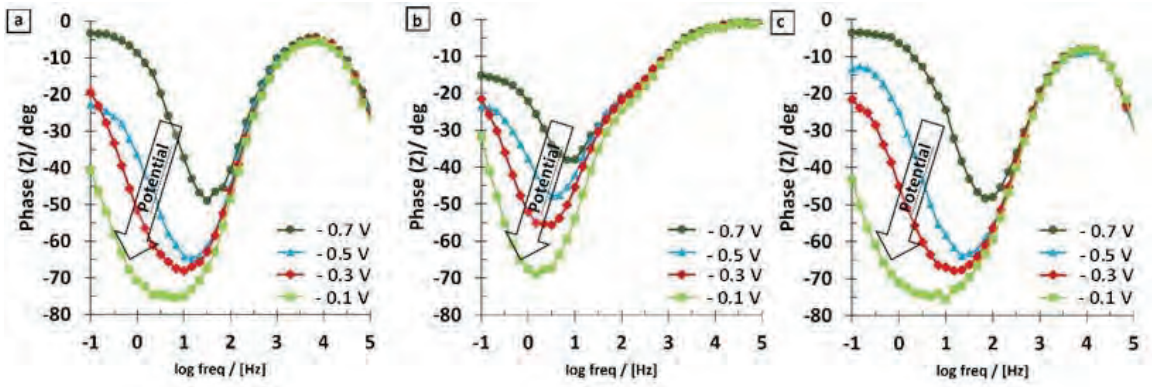

Figure 4. Bode-phase spectra at negative potentials for (**a**) $Al_{1.0}$, (**b**) $Al_{0.8}$, and (**c**) $Al_{0.6}$.

The Bode-phase spectra show the phase shift as a function of frequency for different potentials vs. the reference electrode. The single-phase shift peak for the potentials between −0.7 and −0.1 V indicates that any time constants associated with the corrosion process must be close in frequency. The maximum phase shift is centered at about 10 Hz for $Al_{0.8}$ and 100 Hz for $Al_{0.6}$ and systematically shifts to lower frequencies as the potential increases, reaching a value of about 1 Hz for $Al_{0.8}$ and 5 Hz for $Al_{0.6}$. This shift to lower frequencies is an indication of the increases of the polarization resistance and can occur without a shift in interfacial capacitance.

In the Bode–IZI plots (see Figure 5), for the three HEAs, at high and middle frequencies, the impedance spectra show superimposable curves. All the spectra show a significant drop between −0.1 and +0.1 V. This drop continues with the increasing of potential until the end of the experiment, and the resistance of the film at that moment was reduced more than 200 times for all the HEAs. The impedance of the low-frequency flat surface is associated with the inherent quality of the film. This low-frequency platform represents the addition of the surface layer resistance, the transfer resistance, and the electrolyte resistance. Since both last resistances change slightly for the same HEA, changes in the low-frequency plateau represent changes in the film, and these can be due to the conductive paths through the film.

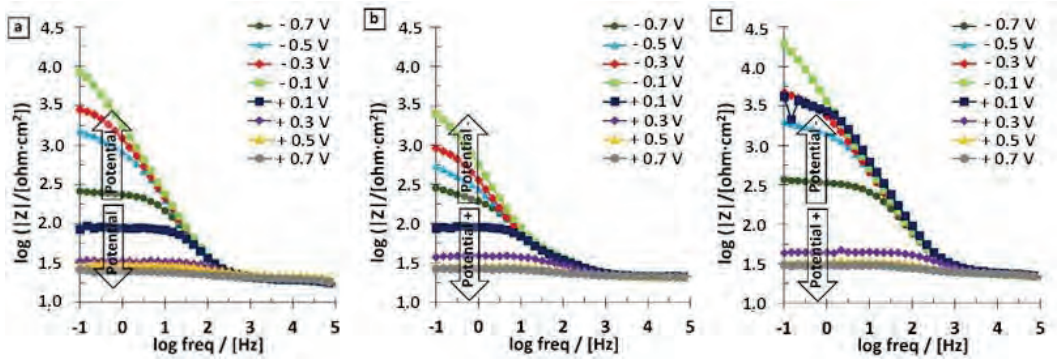

Figure 5. Bode-IZI spectra for (**a**) $Al_{1.0}$, (**b**) $Al_{0.8}$, and (**c**) $Al_{0.6}$.

The increase in low-frequency impedance with the potential is indicative of a richer corrosion resistance of the film formed on the HEA surface. The highest corrosion resistance belongs to the alloy with $x = 0.6$; the value is more than double that for the alloy with $x = 1$, and this confirms that the Al content decrease has changed the passive film characteristics.

In Figure 5, from 0.1 to 0.7 V, a diffusion-controlled process has become a significant part of the total impedance. This is shown by the spectral region with a slope of about 1/4, which occurs from a log frequency of 4.5 to a log frequency of 3.0 and by the spectral region with slope increasing from 1/4 to 1/2, which occurs from a log frequency of 3.0 to 1.0.

These data suggest a corrosion process with diffusion-controlled ionic conductivity [34], and the impedance is dominated by transfer resistance rather than film resistance. This difference in behavior may be attributed to the filling of pores in the film.

When the spectra curve registered from +0.1 to 0.7 V vs. SCE (increasing and decreasing tendency, see Figure 6), strange behavior was observed at lower frequencies where the phase angle changed the direction of evolution at about 50 Hz. This behavior is probably due to a drift of E_{corr} and polarization of the HEA during the impedance measurement [34].

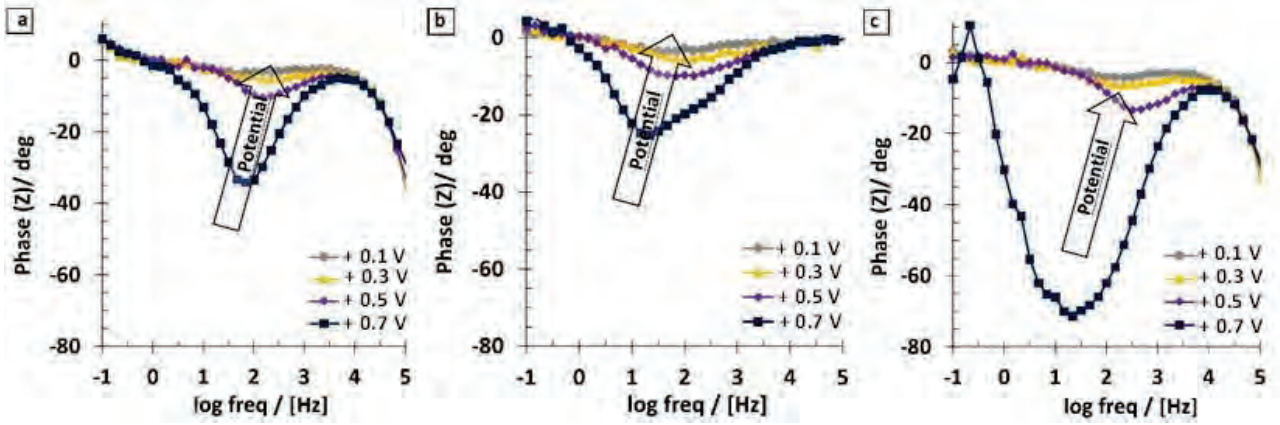

Figure 6. Bode-phase spectra at positive potentials for (**a**) $Al_{1.0}$, (**b**) $Al_{0.8}$, and (**c**) $Al_{0.6}$.

Based on the visual observations of the impedance spectra, the corrosion process parameters have been modeled by the equivalent circuits presented in the Figures 7a and 8a [35].

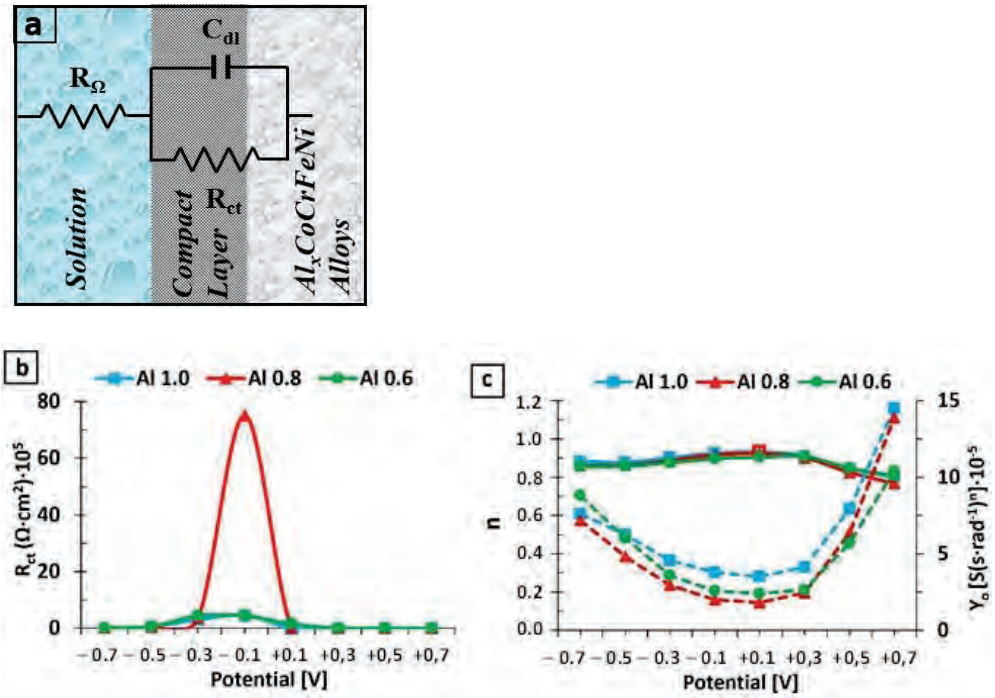

Figure 7. (**a**) Simple equivalent circuit used for the fitting; (**b**) R_{ct} evolution with the potential; (**c**) Y_0 and n parameter corresponding to C_{dl} for the studied alloys.

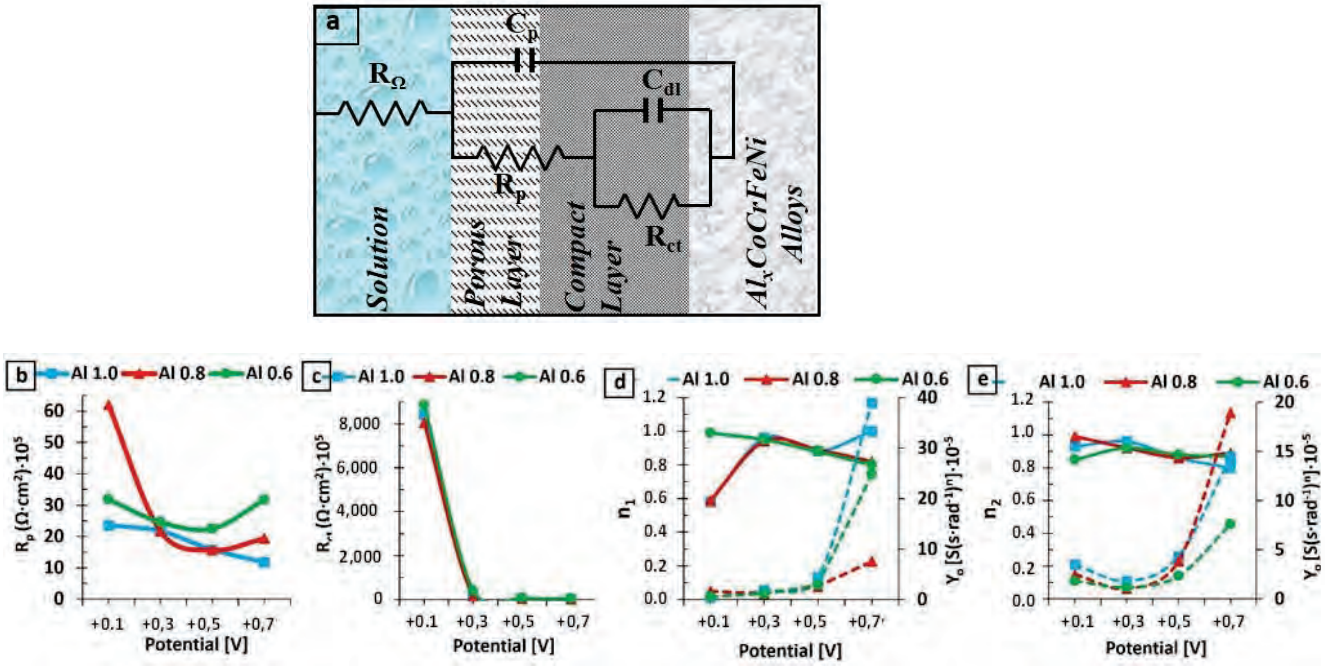

Figure 8. (**a**) Equivalent circuit with two time constants used for the fitting of spectra at positive potentials; (**b**) R_p evolution with the potential; (**c**) R_{ct} evolution with the potential; (**d**) Y_0 and n_1 parameter corresponding to C_p for the external layer; (**e**) Y_0 and n_2 parameter corresponding to C_{dl} for the internal layer.

The elements components of the equivalent circuits are the electrolytic resistance (R_Ω), the resistance of the passive film (R_p), the capacitance of the passive film (C_p), the double-layer capacitance (C_{dl}), and the charge transfer resistance (R_{ct}).

The analysis of the impedance spectra was performed by matching the experimental data with those obtained through the ZSimpWin software. The quality of the fit with an equivalent circuit was initially evaluated by the chi-square value and then by the comparison of the experimental data with the simulated ones. A chi-square value of 10^{-5} indicates a very good fit by using a low number of elements. All elements of the equivalent circuit behaved consistently.

R_Ω is the unbalanced electrolyte resistance and is dependent on the distance from the working electrode to the reference electrode (which remained the same in all the experiments).

R_p is representing the resistance of the passive film pores and is assigned to the resistance of the ion conduction path within the passive layer structure. It indicates the degree of the efficiency of the passive film in protecting the base alloy against corrosion.

R_{ct} represents the polarization resistance at the interface alloy/passive film by considering the entry of the electrolyte into the pores. Fitting procedures have shown that as results of inhomogeneities and porosity, a better coincidence between the theoretical and experimental data is achieved if instead of pure capacitance a constant-phase element is introduced.

CPE constant phase elements were employed (representing the variation from the typical capacitive behavior) and the impedance of a CPE (symbolized with Q) is shown by [36]:

$$Q : Z = (j\omega)^{-n} \cdot Y_0. \quad (2)$$

Z represents the impedance of CPE, j is the imaginary number ($j^2 = -1$), ω is the angular frequency (rad·s^{-1}), Y_0 is the constant of CPE [S(s·rad^{-1})^n] where n is the power number, $n = \alpha(\pi/2)$ where α is the constant phase angle of the CPE (rad). If $n = 1$, CPE = C; if $n = 0$, CPE = R, and if $n = 0.5$, CPE = W.

In this way, all the capacities of the two equivalent circuits have been replaced by phase constant elements.

First, the experimental data have been modeled with the simple circuit of one time constant, the Randles circuit; see Figure 7a. This circuit, called R(QR), is composed of a resistance (R_{ct}) in parallel with Q_{dl}, and these two elements are connected in series with the electrolyte resistance R_Ω. To calculate the total impedance of the equivalent circuit, we calculate the admittance of the parallel combination ($R_{ct}Q_{dl}$):

$$\frac{1}{Z_{eq}} = \frac{1}{Z_{R_{ct}}} + \frac{1}{Z_{Q_{dl}}}. \tag{3}$$

Even a constant phase element was used for fitting the experimental data; because n is close to 1, the obtained Y_0 value is taken as a capacity in the forthcoming discussion:

$$\frac{1}{Z_{eq}} = \frac{1}{R_{ct}} + j\, w\, C_{dl}. \tag{4}$$

Multiplying by R_{ct}, the left side term, Z_{eq}, is:

$$Z_{eq} = \frac{R_{ct} - j\left(w\, C_{dl} {R_{ct}}^2\right)}{1 + \left(w\, C_{dl} R_{ct}\right)^2}. \tag{5}$$

After adding the resistance of the electrolyte, the total impedance is:

$$Z_{eq} = R_\Omega + \frac{R_{ct} - j\left(w\, C_{dl} {R_{ct}}^2\right)}{1 + \left(w\, C_{dl} R_{ct}\right)^2}. \tag{6}$$

R_{ct} is considered the corrosion resistance of the analyzed materials. The values of R_{ct} obtained by adjusting the experimental data with the simulated values from the used equivalent circuit are shown in Figure 7b. Initially, at a potential of −700 mV, the values of R_{ct} for the three HEAs are very similar. As the potential increases, R_{ct} also increases, reaching a maximum value at −100 mV vs. SCE. This increase of R_{ct} (and implicitly of the resistance against the corrosion) with the increase of the potential is due to the passive layer that is formed on the surface of the HEAs modifying its characteristics as a function of the potential: (a) it is more and more compact, since the parameter "n" of the constant phase element approaches 1, the ideal behavior of a capacity and, (b) it is more and more thick (Y_0 decreases with the potential); see Figure 7c. The maximum value of R_{ct} at −100 mV belongs to $Al_{0.8}$, but the one that maintains the maximum value in a longer potential interval is $Al_{0.6}$. This can be explained by the smaller concentration of Al species (oxide and hydroxide) in the passive film, which is a species that promotes a more defective film.

As the potential is shifted from −100 mV to more positive values, R_{ct} decreases (and implicitly decreases the corrosion resistance). This is because the oxide layer on the sample surface is porous; thus, chlorine ions from the electrolyte can easily pass through it and corrode the unprotected metal surface. This process is proved by the decrease of the n-parameter corresponding to the diffusion process, while Y_o increases a lot due to the increase of the surface exposed to the electrolyte (caused by the pores in the passive layer); see Figure 7c.

Considering that at potentials higher than −100 mV, the diffusion stage occupies an increasingly important place in the mechanism of the corrosion process, a better fitting of the experimental data is obtained by using an equivalent electrical circuit with two time constants (see Figure 8a). This circuit, called R(Q(R(QR)), considers both the characteristics of the external porous passive layer (process dominated by ion diffusion) and the internal compact layer (process dominated by charge transfer).

For this circuit, the total impedance is

$$Z_{eq} = R_\Omega + \frac{1}{j\, w\, C_p + \frac{1}{R_p + \frac{1}{\frac{1}{R_{ct}} + j\, w\, C_{dl}}}}. \tag{7}$$

After standard calculations, the following equation was obtained:

$$Z_{eq} = R_1 + \frac{R - w^2RT + w^2AB}{(1 - w^2T)^2 + w^2R^2} + jw\frac{B - RA - w^2TB}{(1 - w^2T)^2 + w^2A^2} \quad (8)$$

where:

$R = R_2 + R_3$
$T = \tau_1\tau_2$
$A = \tau_1 + \tau_2 + C_1R_3$
$B = \tau_2\ R_2$
$\tau_1 \equiv$ time constant of porous layer $[s]$
$\tau_2 \equiv$ time constant of compact layer $[s]$

No significant difference between the R_{ct} values of the analyzed HEAs was observed (see Figure 8c). The evolution of R_p, represented in Figure 8b, shows some differences in the case of sample A0.8: the resistance of the porous passive film decreases slightly with the potential due to pores that increase in number and fill with electrolyte. At 0.7 V vs. SCE, the R_p of the HEAs decreases as the aluminum content grows: increasing the Al content in the alloys leads to a rise of Al and a diminishing of Cr in the passive films. This increase in the amount of Al contained in the passive film takes the form of Al oxides and hydroxides, which effectively build up porous layers that finally result in a thicker passive film. Accordingly, we present in Figure 8d the evolution with the potential of n and Y_{0p}.

It is well known that Co, Ni, and Cr are extremely corrosion-resistant elements and form a strong passive film on the surface. Co^{2+}, Co^{3+}, Ni^{2+}, and Cr^{3+} species, which are generated in the polarization process [36], form a uniform and compact passive film that successfully inhibits the contact of the Cl^- with the metallic surface, thus reducing the corrosion rate and improving the corrosion resistance of the alloy (see R_{ct} evolution in Figure 8c). The decrease of resistance as the applied potential increased at positive values can be attributed to film thinning and breakdown at higher potentials.

There is a small variation in the values of the parameter n of the Y_{dl} associated with the roughness of the electrode surface (see Figure 8e). In the positive range of potential, a variation of "n" is indicative of modifications of non-uniformity and the roughness of the passive film with respect to the metallic surface.

This could be explained by the fact that the dendritic zone of $Al_{0.8}$ has much more chromium than the dendritic zone of $Al_{0.6}$, and being zones of large area, the higher the Cr content in the phase, the better the corrosion resistance property of the passive film formed. However, as the potential increases, the total Al content in the alloy is prevalent, and the higher corrosion resistance is achieved by the alloy with less aluminum.

3.3. Microhardness

For each sample, five indentations were performed, and the average value is then determined.

To correlate the Vickers hardness with yield strength σ_y using a constant C_v that is approximately equal to 3, the Tabor equation [37] can be used:

$$\sigma_y = \frac{HV}{Cv}. \quad (9)$$

Microhardness HV values for HEAs are converted into equivalent yield stress values using this equation (see Table 4).

Table 4. Mechanical properties of analyzed HEAs.

Property	$Al_{1.0}$CrFeCoNi ($Al_{1.0}$)	$Al_{0.8}$CrFeCoNi ($Al_{0,8}$)	$Al_{0.6}$CrFeCoNi ($Al_{0,6}$)
HV (MPa)	562 ± 33	427 ± 17	245 ± 11
σ_y (MPa)	187.5 ± 11	142.3 ± 6	81.9 ± 4

It was observed that the decrease in aluminum concentration significantly decreased the hardness [38] and consequently the Young's modulus and the yield strength of such alloys (see Table 4). Fan et al. observed that by increasing the level of aluminum from 0.5 to 1, the microstructure of the HEA system was changing from an FCC structure to a duplex FCC structure plus BCC and then to a simple BCC structure [39]. A previous study carried out [39] reported that the hardness of the BCC phase is greater than that of the FCC phase, which can be confirmed by our results.

4. Conclusions

The variation of aluminum content in the Al*x*CrFeCoNi system has a significant influence on the microstructure and the behavior of alloys in simulated body fluid.

As the aluminum content decreases, the solidified microstructure varies from equiaxed dendritic grain to equiaxed non-dendritic grain and then to columnar dendritic structure. In the equiaxed non-dendritic grain structure, Widmanstätten side plates can be observed.

The decrease in aluminum content increases the solubility limit of the solid phase for Ni and Co, decreases it for Cr and, Fe is almost unaffected.

Electrochemical Impedance Spectroscopy is a very powerful technique to study the corrosion performance of high-entropy alloys in a simulated human body environment. The obtained results were confirmed by the other techniques that were employed in this study. Circuits composed of one and two time constants in addition to the ohmic resistance of the electrolyte are proposed as equivalent circuits to fit the corrosion behavior of HEAs. The charge transfer resistance in parallel with the double layer capacitance is represented by the low frequency time constant, whereas the medium frequency one is related to the reactions of the alloy´s constituents on the metal surface. Through this technique, information was obtained about the changes of the protective capacity of the passive layers, according with the composition of the alloy and the exposure potential, which demonstrates that the analyzed alloys fulfill the prerequisites for their use as new materials for the manufacturing of medical instruments.

Author Contributions: P.P.S.-P.: writing—original draft preparation, investigation, data curation; N.R.F.-S.: conceptualization, validation, writing—review and editing; I.V.: methodology, investigation, resources; J.C.M.-R.: methodology, visualization, supervision, project administration. All authors have read and agreed to the published version of the manuscript.

Funding: This research received no external funding.

Institutional Review Board Statement: Not applicable.

Informed Consent Statement: Not applicable.

Data Availability Statement: Not applicable.

Acknowledgments: The research was sponsored by the Executive Agency for Higher Education, Research, Development, and Innovation (CNCS CCDI—UEFISCDI), within the framework of grant project Ref. PN-III-P1-1.2-PCCDI-2017-239/60PCCDI 2018—Obtaining and expertise of new biocompatible materials for medical applications—MedicalMetMat; the grant project no. PN-III-P2-2.1-PED-2019-3953/514PED 2019—New composite material with ceramic layers deposited by laser processing for applications at high temperatures and corrosion—LASCERHEA, and project number CABINFR2019-07 Gran Canaria Cabildo.

Conflicts of Interest: The authors declare no conflict of interest.

References

1. Yeh, J.W.; Chen, S.K.; Lin, S.J.; Gan, J.Y.; Chin, T.S.; Shun, T.T.; Tsau, C.H.; Chang, S.Y. Nanostructured high-entropy alloys with multiple principal elements: Novel alloy design concepts and outcomes. *Adv. Eng. Mater.* **2004**, *6*, 299–303. [CrossRef]
2. Chen, H.S.; Tsai, C.W.; Tung, C.C.; Yeh, L.W.; Shun, T.T.; Yang, C.C.; Chen, S.K. Effect of the substitution of Co by Mn in Al-Cr-Cu-Fe-Co-Ni high-entropy alloys. *Ann. Chim. Sci. Mater.* **2006**, *31*, 685–698. [CrossRef]
3. Zhang, Y.; Zuo, T.T.; Tang, Z.; Gao, M.C.; Dahmen, K.A.; Liaw, P.K.; Lu, Z.P. Microstructures and properties of high-entropy alloys. *Prog. Mater. Sci.* **2014**, *61*, 1–93. [CrossRef]

4. Lu, Y.; Dong, Y.; Guo, S.; Jiang, L.; Kang, H.; Wang, T.; Wen, B.; Wang, Z.; Jie, J.; Cao, Z.; et al. A promising new class of high-temperature alloys: Eutectic high-entropy alloys. *Sci. Rep.* **2014**, *4*, 1–5. [CrossRef]
5. Wang, C.; Yu, J.; Yu, Y.; Zhao, Y.; Zhang, Y.; Han, X. Comparison of the corrosion and passivity behavior between CrMnFeCoNi and CrFeCoNi coatings prepared by argon arc cladding. *J. Mater. Res. Technol.* **2020**, *9*, 8482–8496. [CrossRef]
6. Chen, Y.T.; Chang, Y.J.; Murakami, H.; Sasaki, T.; Hono, K.; Li, C.W.; Kakehi, K.; Yeh, J.W.; Yeh, A.C. Hierarchical microstructure strengthening in a single crystal high entropy superalloy. *Sci. Rep.* **2020**, *10*, 1–11. [CrossRef] [PubMed]
7. Ríos, M.L.; Perdomo, P.S.; Voiculescu, I.; Geanta, V.; Crăciun, V.; Boerasu, I.; Rosca, J.M. Effects of nickel content on the microstructure, microhardness and corrosion behavior of high-entropy AlCoCrFeNix alloys. *Sci. Rep.* **2020**, *10*, 1–11. [CrossRef]
8. Zhang, Y. *High-Entropy Materials—A Brief Introduction*; Springer Nature: Singapore, 2019. [CrossRef]
9. Wang, Y.P.; Li, B.S.; Ren, M.X.; Yang, C.; Fu, H.Z. Microstructure and compressive properties of AlCrFeCoNi high entropy alloy. *Mater. Sci. Eng. A* **2008**, *491*, 154–158. [CrossRef]
10. Dasari, S.; Jagetia, A.; Chang, Y.J.; Soni, V.; Gwalani, B.; Gorsse, S.; Yeh, A.C.; Banerjee, R. Engineering multi-scale B2 precipitation in a heterogeneous FCC based microstructure to enhance the mechanical properties of a $Al_{0.5}Co_{1.5}CrFeNi_{1.5}$ high entropy alloy. *J. Alloys Compd.* **2020**, *830*, 154707. [CrossRef]
11. Tang, Z.; Gao, M.C.; Diao, H. Aluminum Alloying Effects on Lattice Types, Microstructures, and Mechanical Behavior of High-Entropy Alloys SystemsNo Title. *JOM* **2013**, *65*, 1848–1858. [CrossRef]
12. Hou, J.; Zhang, M.; Yang, H.; Qiao, J.; Wu, Y. Surface strengthening in $Al_{0.25}$CoCrFeNi high-entropy alloy by boronizing. *Mater. Lett.* **2019**, *238*, 258–260. [CrossRef]
13. Shun, T.T.; Du, Y.C. Microstructure and tensile behaviors of FCC $Al_{0.3}$CoCrFeNi high entropy alloy. *J. Alloys Compd.* **2009**, *479*, 157–160. [CrossRef]
14. Gwalani, B.; Gorsse, S.; Choudhuri, D.; Zheng, Y.; Mishra, R.S.; Banerjee, R. Tensile yield strength of a single bulk Al 0.3 CoCrFeNi high entropy alloy can be tuned from 160 MPa to 1800 MPa. *Scr. Mater.* **2019**, *162*, 18–23. [CrossRef]
15. Csaki, I.; Stefanoiu, R.; Geanta, V.; Voiculescu, I.; Sohaciu, M.G.; Soare, A.; Popescu, G.; Serghiuta, S. Researches regarding the processing technique impact on the chemical composition, microstructure and hardness of AlCrFeNiCo high entropy alloy. *Rev. Chim.* **2016**, *67*, 1373–1377.
16. Lin, C.M.; Tsai, H.L. Evolution of microstructure, hardness, and corrosion properties of high-entropy $Al_{0.5}$CoCrFeNi alloy. *Intermetallics* **2011**, *19*, 288–294. [CrossRef]
17. Chen, M.; Lan, L.; Shi, X.; Yang, H.; Zhang, M.; Qiao, J. The tribological properties of $Al_{0.6}$CoCrFeNi high-entropy alloy with the σ phase precipitation at elevated temperature. *J. Alloys Compd.* **2019**, *777*, 180–189. [CrossRef]
18. Geantă, V.; Voiculescu, I.; Stefănoiu, R.; Chereches, T.; Zecheru, T.; Matache, L.; Rotariu, A. Dynamic Impact Behaviour of High Entropy Alloys Used in the Military Domain. *IOP Conf. Ser. Mater. Sci. Eng.* **2018**, *374*, 012041. [CrossRef]
19. Li, C.; Li, J.C.; Zhao, M.; Jiang, Q. Effect of aluminum contents on microstructure and properties of Al xCoCrFeNi alloys. *J. Alloys Compd.* **2010**, *504*, 515–518. [CrossRef]
20. Wang, W.R.; Wang, W.L.; Wang, S.C.; Tsai, Y.C.; Lai, C.H.; Yeh, J.W. Effects of Al addition on the microstructure and mechanical property of Al xCoCrFeNi high-entropy alloys. *Intermetallics* **2012**, *26*, 44–51. [CrossRef]
21. Kao, Y.F.; Chen, T.J.; Chen, S.K.; Yeh, J.W. Microstructure and mechanical property of as-cast, -homogenized, and -deformed AlxCoCrFeNi ($0 \leq x \leq 2$) high-entropy alloys. *J. Alloys Compd.* **2009**, *488*, 57–64. [CrossRef]
22. Zhao, Y.; Wang, M.; Cui, H.; Zhao, Y.; Song, X.; Zeng, Y.; Gao, X.; Lu, F.; Wang, C.; Song, Q. Effects of Ti-to-Al ratios on the phases, microstructures, mechanical properties, and corrosion resistance of Al2-xCoCrFeNiTix high-entropy alloys. *J. Alloys Compd.* **2019**, *805*, 585–596. [CrossRef]
23. Voiculescu, I.; Geanta, V.; Stefanoiu, R.; Patrop, D.; Binchiciu, H. Influence of the chemical composition on the microstructure and microhardness of alcrfeconi high entropy alloy. *Rev. Chim.* **2013**, *64*, 1441–1444.
24. Kao, Y.F.; Lee, T.D.; Chen, S.K.; Chang, Y.S. Electrochemical passive properties of AlxCoCrFeNi (x = 0, 0.25, 0.50, 1.00) alloys in sulfuric acids. *Corros. Sci.* **2010**, *52*, 1026–1034. [CrossRef]
25. Tang, Z.; Huang, L.; He, W.; Liaw, P.K. Alloying and processing effects on the aqueous corrosion behavior of high-entropy alloys. *Entropy* **2014**, *16*, 895–911. [CrossRef]
26. Kao, Y.F.; Chen, S.K.; Chen, T.J.; Chu, P.C.; Yeh, J.W.; Lin, S.J. Electrical, magnetic, and Hall properties of AlxCoCrFeNi high-entropy alloys. *J. Alloys Compd.* **2011**, *509*, 1607–1614. [CrossRef]
27. Li, Z.; Zhao, S.; Ritchie, R.O.; Meyers, M.A. Mechanical properties of high-entropy alloys with emphasis on face-centered cubic alloys. *Prog. Mater. Sci.* **2019**, *102*, 296–345. [CrossRef]
28. Miracle, D.B.; Senkov, O.N. A critical review of high entropy alloys and related concepts. *Acta Mater.* **2017**, *122*, 448–511. [CrossRef]
29. Levine, D.L.; Staehle, R.W. Crevice Corrosion in Orthopedic Implant Metals. *J. Biomed. Mater. Res.* **1977**, *11*, 553–561. [CrossRef]
30. *ASTM B214-16, Standard Test Method for Sieve Analysis of Metal Powders*; ASTM International: West Conshohocken, PA, USA, 2016. [CrossRef]
31. *ISO 14577-1:2015 Metallic Materials—Instrumented Indentation Test for Hardness and Materials Parameters—Part 1: Test Method n.d*; ISO: Geneva, Switzerland, 2015.
32. *ISO 16773-1-4:2016 Electrochemical Impedance Spectroscopy (EIS) on Coated and Uncoated Metallic Specimens n.d*; ISO: Geneva, Switzerland, 2015.

33. Scully, R.; Silverman, D.C.; Kendig, M. *Electrochemical Impedance: Analysis and Interpretation*; ASTM: Philadelphia, PA, USA, 1993. [CrossRef]
34. González, J.E.G.; Mirza-Rosca, J.C. Study of the corrosion behavior of titanium and some of its alloys for biomedical and dental implant applications. *J. Electroanal. Chem.* **1999**, *471*, 109–115. [CrossRef]
35. Boukamp, B.A. A nonlinear least squares fit procedure for analysis of immittance data of electrochemical systems. *Solid State Ionics* **1986**, *20*, 31–44. [CrossRef]
36. Nascimento, C.B.; Donatus, U.; Ríos, C.T.; Antunes, R.A. Electronic properties of the passive films formed on CoCrFeNi and CoCrFeNiAl high entropy alloys in sodium chloride solution. *J. Mater. Res. Technol.* **2020**, *9*, 13879–13892. [CrossRef]
37. Fan, Q.C.; Li, B.S.; Zhang, Y. Influence of Al and Cu elements on the microstructure and properties of $(FeCrNiCo)Al_xCu_y$ high-entropy alloys. *J. Alloys Compd.* **2014**, *614*, 203–210. [CrossRef]
38. Rios, M.L.; Baldevenites, V.L.; Voiculescu, I.; Rosca, J.M. AlCoCrFeNi High Entropy Alloys as Possible Nuclear Materials. *Microsc. Microanal.* **2020**, *26*, 406–407. [CrossRef]
39. Li, B.; Peng, K.; Hu, A.; Zhou, L.; Zhu, J.; Li, D. Structure and properties of $FeCoNiCrCu_{0.5}Al_x$ high-entropy alloy. *Trans. Nonferrous Met. Soc. China* **2013**, *23*, 735–741. [CrossRef]

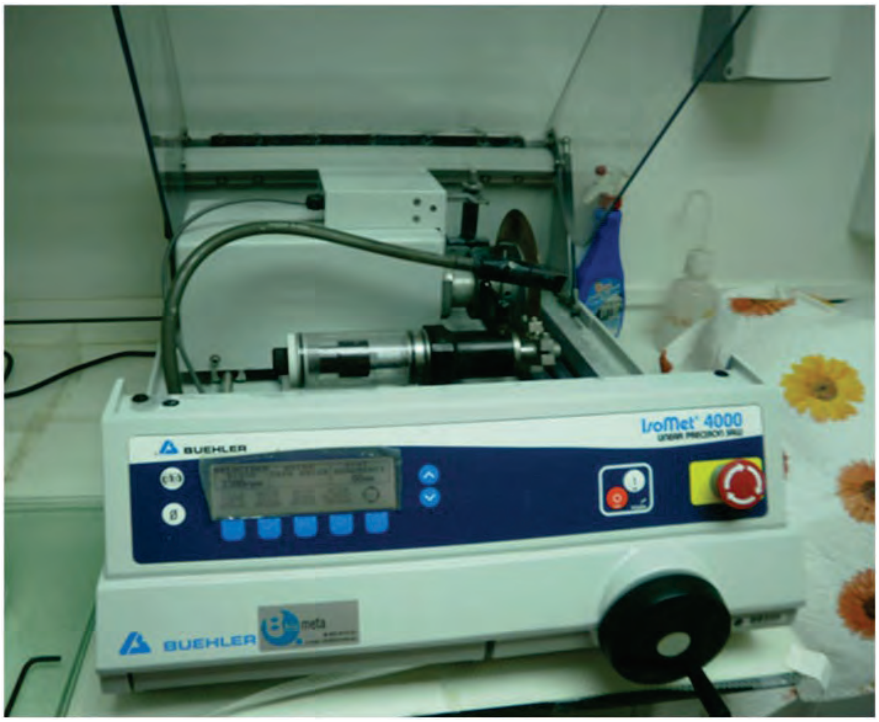

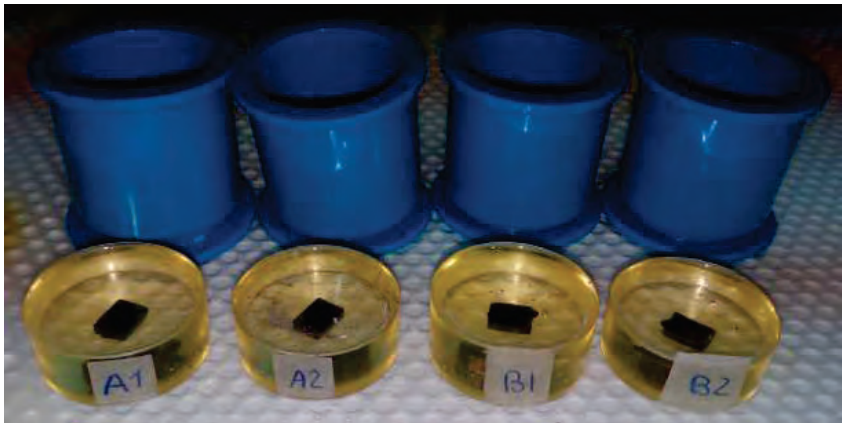

Documento de autoría

4

ULPGC Universidad de Las Palmas de Gran Canaria | Escuela de Doctorado

DOCUMENTO DE AUTORÍA PARA TESIS POR COMPENDIO

Los abajo firmantes, coautores del artículo titulado "EIS Characterization of Ti Alloys in Relation to Alloying Additions of Ta ", publicado en Materials, Vol. 15 No. 476, 2022:

- Reconocemos como autor principal del artículo a D. Pedro Pablo Socorro Perdomo, con DNI 42789076Z.
- Renunciamos a utilizar esta publicación como núcleo principal de otras tesis doctorales, sin perjuicio de que dichas publicaciones puedan ser presentadas como méritos complementarios en las tesis doctorales que pudieran presentar los otros autores de dichas publicaciones.

En Las Palmas de Gran Canaria a 4 de Mayo de 2022

FLORIDO SUAREZ NESTOR RUBEN - 43752800S

Firmado digitalmente por FLORIDO SUAREZ NESTOR RUBEN - 43752800S
Fecha: 2022.05.05 12:16:56 +01'00'

Nestor Ruben Florido Suarez

Mircea Vicentiu Saceleanu

MIRZA ROSCA JULIANA CLAUDIA - 45360672A

Firmado digitalmente por MIRZA ROSCA JULIANA CLAUDIA - 45360672A
Fecha: 2022.05.04 11:20:29 +01'00'

Julia Claudia Mirza Rosca

ULPGC Universidad de Las Palmas de Gran Canaria | Escuela de Doctorado

DOCUMENTO DE AUTORÍA PARA TESIS POR COMPENDIO

Los abajo firmantes, coautores del artículo titulado “Comparative EIS study of titanium-based materials in high corrosive environments“, publicado en International Journal of Surface Science and Engineering, Vol. 15, No. 2, 2021:

- Reconocemos como autor principal del artículo a D.Pedro Pablo Socorro Perdomo, con DNI 42789076Z.
- Renunciamos a utilizar esta publicación como núcleo principal de otras tesis doctorales, sin perjuicio de que dichas publicaciones puedan ser presentadas como méritos complementarios en las tesis doctorales que pudieran presentar los otros autores de dichas publicaciones.

En Las Palmas de Gran Canaria a 4 de Mayo de 2022

FLORIDO SUAREZ NESTOR RUBEN - 43752800S
Firmado digitalmente por FLORIDO SUAREZ NESTOR RUBEN - 43752800S
Fecha: 2022.05.05 12:11:30 +01'00'

Nestor Ruben Florido Suarez

20163025Y MARIA AMPARO VERDU
Firmado digitalmente por 20163025Y MARIA AMPARO VERDU
Fecha: 2022.05.04 13:42:51 +02'00'

Amparo Verdu Vazquez

MIRZA ROSCA JULIANA CLAUDIA - 45360672A
Firmado digitalmente por MIRZA ROSCA JULIANA CLAUDIA - 45360672A
Fecha: 2022.05.04 12:31:57 +01'00'

Julia Claudia Mirza Rosca

ULPGC Universidad de Las Palmas de Gran Canaria | Escuela de Doctorado

DOCUMENTO DE AUTORÍA PARA TESIS POR COMPENDIO

Los abajo firmantes, coautores del artículo titulado “Comparative EIS study of AlxCoCrFeNi Alloys in Ringer´s Solution for Medical Instruments “, publicado en Metals, Vol. 11, No. 928, 2021:

- Reconocemos como autor principal del artículo a D. Pedro Pablo Socorro Perdomo, con DNI 42789076Z.

- Renunciamos a utilizar esta publicación como núcleo principal de otras tesis doctorales, sin perjuicio de que dichas publicaciones puedan ser presentadas como méritos complementarios en las tesis doctorales que pudieran presentar los otros autores de dichas publicaciones.

En Las Palmas de Gran Canaria a 4 de Mayo de 2022

FLORIDO SUAREZ NESTOR RUBEN - 43752800S

Firmado digitalmente por FLORIDO SUAREZ NESTOR RUBEN - 43752800S
Fecha: 2022.05.05 12:37:14 +01'00'

Néstor Rubén Florido Suárez

Ionelia Voiculescu

MIRZA ROSCA JULIANA CLAUDIA - 45360672A

Firmado digitalmente por MIRZA ROSCA JULIANA CLAUDIA - 45360672A
Fecha: 2022.05.05 12:48:37 +01'00'

Julia Claudia Mirza Rosca

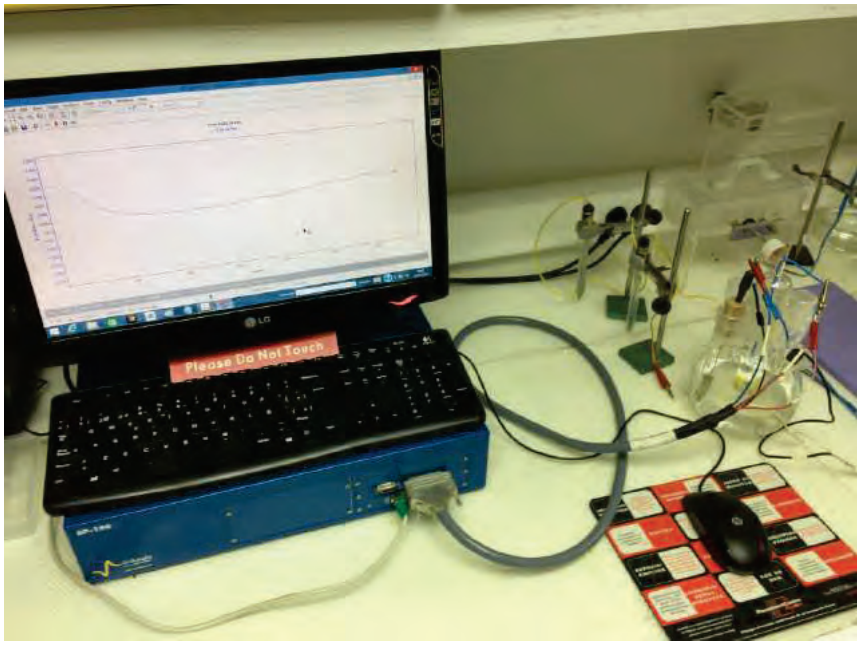

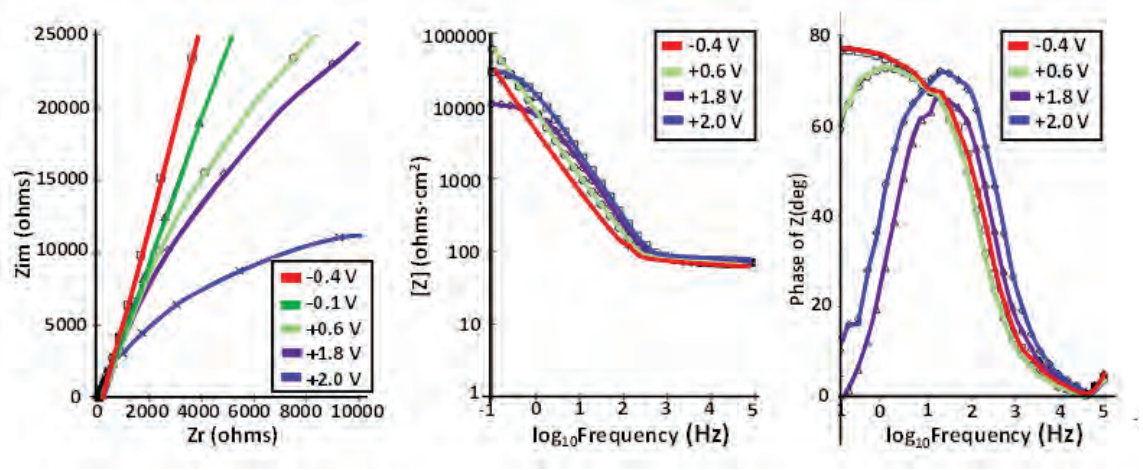

Publicaciones co-participadas

5

5. Publicaciones participadas

5.1 En revistas con índice de impacto

Título:	Analysis of Bone-Implant Interface with Osseoinduction Treatment	
Autores:	Julia Mirza Rosca, Pedro Socorro Perdomo, Nestor Florido Suarez and Maximina Monzón Mayor	
Revista: Microscopy and Microanalysis		
Editorial: Cambridge University Press		Índice Impacto: 3,414 (2019)
Mes/Año: 07 /2020	ISSN: 1431-9276	
Cuartil: Q1	doi:10.1017/S1431927620014142	

Título:	Effects of nickel content on the microstructure, microhardness and corrosion behavior of high-entropy AlCoCrFeNix alloys	
Autores:	M. López-Rios, P.P. Socorro Perdomo, I. Voiculescu, V. Geanta, I. Boerasu, J.C. Mirza Rosca	
Revista: Scientific reports		
Editorial: Cambridge University Press		Índice Impacto: 4.379 (2021)
Mes/Año: 12/2020	ISSN: 2045-2322	
Cuartil: Q1	doi: 10.1038/s41598-020-78108-5	

Título:	Static Testing and Fatigue Behavior of Three High-Entropy Alloys	
Autores:	Nestor Florido-Suarez, Pedro Socorro-Perdomo, Victor Geanta and Julia Mirza-Rosca	
Revista: Microscopy and Microanalysis		
Editorial: Cambridge University Press		Índice Impacto: 3,414 (2020)
Mes/Año: 08 /2021	ISSN: 1431-9276	
Cuartil: Q1	doi:0.1017/S1431927621011260	

Título:	Effect of Heat Treatment on the Microstructure and Corrosión Resistance of AlCoCrFeNi High-Entropy Alloy
Autores:	Nestor Florido-Suarez, Pedro Socorro-Perdomo, Victor Geanta and Julia Mirza-Rosca1
Revista: Microscopy and Microanalysis	
Editorial: Cambridge University Press	Índice Impacto: 3,414 (2020)
Mes/Año: Agosto /2021	ISSN: 1431-9276
Cuartil: Q1	doi:10.1017/S14319276210115942

Título:	Osseo-integration Improvement of Additive Manufactured Dental Alloy
Autores:	Elena-Manuela Stanciu, Nestor Florido-Suarez, Pedro Socorro-Perdomo and Julia Mirza-Rosca
Revista: Microscopy and Microanalysis	
Editorial: Cambridge University Press	Índice Impacto: 3,414 (2020)
Mes/Año: Agosto /2021	ISSN: 1431-9276
Cuartil: Q1	doi:10.1017/S1431927621008564

Título:	Biocompatibility of New High-Entropy Alloys with Non-Cytotoxic Elements
Autores:	Pedro Socorro-Perdomo, Nestor Florido-Suarez, Ionelia Voiculescu and Julia Mirza-Rosca
Revista: Microscopy and Microanalysis	
Editorial: Cambridge University Press	Índice Impacto: 3,414 (2020)
Mes/Año: Agosto /2021	ISSN: 1431-9276
Cuartil: Q1	doi:10.1017/S1431927621006486

Título:	Microstructure and Adjustment in Tensile Strength of Al0.8CoCrFeNi Fibers
Autores:	Nestor Florido-Suarez, Pedro Socorro-Perdomo, Ionelia Voiculescu and Julia Mirza-Rosca
Revista: Microscopy and Microanalysis	
Editorial: Cambridge University Press	Índice Impacto: 3,414 (2020)
Mes/Año: Agosto /2021	ISSN: 1431-9276
Cuartil: Q1	doi:10.1017/S1431927621011648

Título:	Study of Biocompatibility, Mechanical Properties and Microstructural Analysis af Ag-Pd Alloy
Autores:	Jenifer Vaswani-Reboso, Nestor Florido-Suarez, Pedro Socorro-Perdomo and Julia Mirza-Rosca
Revista: Microscopy and Microanalysis	
Editorial: Cambridge University Press	Índice Impacto: 3,414 (2020)
Mes/Año: Agosto /2021	Issn: 1431-9276
Cuartil: Q1	doi:10.1017/S1431927621002415

doi:10.1017/S1431927620014142
Microsc. Microanal. 26 (Suppl 2), 2020

Analysis of Bone-Implant Interface with Osseoinduction Treatment

Julia Mirza Rosca, Pedro Socorro Perdomo, Nestor Florido Suarez and Maximina Monzon mayor

University of Las Palmas de Gran Canaria, Las Palmas de GC, Canarias, Spain

The interactions of tissues, bones and body fluids with biomaterials are an area of crucial importance to all kinds of medical technologies. The implants need to integrate with surrounding tissues to restore adequate function, without releasing harmful chemical products or significantly modifying the local environment.

Even since the 1980s the titanium alloys are intensively applied in the manufacturing of orthopedic devices, it was reported [1] that V is toxic in vitro at concentrations below those of synovial fluids in vivo. The administration of metallic powders to L929 and osteoblast MC3T3-E1 cells showed that Nb had no effect on their relative growth ratios [2] and for this reason it was developed an alternative alloy, Ti6Al7Nb, in which the vanadium was exchanged with niobium. Today Ti6Al7Nb alloy is the preferred choice for cementless total joint replacement.

In this study a chemical treatment was attempted to prepare an osseoinductive surface: immersion in NaOH aqueous solution then dried at 40ºC and heated up to 600ºC for 1 hour and cooled to room temperature [3]. After osseoinductive treatment, the material was implanted in animal´s tibiae (mini-pig). At 6 months after implantation, the animals were sacrificed and the segments of the proximal tibia epiphyses were cut off, fixed in phosphate-buffered formalin and dehydrated; finally, they were embedded in polyester resin and then cutted transversally (metal and bone together) and grounded to a thickness of 75-100 μm. With these samples a lot of observations of interface bone-implant were made: TEM and SEM observations, histological examinations and SEM-EDX analysis.

It can be concluded that there aren´t toxic and carcinogenic responses of animals to implant materials. The EDX detected the following metals: Ti, Ca, P and Al; the calcium and phosphorus presented a Ca/P ratio of 1.65 indicating that it is similar to bone mineral phase. The bone was in intimate contact with the bioactive Ti6Al7Nb implant (see Fig.1). Over time, the amount of bone directly bonding to the implant increased (see Fig.2) and the immature bone had formed in the earlier stages, matured and converted to lamellar bone. All the results revealed that the osseoinductive surface of the implant is in direct contact with newly formed bone without any intervention of a soft tissue layer. We regard osseoinductive ability of nanostructured Ti6Al7Nb as one of the advantages of this implant in consideration for clinical applications.

Figure 1. General view

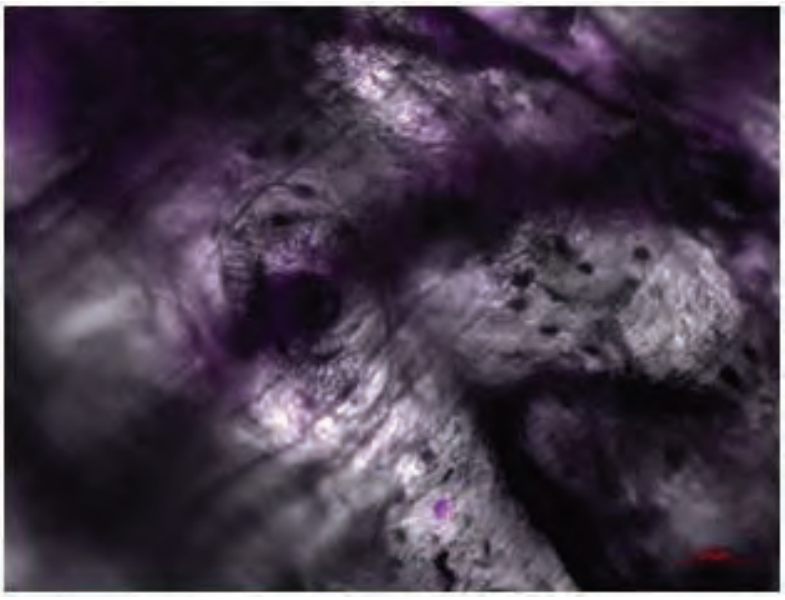

Figure 2. New bone in direct contact with the implant

References

[1]N.J. Hallab , S. Anderson, M.Caicedo, A. Brasher, K. Mikecz, J. Jacobs, *Effects of soluble metals on human peri-implant cells,* J Biomed Mater Res A. 2005;74(1):124-40.
[2] Y. Okazaki, S. Rao, Y.Ito, T. Tateishi, *Corrosion resistance, mechanical properties, corrosion fatigue strength and cytocompatibility of new Ti alloys without Al and V*, Biomaterials 1998, 19:1197-1215.
[3] M.Takemoto, S.Fujibayashi, M.Neo, J.Suzuki, T.Kokubo, T.Nakamura, *Mechanical properties and osteoconductivity of porous bioactive titanium*, Biomaterials 2005, 26(30), 6014-6023.

https://doi.org/10.1017/S1431927620014142

scientific reports

Check for updates

OPEN

Effects of nickel content on the microstructure, microhardness and corrosion behavior of high-entropy AlCoCrFeNix alloys

M. López Ríos[1], P. P. Socorro Perdomo[1], I. Voiculescu[2], V. Geanta[3], V. Crăciun[4,5], I. Boerasu[4] & J. C. Mirza Rosca[1]✉

In this study the effect of three different nickel concentration on the microstructure, hardness and corrosion properties of high entropy alloys (HEAs) from AlCrFeCoNi system as an alternative material for medical instruments fabrication was investigated. The analyzed HEAs were AlCrFeCoNix obtained by vacuum arc remelting from high purity raw materials and having nickel atomic ratio x = 1.0, 1.4 and 1.8. The microscopy examination revealed the dendritic morphology for the reference alloy (AlCrFeCoNi) and that the extent of the interdendritic areas increased with the concentration of nickel while Cr was more segregated in the interdendritic areas than in dendrites. Hardness values decreased as the percentage of nickel increased due to the dissolution of the precipitates in a nickel-rich matrix and consequently the formation of continuous solid solutions. The corrosion properties of the synthesized HEAs were evaluated using a potentiodynamic polarization method. The alloys were immersed in Simulated Body Fluid during one week and the corrosion parameters were recorded. The low corrosion rates, low corrosion currents and high polarization resistance attest the good stability of these HEAs in simulated biological environment indicating their possible use for surgical and dental instruments.

Classic metallic alloys generally contain one metal in a high proportion, called the base metal, and very rarely two metals in similar proportions. Although small amounts of other elements are added, this can make a big difference in the characteristics of the obtained alloy. Due to the great advance of science and technology, new metallic alloys containing more than 2 base metals, with a different metallurgical concept, have been recently explored[1,2].

High-entropy alloys (HEAs) are one of the most promising results of the exploration of new chemical compositions for metallic materials with improved performance[3–5]. Originally, they were defined as an alloy with at least five metallic elements with atomic percentage between 5 and 35%[6].

One of the basic alloy from HEA category, AlCoCrFeNi, was discovered in 2014 by Zhang's group at University of Science and Technology from Beijing, China[2]. Many other groups have joined the research effort to understand this HEA microstructure[7,8], hardness[9,10], strength[11,12], friction and wear[13] and thermal resistance[14,15] particular properties. Although many interesting topics have been explored, only few studies deal with corrosion properties of this high-entropy alloy, in general depending of fabrication method: if is synthesized by laser additive[16], by electrospark process[17] and by spark plasma sintering with pre-alloy powders obtained through gas atomization[18]. Other studies, with different aluminium concentration were performed[19–21].

In the late last century, the progress of materials science led to the rapid development of biomedical materials. Nowadays, titanium alloys are widely used as implants and prosthesis in the human body because of their excellent biocompatibility and low density. However, titanium alloys do not have sufficient strength characteristics

[1]Mechanical Engineering Department, University of Las Palmas de Gran Canaria, Campus Universitario Tafira, Edif.Ingenieria, 35017 Gran Canaria, Spain. [2]Faculty of Industrial Engineering and Robotics, Politehnica University of Bucharest, 313 Splaiul Independentei, 060042 Bucharest, Romania. [3]Faculty of Materials Science and Engineering, Politehnica University of Bucharest, 313 Splaiul Independentei, 060042 Bucharest, Romania. [4]National Institute for Laser, Plasma and Radiation Physic, Magurele, Romania. [5]Extreme Light Infrastructure-Nuclear Physics, IFIN-HH, Magurele, Romania. ✉email: julia.mirza@ulpgc.es

for medical instruments used for surgery or prosthetic devices. The recent development of HEAs provides a new generation of biomaterials which may can be used for medical devices.

To be able to use the high-entropy alloys for the manufacturing of medical instruments (like cutters, saws, scalpels etc.), their mechanical characteristics and corrosion resistance in physiological fluids which contain 1% wt. NaCl, must be tested. Furthermore, if the material corrodes due to chemical attack, some corrosion products that will form can produce undesirable reactions at metal-tissue interface. To avoid this deleterious effect, the chemical composition of the new alloys must be carefully designed[22]. The material needs to be inert in contact with the human body, so it won´t cause any metal contamination when used internally. Together with the mechanical properties[23,24], corrosion resistance plays a critical role in determining the successful use of HEAs for biomedical applications[25,26]. In this study the effect of three different nickel concentrations on the microstructure, hardness and corrosion properties of high entropy alloys from AlCrFeCoNi system has been investigated. The reason for adding nickel is that nickel generally increases ductility and hardness. Nickel improves heat treatment properties by expanding the critical temperature level, it does not form oxides and this increases strength without decreasing ductility. The results presented below indicate that the structure and corrosion behavior of AlCrFeCoNix alloys strongly depends on the Ni content.

Experimental

Materials and samples preparation. The high entropy AlCrFeCoNix alloys (with x = 1.0, 1.4 and 1.8) were obtained in the ERAMET Laboratory of the Politehnica University of Bucharest, using the MRF ABJ 900 Vacuum Arc Remelting (VAR) installation[10,25]. The theoretical degree of assimilation of the chemical elements during melting and the possible losses by vaporization were taken into account for designing the metallic charge. Highly pure raw materials, including Al, Cr, Fe, Co and Ni (at least 99.5%) were used. In order to obtain the adequate homogeneity, the obtained alloys were flipped and re-melted in VAR equipment for 6 times (3 times on each part) under inert atmosphere of Argon.

Samples in the form of rods of about 10 cm long and 1 cm diameter were obtained. The rods were transversally cut and some samples were selected for homogenization (annealing to 1100 °C for 48 h followed by water quenching). For structural, compositional and mechanical analyses the samples were embedded into an epoxy resin cylinder and then their surface was prepared in 3 stages: (1) polishing with SiC abrasive papers of progressive grain size from 240 to 2000 grit; (2) final polishing with 0.1 μm alpha alumina paste; (3) cleaning in ultrasonic deionized water.

Test environment. All the measurements were performed in Ringer Grifols solution (from Grifols Laboratories, Barcelona, Spain) with the following composition in mmol/l: Na^+ 129.9; K^+ 5.4; Ca^{2+} 1.8; Cl^- 111.7 and $C_3H_5O_3^-$ 27.2. It is a modified physiological solution in which part of the sodium ions are replaced by calcium and potassium ions and parts of the chlorine ions by lactate ions. The lactate ions are transformed into bicarbonate ions allowing a regulation of the solution pH. The tests were conducted at 37 ± 0.1 °C in a thermostatic bath.

Microstructural characterization. To study the microstructure of the alloys by optical microscopy, their surface was etched by electrochemical route using a solution of 10% oxalic acid, a current of 5 A and an immersion time of 4 s. The observations of the surface were made using an OLYMPUS PME 3-ADL microscope.

Scanning electron microscope (SEM) observations were made using a S LoVac of the Apreo Field Emission Scanning Electron Microscope (THERMO FISHER SCIENTIFIC, Co., USA) equipped with a TEAM EDX spectrometer. For ensuring the best high vacuum imaging and analytic conditions the microscope was set to run at 20 kV voltage and 1.6 nA beam current, for working distance of 10.0 mm.

Electrochemical measurements. The electrochemical measurements were made with a conventional three-electrode electrochemical cell: the sample as working electrode, Pt as counter electrode and a saturated calomel electrode (SCE) as reference electrode. The used potentiostate was a SP-150 (BioLOGIC Science Instruments) controlled by a computer with EC-LAB software package.

Open circuit potential (OCP). Open circuit potential measurements during 3 days were performed, followed by potentiodynamic polarization measurements. All tests were performed three times and data were processed using EC-LAB software.

Potentiodynamic polarization studies—polarization resistance and Tafel slopes. In order to calculate the Tafel slopes for the partial anodic processes (b_a), and the Tafel slopes for the partial cathodic processes (b_c), the linear polarization curves have been shifted from E_{OCP} − 150 mV to E_{OCP} + 150 mV using a scanning rate of 10 mV/s. The polarization studies to evaluate the passivation process continued with measurements from − 800 mV (vs. SCE) to + 500 mV (vs.SCE), increasing the potential at a scanning rate of 1 mV/s. SP-150 potentiostate was used to perform the tests and data were processed using EC-LAB software, both from BioLOGIC Science Instruments. Results showed the potentiodynamic polarization curves and the breakdown potential.

Microhardness measurements. The HEAs Vickers microhardness has been measured by an indentation test using a REMET HX-1000 Microhardness Tester. The samples, with the surfaces polished to mirror quality for good vision of the prints, were indented every 0.5 mm along the diameter. The tests were carried out according to the regulation UNE-EN ISO 6507-1:2006, applying a load of 100 g during 15 s. A minimum of 5

indentations were made on each sample and the average value was calculated, expressing it as the Vickers hardness (HV).

XRD analysis. X-ray diffraction experiments were performed with the aid of an empyrean diffractometer (MALVERN-PANALYTICAL). The instrument was working with a Cu Kα anode at a power of 45 kV and 40 mA in the Bragg–Brentano geometry. The samples were rotated during acquisition to ensure a better data collection. The acquired patterns were simulated to extract the crystalline phase present, lattice parameter and grain size with the aid of HighScore Plus software from MALVERN-PANALYTICAL.

Results and discussions

Microstructure. The phase structure of an alloy is critical for its biocompatibility and depends on the solubility of the alloying elements. The interaction between the phase structure and the biologic environment determines which elements will be released and, therefore, how the body will respond to the alloy. The grain size affects the corrosion processes because the grain boundaries influence the corrosion behaviour. The smaller the grain size of the samples, the higher the critical current density they will have as the edges of the grains store internal energy that promotes the corrosion[27].

The microstructures of the analysed HEAs before corrosion tests are shown in Fig. 1a–f. The overall look of the optical microstructures is dendritic (Fig. 1a–c). The different concentrations of the alloying elements involves the morphology of the phases. Thus, in the case of AlCrFeCoNi the aspect of the dendrites is quite round, while in the $AlCrFeCoNi_{1.4}$ sample we can observe needle forms that are oriented in different directions. The $AlCrFeCoNi_{1.8}$ sample combines rounded phases with needle-like phases, consistent with the observation reported by Cao et al.[28].

Chrome induces the formation of a protective and compact oxide layer on the surface of nickel alloys, the optimum corrosion resistance being obtained with Cr contents of about 16–27%. If the Cr content is lower, the alloy may not be able to develop a passive film adequate for a good corrosion resistance. AlCrFeCoNi has a spinodal structure quite typical for high entropy alloys, as we reported before[5]. This structure determines the smaller dimension of the phases and higher interfaces area increasing the hardness value.

The SEM observations are presented in Fig. 1d–f. The microstructural aspect is similar to that observed by optical microscopy. In the case of Ni_1 alloy, the crystalline grains with crystallites are observed, organized like Chinese letters, bordered by linear limits (Fig. 1d). As the Ni content increases in the $Ni_{1.4}$ alloy, the appearance of acicular phases is observed (Fig. 1e). As further increase of nickel content in $Ni_{1.8}$ alloy the acicular phases become rounded (Fig. 1f).

The elements Al, Co and Ni can form continuous solid solutions with the same composition in the matrix of dendritic and interdendritic zones while Cr and Fe segregated more in the spherical precipitates of dendritic region[5,7]. This suggests that the partitioning of elements from the solution phase of HEA is inherently related to the enthalpy and miscibility between the various atoms present[22].

The heat treatment performed after casting promoted homogenization of chemical composition and changes of microstructure aspect (Fig. 1g–i). The linear appearance of the grain boundaries was replaced by curved connections and the amount of needle phase decreased. In Fig. 1g three types of phases can be distinguished, as follows: a majority phase (light gray) with dendritic appearance, an inter-dendritic phase (dark gray) and thin needle like phase formed inside the majority phase. As the nickel concentration increased (Fig. 1h,i), there was a compositional change of the 2 major phases (dark gray and light gray) and a decreasing of the needle-like phase number.

The surface of the samples was examined also after performing heat treatment and corrosion test. For all the samples, pitting corrosion was observed. The images of the corroded surfaces highlight the acicular-looking phases that formed in the microstructure after the heat treatment (see Fig. 1j–l). It is observed how the chemical solution partially dissolved the surface film and preferentially attacked the alloy phases. As the Ni content in sample $Ni_{1.8}$ increases to 31 at.% (Fig. 1l), more extended corrosion effects on the alloy phases are observed.

EDS analysis. The EDS analyses have been performed on micro-zones, having the same square area, see Fig. 1g–l. The results of the chemical composition for the three alloys are presented in Table 1.

Analyzing the EDS results from Table 1 it is observed that Al concentration decreases in all samples that were simultaneously heat treated and corroded, from about 10 at% to 2.57–3.03 at%. A similar evolution is observed in terms of Ni concentration, which decreases from the maximum values existing in the heat treated samples (24.99 at% for Ni_1 to 37.68 at% for $Ni_{1.8}$) to just over half of the initial values (12.73 at % Ni for Ni_1 to 25.14 at% Ni for $Ni_{1.8}$). Cr and Fe maintain their concentrations within tight limits (maximum variations of 5 at%), and Co records the largest increases in concentration for simultaneously heat-treated and corroded samples. This behavior emphasizes the high chemical stability of Co in the metal matrix of the analyzed alloys.

Based on the EDS analysis performed on different phases, following the initial values of Co and Cr content in those phases, the specific tendency of segregation and association of these elements to form common phases is observed on atoms distribution maps (see Fig. 2).

In the case of Ni_1 (AlCrFeCoNi) TT sample, the chemical microanalysis on light grey phase indicates that it contains about 5.08 at% Al, 9.14 at% Co, 31.76 at% Cr, 29.80 at% Fe and 20.51 at% Ni. The dark grey phase contains 27 at % Al, 8.55 at% Co, 10.37 at% Cr, 14.15at% Fe and 38.26 at% Ni.

Regarding $Ni_{1.4}$ ($AlCrFeCoNi_{1.4}$) TT sample, the light grey phase contains 4.40 at % Al, 7.16 at % Co, 34.18 at % Cr, 28.96 at % Fe and 21.42% Ni. The dark grey phase contains 23.53 at% Al, 7.21 at % Co, 13.35 at % Cr, 15.21 at % Fe and 39.23 at % Ni.

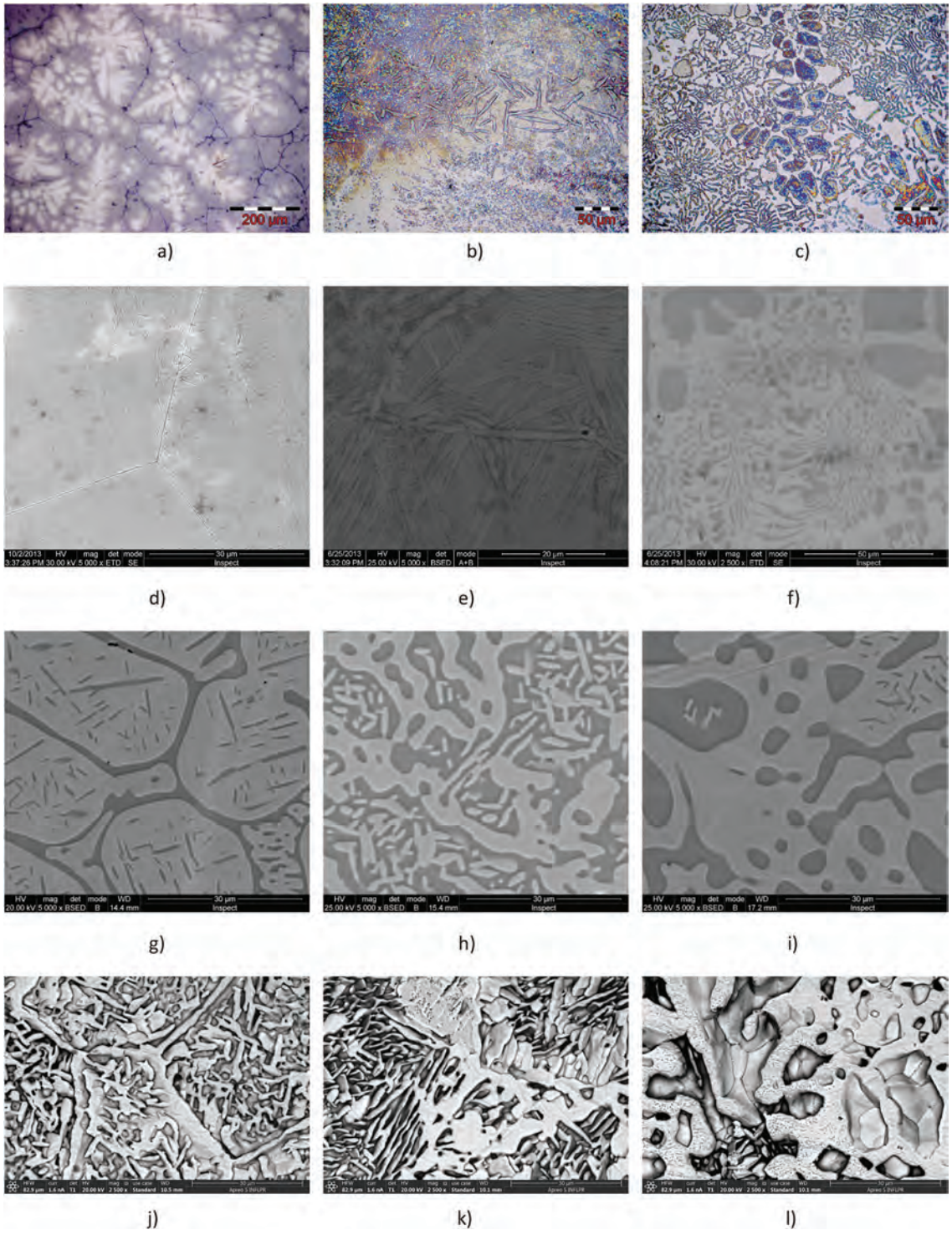

Figure 1. Microstructure evolution of HEAs (Ni_1, $Ni_{1.4}$ and $Ni_{1.8}$) during thermal and chemical processing: (**a**), (**b**), (**c**) optical microstructure; (**d**), (**e**), (**f**) SEM as-cast microstructure; (**g**), (**h**), (**i**) SEM heat treated microstructure; (**j**), (**k**), (**l**) Thermal treated and corroded microstructure.

Finally, in the case of $Ni_{1.8}$ ($AlCrFeCoNi_{1.8}$) TT sample, the light grey phase contains 21.73 at% Al, 5.31 at %Co, 9.85 at% Cr, 12.82 at% Fe and 48.88 at% Ni. The dark grey phase contains 5.51 at % Al, 6.02 at % Co, 29.06 at% Cr, 24.98 at.% Fe and 31.01at % Ni.

These results highlight the tendency of Al and Ni to form stable compounds (dark grey phase) and quite equal distribution of the other elements in light grey phase or in the acicular phases.

	Ni_1			$Ni_{1.4}$			$Ni_{1.8}$		
Element	Corr	TT	T + C	Corr	TT	T + C	Corr	TT	T + C
Al, at%	**12.00**	**9.89**	**2.57**	**11.68**	**14.28**	**3.03**	**10.59**	**10.46**	**2.77**
wt%	6.33	5.14	1.29	6.12	7.54	1.52	5.47	5.37	1.38
Error,%	5.47	5.43	4.13	2.84	5.47	5.74	2.92	5.82	5.76
Co, at%	**6.59**	**8.48**	**21.85**	**3.75**	**7.40**	**21.49**	**3.34**	**5.36**	**20.49**
wt%	7.58	9.62	24.07	4.29	8.54	23.46	3.77	6.01	22.33
Error,%	5.34	5.02	1.79	3.32	4.43	1.79	3.88	4.51	1.76
Cr, at%	**28.72**	**26.98**	**31.83**	**32.61**	**22.67**	**28.51**	**29.62**	**22.95**	**26.16**
wt%	29.17	27.01	30.93	32.93	23.07	27.46	29.50	22.71	25.15
Error, %	1.93	1.90	1.90	1.99	2.00	1.95	2.04	2.11	1.97
Fe, at%	**26.56**	**26.40**	**26.41**	**24.75**	**21.52**	**23.52**	**22.94**	**21.39**	**21.07**
wt%	28.98	28.38	27.57	26.85	23.53	24.33	24.54	22.73	21.76
Error,%	2.05	1.95	1.87	1.81	2.11	1.94	1.90	2.30	1.99
Ni, at%	**23.28**	**24.99**	**12.73**	**24.78**	**31.13**	**19.62**	**31.33**	**37.68**	**25.14**
wt%	26.58	28.24	13.97	28.26	35.78	21.33	35.24	42.10	27.29
Error,%	2.12	1.94	2.05	1.73	2.11	1.93	1.67	1.98	1.85
O, at%	**2.38**	**2.46**	**3.54**	**1.39**	**2.22**	**2.77**	**1.08**	**1.61**	**3.25**
wt%	0.74	0.76	1.06	0.43	0.70	0.82	0.33	0.49	0.96
Error, %	5.15	4.57	4.13	2.78	5.21	4.40	2.73	6.24	4.28

Table 1. EDS global analyses on micro areas for HEAs after different processing stages. Corr, corroded; TT, Thermal treated; T + C, Thermal treated and corroded.

X-ray diffraction. The XRD patterns acquired from as-cast samples are displayed in Fig. 3. The Ni_1 sample exhibited a pure primitive cubic phase (space group Pm-3m, number 221), matched very well by reference pattern 04-018-5047, Al0.4Co0.4Cr0.4Fe0.4Ni0.4. Increasing the Ni content resulted in the appearance of a new FCC phase (Fm-3m, group 225, a = 3.5643 Å), that was matched by reference pattern 04-022-2301, $Co_{0.25}Cr0.25Fe_{0.25}Ni_{0.25}$ and indicated by symbol # in front of the Miller indices in Fig. 3. Also, $Al_{0.9}Ni_{4.22}$ (pattern 00-050-1294) with a slightly different lattice parameter (FCC, a = 3.5700 Å) and $Cr_{0.10}Fe_{0.65}Ni_{0.25}$ (pattern 04-019-2390) with a slightly different lattice parameter (FCC, a = 3.5920 Å) are good matches. The presence of an Al-Ni FCC type compound after the thermal treatment is strongly supported by the EDS results. After corrosion treatment, a strong decrease in Ni and Al concentrations was observed, which was probably caused by the dissolution of this compound, while the others elements were not that much affected. SEM images of the corroded surface also suggest that a phase initially present was dissolved and disappeared from the surface region.

XRD patterns acquired from samples after the thermal treatment exhibited a mixture of two cubic phases: a primitive one and a FCC one (Fig. 3), with the relative percentage displayed in Table 2, although the presence of other FCC type compounds as those mentioned above could not be ruled out. The patterns also displayed narrower diffraction peaks, indicative of grain growth. The lattice parameters of the Pm-3 m and FCC phases, also displayed in Table 2 did not significantly changed with the increase of Ni content or the thermal treatment.

With the increasing of nickel concentration, the lattice parameter of the primitive cubic phase varies very slightly, from 2.876 Å to 2.870 Å, while the grain size remains almost the same (from 398 to 414 and 365 Å) for as-cast samples. For the FCC phase, the lattice parameters also vary very slightly but the grain size increases with the nickel content for both as-cast andannealed samples. It can be seen that, for all the studied alloys, the lattice parameter of the two phases varies marginally, which was also reported for other HEAs[29].

The results show a good homogeneity of the samples with two main solid solutions formed and some minor compounds segregating in the dendritic zone.

After the thermal treatment, the elemental composition of HEAs does not change; however, after the corrosion stage, the Al concentration in the surface region significantly dropped, followed by Ni; Co concentration went up, while Fe and Cr did not change much.

To explain these results, the formation after the thermal treatment of an Al-Ni compound is hypothesized, which should be corroded faster than the main HEA phase. There are several Al-Ni compounds having an FCC lattice and a lattice parameter very close to that of FCC AlCoCrFeNi HEA that could explain the results.

Open circuit potential (OCP). Open circuit potential measurement curves during one-week immersion are shown in Fig. 4.

For all analyzed HEAs, after a short immersion time of about some hours, there is an increase in the corrosion potential due to the growth of passive layers on the surface of the alloys. During the first 24 h, the OCP for all the three alloys increases with 30–50 mV due to the build-up of the passive layers on the surface of the HEAs. The maximum value of OCP is 236 mV for AlCrFeCoNi and 235 $AlCrFeCoNi_{1.8}$ and almost half of this value, 102 mV, for $AlCrFeCoNi_{1.4.}$

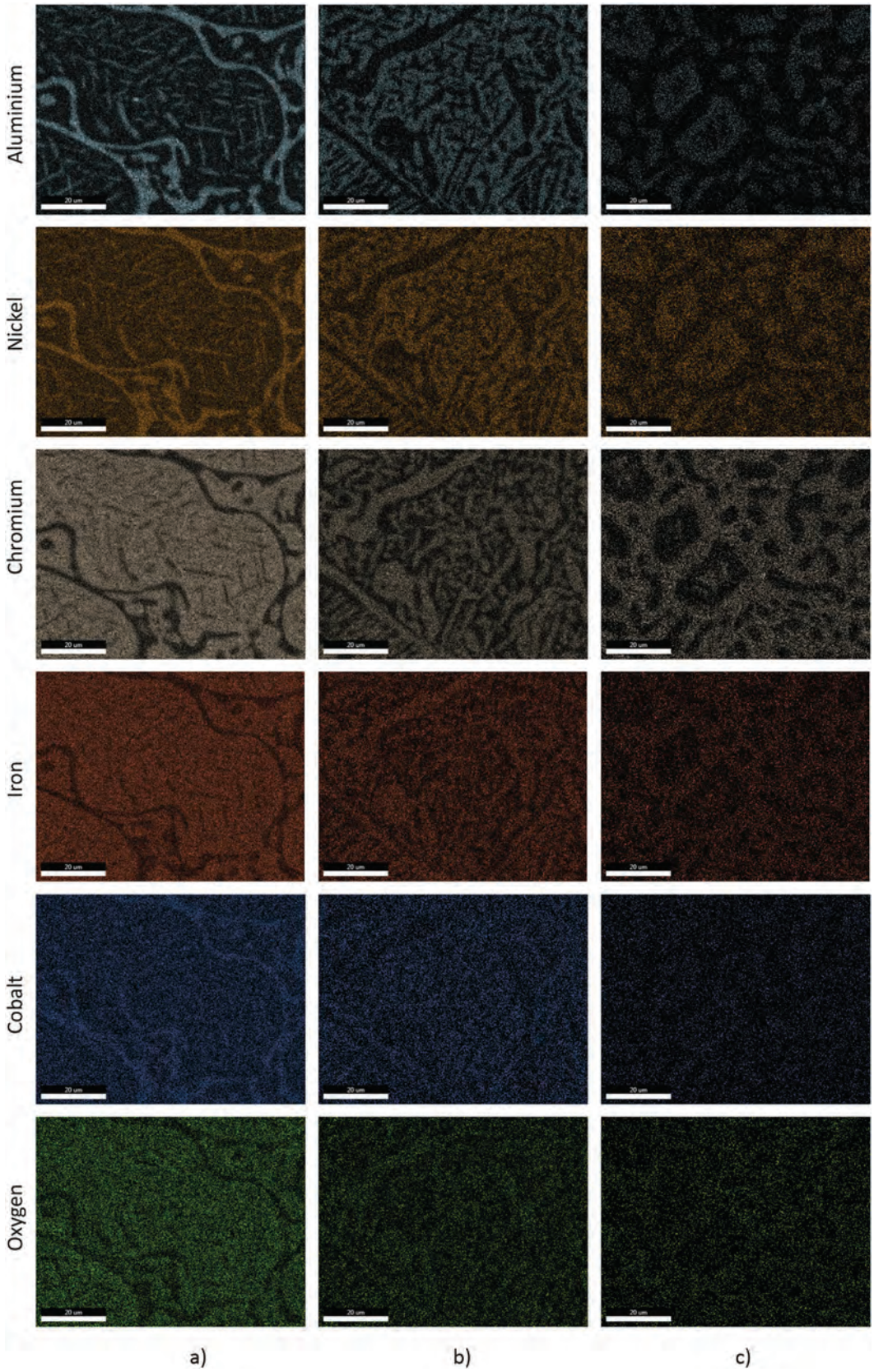

Figure 2. Atoms distribution of main elements of HEAs micro-area. (**a**) in Ni_1 TT sample; (**b**) $Ni_{1.4}$ TT sample; (**c**) $Ni_{1.8}$ TT sample.

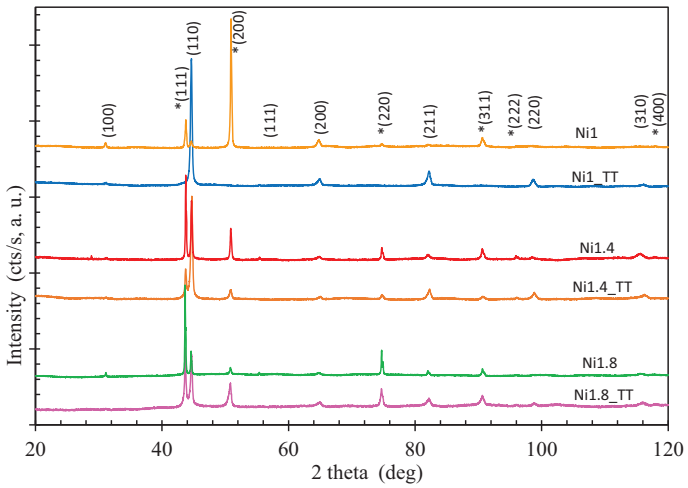

Figure 3. XRD patterns acquired from as-cast samples and from thermal treated samples (Miller indices for the new FCC phase induced by a higher Ni content are marked by symbol #).

	Pm-3m (PDF 04-018-5047)			Fm-3m (PDF 04-022-2301)		
Sample	Content (%)	Lattice parameter (Å)	Grain size (Å)	Content (%)	Lattice parameter (Å)	Grain size (Å)
Ni_1	100	2.876	398	–	–	–
$Ni_{1.4}$	78	2.870	414	22	3.595	327
$Ni_{1.8}$	37	2.873	365	63	3.599	402
Ni_1_TT	16	2.875	574	84	3.588	562
$Ni_{1.4}$_TT	73	2.871	937	27	3.591	1813
$Ni_{1.8}$_TT	75	2.872	1258	25	3.591	1259

Table 2. Samples phase composition, lattice parameters and grain size.

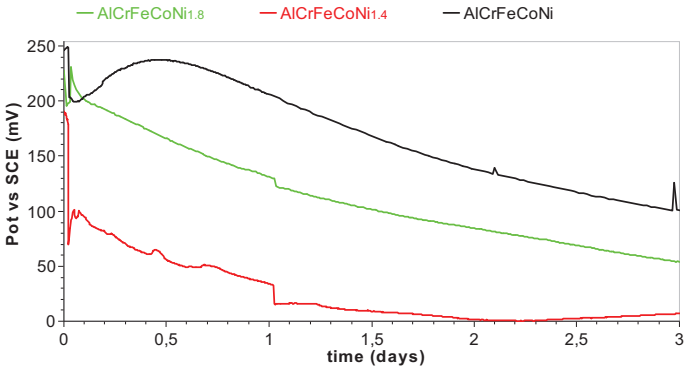

Figure 4. Variation of open circuit potential with time for the three alloys (AlCrFeCoNi, $AlCrFeCoNi_{1.4}$, $AlCrFeCoNi_{1.8}$) in Ringer solution.

After the OCP reaches the maximum value, it begins to decrease. This decrease is due to the changes in the characteristics of the surface film.

From the curves can be seen continuous breakages and repairs of the passive layer.

Potentiodynamic polarization result. Polarization techniques have been used respecting the indications of ASTM Subcommittee G01.11 on Electrochemical Measurements in Corrosion Testing regarding the reproducibility of cyclic potentiodynamic polarization measurements for determining the susceptibility to localized corrosion[30].

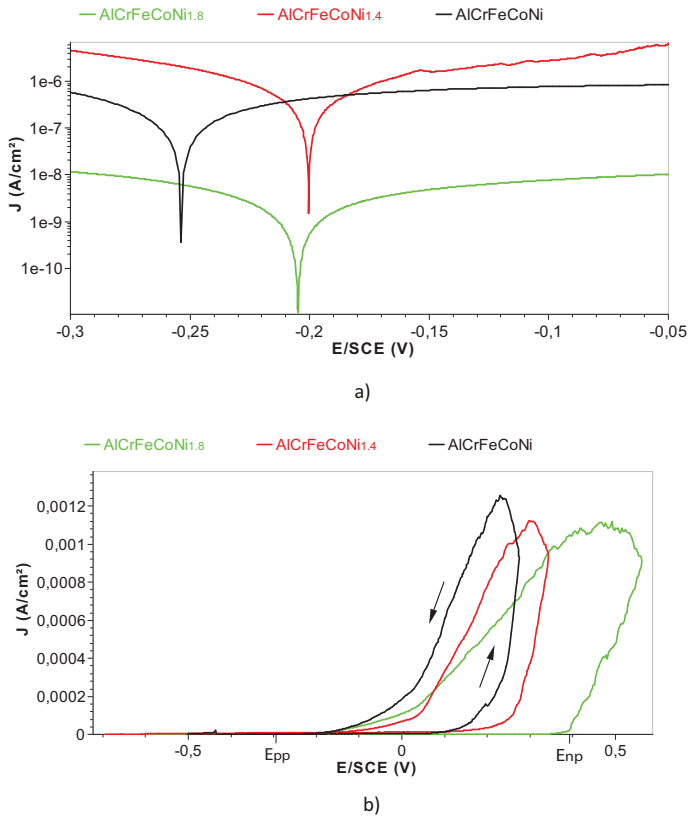

Figure 5. (**a**) Tafel curves for $AlCrFeCoNi_1$, $AlCrFeCoNi_{1.4}$ and $AlCrFeCoNi_{1.8}$ after one-week immersion. (**b**) Potentiodynamic polarization curves for AlCrFeCoNi, $AlCrFeCoNi_{1.4}$, $AlCrFeCoNi_{1.8}$ presented in linear axis in order to reveal the nucleation pitting potential and pitting protection potential).

Alloy	E_{corr} (mV)	i_{corr} (nA/cm²)	b_a (mV)	b_c (mV)	Corrosion rate (mmpy)
AlCrFeCoNi	− 255.59	428	638.4	255.1	5.92E−03
$AlCrFeCoNi_{1.4}$	− 199.7	748	169.2	124.5	3.00E−02
$AlCrFeCoNi_{1.8}$	− 206.86	374	347	185.8	1.25E−02

Table 3. Electrochemical parameters of corrosion process estimated through Tafel approximation.

1. Plots in a semi-logarithmic version between − 150 mV (vs OCP) and + 150 mV (vs OCP) after 1 week in Ringer solution are displayed (see Fig. 5a).

   The values of E_{corr}, i_{corr}, b_a, b_c and V_{corr} were determined by EC-Lab software and presented in Table 3. An alloy will corrode if b_c is greater than b_a and will be subjected to passivity if b_c is smaller than b_a. The higher values of b_a vs b_c for all the three alloys indicates an anodic control of the corrosion process which implies the existence of a passive layer on the sample's surface. The point resulted in the intersection of the two Tafel slopes has the coordinates i_{corr} and ZCP (zero current potential). It can be seen that in all the cases, the difference between OCP and ZCP is only few mV. This indicates that the errors introduced into the values of kinetic parameters are negligible with the variations of the charging current.

   The corrosion current densities obtained for the analyzed HEAs are much lower than that of the 304SS[31], which means that these HEAs are more resistant to general corrosion than 304SS.

   With the increase of Ni content, the corrosion rate of the alloy presents a non-linear trend mainly due to the fact that Ni content is not the only factor affecting the corrosion process (for example: microstructure, element distribution, etc.).
2. Pitting potential

   The pitting potential (or pit nucleation potential E_{np}) is one of the most important parameter characterizing the susceptibility of HEA to pitting corrosion. It is the potential at which the passive film formed on the HEA surface is damaged and the current density begins to increase drastically in the passive range due to the pits nucleations. Plots in a linear version of I vs E between − 0.8 V and + 0.5 V vs Ref (see Fig. 5b) were performed in order to determine the pit nucleation potential (pitting potential) and pitting protection potential (the potential in the reverse scan associated with a drop in current density caused by the repasivation of pits).

A scan rate of 1 mV/s was used and considered to be sufficiently slow to prevent any distortion of the curves. The values of nucleation pitting potential were 185 mV for AlCrFeCoNi, 245 mV for $AlCrFeCoNi_{1.4}$ and 385 mV for $AlCrFeCoNi_{1.8}$. The obtained values characterize the resistance of the analyzed HEA to pitting corrosion and can therefore be considered a measure of the susceptibility of HEA in simulated body fluid. $AlCrFeCoNi_{1.8}$ has the most positive pit nucleation potential: the more positive Enp, the more resistant the alloy is to pitting.

Among the three tested alloys, the difference between E_{np} and E_{pp} for $AlCrFeCoNi_{1.8}$ is the largest, which suggests that the repasivation tendency of pits on this alloy is large and only at higher potential these pits can transform to stable pits.

Microhardness. Five indentations have been made for each sample and the average value was calculated. The hardness values decrease with the increase of nickel concentration (562HV for AlCrFeCoNi, 455HV for $AlCrFeCoNi_{1.4}$ and 316HV for $AlCrFeCoNi_{1.8}$) as a result of dissolution of Cr and Fe precipitates in the nickel-rich matrix, forming a stable solid solution as we reported before[10]. For other HEA system, substitution of Al with different Zr concentrations, determine changes in the microhardness values, attributed to the phase changes in the alloy structure[23].

As has been demonstrated in a few studies[11,24] most metals and alloys exhibit strengthening effect by grain refinement due to the boundaries that function as impediments to dislocations. The decreasing of grain boundary density lead to the microhardness (and equivalent yield strength) values decreasing in HEAs which is consistent with the concept that the lattice of the crystal is seriously distorted and dislocations movement is more difficult than in conventional alloys[32,33].

Conclusions

In this study, the effects of nickel content on the microstructure, microhardness and corrosion behavior of high-entropy entropy $AlCoCrFeNi_x$ alloys in simulated body fluid were investigated and following conclusions were drawn:

1. The microscopy examination revealed the dendritic morphology for as cast alloy $AlCrFeCoNi_{1.0}$ and the increase of the extent of the interdendritic areas by increasing the nickel concentration for $AlCrFeCoNi_{1.4}$ and $AlCrFeCoNi_{1.8}$. The annealing determined a more uniform distribution of the phases for the three high-entropy alloys and the modification of the morphology of the grain boundaries. It also resulted in a significant increase of the grain sizes.
2. The formation after the annealing treatment of an Al-Ni compound is hypothesized, which should be corroded faster than the main HEA phase. There are several Al-Ni compounds having an FCC lattice and a lattice parameter very close to that of FCC AlCoCrFeNi.
3. The low corrosion rates and low corrosion currents demonstrate the good stability of the studied samples of $AlCoCrFeNi_x$ (x = 1.0, 1.4 and 1.8) in simulated biological environment.
4. The lattice parameter of the cubic phase varies very slightly, from 2876 to 2870 Å by increasing the Ni content, but the grain size decreases considerably (from 398 to 206 Å) for as-cast samples. For the FCC phase, the lattice parameters also vary very slightly but the grain size increases with the nickel content for both as-cast and annealing samples.
5. The results proved that by manipulating the composition and structure of HEAs their mechanical and chemical performance could be optimized to meet the requirements for their usage as novel medical instruments materials.

Data availability

The datasets generated during the current study are available from the corresponding author on reasonable request.

Received: 4 June 2020; Accepted: 17 November 2020
Published online: 03 December 2020

References

1. Yeh, J. W. & Lin, S. J. Breakthrough applications of high-entropy materials. *J. Mater. Res.* **33**, 3129–3137 (2018).
2. Zhang, Y. *High-Entropy Materials A Brief Introduction*. https://doi.org/10.1007/978-981-13-8526-1 (2019).
3. Ching, W. Y. *et al.* Fundamental electronic structure and multiatomic bonding in 13 biocompatible high-entropy alloys. *npj Comput. Mater.* **6**, 1–10 (2020).
4. Zhang, C. *et al.* Understanding phase stability of Al-Co-Cr-Fe-Ni high entropy alloys. *Mater. Des.* **109**, 425–433 (2016).
5. Csaki, I. *et al.* Researches regarding the processing technique impact on the chemical composition, microstructure and hardness of AlCrFeNiCo high entropy alloy. *Rev. Chim.* **67**, 1373–1377 (2016).
6. Yeh, J. W. *et al.* Nanostructured high-entropy alloys with multiple principal elements: Novel alloy design concepts and outcomes. *Adv. Eng. Mater.* **6**, 299-303+274 (2004).
7. Wang, Y. P., Li, B. S., Ren, M. X., Yang, C. & Fu, H. Z. Microstructure and compressive properties of AlCrFeCoNi high entropy alloy. *Mater. Sci. Eng. A* **491**, 154–158 (2008).
8. Ye, Y. F., Wang, Q., Lu, J., Liu, C. T. & Yang, Y. High-entropy alloy: challenges and prospects. *Mater. Today* **19**, 349–362 (2016).
9. Alabd Alhafez, I., Ruestes, C. J., Bringa, E. M. & Urbassek, H. M. Nanoindentation into a high-entropy alloy—an atomistic study. *J. Alloys Compd.* **803**, 618–624 (2019).
10. Voiculescu, I., Geanta, V., Stefanoiu, R., Patrop, D. & Binchiciu, H. Influence of the chemical composition on the microstructure and microhardness of alcrfeconi high entropy alloy. *Rev. Chim.* **64**, 1441–1444 (2013).

11. Li, Z., Zhao, S., Ritchie, R. O. & Meyers, M. A. Mechanical properties of high-entropy alloys with emphasis on face-centered cubic alloys. *Prog. Mater. Sci.* **102**, 296–345 (2019).
12. Chen, C., Pang, S., Cheng, Y. & Zhang, T. Microstructure and mechanical properties of. *J. Alloys Compd.* **659**, 279–287 (2016).
13. Yang, S., Liu, Z. & Pi, J. Microstructure and wear behavior of the AlCrFeCoNi high-entropy alloy fabricated by additive manufacturing. *Mater. Lett.* **261**, 127004 (2020).
14. Chen, J. *et al.* A review on fundamental of high entropy alloys with promising high-temperature properties. *J. Alloys Compd.* **760**, 15–30 (2018).
15. Miracle, D. B. & Senkov, O. N. A critical review of high entropy alloys and related concepts. *Acta Mater.* **122**, 448–511 (2017).
16. Shon, Y., Joshi, S. S., Katakam, S., Shanker Rajamure, R. & Dahotre, N. B. Laser additive synthesis of high entropy alloy coating on aluminum: corrosion behavior. *Mater. Lett.* **142**, 122–125 (2015).
17. Li, Q. H., Yue, T. M., Guo, Z. N. & Lin, X. Microstructure and corrosion properties of alcocrfeni high entropy alloy coatings deposited on AISI 1045 steel by the electrospark process. *Metall. Mater. Trans. A Phys. Metall. Mater. Sci.* **44**, 1767–1778 (2013).
18. Zhou, P. F., Xiao, D. H. & Yuan, T. C. Microstructure, mechanical and corrosion properties of AlCoCrFeNi high-entropy alloy prepared by spark plasma sintering. *Acta Metall. Sin. (English Lett.)* **33**, 937–946 (2020).
19. Yamanaka, K. *et al.* Corrosion mechanism of an equimolar AlCoCrFeNi high-entropy alloy additively manufactured by electron beam melting. *npj Mater. Degrad.* **4**, 1–12 (2020).
20. Shi, Y. *et al.* Homogenization of AlxCoCrFeNi high-entropy alloys with improved corrosion resistance. *Corros. Sci.* **133**, 120–131 (2018).
21. Shi, Y. *et al.* Corrosion of Al x CoCrFeNi high-entropy alloys : Al-content and potential scan-rate dependent pitting behavior. *Eval. Program Plann.* **119**, 33–45 (2017).
22. Chen, H. Y. *et al.* Effect of the substitution of Co by Mn in Al-Cr-Cu-Fe-Co-Ni high-entropy alloys. *Ann. Chim. Sci. Mater.* **31**, 685–698 (2006).
23. Feng, X. *et al.* Effect of Zr addition on microstructure and mechanical properties of CoCrFeNiZrx high-entropy alloy thin films. *Appl. Nanosci.* https://doi.org/10.1007/s13204-019-01057-7 (2019).
24. Huang, Y. C., Su, C. H., Wu, S. K. & Lin, C. A study on the hall-petch relationship and grain growth kinetics in FCC-structured high/medium entropy alloys. *Entropy* **21**, 297 (2019).
25. Geanta, V., Voiculescu, I., Vizureanu, P. & Victor Sandu, A. High entropy alloys for medical applications. *Eng. Steels High Entropy Alloys* https://doi.org/10.5772/intechopen.89318 (2020).
26. Qiu, Y. *et al.* Corrosion characteristics of high entropy alloys corrosion characteristics of high entropy alloys. *Mater. Sci. Technol.* **31**, 1235–1243 (2015).
27. Guérin, M. *et al.* Identification of the metallurgical parameters explaining the corrosion susceptibility in a 2050 aluminium alloy. *Corros. Sci.* **102**, 291–300 (2016).
28. Cao, L. *et al.* Microstructural evolution, phase formation and mechanical properties of multi-component AlCoCrFeNix alloys. *Appl. Phys. A Mater. Sci. Process.* **125**, 1–11 (2019).
29. Krapivka, N. A., Firstov, S. A., Karpets, M. V., Myslivchenko, A. N. & Gorban, V. F. Features of phase and structure formation in high-entropy alloys of the AlCrFeCoNiCux system (x = 0, 0.5, 1.0, 2.0, 3.0). *Phys. Met. Metallogr.* **116**, 467–474 (2015).
30. Baboian R. & Haynes, S. G. *Cyclic polarization measurements-experimental procedure and evaluation of test data*. https://doi.org/10.1520/STP28038S (1981).
31. Chen, Y. Y., Duval, T., Hung, U. D., Yeh, J. W. & Shih, H. C. Microstructure and electrochemical properties of high entropy alloys—a comparison with type-304 stainless steel. *Corros. Sci.* **47**, 2257–2279 (2005).
32. Liu, W. H., Wu, Y., He, J. Y., Nieh, T. G. & Lu, Z. P. Grain growth and the Hall–Petch relationship in a high-entropy FeCrNiCoMn alloy. *Scr. Mater.* https://doi.org/10.1016/j.scriptamat.2012.12.002 (2013).

Acknowledgements

The research was supported by the Romanian National Authority, Executive Agency for Higher Education, Research, Development and Innovation (CNCS CCDI—UEFISCDI), project number PN-III-P1-1.2-PCCDI-2017-239/60PCCDI and Romanian National Nucleu Program LAPLAS VI – contract n°. 16N/2019.

Author contributions

M. López Ríos—Conceptualization, methodology, writing—original draft preparation, investigation. P. Socorro Perdomo—data curation (Figs. 4, 5 and Table 3). V. Geanta—investigation, Figs. 1, 2 and Table 1, resources. I. Voiculescu—investigation (Figs. 1, 2, Table 1), data curation, writing—review and editing. V. Craciun—investigation (Fig. 3 and Table 2), data curation, writing—review and editing. I. Boerasu –investigations. J.Mirza Rosca: data curation, project administration, visualization, writing—review and editing (data curation, supervision, validation of data). All authors reviewed the manuscript and agreed to the published version of the manuscript.

Competing interests

The authors declare no competing interests.

Additional information

Correspondence and requests for materials should be addressed to J.C.M.R.

Reprints and permissions information is available at www.nature.com/reprints.

Publisher's note Springer Nature remains neutral with regard to jurisdictional claims in published maps and institutional affiliations.

doi:10.1017/S1431927621011260
Microsc. Microanal. 27 (Suppl 1), 2021

Static Testing and Fatigue Behavior of Three High-Entropy Alloys

Nestor Florido-Suarez[1], Pedro Socorro-Perdomo[1], Victor Geanta[2] and Julia Mirza-Rosca[1]

[1]University of Las Palmas de Gran Canaria, United States, [2]Politehnica University of Bucharest, United States

Introduction The term "high entropy alloys" (HEA) was first introduced in 2004 to describe alloys with multiple major elements in equiatomic or near-equiatomic proportions [1,2]. A novel metallurgy was created that did not consider one or two major elements with the others as only minor additions, but rather all elements solidifying on equal conditions from the liquid state. High entropy alloys (HEA), that have been identified as multicomponent alloys which contain a at least five metallic elements with quantities in the range of 5 - 35 %, can easily lead to multicomponent solid solution phases and yield an interesting combination of high strength and toughness performance, superior ductility, excellent wear and corrosion resistance. One of the basic alloy from HEA category, AlCoCrFeNi, was discovered in 2014 by Zhang's group at University of Science and Technology from Beijing, China [3]. Many other groups have joined the research effort to understand this HEA characteristics as microstructure, hardness, strength, friction, thermal and corrosion resistance [4]. Although many interesting topics have been explored, only few studies deal with fatigue properties of this high-entropy system, in general depending of fabrication method. Experimental The high entropy alloys from the system AlCrFeCoNi were obtained in the ERAMET Laboratory of the Politehnica University of Bucharest, using the MRF ABJ 900 Vacuum Arc Remelting (VAR) installation [5]. The theoretical degree of assimilation of the chemical elements during melting and the possible losses by vaporization were taken into account for designing the metallic charge. Highly pure raw materials, including Al, Cr, Fe, Co and Ni (at least 99.99%) were used. In order to obtain the adequate homogeneity, the obtained alloys were flipped and re-melted in VAR equipment for 6 times (3 times on each part) under inert atmosphere of Argon. Tensile tests were performed at room temperature using a standard ASTM E8M specimen. The tensile test was performed at an initial strain rate of 10-3s-1 using a Bose Electro Force 3100 universal testing machine (Bose Corporation, Minnesota, USA) and the tensile test was carried out three times for every alloy. The high cycle fatigue test was conducted employing a standard ASTM E466 specimen. High-cycle fatigue terms were a frequency of 20 Hz and a stress ratio of R = 0.1 at room temperature. The fatigue resistance (fatigue limit) was fixed at the maximum stress level that does not produce fractures at 106 cycles. Prior to fatigue testing, the specimens were ground using 600 - 2500 grit emery paper and 0.3 μm alumina suspension to significantly minimize the influence of surface roughness as mentioned in the laboratory protocol [6,7]. Results and discussion Currently, many test procedures and models have been employed to estimate the fatigue behavior of materials. However, various test methods and types of materials have a substantial impact on the evaluation of fatigue performance. Therefore, to analyze the fatigue characteristics of different materials under various test procedures, the strength and fatigue properties of high entropy alloys were evaluated through tensile and compression tests at several different loading rates and stress ranges. In this work, three high entropy alloys of the AlCrFeCoNi system were tested (see Fig. 1). Based on this, the strength creep surface models associated with the loading cycles and the unified normalized fatigue model of the analyzed alloys under different stress conditions were determined. By comparing the differences between the fatigue performance of the three alloys, the results reveal that the fatigue performance of the analyzed materials were totally distinct under various test procedures. The standard fatigue equation cannot estimate the effect of sample size and stress level on the fatigue properties. Therefore, the fatigue model obtained in this paper can solve these difficulties. It is of course also clear that the fatigue behaviour of one sample is better than that of the other two alloys when the stress value is low. Therefore, the fatigue lifetime of this sample is considerably more sensible to the stress value than that of the other two alloys. On the basis of the settlement and the comparative examination of the standardized models of the fatigue properties of different high entropy alloys, the scientific transformation from alloy fatigue

to structural fatigue is carried out, which offers perspectives on the anti-fatigue engineering of high entropy alloys. Conclusions The mechanical properties obtained from static testing and fatigue behavior of high-entropy alloys were correlated with other mechanical parameters (hardness and rugosity). From the comparison of the fatigue resistance grade of AlCrFeCoNi HEA with other metallic materials, it is clear that the fatigue resistance of the investigated materials is significantly higher than that of other tested materials.

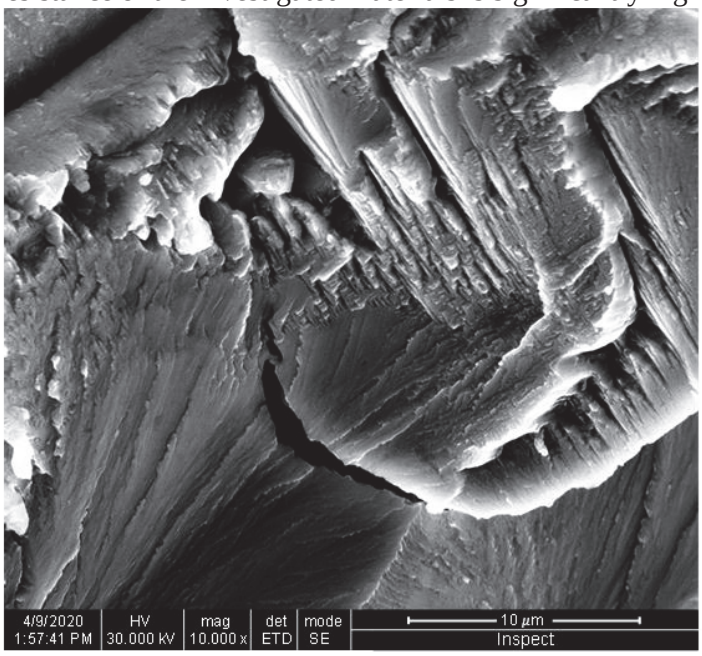

Figure 1. Fatigue fractography of the high-entropy alloy

References

[1] Ye YF, Wang Q, Lu J, Liu CT, Yang Y. High-entropy alloy: challenges and prospects. Mater Today 2016;19:349–62. https://doi.org/10.1016/j.mattod.2015.11.026.

[2] George EP, Raabe D, Ritchie RO. High-entropy alloys. Nat Rev Mater 2019;4. https://doi.org/10.1038/s41578-019-0121-4.

[3] Zhang Y. High-Entropy Materials A Brief Introduction. 2019. https://doi.org/10.1007/978-981-13-8526-1.

[4] López Ríos M, Socorro Perdomo PP, Voiculescu I, Geanta V, Crăciun V, Boerasu I, et al. Effects of nickel content on the microstructure, microhardness and corrosion behavior of high-entropy AlCoCrFeNix alloys. Sci Rep 2020;10:1–11. https://doi.org/10.1038/s41598-020-78108-5.

[5] Csaki I, Stefanoiu R, Geanta V, Voiculescu I, Sohaciu MG, Soare A, et al. Researches regarding the processing technique impact on the chemical composition, microstructure and hardness of AlCrFeNiCo high entropy alloy. Rev Chim2016;67:1373–7.

[6] Rosca JM, Perdomo PS, Suarez NF, Monzon Mayor M. Analysis of bone-implant interface with osseoinduction treatment. MicroscMicroanal 2020. https://doi.org/10.1017/S1431927620014142.

[7] Garcia-Falcon CM, Gil-Lopez T, Verdu-Vazquez A, Mirza-Rosca JC. Electrochemical characterization of some cobalt base alloys in Ringer solution. Mater Chem Phys 2021. https://doi.org/10.1016/j.matchemphys.2020.124164.

doi:10.1017/S1431927621011594
Microsc. Microanal. 27 (Suppl 1), 2021

Effect of Heat Treatment on the Microstructure and Corrosión Resistance of AlCoCrFeNi High-Entropy Alloy

Nestor Florido-Suarez[1], Pedro Socorro-Perdomo[1], Victor Geanta[2] and Julia Mirza-Rosca[1]

[1]University of Las Palmas de Gran Canaria, United States, [2]Politehnica University of Bucharest, United States

Introduction In the early 2000s, a distinctly different approach emerged based on conceptually equiatomic or near-equiatomic multicomponent alloys, commonly with five or more metallic elements, which were assumed to form stable single-phase solid solutions [1]. This stability was then attributed to the high entropy of the mixture coupled with a disordered multi-element solution, which was assumed to be in competition with the enthalpy of phase formation. This concept, initially proposed by Yeh et al [2] in Taiwan and separately by Cantor et al [3] in the UK, has come to be called high-entropy alloys (HEA) and has been found to be of great importance in the formulation of new alloys. AlCoCrFeNi is one of the most studied alloy systems from the area of high entropy alloys (HEA) due to it's attractive microstructure and mechanical properties. AlCoCrFeNi alloys are mainly prepared by vacuum arc remelting (VAR), which is based on the remelting of the raw elemental metals by means of the arc generated between the electrode and the metallic powder to be melted. However, arc remelting method requires high energy and the phase composition is not uniform, which is prejudicial to the mechanical properties of the alloy. It is often necessary to homogenize at high temperature and continue hot or cold working, followed by annealing treatment, to disintegrate the microstructure of the melt and thus obtain homogeneous materials with a fine-grained structure [4]. In this work the effect of annealing treatment on the microstructure and corrosion resistance of AlCoCrFeNi in simulated body fluid is studied for the possible use as new material for nuclear applications. Experimental procedure The alloy AlCoCrFeNi was obtained from high purity powders of Al, Cr, Co, Fe and Ni in a MRF ABJ 900 Vacuum Arc Remelting installation. The heat treatment consists of heating the samples at 1100ºC, maintaining them at this temperature during 72 hours and then cooling in water at room temperature. Microstructural characterization with Optical Microscopy (Zeiss AxioVert A1), Scanning Electron Microscopy and Energy-dispersive X-ray Spectroscopy (Fei XL30 ESEM with LaB6 cathode coupled to an EDAX Saphire) was performed. Electrochemical Impedance Spectroscopy (PAR 263A connected with a lock-in amplifier PAR 5210) was used to analyze the behavior of the samples in high concentration salts solutions and the results were correlated with the corrosion potential and the corrosion rate in the same conditions. Results and discussion It can be observed that the overall look of AlCoCrFeNi without heat treatment (see Fig.1) is polygonal grains with no obvious particles and only small pores and nanoprecipitates are detected. Two different zones are highlighted, one dendritic and other interdendritic with significant compositional differences of the elements. The nanoscale analysis revealed the dendritic region rich in Al and Ni but depleted in Cr and Fe and the interdendritic region rich in Cr and Fe but depleted in Al and Ni. Only cobalt shows no significant difference in the two areas with a somewhat higher concentration in the interdendritic zone. After heat treatment, a wall-shaped structure is predominant (see Fig.2). Both size and quantity of the precipitates increase, indicating that the heat treatment promote the homogeneous structure formation. The analysis indicates that the nanoscale precipitates are phases with all the elements (Ni, Cr, Al, Fe and Ni) of near-equimolar ratio and the matrix is Cr and Fe rich phase. Because the matrix is the predominant phase and in it the concentration of Cr is high, the predominant component of the uniform and compact passive film is Cr2O3 that successfully inhibits the contact of the chloride ions with the metallic surface, thus reducing more than 50 times the corrosion rate and improving the corrosion resistance of the alloy. Electrochemical Impedance Spectroscopy is a very powerful technique to study the corrosion performance of high entropy alloys in a very concentrated salt solution and the obtained results were confirmed by the other

electrochemical techniques employed in this study. Through all these techniques, information was obtained about the changes of the protective capacity of the passive layers, according with and without the heat treatment of the alloy and the exposure potential. Conclusions The heat treatment has a significant influence on the microstructure and the behavior of the alloys in simulated body fluid. With the heat treatment, the solidified microstructure varies from equiaxed dendritic grain to a wall-shaped structure with nanoprecipitates. The very high resistance of the heat treated alloy implies a high corrosion resistance which can be assigned to the formation of the protective chromium oxide layer. The obtained results demonstrate that the heat treatment alloy fulfill the prerequisites for its use as new material for nuclear applications.

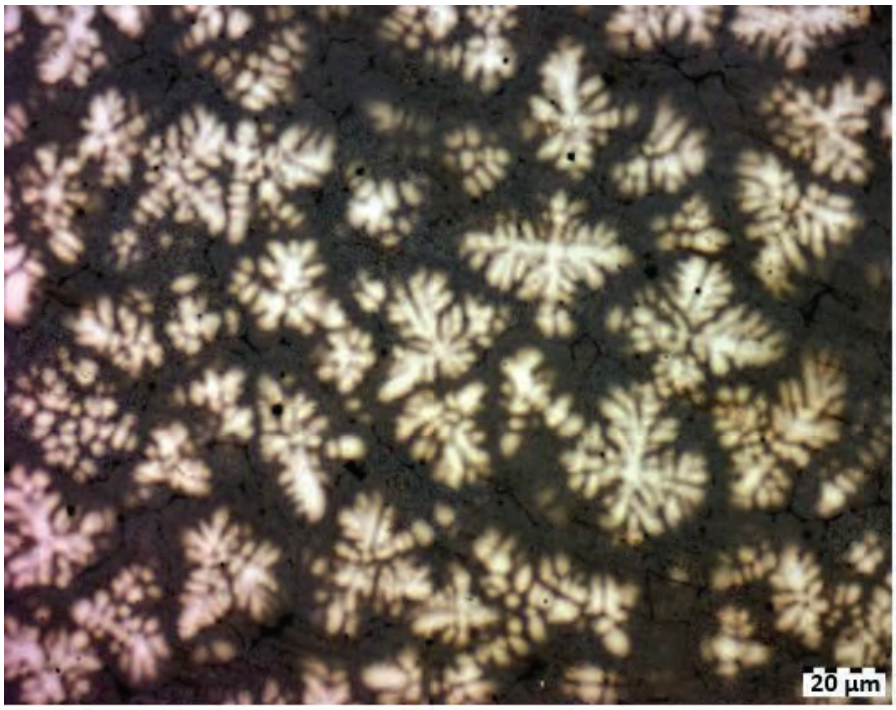

Figure 1. Fig.1 As-cast microstructure of AlCrFeCoNi alloy

https://doi.org/10.1017/S1431927621011594

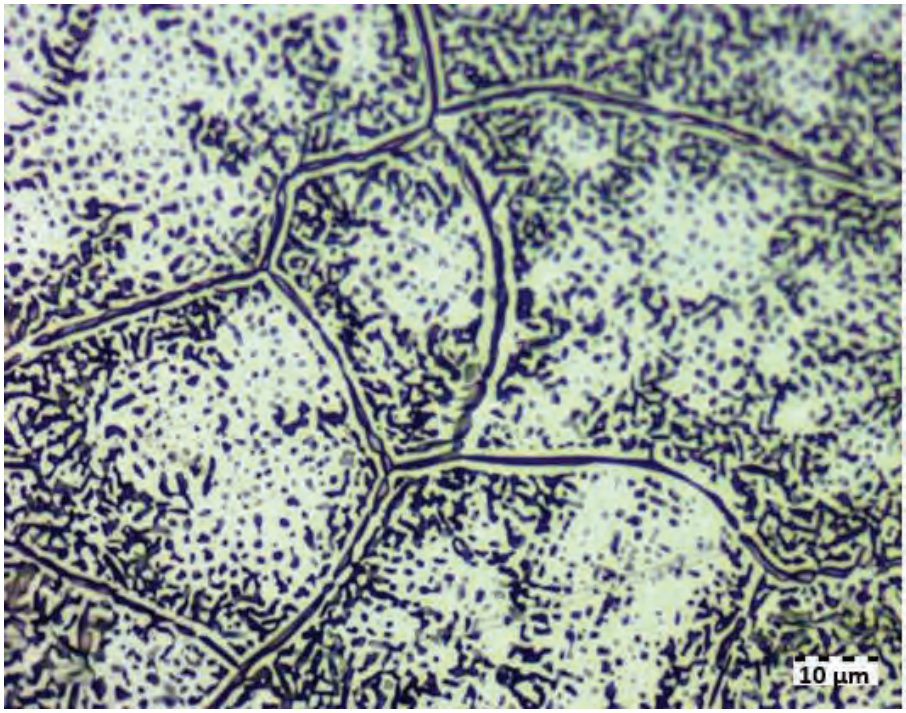

Figure 2. Fig.2 Heat treated microstructure of AlCrFeCoNialloy

References

[1] Z. Li, S. Zhao, R. O. Ritchie, and M. A. Meyers, "Mechanical properties of high-entropy alloys with emphasis on face-centered cubic alloys," *Progress in Materials Science*, vol. 102, no. March 2018, pp. 296–345, 2019, doi: 10.1016/j.pmatsci.2018.12.003.

[2] J. W. Yeh *et al.*, "Nanostructured high-entropy alloys with multiple principal elements: Novel alloy design concepts and outcomes," *Advanced Engineering Materials*, vol. 6, no. 5, pp. 299–303, 2004, doi: 10.1002/adem.200300567.

[3] B. Cantor, I. T. H. Chang, P. Knight, and A. J. B. Vincent, "Microstructural development in equiatomic multicomponent alloys," *Materials Science and Engineering A*, vol. 375–377, no. 1-2 SPEC. ISS., pp. 213–218, 2004, doi: 10.1016/j.msea.2003.10.257.

[4] López Ríos M, Socorro Perdomo PP, Voiculescu I, Geanta V, Crăciun V, Boerasu I, et al. Effects of nickel content on the microstructure, microhardness and corrosion behavior of high-entropy AlCoCrFeNix alloys. Sci Rep 2020;10:1–11. https://doi.org/10.1038/s41598-020-78108-5.

doi:10.1017/S1431927621008564
Microsc. Microanal. 27 (Suppl 1), 2021

Osseo-integration Improvement of Additive Manufactured Dental Alloys

Elena-Manuela Stanciu[1], Nestor Florido-Suarez[2], Pedro Socorro-Perdomo[2] and Julia Mirza-Rosca[2]

[1]Transilvania University of Brasov, United States, [2]University of Las Palmas de Gran Canaria, United States

Introduction

Titanium and titanium alloys, being biologically inert materials, are not chemically bonded to bone tissue. Consequently, in clinical use they must be fixed to the bone by mechanical interlocking, and the potentially loosening over an extended period can be a serious challenge (Zhang and Chen 2019; Kaur and Singh 2019). It has been found that biologically active materials, like hydroxyapatite and some glasses, were found that form strong chemical links with bone tissue and are being used extensively to fill bone defects. However, due to their brittleness, they are only suitable in situations where mechanical loads are absent or principally compressive. Titanium and its alloys are the most suitable to exhibit bioactivity in case of load-bearing components but must be previously subjected to a special surface treatment, involving changes in the passive film properties. In this paper, the improvement of osseointegration of two titanium alloys was studied.

Experimental

Ti-6Al-4V and Ti-6Al-4Fe alloys were obtained by Electron Beam Melting (Arcam AB, Sweden), built layer-by-layer on a titanium commercially pure grade 2 as substrate. The samples obtained in the form of flat discs (approx. 0.5 cm in diameter) were initially polished on a Struers Tegrapol-11 polishing machine (López Ríos et al. 2020) with emery discs of various sizes (800 to 3000) and then with diamond paste (0.1 μm) on a polishing cloth. The surface of each sample has been left as a mirror surface to ensure reproducibility of results (Pałka and Pokrowiecki 2018). The samples were immersed for one day in a 10M NaOH aqueous solution at a temperature of 60°C and then immersed for 3 months in Carter-Brugirard artificial saliva. For comparison, samples with the same composition but without chemical treatment were immersed in the same conditions to differentiate the effects of the treatment.

Data on mechanical and electrochemical behavior are reported. SEM observations of the surface film and EDX measurements were carried out. Elemental distribution by EDX maps were employed to establish the composition of the oxide layer, the alloy morphology and to detect any contamination particles. Optical metallography, Vickers microhardness and tensile tests were used to analyse the mechanical behavior. The electrochemical performance of these alloys was determined in artificial saliva by electrochemical polarization and electrochemical impedance spectroscopy.

Results and discussion

During the study of the mechanism of bone union of biologically active ceramics, it has been shown that the fundamental requirement for synthetic materials to be bonded to a living bone is the development of a bone-like apatite film on their surface.

The resulting apatite is very close in composition and structure to the bone material. Therefore, osteoblasts favourably regenerate and differentiate to form apatite and collagen in this apatite film and, consequently, the adjacent bone can come into proximal contact with the apatite film from the surface. After this happens, a vigorous chemical link is created between the bone minerals and the surface of the apatite layer to decrease the energy of the interface between both (Zhenhuan et al. 2020).

Titanium and its alloys are generally covered with a thin TiO2 passive layer, and hence is chemically durable. However, even this stable TiO2 layer reacts with NaOH solution to form a sodium titanate gel, and this layer can be stabilized as an amorphous sodium titanate by a suitable heat treatment (Kokubo et al. 2004). This sodium titanate layer forms many Ti-OH groups on its surface in the living body via the exchange of its Na+ ions from the surface with H3O+ ions in the surrounding body fluid.

The apatite layer is so tightly bonded to the substrates that a fracture occurs not at the apatite-substrate interface but in the glue or the apatite layer when a tensile stress is applied normally to the substrate at a crosshead speed of 1 mm.min-1 (see Fig.1 and Fig.2). The estimated adhesive strengths between the apatite layer and the substrate ranged from 9.8 to 11.5 MPa.

The observation that apatite deposition occurred better on the contact substrates indicates that the increase of pH in the simulated body fluid could play a decisive role in the formation of apatite on NaOH-treated alloys. Evidently, a much higher pH is predicted to accumulate in the gap under the contact substrates due to the narrow pathway for ion diffusion, while a higher pH, necessary for apatite nucleation, could not be achieved in the proximity of the open surface due to the greater ease of ion diffusion. Thus, the decisive role of ion diffusion in the bioactivity of sodium titanate gel can be demonstrated. It also suggests that the biologically activity of sodium titanate gel decreases with contact with aqueous solution because of the dissolution of the sodium component of the gel.

Conclusions

It turned out that the oxide films on the metal surface showed a tendency to passivation and very high stability and no evidence of any form of local corrosion was noted. The experimental electrochemical performance data of such layers were fitted by an equivalent circuit having two-time constants. The mechanical and EDX results support the existence of a porous outer passive film with a high oxygen concentration and a dense and protective inner passive film where titanium dioxide is the predominant compound. EIS results confirmed the mechanistic findings. The outcomes show that the employment of a surface processing improves the adherence of the passive film to the alloy surface and enhances the biocompatibility of the medical implants.

https://doi.org/10.1017/S1431927621008564

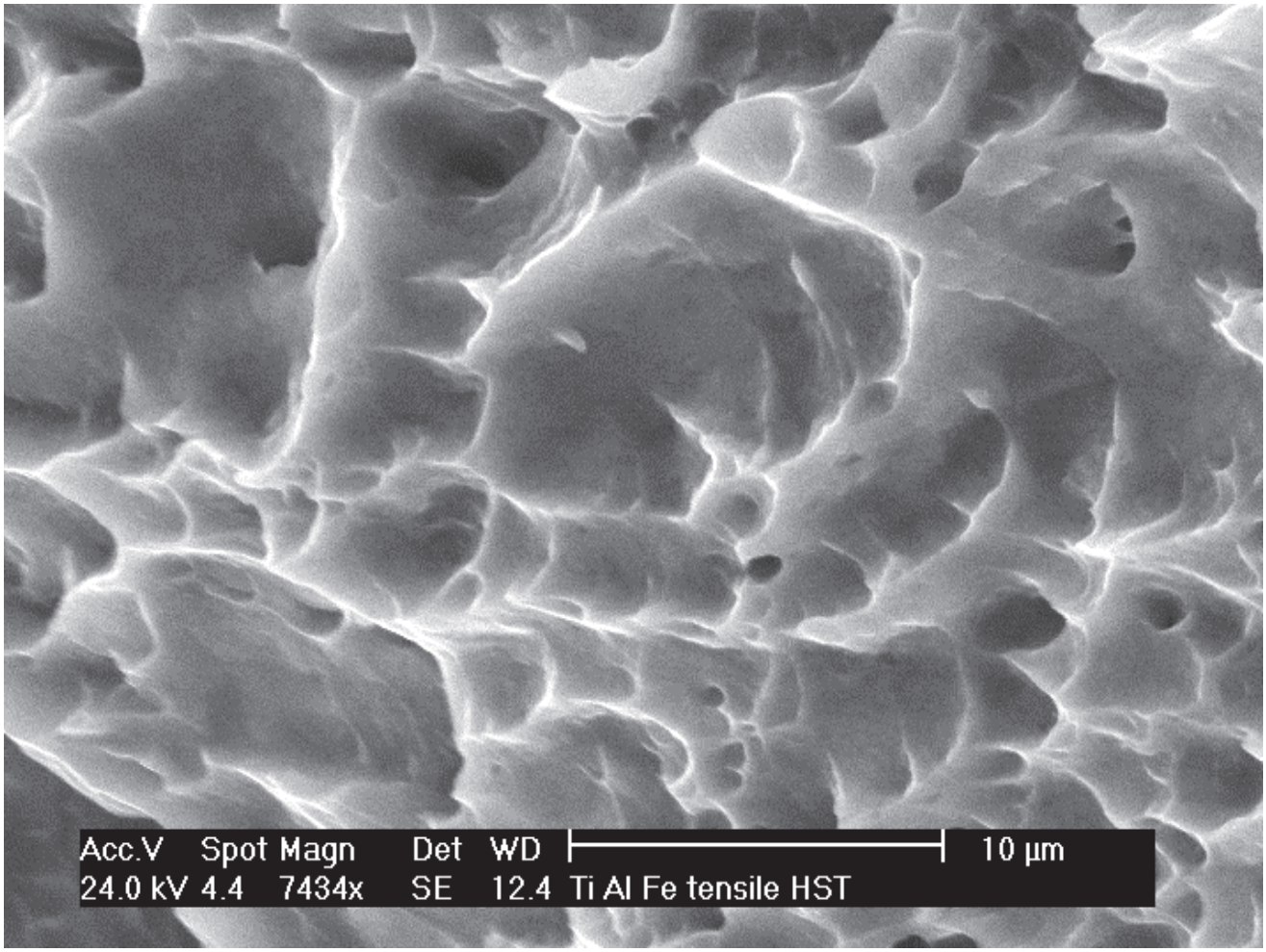

Figure 1. Fig.1 Ti6Al4Fe tensile test after NaOH treatment

https://doi.org/10.1017/S1431927621008564

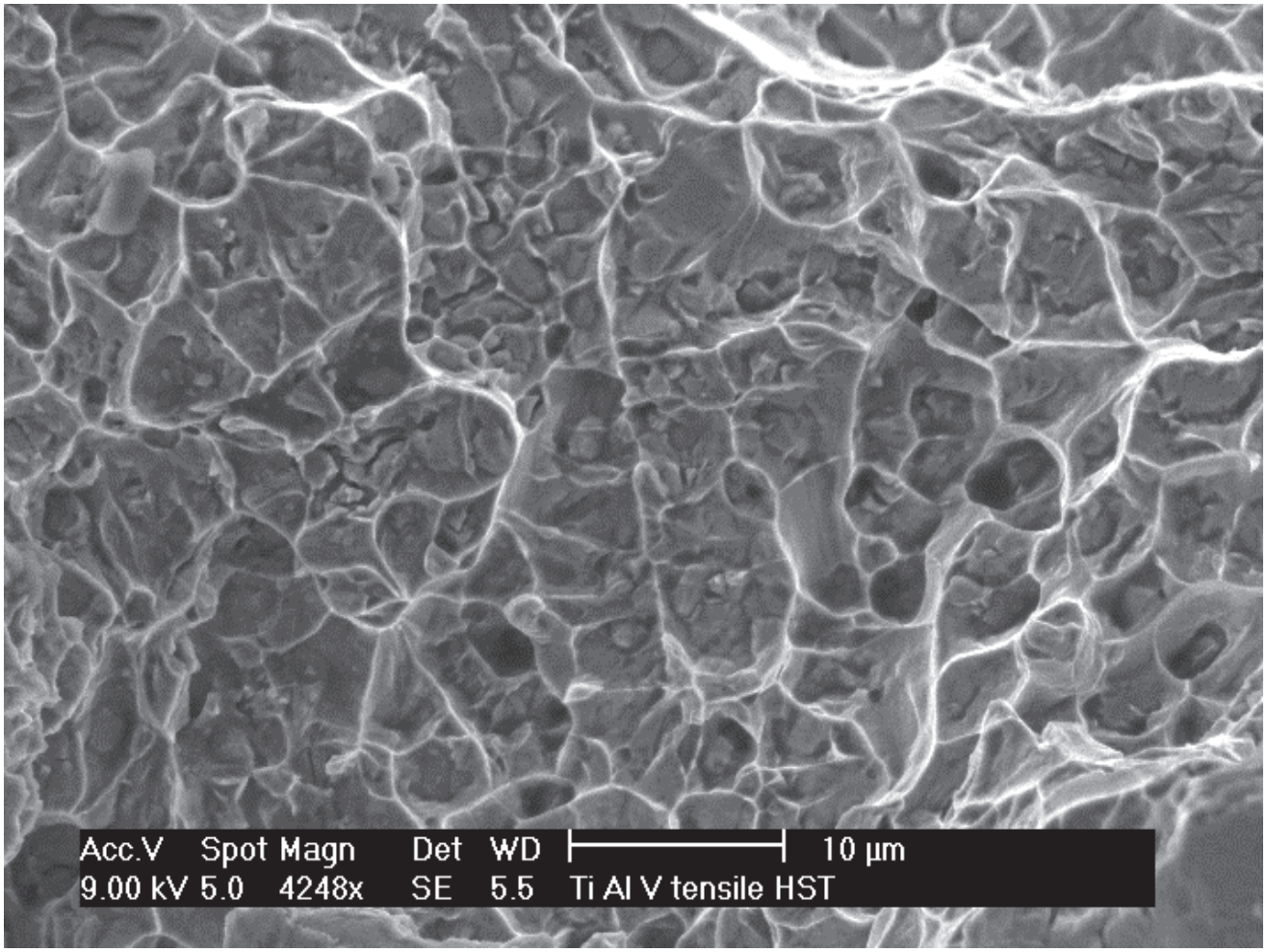

Figure 2. Fig.2 Ti6Al4V tensile test after NaOH treatment

References

Kaur, Manmeet, and K. Singh. 2019. "Review on Titanium and Titanium Based Alloys as Biomaterials for Orthopaedic Applications." *Materials Science and Engineering C*. https://doi.org/10.1016/j.msec.2019.04.064.

Kokubo, T., H.-M. Kim, M. Kawashita, and T. Nakamura. 2004. "Bioactive Metals: Preparation and Properties." *Journal of Materials Science: Materials in Medicine* 15 (2): 99–107. https://doi.org/10.1023/B:JMSM.0000011809.36275.0c.

López Ríos, M., P. P. Socorro Perdomo, I. Voiculescu, V. Geanta, V. Crăciun, I. Boerasu, and J. C. Mirza Rosca. 2020. "Effects of Nickel Content on the Microstructure, Microhardness and Corrosion Behavior of High-Entropy AlCoCrFeNix Alloys." *Scientific Reports*. https://doi.org/10.1038/s41598-020-78108-5.

Pałka, Krzysztof, and Rafał Pokrowiecki. 2018. "Porous Titanium Implants: A Review." *Advanced Engineering Materials*. https://doi.org/10.1002/adem.201700648.

Zhang, Lai Chang, and Liang Yu Chen. 2019. "A Review on Biomedical Titanium Alloys: Recent Progress and Prospect." *Advanced Engineering Materials* 21 (4): 1–29. https://doi.org/10.1002/adem.201801215.

Zhenhuan, Wu, Dai Yu, Luo Junsi, Ji Xiaowei, Xie Zongyu, Li Li, and Xie Xiaoli. 2020. "Physiochemical and Biological Evaluation of SLM-Manufactured Ti-10Ta-2Nb-2Zr Alloy for Biomedical Implant Applications." *Biomedical Materials (Bristol)* 15 (4). https://doi.org/10.1088/1748-605X/ab7ff4.

doi:10.1017/S1431927621006486
Microsc. Microanal. 27 (Suppl 1), 2021

Biocompatibility of New High-Entropy Alloys with Non-Cytotoxic Elements

Pedro Socorro-Perdomo[1], Nestor Florido-Suarez[1], Ionelia Voiculescu[2] and Julia Mirza-Rosca[1]

[1]University of Las Palmas de Gran Canaria, United States, [2]Politehnica University of Bucharest, United States

Introduction

In the 1980s, the possibility of creating alloys by combining different elements or materials began to be developed theoretically. By changing the proportion of each of the elements that form part of the alloy, the properties of the alloy can be improved, making the different components "work as a team", giving rise to materials with better behavior against corrosion attacks, others against impacts, etc. [1][2]. This theoretical development gave rise to the idea of high entropy alloys (HEA). In 1995, Professor Jen-Wei Yeh, National Tsing Hua University, Hsinchu, Taiwan, suggested making alloys using five or more different metals in similar proportions to make them alloys with many major elements. The name High Entropy Alloys is in fact due to the fact that the high stability of these alloys is because of their high entropy, which increases with the number of elements used for their preparation and composition. In parallel, Brian Cantor, from the University of Bradford, together with his research team, was also working with high entropy alloys [3]. It was Professor Yeh who gave the name to this type of alloys, but Brian Cantor, despite not referring to them with that terminology when working with them, developed a high-entropy alloy using the same number of atoms of each element, which has been and is the basis of the studies carried out since then within this field of research. In this work, the behavior of two HEA (High Entropy Alloys) of different composition, in simulated body fluid, is studied in order to determine whether these alloys are suitable for use in the field of medical prosthesis and implants.

Experimental

The studied materials, namely HEA 1 and HEA2, have the following composition:

HEA 1: 20.45%Mo, 32.45%Ta, 12.67%Ti, 18.97%Zr and 15.46%Fe

HEA 2: 17.32%Mo, 38.95%Ta, 13.21%Ti, 17.45%Zr and 13.07%Nb.

In order to characterize the properties of these two alloys, different electrochemical methods were used. Electrochemical Impedance Spectroscopy and the analysis of the spectra was carried out by fitting different equivalent circuits to the experimental data [4], [5]. The spectroscopy impedance results were correlated with the microstructure which was characterized by Optical Microscopy, Scanning Electron Microscopy and Energy-dispersive X-ray Spectroscopy.

The electrochemical studies were performed in Ringer solution, an isotonic solution typically composed of potassium chloride, sodium bicarbonate, calcium chloride and sodium chloride. A solution that resembles the plasma contained in the blood of human beings and is therefore useful for tests such as those carried out in this study, where the aim is to work by simulating as a working environment, body fluids, which help the body to balance its pH, the activation of muscles and nervous systems.

Results and discussion

The microstructures of the studied alloys are presented in Fig.1 and Fig.2.

Both HEA 1 and HEA 2 have an apparently homogeneous structure and the presence of dendrites due to the rapid cooling of these in the copper base where they have been manufactured can be clearly observed.

From the electrochemical tests we can say that HEA 1 has a lower corrosion potential than HEA 2, which means that HEA 1 is more susceptible to corrosion than HEA 2.

On the other hand, HEA 1 shows a pitting potential of 0.700 V and a repassivation potential of 0.331 V while HEA 2 is the most resistant to this type of corrosion, showing no damage during the test.

Conclusions

Both alloys exhibit spontaneous passivation with a low passive current density, low corrosion rate and high electrochemical impedance in Ringer solution, indicating a better bio-corrosion resistance than Ti6Al4V used nowadays. The good biocompatibility of the two alloys in simulated body fluid can be mainly attributed to the non-cytotoxic surface film and to the high corrosion resistance of the studied alloys. The surface film is non-cytotoxic because is consisted of oxides of high biocompatible elements as Nb, Ta and Ti. The high corrosion resistance leads to a less release of corrosion products during service life. Therefore, all the results further demonstrated the potential of the analyzed high-entropy alloys for biomedical applications.

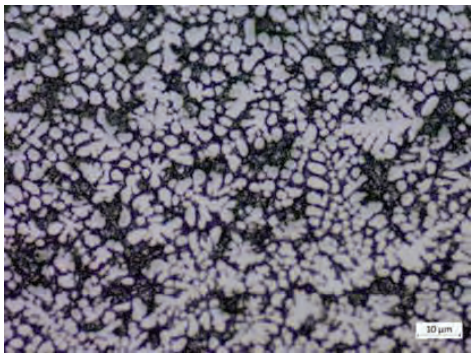

Figure 1. Microstructure of HEA1

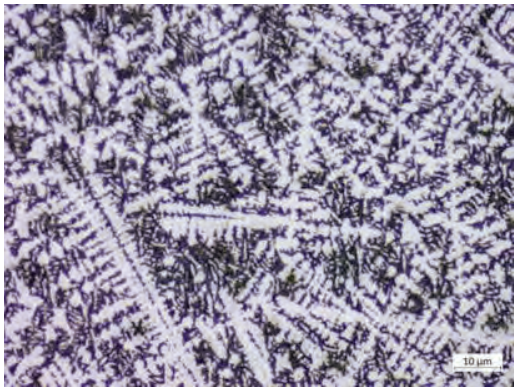

Figure 2. Microstructure of HEA2

References

[1] M. L. Rios, V. L. Baldevenites, I. Voiculescu, and J. M. Rosca, “AlCoCrFeNi High Entropy Alloys as Possible Nuclear Materials,” *Microsc. Microanal.*, 2020, doi: 10.1017/s1431927620014555.

[2] M. López Ríos *et al.*, “Effects of nickel content on the microstructure, microhardness and corrosion behavior of high-entropy AlCoCrFeNix alloys,” *Sci. Rep.*, vol. 10, no. 1, pp. 1–11, 2020, doi: 10.1038/s41598-020-78108-5.

[3] Y. F. Ye, Q. Wang, J. Lu, C. T. Liu, and Y. Yang, “High-entropy alloy: challenges and prospects,” *Materials Today*, vol. 19, no. 6. Elsevier B.V., pp. 349–362, Jul. 01, 2016, doi: 10.1016/j.mattod.2015.11.026.

[4] N. Ibriş and J. C. Mirza Rosca, "EIS study of Ti and its alloys in biological media," *J. Electroanal. Chem.*, 2002, doi: 10.1016/S0022-0728(02)00814-8.
[5] D. Mareci, G. Ungureanu, N. Aelenei, R. Chelariu, and J. C. M. Rosca, "Eis diagnosis of some dental alloys in artificial saliva," *Environ. Eng. Manag. J.*, 2007, doi: 10.30638/eemj.2007.034.

doi:10.1017/S1431927621011648
Microsc. Microanal. 27 (Suppl 1), 2021

Microstructure and Adjustment in Tensile Strength of $Al_{0.8}$CoCrFeNi Fibers

Nestor Florido-Suarez[1], Pedro Socorro-Perdomo[1], Ionelia Voiculescu[2] and Julia Mirza-Rosca[1]

[1]University of Las Palmas de Gran Canaria, United States, [2]Politehnica University of Bucharest, United States

Introduction

The notion of high entropy alloys is a significant new change in alloys design, as they emphasize compositions that are close to the center of a multicomponent phase diagram, in contrast to conventional alloys that are controlled by one basic element. The high entropy alloys can potentially stack solid-solution phases with respect to intermetallic compounds and can give rise to interesting properties such as superior hardness, notable toughness, superior fracture toughness and corrosion resistance [1][2] As potentially remarkable engineering alloys, the AlCoCrFeNi HEA system has stimulated considerable research activities because it possesses a series of attractive physical, chemical and mechanical qualities [3].

The objective of this research is the assessment of the microstructure progression and tuning of the mechanical properties of Al0.8CoCrFeNi fibers produced by cutting followed by annealing at 1100 °C. By thermomechanical treatment and microstructure monitoring, equilibrated tensile properties were obtained at room temperature. In comparison to the bulk as-cast alloy, the heat-treated fibers exhibit an elongation significantly major [4]. The disadvantage in improving the ductility of the fibers was a decrease in yield strength and fracture toughness.

Experimental

The Al0.8CoCrFeNi ingot was prepared from high purity elements by vacuum-arc melting. The molten ingot was cutted into very thin samples (0.5 mm in height) and prepared by grinding (2500 grit SiC abrasive paper) and then polishing them until they were optically flat (0.3μm alumina paste). High-entropy alloy fibers with diameters of 0.4 mm and 1.5 cm in length were then cut from these samples. Afterwards, the HEA fibers were annealed at 1100 °C for 15 min. Tensile tests were performed on a Bose Electro Force 3100 universal testing machine (Bose Corporation, Minnesota, USA) using a strain rate of 10-3s-1 at room conditions (approx. 22°C).

Results and discussion

It was observed that the fibers had an equiaxed grain structure after heat treatment. The ultimate tensile strength (σf), elongation at fracture (εf)) and yield strength (σy) of the fibers were determined. The tensile strength (σf) of the heat-treated fibers at room temperature is comparable to that of the as-cast Al0.8CoCrFeNi alloy.

Fracture images of alloys are routinely examined to identify possible deformation patterns and failure factors. Fig. 1 displays a fractograph of the core area of a typical tensile sample for the fiber with 0.4 mm diameter. The fracture surface morphology exhibits a typical ductile failure.

For Al0.8CrFeCoNi the EDAX nanoscale analysis revealed the dendritic region rich in Fe and Cr but depleted in Ni and Al and the interdendritic region rich in Al and Ni but depleted in Cr and Fe. Only cobalt shows no significant difference in the two areas with a somewhat higher concentration in the interdendritic zone.

It is well known that Co, Ni and Cr are extremely corrosion resistant elements and form a strong passive film on the surface. Co2+, Co3+, Ni2+ and Cr3+ species which are generated in the polarization process form a uniform and compact passive film that successfully inhibits the contact of the Cl- with the metallic surface, thus reducing the corrosion rate and improving the corrosion resistance of the alloy [5].

Conclusions

A systematical survey of the microstructure progression and its effect on the mechanical performance of Al0.3CoCrFeNi HEA fibers before and after annealing at 1100°C was carried out. The following conclusions were reached:

Tensile samples annealed at 1100 ℃ exhibit significant ductility, i.e., >15%, and higher tensile strength values. These outcomes indicate that the mechanical performance of HEA fibers can be customized to particular class of properties with an adequate selection of the high-entropy alloy and annealing temperature.

The improved ductility of high-entropy alloy fibers may be caused by the reduction of casting defects, the "curing" of small casting imperfections and the reduction of residual stress by annealing treatment and subsequent cutting process. These characteristics clearly demonstrate that the high-entropy alloys fibers can be recommended for low-dimensional products as wires, that require good strength, excellent thermal stability and high ductility.

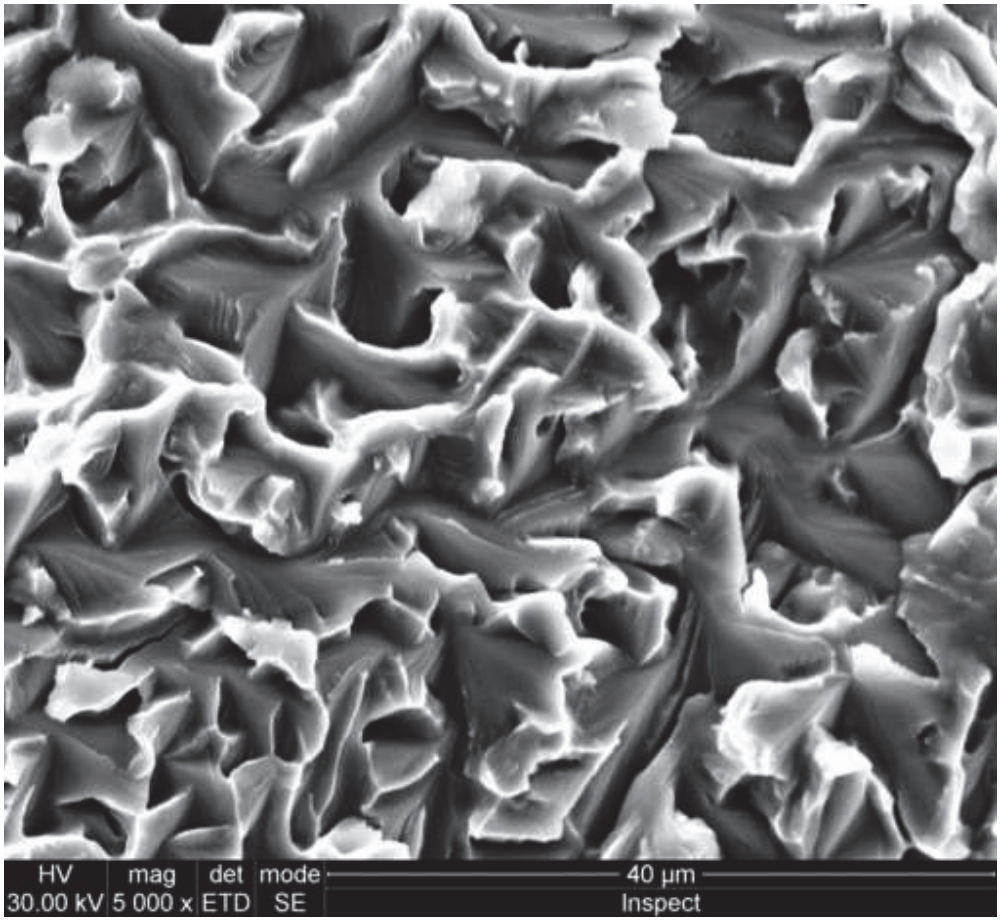

Figure 1. Fig.1 Fractograph of the core area of a tensile sample for the fiber with 0.4 mm diameter.

https://doi.org/10.1017/S1431927621011648

References

[1] Zhang Y. High-Entropy Materials A Brief Introduction. 2019. https://doi.org/10.1007/978-981-13-8526-1.

[2] Pascu A, Rosca JM, Stanciu EM. Laser cladding: From experimental research to industrial applications. Mater. Today Proc., 2019. https://doi.org/10.1016/j.matpr.2019.08.021.

[3] López Ríos M, Socorro Perdomo PP, Voiculescu I, Geanta V, Crăciun V, Boerasu I, et al. Effects of nickel content on the microstructure, microhardness and corrosion behavior of high-entropy AlCoCrFeNix alloys. Sci Rep 2020;10:1–11. https://doi.org/10.1038/s41598-020-78108-5.

[4] Li D, Gao MC, Hawk JA, Zhang Y. Annealing effect for the Al 0.3 CoCrFeNi high-entropy alloy fibers. J Alloys Compd2019;778:23–9. https://doi.org/10.1016/j.jallcom.2018.11.116.

[5] Garcia-Falcon CM, Gil-Lopez T, Verdu-Vazquez A, Mirza-Rosca JC. Electrochemical characterization of some cobalt base alloys in Ringer solution. Mater Chem Phys 2021. https://doi.org/10.1016/j.matchemphys.2020.124164.

550
doi:10.1017/S1431927621002415
Microsc. Microanal. 27 (Suppl 1), 2021

Study of Biocompatibility, Mechanical Properties and Microstructural Analysis af Ag-Pd Alloy

Jenifer Vaswani-Reboso, Nestor Florido-Suarez, Pedro Socorro-Perdomo and Julia Mirza-Rosca

University of Las Palmas de Gran Canaria, United States

Introduction

Using biomaterials to reconstruct damaged parts of the human body is a reality, and to do so they must meet a series of conditions and ensure a certain duration. Until relative recently, the biomaterials were basically engineering materials selected on the criteria of their ability to meet specific biological acceptability requirements. Nowadays, many of them are designed, produced, and manufactured with the unique objective of having an applicability in the medical sector [1] [2].

Regarding the alloys for dental use, it was found that, in addition to corrosion resistance, the different alloys with high noble metal content present mechanical and biological properties that are perfectly compatible for oral use. However, due to the economic situation and the consequent increase in the price of gold, the use of these alloys currently has very high costs for a significant fraction of patients. As a solution to this problem, the study of economically alternative alloys is proposed [3].

Due to their attractive properties from a dental point of view and not least due to their reduced price compared to gold, Ag-Pd alloys have been used extensively in prosthetic dentistry in recent years [4]. According to the classification system of the American Dental Association, Ag-Pd alloys are categorized as noble alloys, while Au-based alloys are considered high noble alloys [5].

Experimental

The study focuses on the alloy Ag-Pd-Cu-Au-Zn-Ir or PALLIAG (commercial name) which, even with a lower content of noble metals, still presents good resistance to corrosion, being suitable for use in the mouth.

The corrosion resistance of metals and their alloys is principally governed by the surface passivation process. In this way, the Palliag alloy should be examined more closely in order to acquire a better understanding of its behavior and to check its viability. Therefore, a study of the physical and mechanical properties will be made by means of metallographic aspects (with Zeiss AxioVert A1 optical microscope) and by means of Vickers hardness (with Buehler microhardness tester). Its electrochemical behavior will also be determined (using a PAR 263A potentiostat-galvanostat connected with a lock-in amplifier PAR 5210), which will allow the comparison of the trends exhibited. It is concluded that the chemical properties are acceptable when compared with reference dental alloys. This locally limits the passivity of the metal, a very small anodic area surrounded by a large cathodic area is generated and as a consequence, local corrosion (pitting) develops rapidly.

Results and discussion

The microstructure of the Palliag alloy after chemically attack is presented in Fig.1. The Vickers hardness was measured at different test loads (0.001; 0.005; 0.01, 0.025, 0.05 and 0.1 Kg) and a Vickers hardness footprint is shown in Fig.2.

The stabilization potential for the Palliag alloy at 40°C is -0.055V and it remains stable for the next 24 hours. These results show that this alloy does not suffer alterations by the electrolyte, this is indicative that they will present low corrosion speeds. This behavior is not indicative that the material is passivated, however, presents a stability that allows use as a dental prosthesis.

It is clear from this that it is a biphasic alloy in which there is an alpha and a beta phase, one soft (approx.110HV) and one hard (approx.180HV). With these obtained results, it is possible confirm that the alloy is homogeneous in all its area and thickness and that there is an absence of different layers superficial, as could be the case of some compact layer in the superficial of thickness considered.

Conclusions

According to the results obtained during the corrosion potential tests during 30 minutes and 24 hours at room temperature and at 40 ºC, it can be concluded the following:

After immersion in Ringer solution, the potential value of the sample studied decreases until it reaches equilibrium, when it stabilizes and remains constant.

The open circuit potential evolution of Ag-Pd is assigned to the passivation of the sample followed by an Ag superficially enrichment and the potential development of an insoluble AgCl film on the surface of the alloy.

The corrosion rate of the analyzed sample, calculated by means of Tafel's curves, tells us that its value is 0.012, which is very good.

It is concluded that the chemical and mechanical properties are acceptable when compared with reference dental alloys.

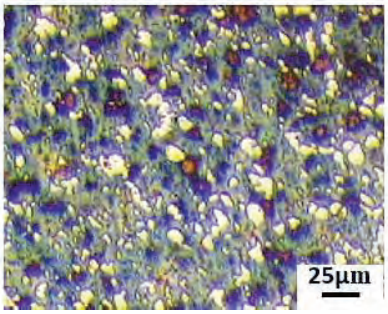

Figure 1. Figure 1. Metallographic analysis polished and chemically attacked surface

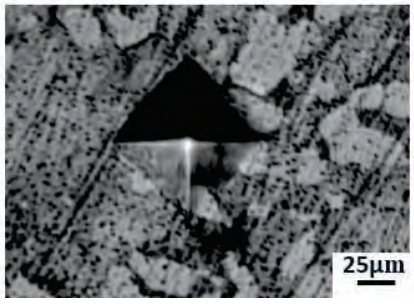

Figure 2. Figure 2. Vickers hardness footprint with 0.025 kgf load

https://doi.org/10.1017/S1431927621002415

References

[1] M. López Ríos *et al.*, "Effects of nickel content on the microstructure, microhardness and corrosion behavior of high-entropy AlCoCrFeNix alloys," *Sci. Rep.*, 2020, doi: 10.1038/s41598-020-78108-5.

[2] C. M. Garcia-Falcon, T. Gil-Lopez, A. Verdu-Vazquez, and J. C. Mirza-Rosca, "Electrochemical characterization of some cobalt base alloys in Ringer solution," *Mater. Chem. Phys.*, vol. 260, no. September 2020, p. 124164, 2021, doi: 10.1016/j.matchemphys.2020.124164.

[3] G. W. Ali, W. El-Hotaby, B. Hemdan, and W. I. Abdel-Fattah, "Thermosensitive chitosan/phosphate hydrogel-composites fortified with Ag versus Ag@Pd for biomedical applications," *Life Sci.*, 2018, doi: 10.1016/j.lfs.2017.12.021.

[4] A. Lubojanski *et al.*, "Application of selected nanomaterials and ozone in modern clinical dentistry," *Nanomaterials*. 2021, doi: 10.3390/nano11020259.

[5] A. D. Association, "Glossary of Dental Clinical and Administrative Terms," *Gloss. Dent. Clin. Adm. Terms*, 2014.

5.2 En revistas sin índice de impacto

Título:	Past Advances and Future Perspective of Ti-Ta Alloys	
Autores:	Nestor R Florido-Suarez, Amparo Verdu-Vazquez, Pedro P Socorro-Perdomo and Julia C Mirza-Rosca	
Revista: Global Journal of Engineering Sciences		
Editorial: Iris Publishers		
Mes/Año: 04/2021	Vol.: 7 Issue 3	Issn.: 2641-2039
	DOI: 10.33552/gjes.2021.07.000668	

Título:	Corrosion Behavior of two new Co-Cr dental alloys for porcelain-fused-to-metal crowns
Autores:	C.M.Garcia-Falcon, T.Gil-Lopez, P.P.Socorro-Perdomo, N.R.Florido-Suarez, J.C.Mirza-Rosca
Revista: International Journal of Medical Dentistry	
ISSN: 2066-6063	

Título:	New option for biomaterials of medical prosthesis and implants
Autores:	P.P. Socorro-Perdomo, N.R.Florido-Suarez, I.Voiculescu, V.Geanta, J.C. Mirza-Rosca
Revista: International Journal of Medical Dentistry	
ISSN: 2066-6063	

ISSN: 2641-2039
DOI: 10.33552/GJES.2021.07.000668
Global Journal of Engineering Sciences
Iris Publishers

Mini Review

Past Advances and Future Perspective of Ti-Ta Alloys

Nestor R Florido-Suarez[1], Amparo Verdu-Vazquez[2], Pedro P Socorro-Perdomo[1] and Julia C Mirza-Rosca[1]*

[1]*Mechanical Eng. Dept., University of Las Palmas de Gran Canaria, Spain*

[2]*Building Technology Dept., Politecnica University of Madrid, Spain*

***Corresponding author:** Julia C Mirza-Rosca, Mechanical Eng. Dept., University of Las Palmas de Gran Canaria, Spain.

Received Date: April 19, 2021

Published Date: April 26, 2021

Abstract

In the case of conventional Ti-based biomaterials, such as Ti-6Al-4V and Nitinol, the release of Al, V and Ni has been shown to be detrimental to the human body and in this context, Ti-Ta alloys have been proposed as one of the best options for biomedical devices. The main focus of this study is to review the different chemical composition of manufactured Ti-Ta alloys, their various techniques of fabrication as well as the microstructure, mechanical properties and corrosion resistance. The paper sought to give an idea of the scope of the research and effort that has gone into developing a high-quality titanium medical device.

Keywords: Ti-Ta alloys; Arc-melting; Microstructure; Mechanical properties; Corrosion; EIS

Introduction

The market request for suitable materials for permanent devices in the human body is growing as people live longer and their bones are weakening with age. The most widely used biomaterial today is titanium, whose corrosion resistance is due to the stability of the oxide film that grows on its surface and can be re-formed at human body temperature and in physiological media if injured. The use of Ti and its alloys as biomaterials is increasing due to their reduced modulus, higher biocompatibility, superior strength and increased corrosion resistance compared to conventional biomaterials such as stainless steel and Co-Cr alloys. But in the case of traditional Ti-based biomaterials such as Ti-6Al-4V and Nitinol, the liberation of Al, V and Ni has been shown to be detrimental to the human organism [1,2]. In this context, Ti-Ta alloys have been proposed as one of the best options for biomedical devices due to their exceptional biocompatibility in the human body environment, superior strength, relatively lower elastic moduli and superior corrosion resistance [3–5].

Chemical Composition of Titanium-Tantalum Alloys

Various types of binary titanium- tantalum alloys have been designed, manufactured and analyzed as follows: Ti-10Ta [6–10]; Ti-20Ta [10]; Ti-30Ta [6–8,10–12]; Ti-40Ta [6,10,12,13]; Ti-50Ta [6,8,10–15]; Ti-60Ta [6,10]; Ti-70Ta [7,10]; Ti-80Ta [6,10].

Fabrication

To present date, Ti-Ta alloys were satisfactorily produced by arc-melting [7,11–14,16,17], powder metallurgy [17,18], mechanical alloying [19,20] and additive manufacturing [21–25]. Scientists have made enormous efforts for the production of titanium-tantalum alloys by arc melting in a high-frequency induction furnace. Because of the large discrepancies in melting point and

density values of Ti and Ta, Ti-Ta alloys used to be remelted many times to obtain a homogeneous elemental composition, which entailed a long processing time. The challenge in the production process by the melting technique suggests that fabrication of the alloy by powder metallurgy is a reasonable option because it is a complete and simple technique that implies the fractionation and synthesis of the alloy. Although melting, powder metallurgy and mechanical alloying are able to manufacture Ti-Ta alloy ingots with good performances, it is however difficult to fabricate Ti-Ta alloy products with personalized complex shapes. Selective laser melting, SLM is a powder melting additive manufacturing AM process, can fabricate complex metallic devices directly from CAD models with a layer-by-layer method.

Microstructure Characterization

Tantalum has an α-BCC crystal structure and is an isomorphic β-stabilizer of titanium, which implies that the lattice pattern of the alloying element (tantalum in this case) is identical to the lattice pattern of the body-centered β-phase of titanium, BCC [26,27]. The α' phase is a distorted, hexagonal, closed-packet crystal framework which results from the uncompleted diffusion less conversion of the β-phase to the α phase [28]. The α´phase is stabilized by the addition of up to 10% or 20% Ta [29]. The α´´ phase is an orthorhombic martensitic crystal framework formed by the rapid cooling or quenching of Ti or Ti alloys from above the beta transus to below the beta transus [30]. There are experimental data that above 80%Ta s homogenous β-phase was stabilized [6,7,27,29]. The ω phase with the closed hexagonal HCP structure can be formed as a result of either β-zone cooling or during aging of quenched Ti alloys [31].

Thus, it is well established that in binary titanium-tantalum alloys there are only two stable solid phases (α and β) and four non-equilibrium solid phases (martensite α', α'', ω and metastable β phase) [19,27]. The formation of one phase or other depends on Ta content and posterior treatment of the alloy.

The microstructures of the Ti-Ta alloys were analyzed by X-ray diffraction analysis (XRD), scanning electron microscopy (SEM) and transmission electron microscopy (TEM). Metallographic examinations were also carried out to determine the as received and heat-treated microstructures [13].

Mechanical Properties

The tantalum concentration plays an essential contribution to the mechanical properties of Ti-Ta alloys. It is assumed that higher Ta concentration is not necessarily better for the improvement of the mechanical properties of titanium-tantalum alloys. Hardness values as a function of aging temperature were determined [6–8,13,15,32] and varies from 175HV 7 for Ti-10Ta to 743±12.93 for Ti-25Ta heat treated at 900 °C for 30 minutes. Dynamic Young's modulus and tensile tests were carried out on Ti-Ta alloys [3,6,8–11,14,15,21,33]. The Young´s modulus varies from 64 GPa for Ti-25Ta3 to 110 GPa for Ti-10Ta obtained by selective laser melting (SLM) [8]. The ultimate tensile strength has values from 500 MPa for Ti-10Ta 5 to 1029±8 MPa for Ti-25Ta 15.

The wear resistance of Titanium-Tantalum alloys and the biocompatibility were evaluated by assessing cytotoxicity through the MTT assay [7]. Between these techniques, to detect transus beta, electrical resistivity is a very accurate tool for measuring structural variations in Ti-based alloys [34,35].

Corrosion Resistance

Corrosion resistance of Ti-Ta alloys was validated by different dc techniques as open-circuit potential measurements, linear polarization, potentiodynamic polarization and coulometric zone analysis [6,7,12,13,15,36,37].

The electrochemical impedance spectroscopy (EIS) is employed to describe the performance of various metals and alloys in diverse media and to supply new information that could not previously be acquired with traditional direct current methods 38. Although there has been a substantial volume of research using EIS to analyze biomaterials, there are only a few with respect to EIS measurements on Ti-Ta alloys and Ti-Ta alloys [12,37,39].

It is noted that it is critical for all cases to develop proper impedance models, which can be employed to fit the experimental data and obtain the parameters that describe the corrosion process [38,39].

Conclusion

Ti-Ta alloys have not yet been widely adopted in medical applications and the primary reason is the difficulty in combining these two metals; in recent years, additive manufacturing processes have been successfully developed and approved for the fabrication of biomedical devices, including for Ti-Ta alloys. But detailed research on the effect of Ta concentration on the microstructure and performance of Ti-Ta alloys processed by additive manufacturing is still limited.

Acknowledgement

None.

Conflict of Interest

No conflict of interest.

References

1. Chen Q, Thouas GA (2015) Metallic implant biomaterials. *Mater Sci Eng R Reports* 87: 1-57.
2. Biesiekierski A, Wang J, Abdel-Hady Gepreel M, Wen CA (2012) New look at biomedical Ti-based shape memory alloys. *Acta Biomater* 8: 1661-1669.
3. Zhou YL, Niinomi M (2009) Ti-25Ta alloy with the best mechanical compatibility in Ti-Ta alloys for biomedical applications. *Mater Sci Eng C 29(3): 1061-1065*.
4. Zhou YL, Niinomi, M, Akahori T, Fukui H, Toda H (2005) Corrosion resistance and biocompatibility of Ti-Ta alloys for biomedical applications. *Mater Sci Eng A* 398: 28-36.

5. Zhou YL, Niinomi M, Akahori T (2008) Changes in mechanical properties of Ti alloys in relation to alloying additions of Ta and Hf. *Mater Sci Eng A* 483-484: 153-156.
6. Zhou YL, Niinomi M, Akahori T (2004) Effects of Ta content on Young's modulus and tensile properties of binary Ti-Ta alloys for biomedical applications. *Mater Sci Eng A* 371: 283-290.
7. DM Gordin, E Delvat, R Chelariu, G Ungureanu, M Besse *et al.* (2008) Characterization of Ti-Ta alloys synthesized by cold crucible levitation melting. *Adv Eng Mater* 10: 714-719.
8. Zhou YL, Niinomi M, Akahori T, Fukui H, Toda H (2005) Corrosion resistance and biocompatibility of Ti-Ta alloys for biomedical applications. *Mater Sci Eng A* 398: 28-36.
9. Huang S, Sing SL, de Looze G, Wilson R, Yeong WY (2020) Laser powder bed fusion of titanium-tantalum alloys: Compositions and designs for biomedical applications. *J Mech Behav Biomed Mater* 108: 103775.
10. Chen G, Yin J, Zhao S, Tang H, Qu X (2019) Microstructure and tensile properties of a Ti-28Ta alloy studied by transmission electron microscopy and digital image correlation. *Int J Refract Met Hard Mater* 81: 71-77.
11. Zhou YL, Niinomi M, Akahori T (2004) Decomposition of martensite α″ during aging treatments and resulting mechanical properties of Ti-Ta alloys. *Mater Sci Eng A* 384: 92-101.
12. Mareci D, Chelariu R, Gordin DM, Ungureanu G, Gloriant T (2009) Comparative corrosion study of Ti-Ta alloys for dental applications. *Acta Biomater* 5: 3625-3639.
13. EA Trillo, C Ortiz, P Dickerson, R Villa, SW Stafford. *et al.* (2001) Evaluation of mechanical and corrosion biocompatibility of TiTa alloys. *J Mater Sci Mater Med* 12: 283-292.
14. Zhou YL, Niinomi M (2008) Microstructures and mechanical properties of Ti-50 mass% Ta alloy for biomedical applications. *J Alloys Compd* 466: 535-542.
15. Danlei Zhao,Changjun Han,Yan Li,Jingjing Li,Kun Zhou. *et al.* Improvement on mechanical properties and corrosion resistance of titanium-tantalum alloys in-situ fabricated via selective laser melting. *J Alloys Compd* 804: 288-298.
16. Margevicius RW, Cotton JD (1998) Stress-assisted transformation in Ti-60 Wt pct Ta alloys. *Metall Mater Trans A Phys Metall Mater Sci* 29: 139-147.
17. JO Yin, G Chen, SY Zhao, Y Ge, ZF Li, *et al.* (2017) Microstructural characterization and properties of Ti-28Ta at.% powders produced by plasma rotating electrode process. *J Alloys Compd* 713: 222-228.
18. Barzilai S, Hayun S (2015) Mechanical alloying and thermal analysis of Ta-Ti alloys. *J Mater Sci* 50: 6833-6838.
19. MehdiShahedi Asl, Seyed Ali Delbari, Maziyar Azadbeh, Abbas Sabahi Naminid, Mehdi Mehrabian, *et al.* (2020) Nanoindentational and conventional mechanical properties of spark plasma sintered Ti-Mo alloys. *J Mater Res Technol* 9: 10647-10658.
20. Sing SL, Yeong WY, Wiria FE (2016) Selective laser melting of titanium alloy with 50 wt% tantalum: Microstructure and mechanical properties. *J Alloys Compd* 660: 461-470.
21. Sing SL, Wiria FE, Yeong WY (2018) Selective laser melting of titanium alloy with 50 wt% tantalum: Effect of laser process parameters on part quality. *Int J Refract Met Hard Mater* 77: 120-127.
22. Nicolas Soro, Hooyar Attar, Erin Brodie, Martin Veidt, Andrey Molotnikov, *et al.* (2019) Evaluation of the mechanical compatibility of additively manufactured porous Ti-25Ta alloy for load-bearing implant applications. *J Mech Behav Biomed Mater* 97: 149-158.
23. Huang S, Sing SL, de Looze G, Wilson R, Yeong WY (2020) Laser powder bed fusion of titanium-tantalum alloys: Compositions and designs for biomedical applications. *J Mech Behav Biomed Mater* 108: 103775 (2020).
24. Dutta B, Froes FH (2017) Additive manufacturing of titanium alloys. in *Additive Manufacturing Handbook: Product Development for the Defense Industry*.
25. Fuerst J, Medlin D, Carter M, Sears J, Voort G Vander (2015) LASER Additive Manufacturing of Titanium-Tantalum Alloy Structured Interfaces for Modular Orthopedic Devices 67.
26. Barzilai S, Toher C, Curtarolo S, Levy O (2016) Evaluation of the tantalum-titanium phase diagram from ab-initio calculations. *Acta Mater* 120: 255-263.
27. Peters M, Leyens C (2003) *Titanium and Titanium Alloys: Fundamentals and Applications*. *Titanium and Titanium Alloys Fundamentals and Applications*.
28. Dobromyslov AV, Dolgikh GV, Dutkevich Y, Trenogina TL (2009) Phase and structural transformations in Ti-Ta alloys. *Phys Met Metallogr* 107: 502-510.
29. Li C, Li G, Yang Y, Varlioglu M, Yang K (2011) Martensitic Twinning in Alpha + Beta Ti-3.5Al-4.5Mo Titanium Alloy. *J Metall*, 1-5.
30. Chen G, Yin J, Zhao S, Tang H, Qu X (2019) Microstructure and tensile properties of a Ti-28Ta alloy studied by transmission electron microscopy and digital image correlation. *Int J Refract Met Hard Mater* 81: 71-77.
31. Dercz G, Izabela Matula, Zubko Maciej, Alicja Kazek-Kesik, Maszybrocka Joanna, *et al.* Synthesis of porous Ti-50Ta alloy by powder metallurgy. *Mater Charact* 142: 124-136.
32. Buciumeanu M, Bagheri A, Souza JCM, Silva FS, Henriques B (2016) Tribology International Tribocorrosion behavior of hot pressed CoCrMo alloys in arti fi cial saliva. *Tribiology Int* 97: 423-430.
33. S Mendis, W Xu, HP Tang, LA Jones, D Liang, *et al.* (2020) Applied Surface Science Characteristics of oxide films on Ti- (10 - 75) Ta alloys and their corrosion performance in an aerated Hank ' s balanced salt solution. 506.
34. Wu C, Peng P, Chou H, Ou K (2018) Microstructural , mechanical and biological characterizations of the promising titanium-tantalum alloy for biomedical applications. *J Alloys Compd* 735: 2604-2610.
35. Gloriant T, G Texier, F Prima, D Laillé, DM Gordin, *et al.* (2006) Synthesis and Phase Transformations of Beta Metastable Ti-Based Alloys Containing Biocompatible Ta, Mo and Fe Beta-Stabilizer Elements. 8(10): 961-965.
36. Mareci D, Chelariu R, Gordin DM, Ungureanu G, Gloriant T (2009) Comparative corrosion study of Ti-Ta alloys for dental applications. *Acta Biomater* 5: 3625-3639.
37. Gloriant T, G Texier, F Prima, D Laillé, DM Gordin, *et al.* (2006) Synthesis and Phase Transformations of Beta Metastable Ti-Based Alloys Containing Biocompatible Ta, Mo and Fe Beta-Stabilizer Elements. 8(10): 961-965.
38. Scully J, Silverman D, Kendig M (1993) *Electrochemical Impedance: Analysis and Interpretation. 45(10): 582-582*.
39. Liu Y, Kaiyang Li, Hong Wu, Min Song, Wen Wang, *et al.* (2015) Synthesis of Ti-Ta alloys with dual structure by incomplete diffusion between elemental powders. *J Mech Behav Biomed Mater* 51: 302-312.

longer analogues, most probably due to more facile/efficient mixing and/or ordering of shorter polymer chains in the presence of micrometer sized RGO flakes.

Acknowledgements*: The authors acknowledge the financial support of the Romanian National Authority for Scientific Research and Innovation, CNCS – UEFISCDI, project no. PN-III-P2-2.1-PED-2019-3995.*

Keywords: *optoelectronic properties, polymers, graphene oxide.*

P11. HYDROGELS BASED ON PVA AND PULLULAN WITH SELF-HEALING BEHAVIOR

Raluca-Ioana Baron[1], Gabriela Biliuta[1], Sergiu Coseri[1]

[1]"Petru Poni" Institute of Macromolecular Chemistry, Iasi, Romania

Abstract

We have prepared and characterized composite hydrogels based on polyvinyl alcohol (PVA) and oxidized pullulan (OxP) using TEMPO reagent. Hydrogels prepared with varied content of OxP and PVA were subjected to the freeze/thaw technique. In order to evaluate the degree of interaction between the two polymers in the physical network, we used FTIR and NMR techniques. An excellent distribution of OxP inside the PVA matrix was noticed with the help of SEM images. An optimal composition was noted for the hydrogel with a content of 7.5% OxP, which is characterized by crystallinity and high resistance. Also, the self-healing ability of hydrogels was revealed, by the fact that after subjecting the sample to a large deformation, it recovers very quickly the initial structure. The favorable association between OxP and PVA through physical bonds recommends these hydrogels for biomedical applications.

Acknowledgements*: This work was supported by a grant from Ministry of Research and Innovation, CNCS - UEFISCDI, project number PN-III-P2-2.1-PED-2019-0169, acronym "HISENSE".*

Keywords: *hydrogels, pva, pullulan, self-healing behavior.*

P12. CELLULOSE - CARBON NANOTUBES HYBRID MATERIALS ACTING AS ELECTROMAGNETIC SHIELDING MATERIALS

Gabriela Biliuta[1], Raluca-Ioana Baron[1], Sergiu Coseri[1]

[1]"Petru Poni" Institute of Macromolecular Chemistry, Iasi, Romania

Abstract

A convenient approach for the preparation of cellulose - carbon nanotubes (CNT) hybrid materials owning electromagnetic shielding properties, based on viscose (V) and TEMPO-oxidized viscose fibers (VO) is proposed. Viscose - carbon nanotubes (V-CNT) and TEMPO-oxidized viscose - carbon nanotubes (VO-CNT) composites were prepared by embedding carbon nanotubes on the surface of two types of cellulose fibers, that is, viscose and its C6-oxidized derivative. The chemical composition, morphology, and thermal stability of the prepared hybrid materials were thoroughly investigated by FTIR, SEM, and thermogravimetric analyses.

Acknowledgements*: This work was supported by a grant of Ministry of Research and Innovation, CNCS-UEFISCDI, project number PN-III-P4-ID-PCE2020-0476, acronym EXCELLFUEL.*

Keywords: *nanotubes, electromagnetic, biomaterials.*

P13. CORROSION BEHAVIOR OF TWO NEW CO-CR DENTAL ALLOYS FOR PORCELAIN-FUSED-TO-METAL CROWNS

C.M. Garcia-Falcon[1], T. Gil-Lopez[2], P.P. Socorro-Perdomo[1], N.R. Florido-Suarez[1], J.C. Mirza-Rosca[1]

[1]University of Las Palmas de Gran Canaria, Spain

[2]Madrid Polytechnic University, Spain

Abstract

CoCr alloys have been used in dentistry for porcelain-fused-to-metal crowns due to their good biocompatibility, wear resistance, long service duration, good mechanical properties and last but

not least, superior corrosion. The present investigation evaluated and compared two new Co-Cr based dental alloys, studying their microstructures and corrosion behavior in Ringer solution using different techniques. The results of the study exhibit that the contact of alloys during 24-hours with Ringer's solution, from a qualitative point of view, reveals that both alloys show a high passivation tendency. The two alloys presented formation of protective layers on their surface after electrochemical treatment. The alloys showed a general corrosion behavior, homogeneous on the surface. In terms of susceptibility to corrosion, findings in this study show that all alloys investigated have a more than adequate corrosion resistance in Ringer´s solution, although one of the dental alloys presented a higher corrosion resistance than the other one.

Keywords: *Co-Cr dental alloys, corrosion, Ringer solution.*

P14. NEW OPTION FOR BIOMATERIALS OF MEDICAL PROSTHESIS AND IMPLANTS

P.P. Socorro-Perdomo[1], N.R. Florido-Suarez[1], I. Voiculescu[2], V. Geanta[2], J.C. Mirza-Rosca[1]
[1]University of Las Palmas de Gran Canaria, Spain
[2]Politehnica University of Bucharest, Romania

Abstract

The behavior of two High Entropy Alloys of different composition, in simulated body fluid, is studied in order to determine whether these alloys are suitable for use in the field of medical prosthesis and implants. The studied materials, have the following composition: A) 20.45%Mo, 32.45%Ta, 12.67%Ti, 18.97%Zr and 15.46%Fe; B) 17.32%Mo, 38.95%Ta, 13.21%Ti, 17.45%Zr and 13.07%Nb. In order to characterize the properties of these two alloys, different electrochemical methods were used. First of them was Electrochemical Impedance Spectroscopy and the analysis of the spectra was carried out by fitting different equivalent circuits to the experimental data. The spectroscopy impedance results were correlated with the microstructure which was characterized by Optical Microscopy, Scanning Electron Microscopy and Energy-dispersive X-ray Spectroscopy. The surface film is non-cytotoxic because is consisted of oxides of high biocompatible elements as Nb, Ta and Ti and all the results demonstrated the potential of the analyzed alloys for biomedical applications.

Keywords: *biomaterials, prosthesis, implants.*

P15. BIOCOMPATIBLE APATITIC MATERIALS FOR BONE TISSUE ENGINEERING: NEW APPROACHES IN MODERN MEDICINE

Toma Fistos[1,2], Roxana Ioana Brazdis[1,2], Anda Maria Baroi[1,3], Irina Fierascu[1,3], Radu Claudiu Fierascu[1,2]
[1]National Institute for Research & Development in Chemistry and Petrochemistry – ICECHIM, Bucharest, Romania;
[2]University "Politehnica" of Bucharest, Romania;
[3]University of Agronomic Sciences and Veterinary Medicine of Bucharest, Romania

Abstract

Approximatively 40% of the total human body weight is represented by bones, with specific shapes, sizes and structures. In the course of time, these skeletal tissues suffer from different diseases which damage their physical properties and good functioning. The most common treatments for fixing and replacing bone materials are metal implants due to their hard mechanical properties, but they also present several disadvantages: low biocompatibility, high possibility of corrosion and lack of anti-infection properties. In these recent years, the scientific area proposed the deployment of naturally synthesized biomaterials in bone tissue engineering. Hydroxyapatite (HAP), a calcium phosphate, represents an alternative solution for biomedical implants on the strength of its high biocompatibility, providing a quick fixation of the implant and creating a strong bond with the bone.

5.3 Capítulos de libros

ELECTRONIC POWER SYSTEM FOR THE DYNAMIC CORROSION CONTROL

J.M. Cabrera-Peña, N.R. Florido-Suarez*, P.P. Socorro-Perdomo, S.J. Brito-García, J.C. Mirza-Rosca

University of Las Palmas de Gran Canaria, Campus Tafira, Edificio Ingeniería, 35017, SPAIN

nestor.florido@ulpgc.es
Corresponding Author ORCID: 0000-0002-1824-6792

ABSTRACT

Introduction

Corrosion is currently a worldwide source of economic, material, environmental damage and in the worst case, even human loss due to corrosion in infrastructure. To combat it there are a variety of techniques and treatments, but even applying them in their strictest form, sooner or later, the phenomenon cannot be avoided. Cathodic protection is a technique used to control the corrosion of a metal surface by making it the cathode of an electrochemical cell. Impressed current cathodic protection systems consist of anodes that are connected to a power source that provides a perpetual source of electrical flow. This method can often provide much longer protection than a sacrificial anode, as the anode is supplied by an unlimited power source.

Purpose

The objective is the study, design and elaboration of the prototype, continuing a preliminary study called "Study of the protection against corrosion of a metallic structure" in order to introduce modifications and improvements to the prototype to allow to overcome corrosion in metallic structures.

Experimental

Therefore it is proposed a prototype based on cathodic protection is proposed, since it is defined as the method to reduce or eliminate the corrosion of a metal. To do this, the surface

must be made to function as a cathode when it is in an electrolyte, that is, a medium, whether aquatic, atmospheric or terrestrial. This is done by impressed current cathodic protection. Continuing with an already open line of research, design of a prototype starting from a DC - DC Buck - Boost converter to which a closed loop power system is incorporated, thus allowing control of the printing current and the relative humidity of the environment through of a voltage and humidity sensor, respectively.

For the characterization and viability of the prototype, different tests are carried out, among them, it tested in a salt spray chamber using steel specimens to test for corrosion by generation of an adverse environment in an accelerated manner.

Results and discussion

The conditions of the test, suppose an extreme reproduction to which any structure could face against the corrosion, the commutation between the values of intensity of polarization and maintenance can take a second plane, reason why all the attention was focused on the verification whether the current protection technique printed with the values calculated on the bias current during this line of research were capable of correctly protecting. When conducting the test using the impressed current technique, it was done with a zinc anode, a material that is not recommended for this type of protection due to its rapid consumption, which is why it has been changed in the current study for the installation of platinum anodes. The specific details of how structures are constructed can also add to the complexity — and therefore cost — of cathodic protection. In addition to this cost, the system also requires routine maintenance, including periodic visual inspection. In the case of impressed current cathodic protection there is also the ongoing cost of electricity. Sacrificial anodes in particular have a limited amount of current available, are subject to rapid corrosion, and therefore have a limited lifespan.

Conclusions

In conclusion, the design proposed for the device has flaws, so it would represent a new line of research open to optimization. Regarding the tests carried out in a saline mist chamber, they proved that a greater resistance to corrosion is achieved than that obtained with the control specimen, so that different ways of applying it could be analyzed. At the same time, it is interesting to continue with the use of the new tests on the cathodic protection technique by impressed current.

Keywords: *Corrosion, Cathodic Protection, Prototype*

A STUDY OF METALLIC GLASS $Al_{93}Ti_3Cr_2Fe_3$ FOR BIOMEDICAL APPLICATIONS

S.J. Brito-Garcia[1], P.P. Socorro-Perdomo[1], N.R. Florido-Suarez[1], T. Gil-Lopez[2], J.C. Mirza-Rosca[1*]

[1]*University of Las Palmas de Gran Canaria, Campus Tafira, Edificio Ingeniería, 35017, SPAIN*
[2] *Madrid Polytechnic University, Department of Building Technology, Madrid 28040, SPAIN*
julia.mirza@ulpgc.es
Corresponding Author ORCID: 0000-0003-0623-3318

ABSTRACT

Introduction

Metallic glasses are those which share the properties of both metals and glasses. As promising materials for different applications, metallic glasses are preferred over metals, ceramics, magnetic and some other types of existing materials due to their enhanced properties. Some of the important reasons for which we consider these glasses for specific application like biomaterials are discussed in this study.

Purpose

A study of two samples with the same chemical composition, $Al_{93}Ti_3Cr_2Fe_3$, produced by the "Metal spinning cooling" method but cooled at different speeds of the rotating wheel: one at 1700 rpm (which we call Al - 17) and the other at 2500 rpm (which we call Al - 25), is carried out to evaluate the possible biomedical applications. The thin film samples have thicknesses of less than 20µm and widths of no more than 5mm.

Experimental

For their characterization, mechanical and electrochemical tests are carried out, which will allow to know the main properties of the material in order to decide the possible biomedical applications of the alloys. A tensile test will be carried out to calculate the Young's modulus of elasticity and the tensile strength, a metallographic study in order to define the characteristics

of the microscopic structure of the alloys and, finally, corrosion tests, for the corrosion potential and corrosion rate determinations.

Results

To calculate the Young's modulus of elasticity E, the graphs are obtained with the values of each of the tested specimens. A rectilinear section of the graph is selected and we calculate the linear dispersion equation $y = ax + b$ where 'a' represents the slope of the line and gives us the E value. Finally, the coefficient of determination R^2 is calculated to verify the optimality of the model used. In all cases the value of R^2 is above 0.99 so we can say that the model fitts more than 99% of the calculated variable. The corrosion tests are performed in Ringer's solution, which simulates the physiological fluid of the human body. An open circuit potential test is performed and the evolution of the potential E is represented with respect to time and the profile of the obtained curve will allow us to know the tendency to passivation or to corrosion of each sample. A linear polarization is performed on each specimen in the electrolytic cell. The data are processed in the Ec-Lab program obtaining the values of corrosion current I_{corr} and the Tafel coefficients β_a and β_c from which the corrosion rate is calculated in mmpy.

Conclusions

The values of the tensile strength σ_{ten} can be considered low in comparison with other alloys used as titanium-based biomaterials or stainless steels, although in none of the two metallic glass samples studied is this value lower than that of cortical bone (50 - 150 MPa). To highlight the average value obtained for the σ_{ten} for the Al-25 sample, which is of the order of 2.2 times that of Al-17. In all the microphotographs taken of the metallic glass samples, without attack and with the attacks carried out with hydrofluoric acid, a non-crystalline structure is observed, as is to be expected in a material with a glassy structure. The samples studied show good corrosion behavior, although they show a notable increase in corrosion rate when tested at body temperature (40ºC). Comparing the corrosion rate between the samples Al-17 and Al-25 at each temperature analyzed, it is observed that Al-17 at room temperature has a corrosion rate increase of about 4.5 times with respect to the corrosion rate of Al-25. It is concluded that the Al-25 sample presents a better behavior as biomaterial due to the higher mechanical resistance, a low Young's modulus and a lower corrosion rate. The metallographic study confirms the amorphous structure of the samples, in none of the micrographs crystalline structures are observed.

Keywords: *Metallic glass, Tensile strength, Corrosion*

GLOBCER'21

Global Conference on Engineering Research

2-5 June 2021

GLOBAL CONFERENCE on ENGINEERING RESEARCH

Conference Proceedings

ISBN: 978-625-44365-9-8

Biocompatibility of High Entropy Alloys Based on FeMoTaTiZr AND MoTaNbTiZr

V.I. Iovu[*,1], P. Socorro-Perdomo[1], N. Florido-Suarez[1], I. Voiculescu[2], J.C. Mirza-Rosca[1]

[*]: viorel.iovu101@alu.ulpgc.es, ORCID: 0000-0003-0623-3318
[1]: *Dept. of Mechanical Engineering, University of Las Palmas de Gran Canaria, Spain*
[2]: *Faculty of Industrial Engineering and Robotics, Politehnica University of Bucharest, Romania*

ABSTRACT

Introduction: So far, a lot of metallic biomaterials have been developed, including various alloys. Yet, there is a great need in the field of medicine for solutions regarding metallic biomaterials with superior biocompatibility and mechanical properties capable of meeting the increasingly demanding requirements. Ti alloys are widely used as implants in the human body because of their great biocompatibility and low density but they don't have enough strength for most exigent devices [1]. High Entropy Alloys (HEAs) could be one of these solutions: they may potentially break the properties limits of traditional alloys based on one dominant element. A HEA consists of the mixture of at least five principal metallic elements with near equiatomic percentage [2]. Since the 2000s, extensive worldwide research has been carried out in this field and articles published in journals have grown exponentially.

Purpose: To carry out this study, we have received from the Polytechnic University of Bucharest a total of six samples of two different HEAs (three samples per alloy), named A and B, based on FeMoTaTiZr and MoTaNbTiZr, respectively. These alloys were obtained by vacuum arc remelting (VAR) from high purity raw materials. The main objective of the study is to determine the biocompatibility of both alloys. To do so, their microstructure will be examined through metallography and corrosion tests will be carried out to find out their behavior while submerged in a liquid which simulates the human body fluid.

Experimental: Before the analysis of the samples, they have undergone a preparation process that includes grinding and polishing on an automatic machine. Abrasive papers of SiC in successively finer grit sizes (from 300 - 2500) were used for grinding. The samples were polished with a soft polishing cloth and an agglomerated alpha alumina suspension. Then, the specimens were embedded in a resin to facilitate their handling and get more accurate results. The result after the preparation can be observed in Figure 1. Subsequently, the microstructure of the areas to be observed was revealed through chemical etching with Kroll's reagent and analyzed by bright-field microscopy.

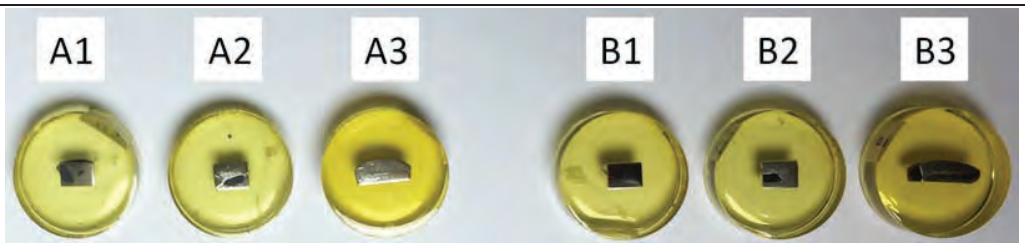

Figure 1 - Samples of HEAs A and B after preparation process

Results: During the macroscopic metallographic analysis non-homogeneous areas and porosity were observed on samples A1, A2, B1 and B2. This might be an indication that the melting and the mixture of the powders were not perfect. Samples A3 and B3 come from another melting batch and they seem to be more promising. Under the microscope the suspicion about the A1, A2, B1 and B2 specimens was confirmed. Figure 2 shows two main areas on sample A1 and B2, and even a microcrack on B2 can be seen; two main phases are observed with regular dendritic structures that have formed during a rapid cooling. Samples A2 and B1 show a very similar microstructure. A3 and B3 show a more homogeneous structure than the previous samples, yet the mixture is not perfect since two main areas are observable with diverse grain sizes. The homogenization process must be improved.

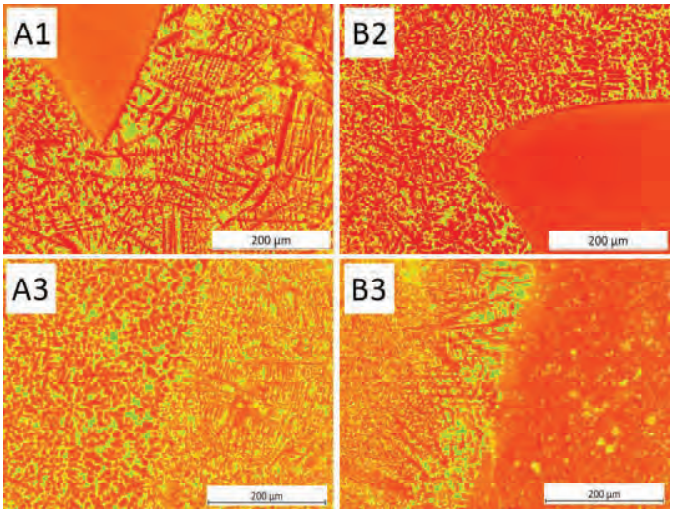

Figure 2 – Samples seen under the microscope after etching (x10 magnification)

From the corrosion tests we found out that HEA B has a higher corrosion potential, then HEA B is less susceptible to corrosion than HEA A. In addition, the pitting potential of HEA A is 0.7V while there are no clear signs of pitting on HEA B, it behaves passively. There are no signs of surface degradation on HEA B after the electrochemical attack either, this suggests HEA B has a good resistance to pitting due to the Nb presence in the composition of the alloy.

Keywords—*BioHEA; High Entropy Alloys; Biocompatibility; Mechanical Properties; FeMoTaTiZr; MoTaNbTiZr*

References

[1] M. López Ríos *et al.*, "Effects of nickel content on the microstructure, microhardness and corrosion behavior of high-entropy AlCoCrFeNix alloys," *Sci. Rep.*, vol. 10, no. 1, 2020, doi: 10.1038/s41598-020-78108-5.

[2] M. L. Rios, V. L. Baldevenites, I. Voiculescu, and J. M. Rosca, "AlCoCrFeNi High Entropy Alloys as Possible Nuclear Materials," *Microsc. Microanal.*, vol. 26, no. S2, 2020, doi: 10.1017/s1431927620014555.

APOLLONIA UNIVERSITY OF IAŞI

in collaboration with

Academy of Romanian Scientists

Iaşi branch

Proceedings of International Congress

"By promoting excellence we prepare the future"

- Selection of Abstracts -

1st-3rd of March 2021

IAŞI, ROMANIA

longer analogues, most probably due to more facile/efficient mixing and/or ordering of shorter polymer chains in the presence of micrometer sized RGO flakes.

Acknowledgements*: The authors acknowledge the financial support of the Romanian National Authority for Scientific Research and Innovation, CNCS – UEFISCDI, project no. PN-III-P2-2.1-PED-2019-3995.*

Keywords: *optoelectronic properties, polymers, graphene oxide.*

P11. HYDROGELS BASED ON PVA AND PULLULAN WITH SELF-HEALING BEHAVIOR

Raluca-Ioana Baron[1], Gabriela Biliuta[1], Sergiu Coseri[1]

[1]"Petru Poni" Institute of Macromolecular Chemistry, Iasi, Romania

Abstract

We have prepared and characterized composite hydrogels based on polyvinyl alcohol (PVA) and oxidized pullulan (OxP) using TEMPO reagent. Hydrogels prepared with varied content of OxP and PVA were subjected to the freeze/thaw technique. In order to evaluate the degree of interaction between the two polymers in the physical network, we used FTIR and NMR techniques. An excellent distribution of OxP inside the PVA matrix was noticed with the help of SEM images. An optimal composition was noted for the hydrogel with a content of 7.5% OxP, which is characterized by crystallinity and high resistance. Also, the self-healing ability of hydrogels was revealed, by the fact that after subjecting the sample to a large deformation, it recovers very quickly the initial structure. The favorable association between OxP and PVA through physical bonds recommends these hydrogels for biomedical applications.

Acknowledgements*: This work was supported by a grant from Ministry of Research and Innovation, CNCS - UEFISCDI, project number PN-III-P2-2.1-PED-2019-0169, acronym "HISENSE".*

Keywords: *hydrogels, pva, pullulan, self-healing behavior.*

P12. CELLULOSE - CARBON NANOTUBES HYBRID MATERIALS ACTING AS ELECTROMAGNETIC SHIELDING MATERIALS

Gabriela Biliuta[1], Raluca-Ioana Baron[1], Sergiu Coseri[1]

[1]"Petru Poni" Institute of Macromolecular Chemistry, Iasi, Romania

Abstract

A convenient approach for the preparation of cellulose - carbon nanotubes (CNT) hybrid materials owning electromagnetic shielding properties, based on viscose (V) and TEMPO-oxidized viscose fibers (VO) is proposed. Viscose - carbon nanotubes (V-CNT) and TEMPO-oxidized viscose - carbon nanotubes (VO-CNT) composites were prepared by embedding carbon nanotubes on the surface of two types of cellulose fibers, that is, viscose and its C6-oxidized derivative. The chemical composition, morphology, and thermal stability of the prepared hybrid materials were thoroughly investigated by FTIR, SEM, and thermogravimetric analyses.

Acknowledgements*: This work was supported by a grant of Ministry of Research and Innovation, CNCS-UEFISCDI, project number PN-III-P4-ID-PCE2020-0476, acronym EXCELLFUEL.*

Keywords: *nanotubes, electromagnetic, biomaterials.*

P13. CORROSION BEHAVIOR OF TWO NEW CO-CR DENTAL ALLOYS FOR PORCELAIN-FUSED-TO-METAL CROWNS

C.M. Garcia-Falcon[1], T. Gil-Lopez[2], P.P. Socorro-Perdomo[1], N.R. Florido-Suarez[1], J.C. Mirza-Rosca[1]

[1]University of Las Palmas de Gran Canaria, Spain

[2]Madrid Polytechnic University, Spain

Abstract

CoCr alloys have been used in dentistry for porcelain-fused-to-metal crowns due to their good biocompatibility, wear resistance, long service duration, good mechanical properties and last but

not least, superior corrosion. The present investigation evaluated and compared two new Co-Cr based dental alloys, studying their microstructures and corrosion behavior in Ringer solution using different techniques. The results of the study exhibit that the contact of alloys during 24-hours with Ringer's solution, from a qualitative point of view, reveals that both alloys show a high passivation tendency. The two alloys presented formation of protective layers on their surface after electrochemical treatment. The alloys showed a general corrosion behavior, homogeneous on the surface. In terms of susceptibility to corrosion, findings in this study show that all alloys investigated have a more than adequate corrosion resistance in Ringer´s solution, although one of the dental alloys presented a higher corrosion resistance than the other one.

Keywords: *Co-Cr dental alloys, corrosion, Ringer solution.*

P14. NEW OPTION FOR BIOMATERIALS OF MEDICAL PROSTHESIS AND IMPLANTS

P.P. Socorro-Perdomo[1], N.R. Florido-Suarez[1], I. Voiculescu[2], V. Geanta[2], J.C. Mirza-Rosca[1]
[1]University of Las Palmas de Gran Canaria, Spain
[2]Politehnica University of Bucharest, Romania

Abstract

The behavior of two High Entropy Alloys of different composition, in simulated body fluid, is studied in order to determine whether these alloys are suitable for use in the field of medical prosthesis and implants. The studied materials, have the following composition: A) 20.45%Mo, 32.45%Ta, 12.67%Ti, 18.97%Zr and 15.46%Fe; B) 17.32%Mo, 38.95%Ta, 13.21%Ti, 17.45%Zr and 13.07%Nb. In order to characterize the properties of these two alloys, different electrochemical methods were used. First of them was Electrochemical Impedance Spectroscopy and the analysis of the spectra was carried out by fitting different equivalent circuits to the experimental data. The spectroscopy impedance results were correlated with the microstructure which was characterized by Optical Microscopy, Scanning Electron Microscopy and Energy-dispersive X-ray Spectroscopy. The surface film is non-cytotoxic because is consisted of oxides of high biocompatible elements as Nb, Ta and Ti and all the results demonstrated the potential of the analyzed alloys for biomedical applications.

Keywords: *biomaterials, prosthesis, implants.*

P15. BIOCOMPATIBLE APATITIC MATERIALS FOR BONE TISSUE ENGINEERING: NEW APPROACHES IN MODERN MEDICINE

Toma Fistos[1,2], Roxana Ioana Brazdis[1,2], Anda Maria Baroi[1,3], Irina Fierascu[1,3], Radu Claudiu Fierascu[1,2]
[1]National Institute for Research & Development in Chemistry and Petrochemistry – ICECHIM, Bucharest, Romania;
[2]University "Politehnica" of Bucharest, Romania;
[3]University of Agronomic Sciences and Veterinary Medicine of Bucharest, Romania

Abstract

Approximatively 40% of the total human body weight is represented by bones, with specific shapes, sizes and structures. In the course of time, these skeletal tissues suffer from different diseases which damage their physical properties and good functioning. The most common treatments for fixing and replacing bone materials are metal implants due to their hard mechanical properties, but they also present several disadvantages: low biocompatibility, high possibility of corrosion and lack of anti-infection properties. In these recent years, the scientific area proposed the deployment of naturally synthesized biomaterials in bone tissue engineering. Hydroxyapatite (HAP), a calcium phosphate, represents an alternative solution for biomedical implants on the strength of its high biocompatibility, providing a quick fixation of the implant and creating a strong bond with the bone.

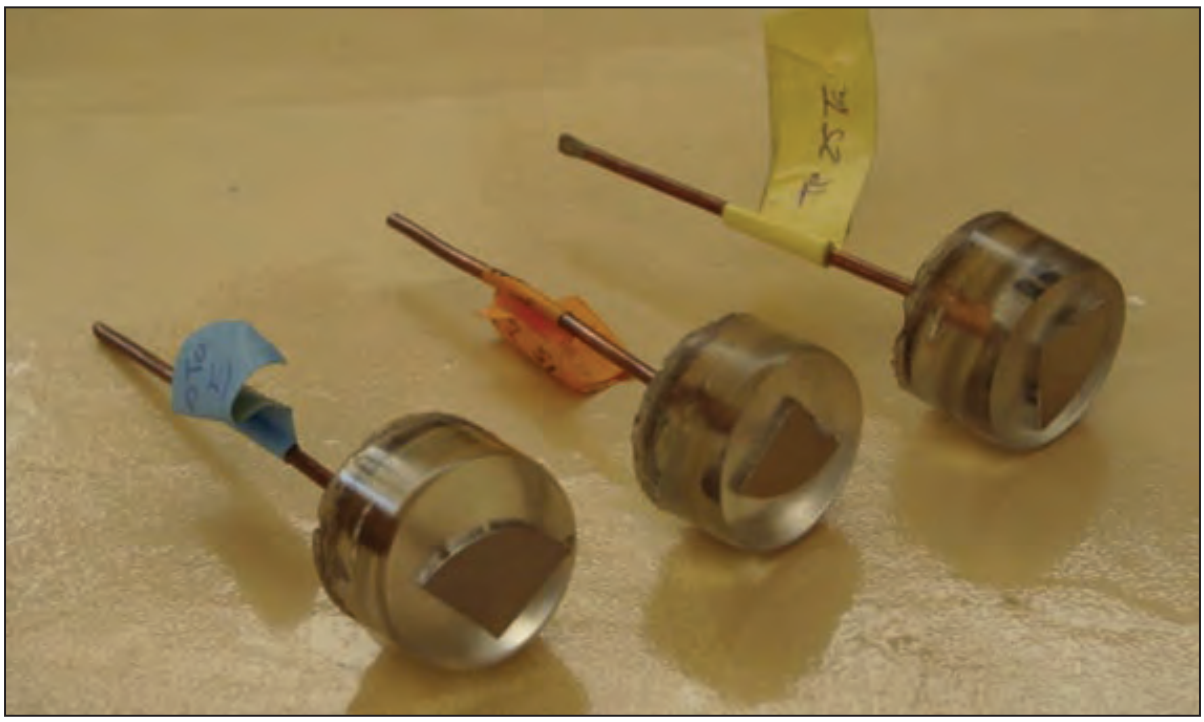

Eventos científicos 6

BIOREMED2019

International Seminar on Biomaterials and Regenerative Medicine

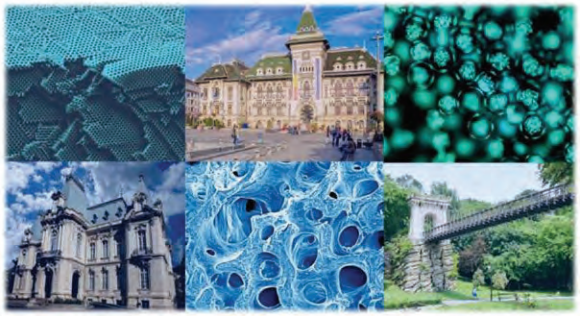

September 26-28, 2019
Craiova, Romania

SRB
Societatea Română de Biomateriale

www.srb.ro

COMPARATIVE STUDY OF DIFFERENT NI-CR DENTAL MATERIALS FOR CASTING DENTAL CROWNS AND BRIDGES

L.S. Baltes[1], P.P. Socorro Perdomo[2], J.C. Mirza Rosca[3*], M.H. Tierean[4]

[1] Department of Materials Engineering and Welding,Transilvania University of Brasov, 29 Eroilor Blvd., 500036, Brasov, Romania,e-mail:baltes@unitbv.ro
[2]Department of Mechanical Engineering, University of Las Palmas de Gran Canaria (ULPGC), Tafira 35017, Canary Islands, Spain, e-mail:pedro.soccoro@ulpgc.es
*[3] Department of Mechanical Engineering, University of Las Palmas de Gran Canaria (ULPGC), Tafira 35017, Canary Islands, Spain,*corresponding author e-mail: julia.mirza@ulpgc.es*
[4]Department of Materials Engineering and Welding,Transilvania University of Brasov, 29 Eroilor Blvd., 500036, Brasov, Romania,e-mail:mtierean@unitbv.ro

Abstract: The materials used for the porcelain-fused-to-metal and casting dental crown and bridge are required to have a simple manufacturing process, low cost price and surely a very good corrosion resistance. The nickel from Ni-based alloys is known as highly toxic, with epithelial cells and fibroblasts and despite the common allergies to nickel, it was allied with chromium, so the use of Ni-Cr alloys in the oral cavity does not always lead to an allergic reaction; so the use of Ni-Cr dental alloys is increasing.
Due to the spread of Ni-Cr alloys, the present paper made a comparative study of six alloys: Wiron NT, Wirolloy and Heraenium (Germany), Verasoft (USA) and Nicromal Soft and V (Romania) regarding microstructure characterization and corrosion behaviour (Open Circuit Potential, Polarization Resistance, Tafel slopes and Electrochemical Impedance Spectroscopy) in simulated body fluid (Ringer solution).
The obtained results showed that mentioned alloys are under the influence of an anodic control, due to the formation of protective layers, most likely of oxide, on the surface. Also, according to the type of corrosion these alloys can be divided into two categories. A uniform general corrosion behaviour was found on the surface of Wiron NT and Heraenium Ni-Cr alloys and pitting corrosion for Wirolloy, V, VeraSoft and Nicromal Soft Ni-Cr alloys. In terms of susceptibility to corrosion, the biologic safety of the studied alloys is very high for the Heraenium and Wiron NT and adequate for the rest.

Key words: Ni-Cr dental alloys, corrosion, biomaterials

NanoMed 2019

NanoMedicine International Conference 2019

Since the advent of nanotechnology, there has been a tremendous growth in this field of nano-bio-technology. Many products introduced into the market are based on nano-bio-technology and are useful to environment monitoring, rapid diagnostics, diseases monitoring, diseases management, and personalized health care. The ultimate aim of this approach is to make a better and healthier tomorrow for everybody. **NanoMedicine 2019** will cover the most recent international developments in the field of Nanobiotechnology and Nanomedicine. Participants will get a complete overview on the state of the art in these fields and on the research carried out and the latest results. Recent advances, difficulties and breakthroughs as well as emerging and future trends of the converging fields of Nanotechnology, Biotechnology and Medicine will be discussed. The event offers to the participants from both science and industry the opportunity to discuss new cooperation projects.

The **NanoMedicine 2019** will cover the following themes:

Effects of Nickel Content on the Microstructure, Microhardness and Corrosion Behavior of High-entropy $AlCoCrFeNi_x$ Alloys

M .López Ríos,[1] P. P. Socorro Perdomo[1], V .Lucero Baldevenites[1], I.Voiculescu[2], V. Geanta[2], J. C. Mirza Rosca[1*]
[1] Las Palmas de Gran Canaria University, Mech. Eng. Dept.,Spain
[2] Politehnica University of Bucharest, LAMET, Bucharest, Romania

SPECIMENS PREPARATION

The pioneering efforts in obtaining the high entropy alloys (HEAs) created the groundwork for a new concept of solid solutions multi-principal element alloys with unique properties at the nanoscale. In this study we investigate the effect of different nickel concentration on the microstructure, hardness and corrosion properties of high entropy alloys from AlCrFeCoNi system.

COMPONENTS	HEA 1 AlCrFeCoNi	HEA 5 $Al_{0.8}CrFeCoNi$	HEA 6 $Al_{0.6}CrFeCoNi$	HEA 12 $AlCrFeCoNi_{1.4}$	HEA 14 $AlCrFeCoNi_{1.8}$
Al, wt%	10,67	8,72	6,68	9,76	8,99
Cr, wt%	20,55	21,00	21,47	18,8	17,32
Fe, wt%	22,13	22,61	23,12	20,24	18,65
Co, wt%	23,32	23,82	24,36	21,33	19,65
Ni, wt%	23,33	23,85	24,36	29,86	35,38

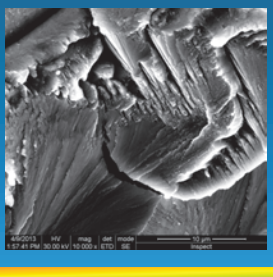

Nanometric image of HEA1 surface after fracture (Scanning Electron Microscope)

TESTS AND RESULTS

METALLOGRAPHY

HEA1

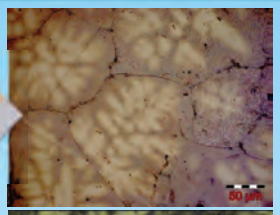

HEA12

HEA14

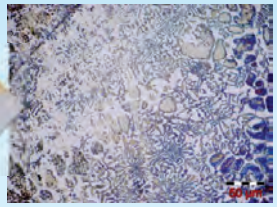

The microscopy examination reveals dendritic morphology for the reference alloy (AlCrFeCoNi) and the increase of the width of the interdendritic zones by increasing the nickel concentration.

HARDNESS

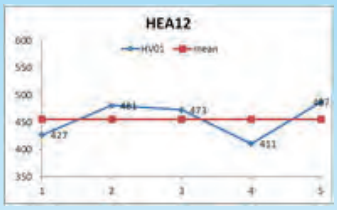

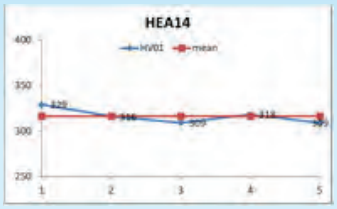

Hardness values decrease with increasing the percentage of nickel because of the dissolution of precipitates in a nickel rich matrix and in consequence forming continuous solid solutions.

CORROSION

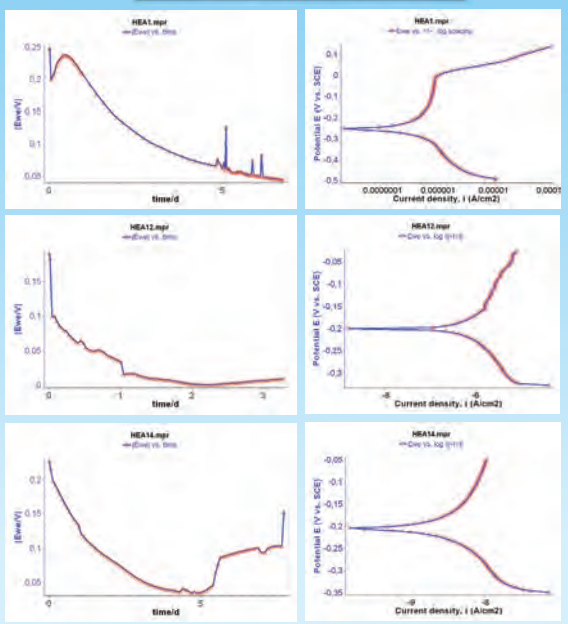

The alloys were immersed in SBS (Simulated Body Fluid) during one week . The low corrosion rates, low corrosion currents and high polarization resistance attest the good stability of HEAs in simulated biological environment.

ADVANCED CONCEPTS in MECHANICAL ENGINEEERING

"GHEORGHE ASACHI" TECHNICAL UNIVERSITY OF IAŞI - FACULTY OF MECHANICAL ENGINEERING

CONFERENCE PROGRAM

THE 9th INTERNATIONAL CONFERENCE ON ADVANCED CONCEPTS IN MECHANICAL ENGINEERING

ACME2020

JUNE 4 – 5, 2020
IAŞI, ROMANIA

Organized by:

FACULTY of MECHANICAL ENGINEERING

THE "GHEORGHE ASACHI" TECHNICAL UNIVERSITY OF IASI

Under the aegis of:

ROMANIAN MINISTRY OF NATIONAL EDUCATION AND SCIENTIFIC RESEACH
ROMANIAN ACADEMY OF TECHNICAL SCIENCES
ACADEMY OF ROMANIAN SCIENTISTS

In partnership with:

AMERICAN UNIVERSITY OF MADABA, JORDAN
SIAR - SOCIETY OF AUTOMOTIVE ENGINEERS OF ROMANIA
ARoTMM - ROMANIAN ASSOCIATION FOR MECHANISMS AND MACHINE SCIENCE
SROMECA – ROMANIAN ASSOCIATION OF MECHATRONICS
ART – ROMANIAN TRIBOLOGY ASSOCIATION
SRT - ROMANIAN SOCIETY OF THERMODYNAMICS
AFCR - ROMANIAN ASSOCIATION FOR REFRIGERATION AND CRYOGENICS ENGINEERS

June 04-05, 2020,
Iasi, Romania

Electrochemical Behavior of New Titanium Alloys

Las Palmas de Gran Canaria
España

V.Lucero Baldevenites, N.Florido Suarez, P.Socorro Perdomo, J.Mirza Rosca
University of Las Palmas de Gran Canaria, Spain
viviana.lucero@ulpgc.es

Keywords:

Titanium, tantalum, corrosion, Ringer solution, medical devices.

1. Introduction:

Increased use of Ti and Ti alloys as biomaterials is occurring due to their lower modulus, superior biocompatibility and high corrosion resistance compared with conventional biomaterials such as stainless steel and Co-Cr alloys. These attractive properties were a driving force for the early introduction of Ti and Ti-6Al-4V as implantable materials [1]. But Ti-6Al-4V has a potential toxicity and adverse tissue reactions [2,3] and new Ti alloys composed of non-toxic and non-allergic elements have been developed for biomedical applications [4]. Among them, titanium-tantalum binary alloys have [5,6] been developed and, in this work, corrosion resistance of Ti-Ta alloys was tested by open-circuit potential measurements, linear polarization, potentiodynamic polarization and Electrochemical Impedance Spectroscopy.

2. Experimental Part:

The studied titanium tantalum alloys were Ti-5Ta, Ti-15Ta, Ti-25Ta and Ti-30Ta from R&D CS (Research & Development Consulting and Services) Bucharest, Romania. The Ti-Ta ingots (diameter = 20 mm, length = 30 mm) were obtained by levitation melting in a high-frequency induction furnace with a cold copper crucible, followed by a homogenization heat treatment in order to eliminate the segregation.
A conventional three-electrode electrochemical cell with a Pt grid as counter electrode and saturated calomel electrode (SCE) as reference electrode was used. AC impedance data were obtained at different potentials using a PAR 2634 A potentiostat connected with a PAR 5210 lock-in amplifier. The amplitude of the AC potential was 10 mV and single sine wave measurements at frequencies between 10-1 and 105 Hz were performed for each sample. In order to characterize the oxide film, the impedance spectra were recorded between -400 mV and 2000 mV with a 100 mV step, polarizing the electrodes continuously and allowing the system to stabilize for 600 s at each potential. Data acquisition and analysis were performed with a personal computer and the spectra were interpreted using the ZSimpWin program.

3. Results and Discussions:

The electric potential difference between electrolyte and metal interface is a relevant factor directly related to the surface conditions. The EIS tests have been carried out at different applied potentials in 3 domains: cathodic-anodic transition, passive and near transpassive transition. The impedance data will be compared in order to evaluate the influence of the potential on the passive oxide characteristics (see Fig.1).

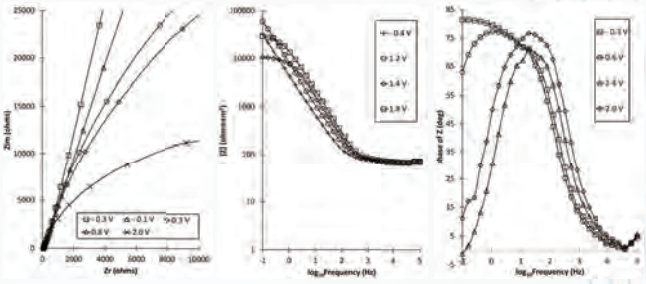

a) b) c)

Figure 1. EIS curves for Ti-15Ta:a) Nyquist, b) Bode IZI and c) Bode phase

Analysis of the impedance spectra was done by fitting these data with ZSimpWin. The quality of fitting to the equivalent circuit was judged firstly by the chi-square value and secondly by comparing experimental with simulated data.
Instead of capacitance, constant phase elements CPE (which represent the deviation from the true capacitive behavior) were used.

Diagnostic criteria for the choice of equivalent circuits for modeling impedance data may be summarized by visual observations of the shifts in experimental Bode plots with changing potential and alloying element(see Fig.2).

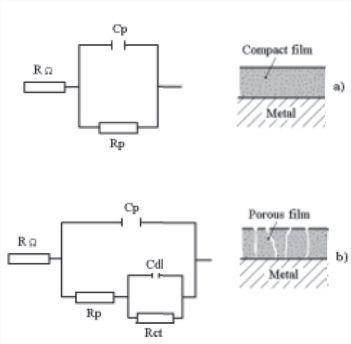

4. Conclusions:

Among Ti-Ta alloys, the Ti-25Ta exhibits superior properties of the passive film and corrosion behavior, therefore it appears to be a promising candidate for metallic biomaterials.

Impedance spectra are fitted with one time constant equivalent circuit, typically for a compact oxide film, for all Ti-Ta alloys in extra-cellular fluids. The Nyquist plots for all the Ti-Ta alloys show the same incomplete semicircles with large diameters increasing with the potential (till a determinated value for each alloy) due to the improvement of the protective properties of the passive film formed on the surface of the alloy.

The passive layer resistance decreases with the potential due to the dissolution processes through the passive film. For all Ti-Ta alloys, the Bode phase plots exhibited one phase angle, typical for a capacitive barrier passive layer formed on the surface of the alloy.

Titanium-tantalum binary alloys are expected to become promising candidates for medical applications due firstly to tantalum which is a non-toxic element and secondly, due to their better compatibility with bone tissue compared with cp-Ti and Ti-6Al-4V alloy.

5. Acknowledgments:

We gratefully acknowledge the support and generosity of The R&D CS (Research & Development Consulting and Services) Bucharest, Romania, without which the present study could not have been completed.

References:

[1] R.M.Souto, G.T.Burnstein, (1996), *A preliminary investigation into the microscopic depassivation of passive titanium implant materials in vitro*, J. Mater. Sci. Mater. Med. 7(6), pp. 337-343.
[2] S.Fujibayashi, T.Nakamura, S.Nishiguchi, J.Tamura, M.Uchida, H-M.Kim, T.Kokubo, (2001*), Bioactive titanium: Effect of sodium removal on the bone-bonding ability of bioactive titanium prepared by alkali and heat treatment,* J. Biomed. Mater. Res. 56(4), pp. 562-570.
[3] S. Piazza, G.Lo Biundo, M.C. Romano, C. Sunseri, F. Di Quarto, (1987), *In situ characterization of passive films on al-ti alloy by photocurrent and impedance spectroscopy*, Corros. Sci. 40, pp.1087-1108.
[4] M. Niinomi, (2002), *Recent metallic materials for biomedical applications*, Metal. Mater. Trans. 33A, 477-486.
[5] Y.L. Zhou, M. Niinomi, T. Akahori, H. Fukui, (2005), *Development of Ti-30 mass% Ta Alloy for Biomedical Applications*, Mater. Sci. Forum 475-479, pp. 2309-2312.
[6] D.M. Gordin, E. Delvat, R. Chelariu, G. Ungureanu, M. Besse, D. Laillé, T. Gloriant, (2008*), Characterization of Ti-Ta Alloys Synthesized by Cold Crucible Levitation Melting*, Adv. Eng. Mater. 10(8), pp 714-719.

June 04-05, 2020,
Iasi, Romania

Las Palmas de Gran Canaria
Spain

"In vivo" Analysis of Osteoinduction Treatment on Ti6Al7Nb

V.Lucero Baldevenites, N.Florido Suarez, P.Socorro Perdomo, J.Mirza Rosca
University of Las Palmas de Gran Canaria, Spain
viviana.lucero@ulpgc.es

Keywords:

Titanium, niobium, aluminum, osseointegration, implant, biological fluids

1. Introduction:

The importance of the mechanical stability of one implant is evaluated by analyzing the quality of the osseointegration at the bone-implant interface through the analysis of the amount of neoformed bone in direct contact with the implant, able to mechanically fix the implant and the type of bone tissue that is formed.
The study of the in vivo behavior of a Ti6Al7Nb implant, subjected to 2 different surface treatments, is of great interest in order to determine and evaluate the possible TOXICITY caused by the implant through the content of metals present in biological fluids of experimental animals, OSTEOINTEGRATION of the implant and OSTEOINDUCTION at the implant-bone interface.

2. Experimental Part:

To study the release of ions from the implant (Ti6Al7Nb) to the body (determination of Aluminum toxicity), the Atomic Absorption Spectrometry (EAA) technique has been used.
This technique has been chosen, since they have very good characteristics: high specificity, selectivity, excellent sensitivity at low concentrations (1000 ppm), speed of determination and a wide field of application (70 elements, which makes it the technique). best suited for measuring Aluminum in biological fluids)

For the bone-implant interface study (osseointegration), the Scanning Electron Microscopy technique with EDX analyzer was used.

3. Results and Discussions:

The area known as the tip-plate was analyzed by means of a 1.5 mm scan, collecting points, as in the other cases, from the bone part, the bone-metal interface and the metal.
Likewise, the interface was carefully examined in order to find out if there is metal contamination in the bone-organic structure.

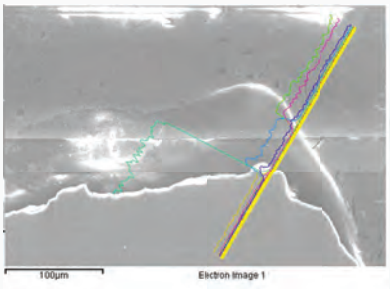

Figure 1. Análisis interfaz hueso-implante en la zona de la punta-placa mediante barrido de 1.5 mm

This new treatment, called SBF (synthetic or simulated body fluids), has the advantage of inducing the formation of apatite (hydroxyapatite coating) in metals and other materials, immersed in solutions that simulate biological fluids (Ringer, Earl, Hanks). The innovation of this treatment is found in the use of biovitroceramic particles as substitutes.

In order to demonstrate the feasibility of this treatment in medical applications, it was evaluated in vitro through its application to implants.

Biocompatibility analyzes consisted of in vitro assays of osteoblastic cells (osteoblast culture) donated by the American Type Culture Collection. Osteoblastic cells were grown with an initial density of 1x104 cell · cm^{-2} in a medium consisting of a 1:1 mixture of Dulbecco's modified Eagle's medium and Ham's F12 medium containing 0.3 mg/ml G418, 10% fetal bovine serum, 100 U/ml of penicillin and 100 g/ml streptomycin, in a humid atmosphere and 5% CO_2.

Depending on the incubation temperature, the cell culture can show similar preosteoblastic characteristics.
Analyzes of the surface of the implants at the microstructural level, as well as the XRS patterns are shown below.

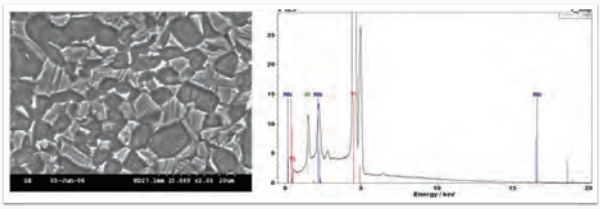

Figure 2. De izq. a der. se muestra la superficie del Ti6Al7Nb y el patrón XRD.

In the image of the Ti6Al7Nb microstructure, the primary grains of the metastable phase are observed and the graph shows the characteristic peaks of the Ti6Al7Nb alloy.

4. Conclusions:

In vitro tests, treatement superficial SBF with biovitroceramic particles to the implants indicate that there is good osteoinduction and biocompatibility in the samples, highlighting immersion time as an important parameter in deposition quality (biocompatibility and cytotoxicity): expression of alkaline phosphatase confirms that osteoblastic cells belong to the osteoblastic phenotype, existing positive histochemical reaction; Cytomorphological analyzes show differences related to the start of the culture: after 24 hours, results are better for samples immersed for 15 days; after 48 hours, results are better for samples immersed for 15 days.

Studies using the EAA technique indicate that the concentration of Al that can affect humans due to the diffusion of Al by wearing an implant is insignificant, and cannot be considered harmful compared to daily consumption due to food intake or other factors.

This last conclusion collides with the arguments found in the existing literature that bet on a change in the implantable material, that is, a change in the widely used Ti6Al4V alloy with satisfactory results for the Ti6Al7Nb alloy object of this study, much more expensive and difficult to obtain

5. Acknowledgments:

We appreciate the support and generosity of ITC (Instituto Tecnológico de Canarias) Las Palmas, Spain, without which the present study could not have been completed.

References:

[1] Savory J, Wills MR., (1989), *Analytical Techniques for the analysis of Aluminium*. [book auth.] H. J. Gitelman. Aluminum and Health: A Critical Review . New York: Marcel Dekker, pp. 1-26.
[2] Ioannou PC, Piperaki EA. (1986), *Kinetic fluorimetric determination of aluminium in serum.* Clinical Chemistry, Vol. 32, pp. 1481-1483.
[3] Berlin A, Mattiello G, Taylor A. (1987), *Quality Assurance for Aluminium Analysis.* Copenhague: s.n., 1987. Trace Elements in human health and disease, WHO Environmental Health report 26. pp. 37-38.
[4] Gilmutdinov KH, Zakharov YA, Ivanov VP, Voloshin AV, Dittrich K. (1992), *Shadow spectral fiming: a method of investigating electrothermal atomization II: Dynamics of formation and structure of the absorption layer of aluminium, indium and gallium molecules.* 4, Journal of analytical atomic spectrometry , Vol. 7, pp. 675-683. ISSN 0267-9477.
[5] Chuni L., Chakrabarti, Albert K. Gilmutdinov, Craig Hutton J. (1993), *Digital imaging of atomization processes in electrothermal atomizers for atomic absorption spectrometry*., Analytical Chemistry, Vol. 65, pp. 716-723.

June 04-05, 2020,
Iasi, Romania

Nanostructurated Ti-20Zr in Artificial Extra-cellular Fluids

Las Palmas de Gran Canaria, Spain

N.Florido Suarez, V.Lucero Baldevenites, P.Socorro Perdomo, J.Mirza Rosca
University of Las Palmas de Gran Canaria, Spain
nestor.florido@ulpgc.es

Keywords:

Titanium, zirconium, biomaterial, corrosion, microhardness

1. Introduction:

Relatively few metals are biocompatible and, therefore used for structural application in the body (e.g., implants for hip, knee, ankle, shoulder, wrist and finger); the principal metals used are: stainless steels, cobalt-based alloys and titanium-based alloys. This is due to their ability to bear significant loads, withstand fatigue loading and undergo plastic deformation prior to failure. Further studies have shown the release of both V and Al ions from the alloy might cause long-term health problems, such as peripheral neuropathy, osteomalacia and Alzheimer diseases [1,2].
Zirconium is similar to titanium in that an adherent, protective oxide film forms on its surface. As a result, zirconium is very resistant to corrosive attack and also exhibits the highest biocompatibility of all metals [3].
The purpose of the present investigation is to correlate the microstructure, microhardness and electrochemical behaviour of nanostructurated Ti-20Zr in artificial extra-cellular fluids for biomedical applications.

2. Experimental Part:

The Ti-20Zr alloy, composed of 80% Titanium and 20% Zirconium, (from R&D CS Bucharest, Romania – Research &Development Consulting and Services) was obtained by vacuum melting. Samples (Fig. 1) were prepared for each one of the different techniques: optical metallography, Vickers microhardness and Electrochemical Impedance Spectroscopy.
For microscopic observations, an Olympus PME 3-ADL microscope was employed. The surface was observed before etching and analysed at different magnifications.
The samples, ground and polished to mirror finish with alumina paste of 0.1 µm, were used to measure the microhardness by means of an indentation test (Remet HX-1000 Microhardness Tester).
Electrochemical measurements were made at 25ºC using a single compartmented cell containing 75 ml of electrolyte. The potential of the working electrode was measured against a NaCl (saturated) - calomel electrode (SSCE) and the mentioned potentials were referred to this electrode. A cylindrical Pt grid was used as a counter electrode.

3. Results and Discussions:

Fig. 1 shows the I-E profiles for Ti-20Zr alloy in Ringer's solution. The positive potential scan at 0.01 V/s runs from -0.5 V to 1.5V and did not show a cathodic current or anodic peaks.

The negative potential-going scan exhibits a cathodic peak at approximately -0.15 V. Current instabilities related to breakdown and repair events of the passive film are not detected and the returning scan does not exhibit a hysteresis loop, so the passive film has been fully restored (Fig. 1).

This behavior demonstrates that Ti-20Zr alloy exhibits excellent corrosion resistance due to the stable oxide layer formed on the surface. It has been demonstrated that Zr offers superior corrosion resistance over most other metals [4].

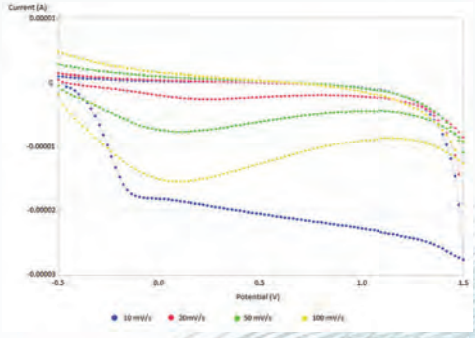

The obtained average values of microhardness permitted the calculation of the measurement depth. It was observed the presence of two phases: one soft and one hard and the correspondence values of microhardness are presented in the Table 1.
It can be seen that α phase is softer than β phase (around 30% less). The hardness of Ti-20Zr alloy is 1.2 times as large as that of commercially pure Ti, confirming the alloy's superior mechanical strength .
In Table 2 the approximate tensile strength is presented for the last three applied loads (50, 100 and 200 gf) using the average Vickers Hardness value.
The obtained tensile strength for Ti-20Zr is also superior to that of commercially pure Ti.

SOFT AND HARD PHASES - Ti-20Zr			
LOAD (gf)	PHASE	HARDNESS (HV)	INDENTATION DEPTH (µm)
0.5	SOFT	37.3	0.712
	HARD	50.0	0.615
1	SOFT	66.2	0.756
	HARD	91.3	0.643
2	SOFT	101.5	0.863
	HARD	145.3	0.721
3	SOFT	127.7	0.942
	HARD	197.2	0.758
4	SOFT	149.8	1.000
	HARD	214.8	0.839
5	SOFT	163.7	1.075
	HARD	288.4	0.809
10	SOFT	194.6	1.394
	HARD	242.4	1.249
20	SOFT	201.9	1.935
	HARD	298.4	1.592
50	SOFT	212.8	2.981
	HARD	255.3	2.722
100	SOFT	201.3	4.335
	HARD	256.2	3.842
200	SOFT	210.5	5.990
	HARD	268.8	5.305

4. Conclusions:

The α + β microstructure obtained by aging at 1273 K for two hours exhibits a better mechanical biocompatibility, hence it is more suitable than the other microstructures for biomedical applications. These results confirm the data obtained with higher Zr content in Ti-based alloys.
The hardness of Ti-20Zr alloy is 20% higher than that of commercially pure Ti, confirming the alloy's superior mechanical strength.
The Ti-20Zr alloy exhibits an excellent corrosion resistance, better than cpTi and taking into account that there is a general agreement that Zr compounds have no local or systemic toxic effects, we can conclude that Ti-20Zr can be a potential biomaterial for use as an artificial surgical implant.

5. Acknowledgments:

We gratefully acknowledge the support and generosity of The R&D CS (Research & Development Consulting and Services) Bucharest, Romania, without which the present study could not have been completed.

References:

[1] J. Yu, Z.J. Zhao, L.X. Li, (1993), *Corrosion fatigue resistances of surgical implant stainless steels and titanium alloy* Corros. Sci. 35(1-4), pp. 587-591.
[2] S. Rao, T. Ushida, T. Tateishi, S. Okasaki, S. Asao, (1996) *Effect of Ti, Al, and V ions on the relative growth rate of fibroblasts (L929) and osteoblasts (MC3T3-E1) cells,* Bio-med Mater. Eng. 6, pp. 79-86.
[3] ASM International: Handbook of Materials for Medical Devices, Ed. by J.R. Davis, 2004.
[4] N. Stojilovic, E.T. Bender, R.D. Ramsier, (2005), *Surface chemistry of zirconium,* Prog. Surf. Sci., 78(3-4), pp.101-184.

June 04-05, 2020,
Iasi, Romania

Microscopic Passivation of Bio High Entropy Alloys: Initial studies

Las Palmas de Gran Canaria, Spain

Nestor R. Florido Suarez[1], Viviana E. Lucero Baldevenites, Pedro P. Socorro Perdomo, Ionelia Voiculescu, Victor Geanta, Julia C. Mirza Rosca,
[1]University of Las Palmas de Gran Canaria, Process Engeneering Dept.
[1]nestor.florido@ulpgc.es

Keywords:

Bio HEA, Corrosion, Biomaterials, corrosion, electrochemical

1. Introduction:

In recent years, due to the great advance of scientific and technological research, new alloys are being explored with a different metallurgical concept: at least three basic components and these alloys are called High Entropy Alloys (HEA) [1]. In this way it was created the groundwork for a new concept in alloy design by looking after combinations of metals to work "in team" for an advanced material with unique properties.
At the end of the last century, the progress of science led to the rapid development of biomedical materials and the recent development of high entropy alloys (HEA) provides a new perspective for a new generation of biomaterials [2].

2. Experimental Part:

Two new experimental alloys (with the composition presented in Table 1) were obtained by Vacuum Arc Remelting from high purity chemical elements (99.5%) that exhibit extremely low bio-toxicity for the human body (for this reason we named them BioHEA).
Both the compositional analysis performed using the dispersive energy probe and the structural characterization by X-ray diffraction revealed the dendritic separation of compounds in the fine dendritic matrix.
In order to analyze the passivation process, the electrochemical impedance spectroscopy technique at different potentials was used and the experimental results were compared with those obtained by potentiostatic and potentiodynamic techniques.

3. Results and Discussions:

Two new experimental alloys (with the composition presented in Table 1) were obtained by Vacuum Arc Remelting from high purity chemical elements (99.5%) that exhibit extremely low bio-toxicity for the human body (for this reason we named them BioHEA).

Table 1. The chemical composition of the alloys used

	Wt.%					
	Mo	Ta	Ti	Zr	Nb	Fe
BioHEA 1	20.45	32.45	12.67	18.97		15.46
BioHEA 2	17.32	38.95	13.21	17.45	13.07	

The EIS results of the analyzed BIo-HEA are shown in figure 1

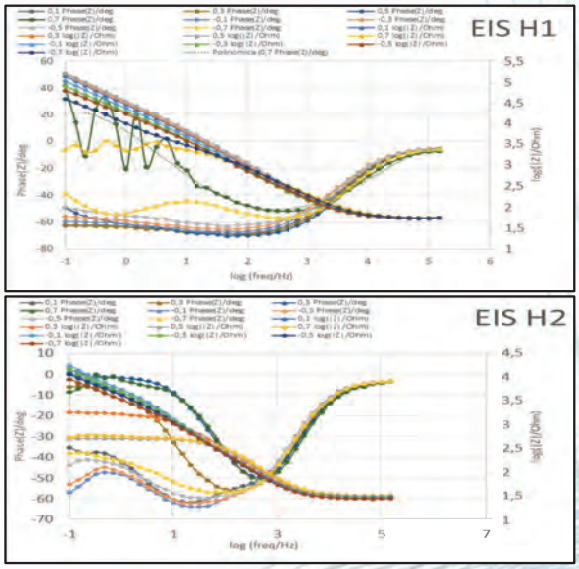

Figure 1. Chemical attack and metallographic analysis Bio-HEA 1 and 2

The alloys were microstructurally characterized (dendritic morphology) and microhardness measurements were performed (Fig.2)

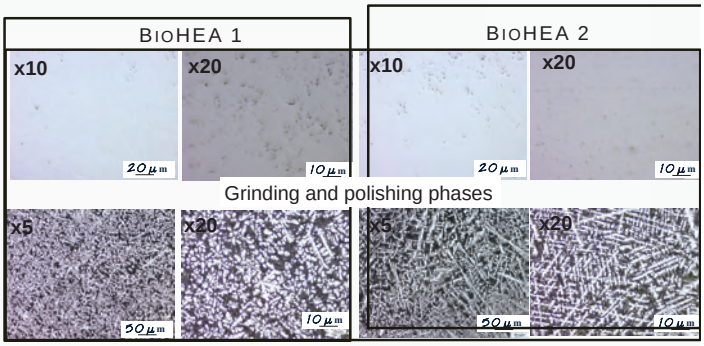

Figure 2. Chemical attack and metallographic analysis

The 24-hour corrosion potential is shown in Figure 3

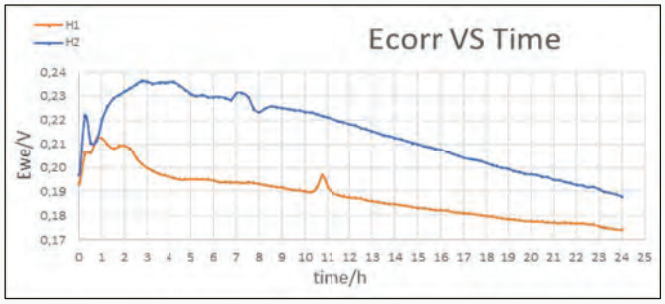

Figure 3. Corrosion potential in 24 hours

4. Conclusions:

The low corrosion rates, low corrosion currents and high polarization resistance attest the good stability of these BioHEA in simulated biological environments.

The effect of the presence of different elements on the HEAs properties in simulated body fluid (SBF). The microstructure, the hardness and the corrosion properties of high entropy alloys and their passive films were analyzed; the alloys were obtained by vacuum arc remelting from raw materials with high purity.
It resulted that the tested oxide films presented passivation tendency and a very good stability at local corrosion was detected. The mechanical data confirm the presence of an outer porous passive layer and an inner compact and protective passive layer. EIS confirms the mechanical results. The thicknesses of these layers were measured. SEM photographs of the surface and EDX profiles for the samples illustrate the appearance of a microporous layer.

5. Acknowledgments:

We gratefully acknowledge the support and generosity of Laboratory The LAMET, Politecnica University of Bucharest, Romani, without which the present study could not have been completed.

References:

[1] B.S. Murty, J.W. Yeh, S. Ranganathan, Chapter 1 - A Brief History of Alloys and the Birth of High-Entropy Alloys, Editor(s): B.S. Murty, J.W. Yeh, S. Ranganathan,High Entropy Alloys,Butterworth-Heinemann, 2014, Pages 1-12, ISBN 9780128002513
[2] Yeh, Jien-Wei. (2006). Recent progress in high-entropy alloys. European Journal of Control - EUR J CONTROL. 31. 633-648. 10.3166/acsm.31.633-648.
[3] Bombac D, Brojan M, Fajfar P, Kosel F, Turk R. «Review of materials in medical applications.» *Materials and Geoenvironment* (RMZ) 54 (2007): 471-499.
[4] Norlin A., Pan J., Leygraf C. «Investigation of electrochemical behavior of stimulation/sensing materials for pacemaker electrode applications.» *Journal of the Electrochemical Society* 152 (2005): 7

Biomaterials 2020

2nd Global Congress & Expo on Biomaterials

Theme: *Historical Development & Classification of Biomaterials*

Download Brochure Meeting Agenda

Date : May 11-12,2020 Venue : DoubleTree by Hilton Hotel : Manchester, UK

2nd Global Congress & Expo on

Biomaterials

May 11-12, 2020 | Manchester, UK

Theme:

Historical development & Classification of Biomaterials

Biomaterials 2020

2nd Global Congress & Expo on Biomaterials
July 22-23, 2020 | Manchester, UK
Biomaterials 2020

TITANIUM-TANTALUM ALLOYS WITH BIOACTIVE SURFACE FOR ORTHOPAEDIC IMPLANTS

E.V. Lucero Baldevenites[1], J.C. Mirza Rosca[1], N.R. Florido Suárez[1], P.P. Socorro Perdomo[1], A. Pascu[2], E. Stanciu[2]

[1]*University of Las Palmas de Gran Canaria, Mechanical Engineering Department, Campus Universitario Tafira, Edificio Ingeniería, 35017, Las Palmas de Gran Canaria, Canary Islands, Spain, email: viviana.lucero@ulpgc.es*

[2]*Transilvania University of Brasov, Materials Engineering and Welding Department, 29 Eroilor Blvd., 500036, Brasov, Romania*

MATERIALS

Alloy	Components	Composition by weight (wh%)	
		Weighted	Measured
Ti5Ta	Ti	95,0	95,0
	Ta	5,0	5,0
Ti15Ta	Ti	85,0	84,8
	Ta	15,0	15,2
Ti25Ta	Ti	75,0	74,6
	Ta	25,0	25,4

METHODS

METALLOGRAPHIC ANALYSIS

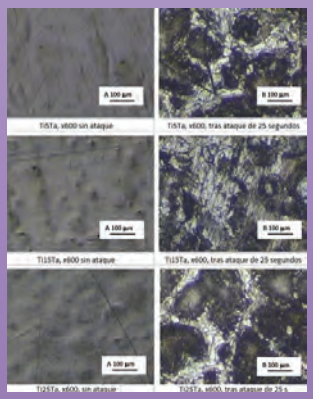

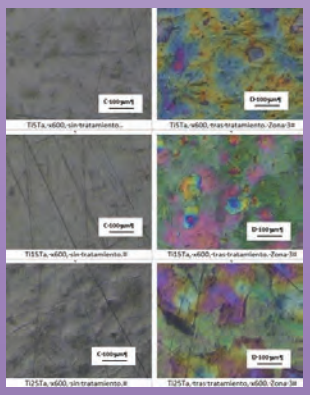

OPEN CIRCUIT POTENTIAL

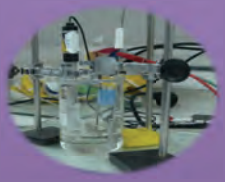

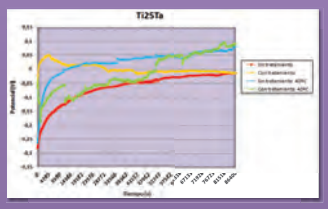

THREE POINT BENDING TEST

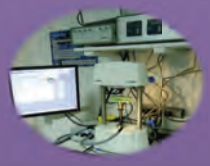

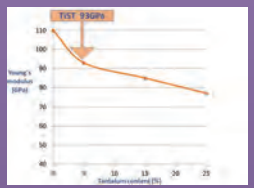

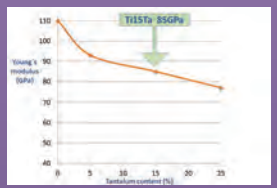

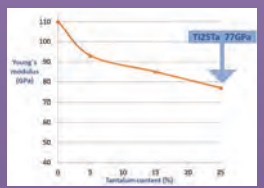

ELECTROCHEMICAL IMPEDANCE SPECTROSCOPY

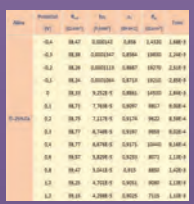

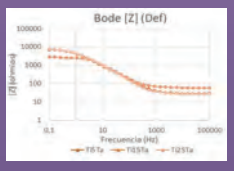

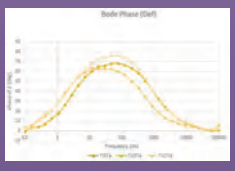

According to microstructure tests result, two crystal structures were observed, a hard one and a soft one. An increase of tantalum content has an effect on increasing material hardness.

Young´s modulus and mechanical properties of TiTa alloys greatly depend on tantalum content, resulting in much lower Young´s modulus than pure titanium.

The open circuit potential of the TiTa alloys stabilizes at a value after a certain period of inmersion in the Ringer´s solution. This phenomenon is due to the rapid formation of the TiO_2 and Ta_2O_5 passive layer and its stabilization.

EIS was used to investigate the corrosion resistance of TiTa alloys, all alloys presented a capacitive behavior, typical of passive systems. Corrosion resistance best results were obtained by the TiTa alloy with the highest tantalum content.

TiTa alloys studied have excellent biocompatibility and corrosion resistant which suggest great possibilities in biomechanical applications.

M&M 2020

Microscopy Society of America

MAS Microanalysis Society

MICROSCOPY & MICROANALYSIS

August 2-6 • Milwaukee, WI

Advance Program & Pre-Meeting Guide

LOOK INSIDE FOR:

At-A-Glance Symposium Schedule | Details on Pre-Meeting Congresses | COVID-19 Planning Update

www.microscopy.org/MandM/2020

UNIVERSIDAD DE LAS PALMAS DE GRAN CANARIA

MICROSCOPY & MICROANALYSIS 2020 August 2-6 • Milwaukee, WI

MILWAUKEE

ANALISYS OF BONE-IMPLANT INTERFACE WITH OSSEOINDUCTION TREATMENT

Julia C. Mirza Rosca[1] , Pedro P. Socorro Perdomo[1],Nestor R. Florido Suarez[2], Maximina Monzón Mayor[3]

[1]Mechanical Engineering Department, University of Las Palmas de Gran Canaria, , julia.mirza@ulpgc.es

[2]Processing Engineering Department, University of Las Palmas de Gran Canaria,

[3]Biology Department, University of Las Palmas de Gran Canaria.

EQUIPMENT

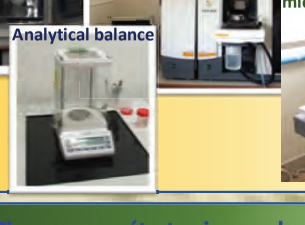

WORKING PROCEDURE

- ✓ There aren´t toxic and carcinogenic responses of animals to implant materials.
- ✓ The EDX detected the following metals: Ti, Ca, P and Al; the ratio Ca/P of 1.65 indicating that it is similar to bone mineral phase.
- ✓ The bone was in intimate contact with the bioactive Ti6Al7Nb implant.

We regard osseo-inductive ability of nanostructured Ti6Al7Nb as one of the advantages of this implant in consideration for clinical applications.

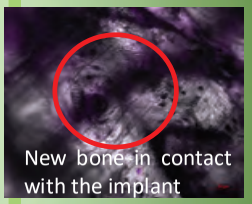

Over time, the amount of bone directly bonding to the implant increased and the immature bone had formed in the earlier stages, matured and converted to lamellar bone.

TECHNIQUES

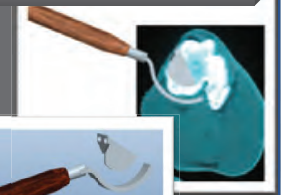

RESULTS

Standar	Conc. Al (µg/L)	Conc. Reales de Al (µg/L)	Absorbance
White Zerp	0	-0.24	0.0882
Master 1	5	5,50	0.1074
Master 2	10	9,68	0.1214
Master 3	15	15,23	0.1400
Master 4	20	19,69	0.1549
Master 5	25	25,14	0.1731

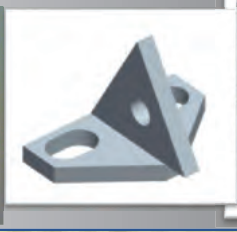

71st Annual Meeting

of the International Society of Electrochemistry

30 August - 4 September 2020
Belgrade, Serbia

Electrochemistry towards Excellence

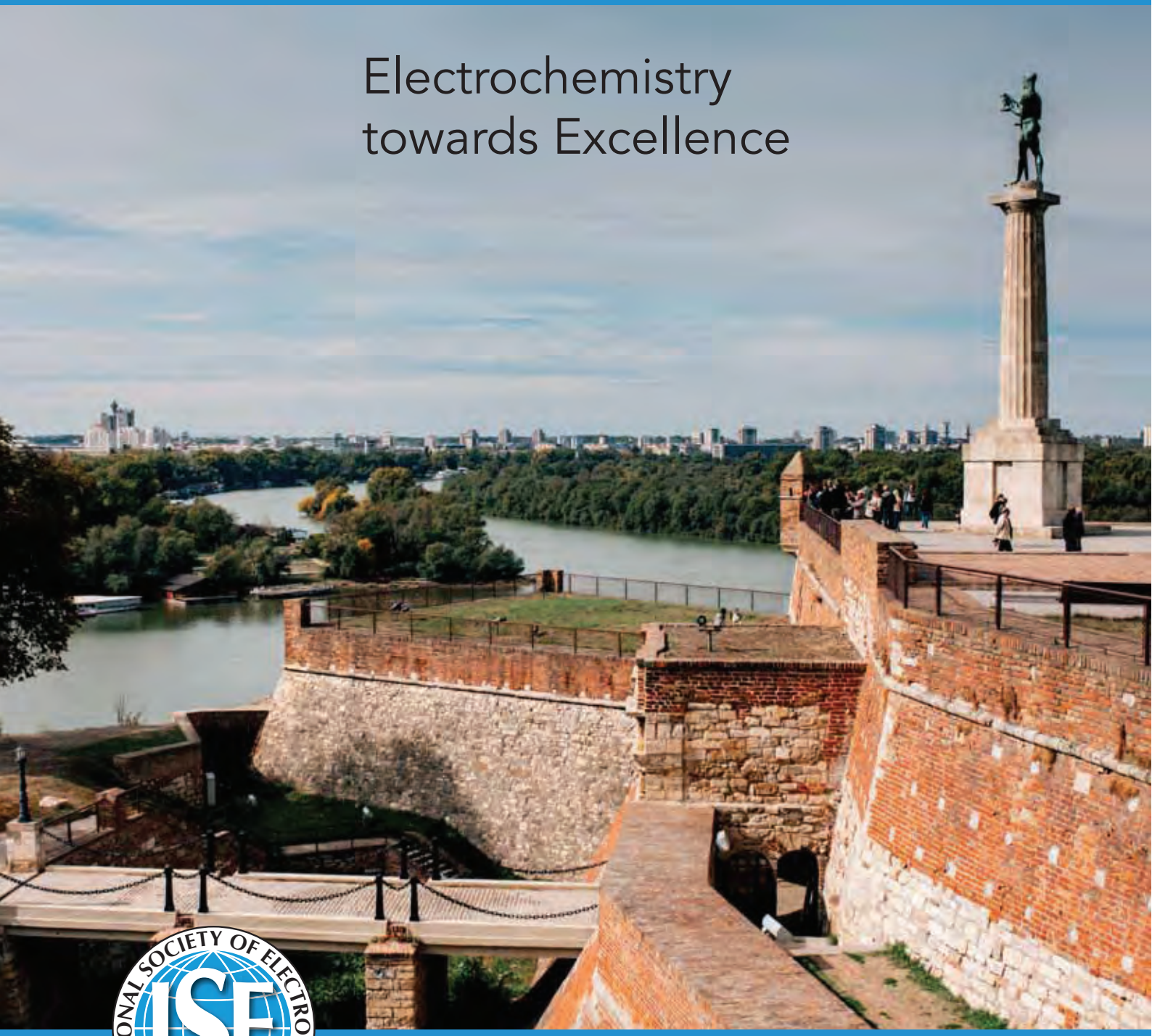

https://annual71.ise-online.org
e-mail: events@ise-online.org

Increasing the Osseoinduction of Ti6Al7Nb Tibia Implant by Surface Treatment and "in vivo" Application

Julia C. Mirza Rosca[1] , Pedro P. Socorro Perdomo[1], Nestor R. Florido Suarez[2], Tomás Gil López[3]

[1]*Mechanical Engineering Department, University of Las Palmas de Gran Canaria, Julia.mirza@ulpgc.es*

[2]*Processing Engineering Department, University of Las Palmas de Gran Canaria,*

[3]*Mechanical Engineering Department, Polytechnic University of Madrid.*

Keywords

Biomaterials, corrosion, electrochemical, orthopedic

ABSTRACT

Animals such as rats, guinea pigs, rabbits, dogs, sheep, goats, pigs and others with a relatively long life expectancy are suitable for long-term testing of subcutaneous tissues, bones and muscles. Pigs are one of the preferred species as they have organs and osseointegration times similar to humans and this is one of the main reasons why the minipig has been chosen as an experimental animal in our study, mainly focused on analyzing the behavior "in vivo" of a titanium alloy plate Ti6Al7Nb with nanostructured surface, from the point of view of its osseointegration and its toxicity.

EQUIPMENT

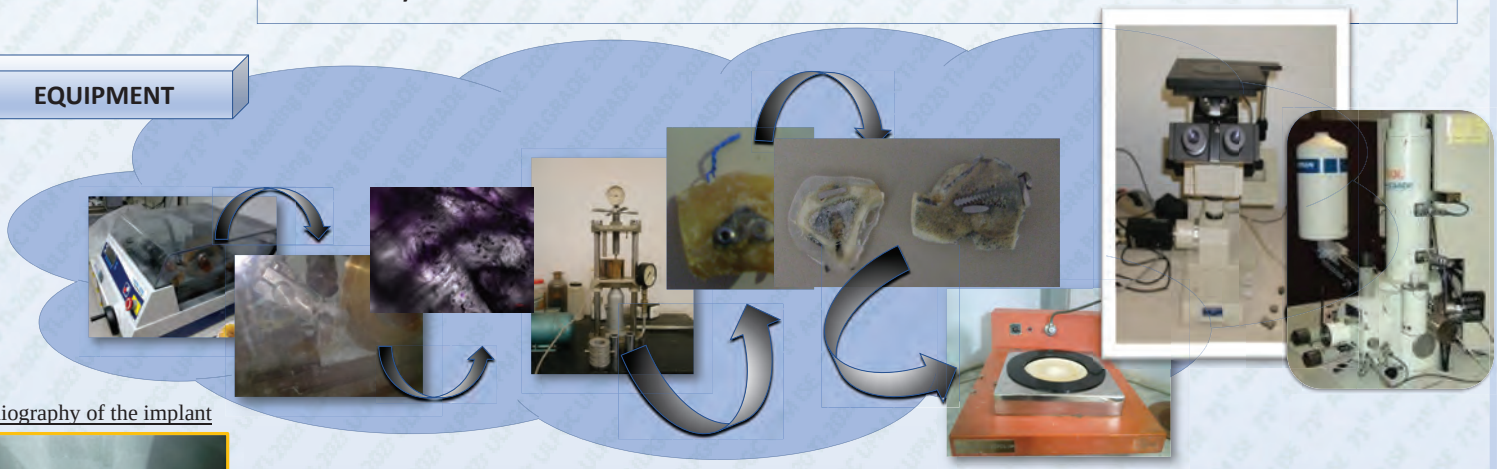

Radiography of the implant

In this study, the implant was designed so that implantation is simple and as minimally invasive as possible, in the tibia, ensuring optimal bone-implant contact as well as load transmission (bone growth induction).

Metal-implant interface analysis

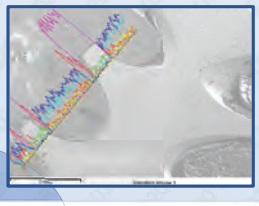

The study of the bone-implant interface of the samples from the experimental animals shows that elements belonging to the mineral part of the bone tissue (calcium, phosphorus) have been found. The average of the results obtained from the Ca/P ratio that have been analyzed for each animal allow us to confirm that there is bone growth.

WORKING PROCEDURE

RESULTS

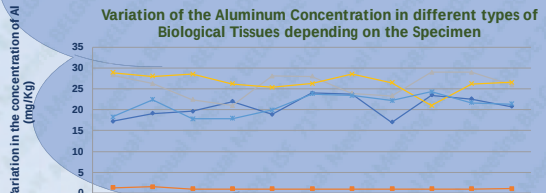

	7	13	15	17	18	24	25 (Sin Tratar)	26	27	34	MEDIA
BRAIN (mg/kg)	17,2	19,1	19,6	22	18,9	24	23,8	17	23,5	22,6	20,77
FAT (mg/kg)	1,3	1,5	1	1	1	1	1	1	1	1	1,085
KIDNEY (mg/kg)	28,3	26,3	22,4	21	28,1	28	23,9	23,3	29	29	25,93
BAZO (mg/kg)	28,9	28	28,5	26,2	25,4	26,3	28,5	26,5	21	26,2	26,55
LIVER (mg/kg)	18,3	22,4	17,8	17,9	19,9	23,8	23,4	22,2	24,3	21,7	21,37

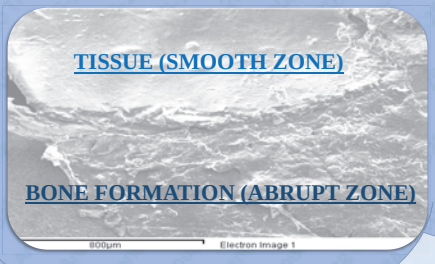

CHEMICAL MICROANALYSIS

Bone to implant interface analysis in the tip area (1.5 mm scan)

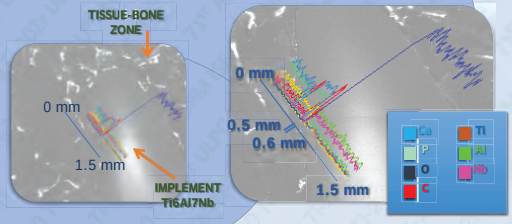

ZONA 1: BONE FPORMATION, Ca, P, O y C (0 mm-0.5 mm)

ZONA 2: INTERPHASE, C y O (0.5 mm-0.6 mm)

ZONA 3: IMPLANTE, Ti, Al, Nb (0.6 mm- 1.4 mm)

Studies using the atomic absorption spectropy technique indicate that the proportion of aluminium that can affect humans due to the diffusion of this element when wearing an implant is insignificant and cannot be considered harmful compared to daily consumption through food intake or other factors.

UNIVERSIDAD DE LAS PALMAS DE GRAN CANARIA

71st Annual Meeting Belgrade 2020

UNIVERSIDAD POLITÉCNICA DE MADRID

Nanostructurated bioactive surface of Ti-Ta alloys for medical devices

Nestor R. Florido Suarez, Pedro P. Socorro Perdomo, Tomas Gil López, Julia C. Mirza Rosca

Processing Engineering Department, University of Las Palmas de Gran Canaria

Campus Universitario de Tafira, EIIC, 35017

nestor.florido@ulpgc.es

Febrero 2012

1 Composition of the Elements

- Composición del titanio

Fe	N_2	O_2	H_2	C	Ti
0.02	0.03	0.018	0.0015	0.008	0.9225

- Composición del tantalio

Fe	Si	Mo	W	Ti	Ni	O_2	C	H_2	N_2	Nb	Ti
0.001	0.005	0.002	0.005	0.001	0.001	0.003	0.001	1.5e-4	0.001	0.002	0.996

2 Cold Crucible Furnace Treatment

3 Alloy Composition

	Alloy 1		Alloy 2		Alloy 3		Alloy 4	
Composition	Tantalum	Titanium	Tantalum	Titanium	Tantalum	Titanium	Tantalum	Titanium
	0.5	0.95	0.15	0.85	0.25	0.75	0.3	0.7
Density	5,11 g/ml		6.33 g/ml		7.54 g/ml		8.15 g/ml	

4 Precision Cutting Machine

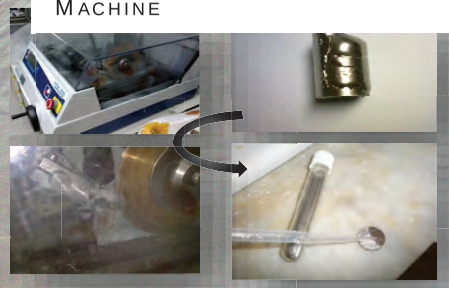

5 Press and Metallographic Polisher

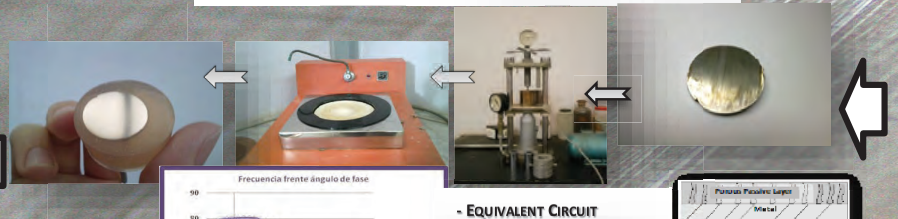

6 Electrochemical Impedance Spectroscopy Test

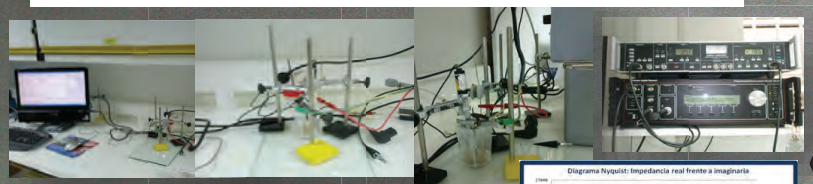

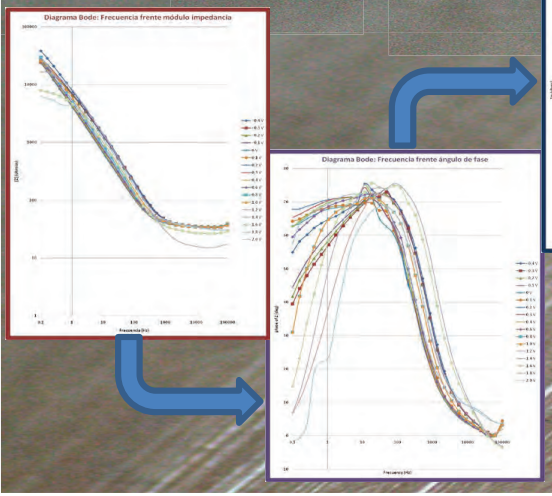

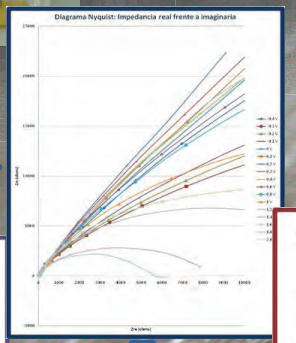

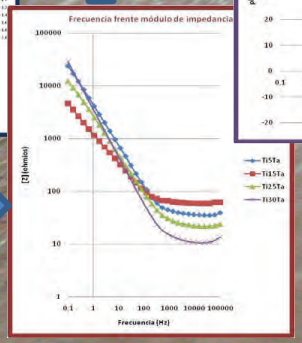

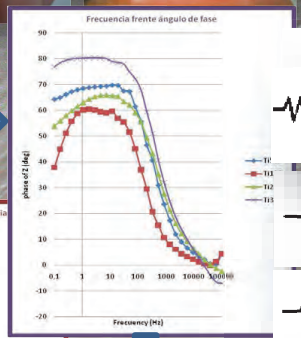

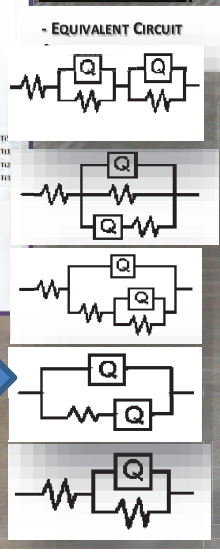

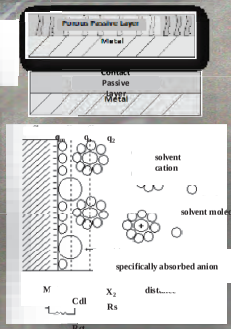

Conclusions:

Titanium alloys with 30% tantalum showed better results. Their electrolytic resistance remains constant in the potential sweep, around 27 Ωcm^{-2}. The capacity of the passive layer decreases slowly as the potential increases. The resistance of the passive layer also decreases slowly with increasing potential up to 1.2 V, at which point there is a drop of one tenth.

Correlation between the electrochemical behavior and mechanical properties of Ti-20Zr as a candidate for orthopedic material

Nestor R. Florido Suarez[1], Pedro P. Socorro Perdomo[2], Amparo Verdú Vazquez[3], Julia C. Mirza Rosca[2]
[1]*Processing Engineering Department, University of Las Palmas de Gran Canaria, nestor.florido@ulpgc.es*
[2]*Mechanical Engineering Department, University of Las Palmas de Gran Canaria,*
[3]*Mechanical Engineering Department, Polytechnic University of Madrid.*

Keywords: Biomaterials, corrosion, electrochemical, orthopedic

ABSTRACT

A combination of titanium with zirconium was evaluated because it has been suggested as a candidate for human body implant material and was primarily developed in response to concerns of potential cytotoxicity and adverse tissue reactions caused by vanadium and aluminum in the actually used biomaterial Ti6Al4V.

Metallography

The Ti-20Zr alloy, composed of 80% Titanium and 20% Zirconium, (from R&D CS Bucharest, Romania – Research & Development Consulting and Services) was obtained by vacuum melting.
From metallographical images can be observed that the sample has an alpha-beta structure. The microhardness measurements concluded that the alloy formed a hard layer on its surface which greatly improves the wear resistance. The obtained tensile strength can be considered good in relation with other similar implant materials.

Materials and Methods

Titanio **Zirconium**

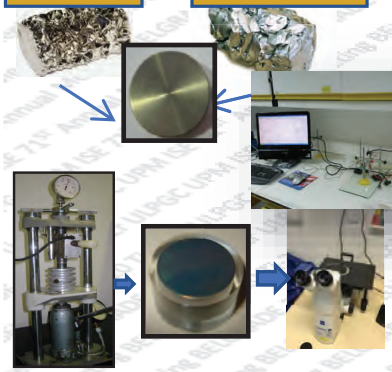

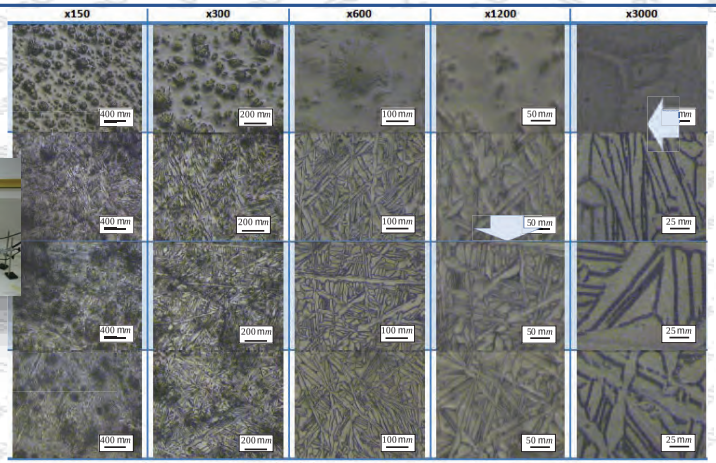

LOAD (gf)	AVERAGE HV	BRINELL HARDNESS	TENSILE STRENGTH (psi)	TENSILE STRENGTH (MPa)
50	234	234	81917	564
100	228	228	80062	552
200	239	239	83877	578

Microhardness

SOFT AND HARD PHASES - Ti-20Zr

LOAD (gf)	PHASE	HARDNESS (HV)	INDENTATION DEPTH (µm)
0.5	SOFT	37.3	0.712
	HARD	50.0	0.615
1	SOFT	66.2	0.756
	HARD	91.3	0.643
2	SOFT	101.5	0.863
	HARD	145.3	0.721
3	SOFT	127.7	0.942
	HARD	197.2	0.758
4	SOFT	149.8	1.000
	HARD	214.8	0.839
5	SOFT	163.7	1.075
	HARD	288.4	0.809
10	SOFT	194.6	1.394
	HARD	242.4	1.249
20	SOFT	201.9	1.935
	HARD	298.4	1.592
50	SOFT	212.8	2.981
	HARD	255.3	2.722
100	SOFT	201.3	4.335
	HARD	256.2	3.842
200	SOFT	210.5	5.990
	HARD	268.8	5.305

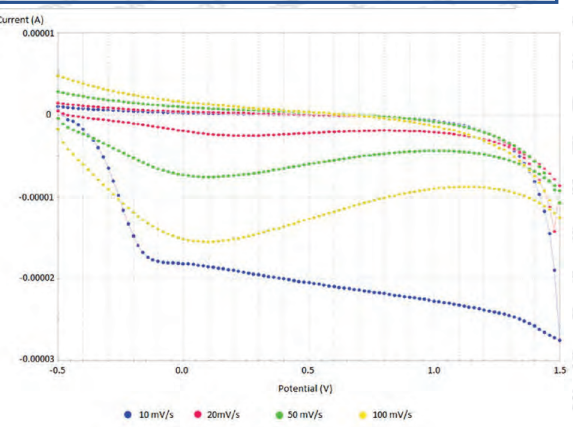

The impedance spectra were fitted with two time constants equivalent circuit and the fitting parameters indicate long-term stability of the passive layers in surgical implant conditions.

CONCLUSIONS

The hardness of Ti-20Zr alloy is 20% higher than that of commercially pure Ti, confirming the alloy's superior mechanical strength.
The results were confirmed by mechanical approach, in terms of two-layer model of the oxide film, consisting of a thin barrier type inner layer and a porous outer layer. The pronounced porous outer layer is expected to facilitate the incorporation of mineral ions and to improve the resistance to electrochemical corrosion over the potential of relevance for human body conditions.

EUROCORR SEPTEMBER 6-10, 2020
BELGIUM BRUSSELS
THE ANNUAL CONGRESS OF THE EUROPEAN FEDERATION OF CORROSION

Biocompatibility of High Entropy Alloys: Science and Design

Néstor R. Florido Suárez[1], E. Viviana Lucero Baldevenites[2], Pedro P. Socorro Perdomo[2], I. Voiculescu[2], V.Geanta[3], J.C.Mirza[2]

[1]*Process Engineering Department, University of Las Palmas de Gran Canaria, Spain* [nestor.florido@ulpgc.es]

[2]*Mechanical Engineering Department, University of Las Palmas de Gran Canaria, Spain*

[3] LAMET, Politecnica University of Bucharest, Romania

CHEMICAL COMPOSITION OF THE ANALYZED BIOHEA

	Wt.%					
	Mo	Ta	Ti	Zr	Nb	Fe
BioHEA 1	20.45	32.45	12.67	18.97		15.46
BioHEA 2	17.32	38.95	13.21	17.45	13.07	

EQUIPMENTS

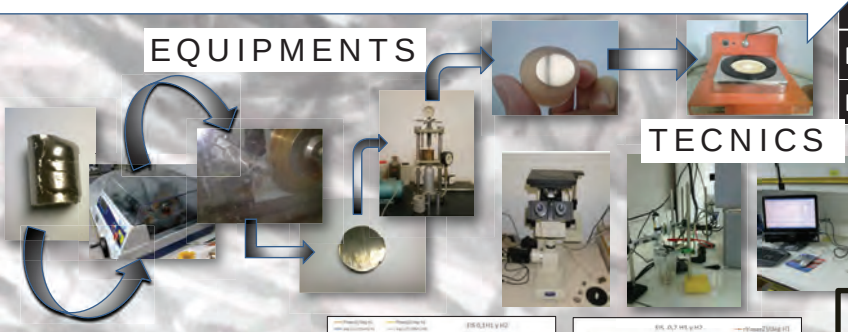

TECNICS

RESULTS

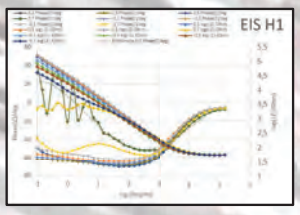

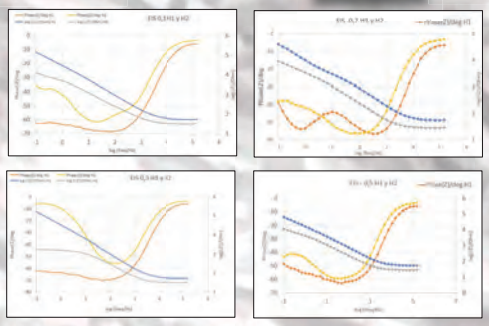

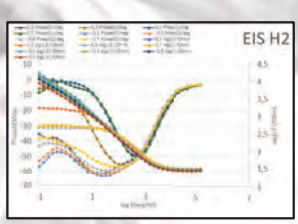

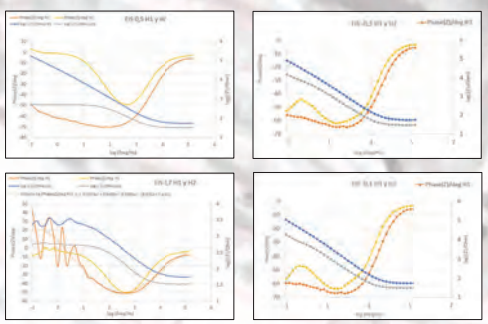

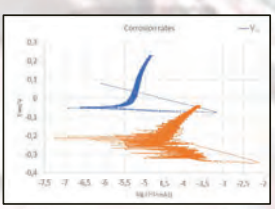

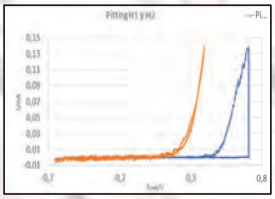

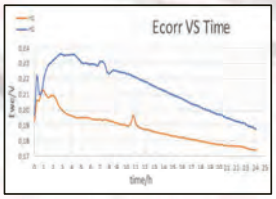

BIOHEA 1

BIOHEA 2

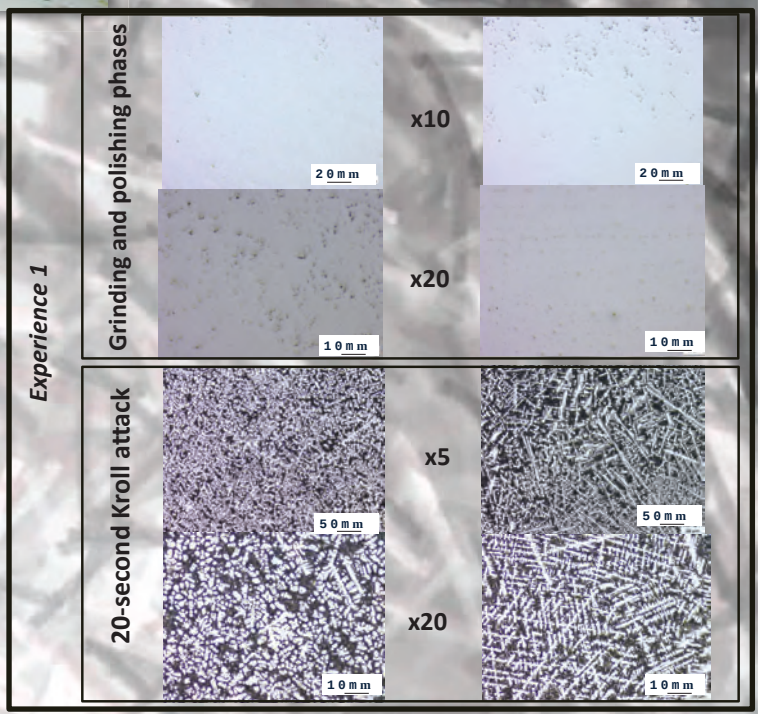

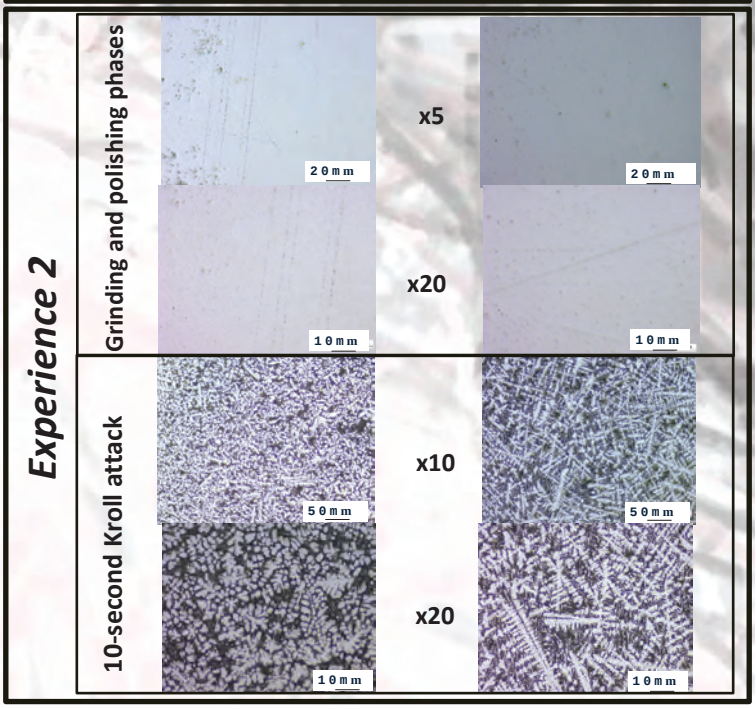

CONCLUSIONS

The effect of the presence of different elements on the HEAs properties in simulated body fluid (SBF). The microstructure, the hardness and the corrosion properties of high entropy alloys and their passive films were analyzed; the alloys were obtained by vacuum arc remelting from raw materials with high purity.

It resulted that the tested oxide films presented passivation tendency and a very good stability at local corrosion was detected. The mechanical data confirm the presence of an outer porous passive layer and an inner compact and protective passive layer. EIS confirms the mechanical results. The thicknesses of these layers were measured. SEM photographs of the surface and EDX profiles for the samples illustrate the appearance of a microporous layer.

The results emphasized that the surface treatment increases the passive layer adhesion to the HEA surface and improves the biocompatibility of the biomedical devices inducing the bone growth on the metallic surface.

TITANIUM-TANTALUM ALLOYS WITH BIOACTIVE SURFACE FOR ORTHOPAEDIC IMPLANTS

E.V. Lucero Baldevenites[1], J.C. Mirza Rosca[1], N.R. Florido Suárez[1], P.P. Socorro Perdomo[1], A. Pascu[2], E. Stanciu[2]

[1]*University of Las Palmas de Gran Canaria, Mechanical Engineering Department, Campus Universitario Tafira, Edificio Ingeniería, 35017, Las Palmas de Gran Canaria, Canary Islands, Spain* viviana.lucero@ulpgc.es

[2]*Transilvania University of Brasov, Materials Engineering and Welding Department, 29 Eroilor Blvd., 500036, Brasov, Romania*

MATERIALS

Alloy	Components	Composition by weight (wh%)	
		Weighted	Measured
Ti5Ta	Ti	95,0	95,0
	Ta	5,0	5,0
Ti15Ta	Ti	85,0	84,8
	Ta	15,0	15,2
Ti25Ta	Ti	75,0	74,6
	Ta	25,0	25,4

METHODS

METALLOGRAPHIC ANALYSIS

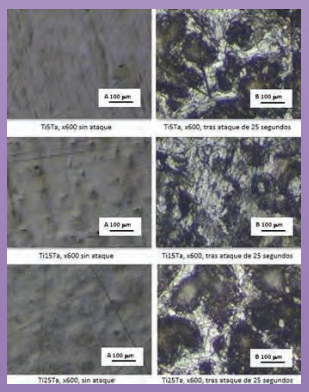

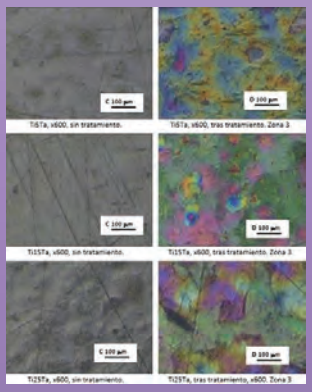

OPEN CIRCUIT POTENTIAL

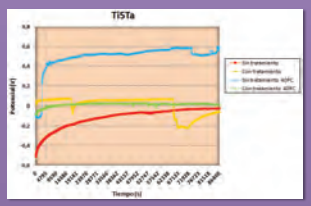

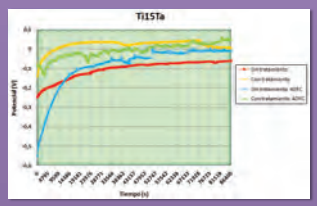

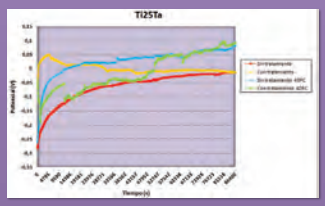

THREE POINT BENDING TEST

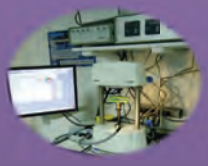

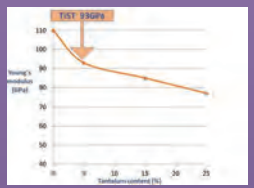

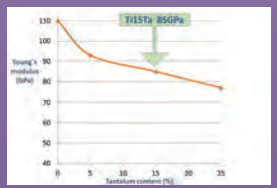

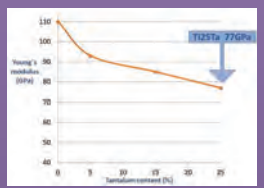

ELECTROCHEMICAL IMPEDANCE SPECTROSCOPY

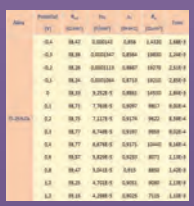

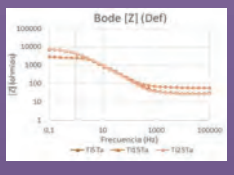

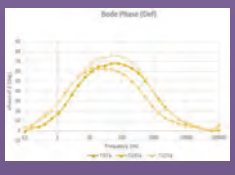

According to microstructure tests result, two crystal structures were observed, a hard one and a soft one. An increase of tantalum content has an effect on increasing material hardness.

Young´s modulus and mechanical properties of TiTa alloys greatly depend on tantalum content, resulting in much lower Young´s modulus than pure titanium.

The open circuit potential of the TiTa alloys stabilizes at a value after a certain period of inmersion in the Ringer´s solution. This phenomenon is due to the rapid formation of the TiO_2 and Ta_2O_5 passive layer and its stabilization.

EIS was used to investigate the corrosion resistance of TiTa alloys, all alloys presented a capacitive behavior, typical of passive systems. Corrosion resistance best results were obtained by the TiTa alloy with the highest tantalum content.

TiTa alloys studied have excellent biocompatibility and corrosion resistant which suggest great possibilities in biomechanical applications.

Uluslararası Bilimsel Araştırmalar ve Yenilikçi Çalışmalar Sempozyumu

International Symposium of Scientific Research and Innovative Studies

ISSRIS'21

ÖZET BİLDİRİLER KİTABI

ABSTRACTS BOOK

22-25 ŞUBAT 2021

22-25 February 2021

ISBN: 978-625-44365-8-1

INTERNATIONAL SYMPOSIUM OF SCIENTIFIC RESEARCH AND INNOVATIVE STUDIES

22- 25 February 2021

ISSRIS'21

ELECTRONIC POWER SYSTEM FOR THE DYNAMIC CORROSION CONTROL

J.M. Cabrera-Peña[1], N.R. Florido-Suarez[1], P.P. Socorro-Perdomo[1] S.J. Brito-Garcia[1], J.C. Mirza-Rosca[1]

[1]University of Las Palmas de Gran Canaria, Campus Tafira, Edificio Ingeniería, 35017, SPAIN

Preparation, testing and results

Battery TCBWORTH 2.2 Ah

Module BMS 4S-30A PRO

TEST RESULTS

SPECIMENS	SURFACE (m^2)	INITIAL WEIGHT (g)	TEST TIME (h)	FINAL WEIGHT (g)	Δ MASS (g)	CORROSION RATE (g/ m^2 · año)
1	0,04	221,97	30,00	221,19	0,78	5.694,00
2	0,04	224,68	30,00	223,84	0,84	6.132,00

Algorithm of the dynamic control system

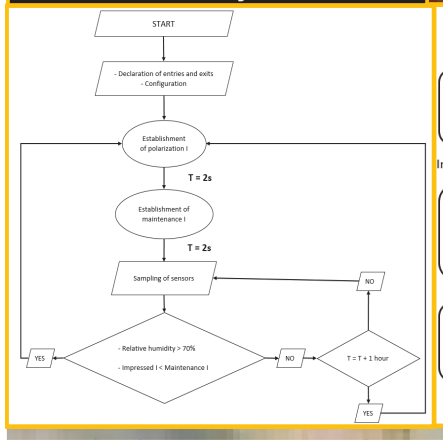

Block diagram of the automated system

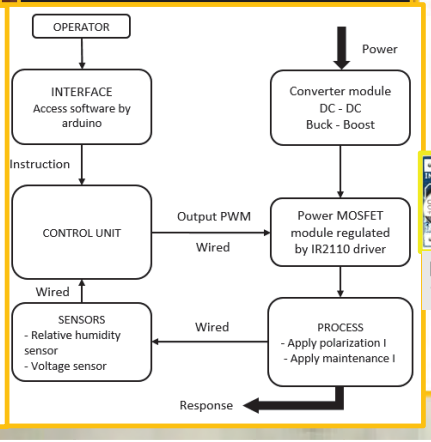

Corrosion is currently a worldwide source of economic, material, environmental damage and in the worst case, even human loss due to corrosion in infrastructure. To combat it there are a variety of techniques and treatments, but even applying them in their strictest form, sooner or later, the phenomenon cannot be avoided. Cathodic protection is a technique used to control the corrosion of a metal surface by making it the cathode of an electrochemical cell. Impressed current cathodic protection systems consist of anodes that are connected to a power source that provides a perpetual source of electrical flow. This method can often provide much longer protection than a sacrificial anode, as the anode is supplied by an unlimited power source.

Connection diagram of the prototype

Module WX - DC2412

MOSFET IRF3205

Sensor DHT22 (AM2302

Sensor FZ0430

Module DC - DC "Buck", LM2596

Module Buck - Boost ZK-SJVA-4X

INTERNATIONAL SYMPOSIUM OF SCIENTIFIC RESEARCH AND INNOVATIVE SUDIES

22- 25 February 2021

A STUDY OF METALLIC GLASS $Al_{93}Ti_3Cr_2Fe_3$ BIOMEDICAL APPLICATIONS

S.J. Brito-Garcia[1], P.P. Socorro-Perdomo[1], N.R. Florido-Suarez[1], T. Gil-Lopez[2], J.C. Mirza-Rosca[1]

[1]University of Las Palmas de Gran Canaria, Campus Tafira, Edificio Ingeniería, 35017, SPAIN

[2] Madrid Polytechnic University, Department of Building Technology, Madrid 28040, SPAIN

Metal Spinning Method

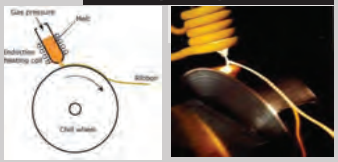

Metallic glass tapes

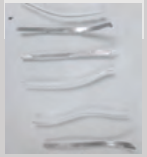

SAMPLES

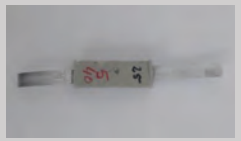

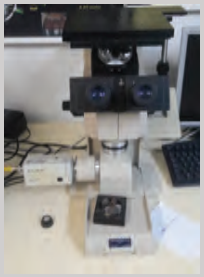

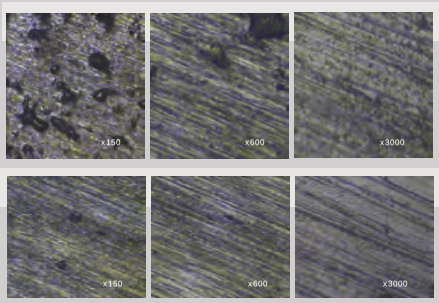

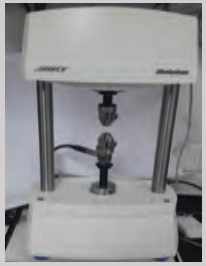

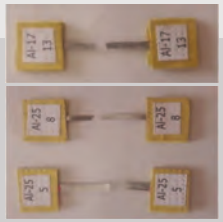

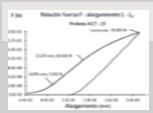

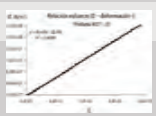

Cinta	σ_{rot} (N/m²)	E (GPa)
Al - 17	$(148 \pm 7) \cdot 10^6$	30,0 ± 2,0
Al - 25	$(316 \pm 70) \cdot 10^6$	31,8 ± 2,6

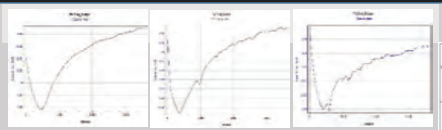

Nº Probeta	OCP, Eaa vs ESC (V) t = 0 seg	t = 3600 seg	ΔE (V)
P-1 17	-0,956	-0,910	0,046
P-2 17	-0,893	-0,873	0,020
P-3 17	-0,863	-0,890	-0,027
P-4 17	-0,998	-0,862	0,136
P-5 17	-0,908	-0,863	0,045
P-6 17	-0,977	-0,862	0,115
P-1 25	-0,572	-0,792	-0,220
P-2 25	-0,812	-0,893	-0,081
P-3 25	-1,093	-0,867	0,226
P-4 25	-0,674	-0,849	-0,175
P-5 25	-0,748	-0,840	-0,092
P-6 25	-0,730	-0,853	-0,123

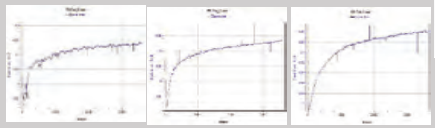

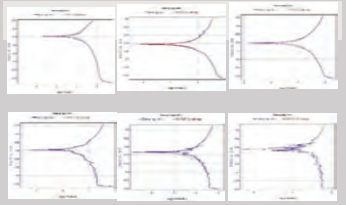

Cinta	Velocidad de corrosión (mmpy)
17 T. Ambiente	$(2,70 \pm 1,00) \cdot 10^{-3}$
17 T. Corporal	$(1,82 \pm 1,57) \cdot 10^{-2}$
25 T. Ambiente	$(6,00 \pm 1,00) \cdot 10^{-4}$
25 T. Corporal	$(7,60 \pm 2,90) \cdot 10^{-3}$

Conclusions

The values of the tensile strength σ_{ten} can be considered low in comparison with other alloys used as titanium-based biomaterials or stainless steels, although in none of the two metallic glass samples studied is this value lower than that of cortical bone (50 - 150 MPa). To highlight the average value obtained for the σ_{ten} for the Al-25 sample, which is of the order of 2.2 times that of Al-17. In all the microphotographs taken of the metallic glass samples, without attack and with the attacks carried out with hydrofluoric acid, a non-crystalline structure is observed, as is to be expected in a material with a glassy structure. The samples studied show good corrosion behavior, although they show a notable increase in corrosion rate when tested at body temperature (40ºC). Comparing the corrosion rate between the samples Al-17 and Al-25 at each temperature analyzed, it is observed that Al-17 at room temperature has a corrosion rate increase of about 4.5 times with respect to the corrosion rate of Al-25. It is concluded that the Al-25 sample presents a better behavior as biomaterial due to the higher mechanical resistance, a low Young's modulus and a lower corrosion rate. The metallographic study confirms the amorphous structure of the samples, in none of the micrographs crystalline structures are observed.

APOLLONIA UNIVERSITY OF IAŞI

in collaboration with

Academy of Romanian Scientists

Iaşi branch

Proceedings of International Congress

"By promoting excellence we prepare the future"

- Selection of Abstracts -

1st-3rd of March 2021

IAŞI, ROMANIA

UNIVERSIDAD DE LAS PALMAS DE GRAN CANARIA

International Congress of „Apollonia" University from Iași
Edition XXXI
1 - 3 March 2021, IASI, ROMANIA

CORROSION BEHAVIOR OF TWO NEW CO-CR DENTAL ALLOYS FOR PORCELAIN-FUSED-TO-METAL CROWNS

C.M. García-Falcón[1], T. Gil-López, P.P. Socorro-Perdomo, N. R. Florido Suarez[1], Julia C. Mirza Rosca[1]
[1]*Mechanical Engineering Department, University of Las Palmas de Gran Canaria*
[2]*Madrid Polytechnic University, Spain*

EQUIPMENT

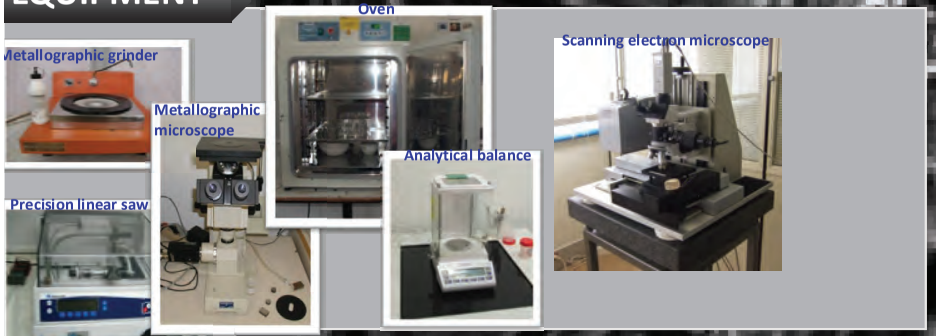

ABSTRACT

CoCr alloys have been used in dentistry for porcelain-fused-to-metal crowns due to their good biocompatibility, wear resistance, long service duration, good mechanical properties and last but not least, superior corrosion. The present investigation evaluated and compared two new Co-Cr based dental alloys, studying their microstructures and corrosion behavior in Ringer solution using different techniques. The results of the study exhibit that the contact of alloys during 24-hours with Ringer's solution, from a qualitative point of view, reveals that both alloys show a high passivation tendency. The two alloys presented formation of protective layers on their surface after electrochemical treatment. The alloys showed a general corrosion behavior, homogeneous on the surface. In terms of susceptibility to corrosion, findings in this study show that all alloys investigated have a more than adequate corrosion resistance in Ringer´s solution, although one of the dental alloys presented a higher corrosion resistance than the other one.

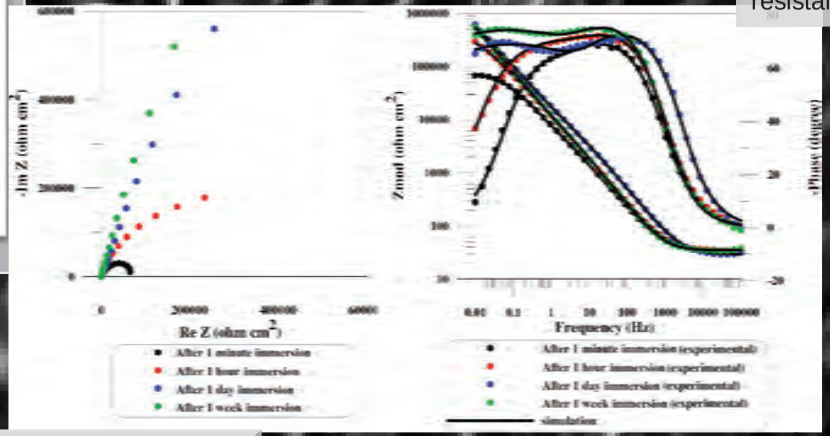

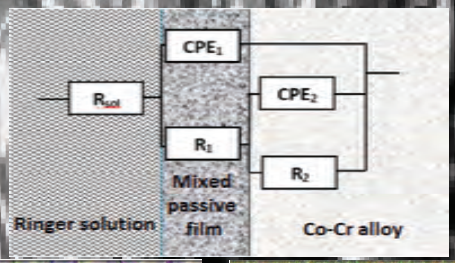

CONCLUSIONS

1. Both alloys tend to spontaneously passivate, and this passivation tendency is very high. The alloys presented the formation of mixed protective layers $Cr_2O_3 \cdot CoO$ with high stability on their surfaces, which substantially improves their biocompatibility in Ringer solution.
2. After electrochemical treatment, the alloys exhibited a uniform or general corrosion behavior, homogeneous on the surface, for areas a and b. However, due to the content of Fe and Ni, a higher degree of corrosion was found in the Vera PDI alloy. Furthermore, the kinetic parameters of the corrosion process in the experiment indicated a two-time constants process with an anodic control, attributable to the formation of passive films on their surfaces.

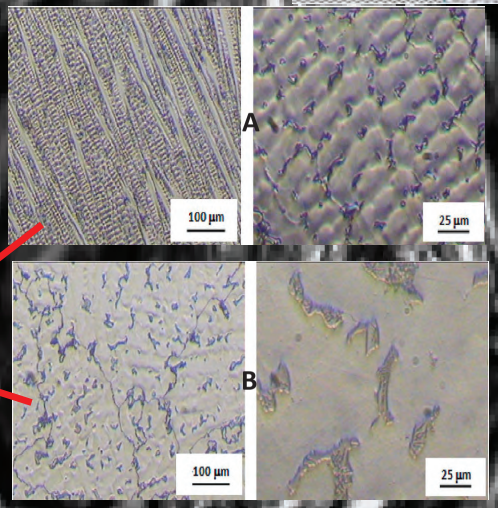

Metallography analysis: (A)- Vitallium 2000 Plus alloy, (B)- Vera PDI alloy

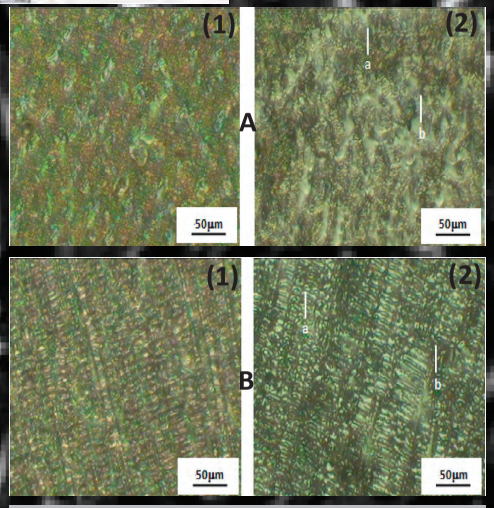

Microstructures (1) after electrochemical treatment, (2) after removal of the sediment: (A)- Vera PDI alloy, (B)- Vitallium 2000 Plus alloy.

International Congress of „Apollonia" University from Iași
Edition XXXI
1 - 3 March 2021, IAȘI, ROMANIA

NEW OPTION FOR BIOMATERIALS OF MEDICAL PROSTHESIS AND IMPLANTS

P. P. Socorro Perdomo[1], N. R. Florido Suarez[1], I. Voiculecu[2], V. Geante[2], Julia C. Mirza Rosca[1]
[1]*Mechanical Engineering Department, University of Las Palmas de Gran Canaria,*
[2]*Politehnica University of Bucharest, Romania*

1 COMPOSITION OF THE ELEMENTS

	Wt.%					
	Mo	Ta	Ti	Zr	Nb	Fe
BioHEA 1	20.45	32.45	12.67	18.97		15.46
BioHEA 2	17.32	38.95	13.21	17.45	13.07	

2 PRECISION CUTTING MACHINE

3 PRESS AND METALLOGRAPHIC POLISHER

4 ELECTROCHEMICAL IMPEDANCE SPECTROSCOPY TEST

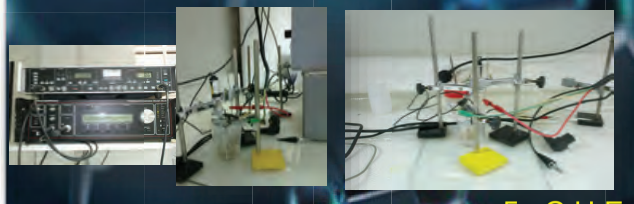

5 CHEMICAL ATTACK AND METALLOGRAPHIC ANALYSIS

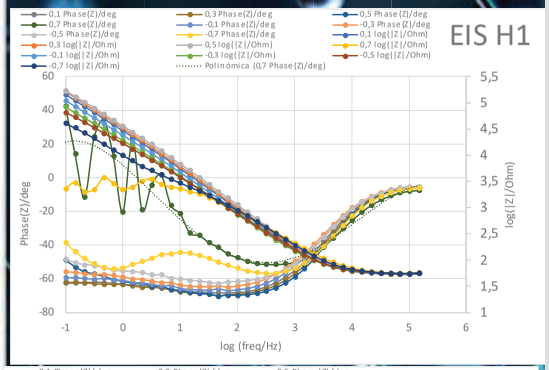

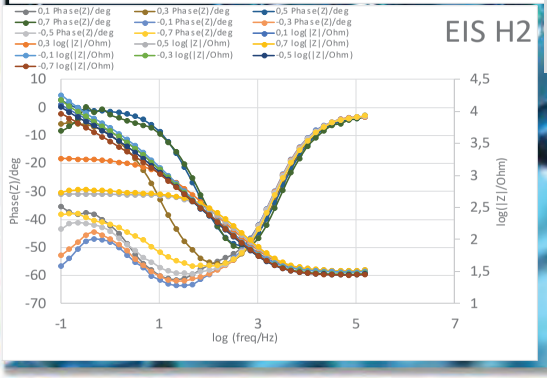

The behavior of two High Entropy Alloys of different composition, in simulated body fluid, is studied in order to determine whether these alloys are suitable for use in the field of medical prosthesis and implants. The studied materials, have the following composition:

A) 20.45%Mo, 32.45%Ta, 12.67%Ti, 18.97%Zr and 15.46%Fe;
B) 17.32%Mo, 38.95%Ta, 13.21%Ti, 17.45%Zr and 13.07%Nb.

In order to characterize the properties of these two allopys, different electrochemical methods were used. First of them was Electrochemical Impedance Spectroscopy and the analysis of the spectra was carried out by fitting different equivalent circuits to the experimental data. The spectroscopy impedance results were correlated with the microstructure which was characterized by Optical Microscopy, Scaning Electron Microscopy and Energy-dispersive X-ray Spectroscopy. The surface film is non-cytotoxic because is consisted of oxides of high biocompatible elements as Nb, Ta and Ti and all the results demonstrated the potential of the analyzed alloys for biomedical applications.

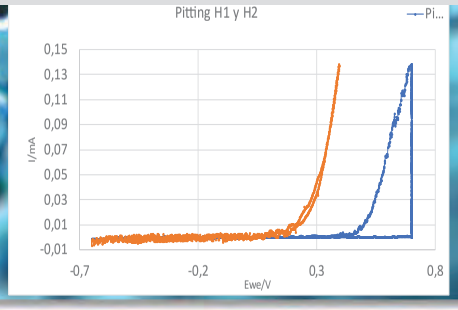

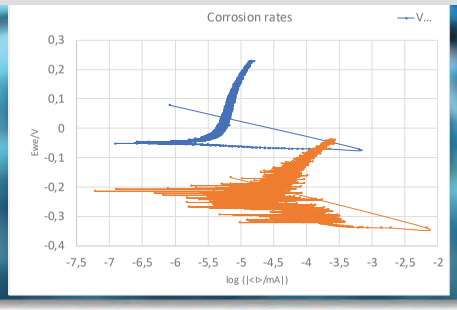

BIO HEA 2

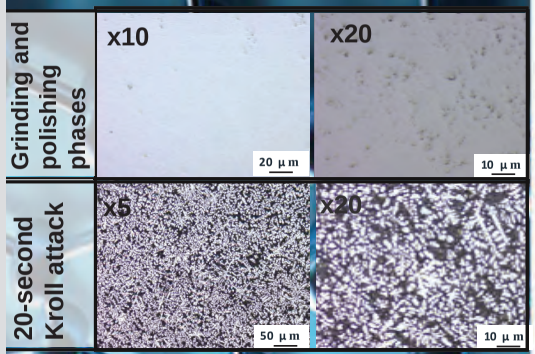

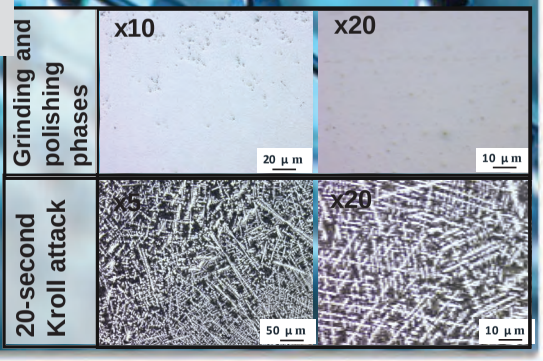

Department of Mechanical Engineering
University of Las Palmas de Gran Canaria

Biocompatibility of High Entropy Alloys based on FeMoTaTiZr and MoTaNbTiZr

Viorel Irinel Iovu, BSc Student, University of Las Palmas de Gran Canaria
Julia Claudia Mirza-Rosca, Prof., University of Las Palmas de Gran Canaria
Pedro Socorro-Perdomo, Prof., University of Las Palmas de Gran Canaria
Nestor Florido-Suarez, Prof., University of Las Palmas de Gran Canaria
Ionelia Voiculescu, Prof., Polytechnic University of Bucharest

ULPGC Universidad de Las Palmas de Gran Canaria | Escuela de Ingenierías Industriales y Civiles

CORROSION OF BIOMATERIALS

University of Las Palmas de Gran Canaria

Julia MiRZA ROSCA
Nestor FLORIDO SUAREZ
Pedro SOCORRO PERDOMO


Portuguese Man O'War nematocyst capsule


Spatter particles

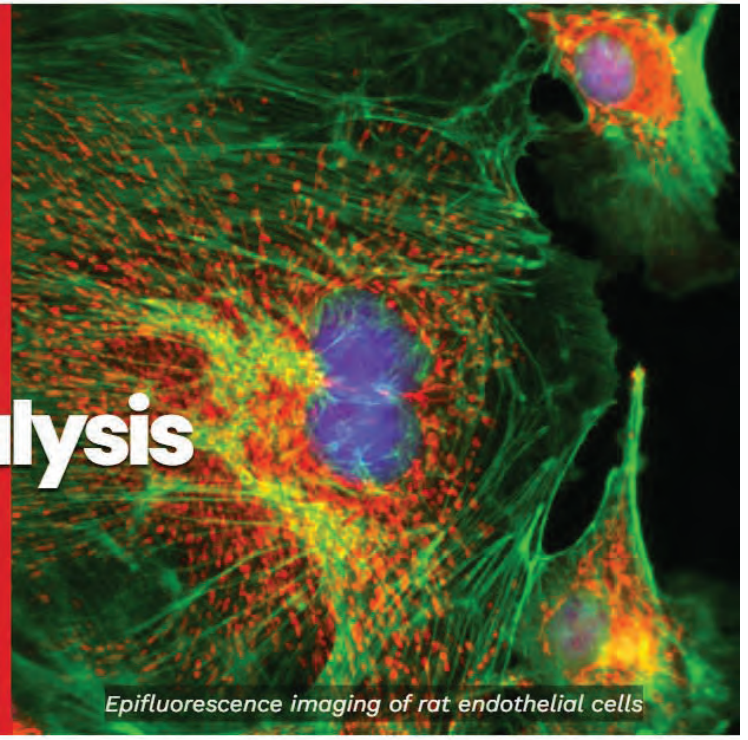
Epifluorescence imaging of rat endothelial cells

M&M 2021
Microscopy & Microanalysis

ABOUT THE SOCIETIES

The Microanalysis Society is a member-driven organization supporting microanalysis, instrumentation, techniques, and applications. The Microanalysis Society annually hosts or sponsors a variety of technical meetings to further its mission, two or more council meetings for the society leadership to confer and make decisions for the benefit of the society, and an annual business meeting.

OSSEO-INTEGRATION IMPROVEMENT OF ADDITIVEMANUFACTURED DENTAL ALLOYS

Elena-Manuela Stanciu[1], Nestor Florido-Suarez[2], Pedro Socorro-Perdomo[2*], Julia Mirza-Rosca[2]

[1]Transilvania University of Brasov, Materials Engineering and Welding Department, Brasov, Romania

[2]University of Las Palmas de Gran Canaria, Canary Island, Spain, *e-mail: pedro.socorro@ulpgc.es

Titanium and its alloys are the most suitable to exhibit bioactivity in case of load-bearing components but must be previously subjected to a special surface treatment, involving changes in the passive film properties .

Ti-6Al-4V and Ti-6Al-4Fe alloys were obtained by Electron Beam Melting (Arcam AB, Sweden), built layer-by-layer on a titanium commercially pure grade 2 as substrate.

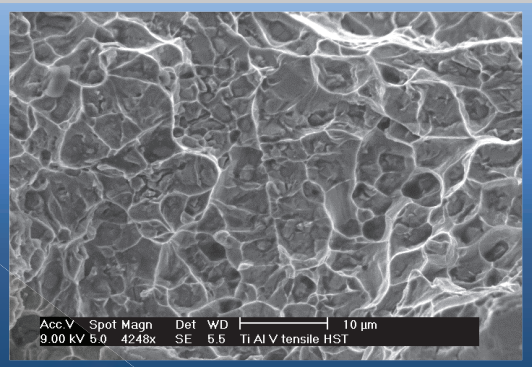

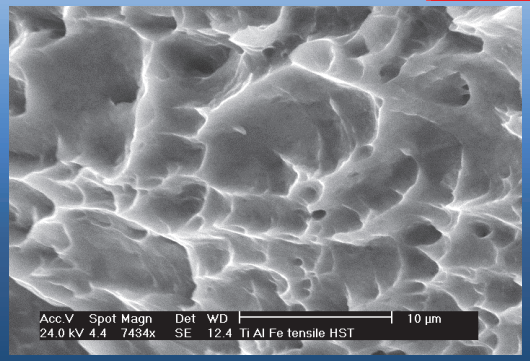

Materials

Methods

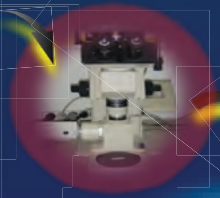

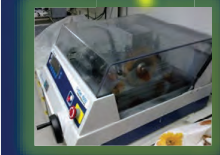

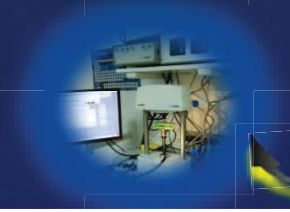

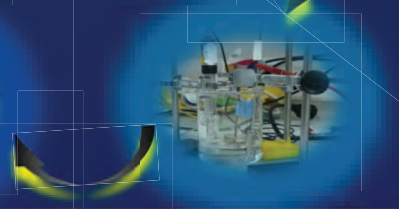

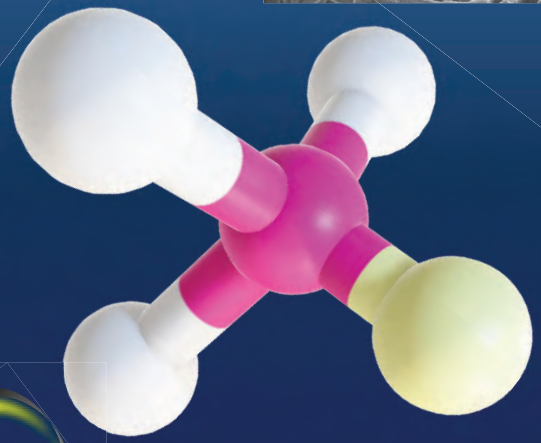

The oxide films on the metal surface showed a tendency to passivation and very high stability and no evidence of any form of local corrosion was noted. The experimental electrochemical performance data of such layers were fitted by an equivalent circuit having two-time constants. The mechanical and EDX results support the existence of a porous outer passive film with a high oxygen concentration and a dense and protective inner passive film where titanium dioxide is the predominant compound. EIS results confirmed the mechanistic findings. The outcomes show that the employment of a surface processing improves the adherence of the passive film to the alloy surface and enhances the biocompatibility of the medical implants.

MICROSCOPY & MICROANALYSIS M&M 2021

STUDY OF BIOCOMPATIBILITY, MECHANICAL PORPERTIES AND MICROSTRUCTURAL ANALYSIS OF Ag-Pd ALLOY

Jenifer Vaswani-Reboso, Nestor Florido-Suarez, Pedro Socorro-Perdomo*, Julia Mirza-Rosca
*University of Las Palmas de Gran Canaria, Canary Island, Spain, *email: pedro.socorro@ulpgc.es*

UNIVERSIDAD DE LAS PALMAS DE GRAN CANARIA

Introuction

Ag–Pd alloys have been used in prosthetic dentistry in recent years because of their low price compared with gold. According to the American Dental Association classification system, the Ag–Pd alloys are classified as noble metal, where as the Au-based alloys are classified as high noble metal.

The study focuses on the alloy Ag-Pd-Cu-Au-Zn-Ir or PALLIAG (commercial name) which, even with a lower content of noble metals, still presents good resistance to corrosion, being suitable for use in the mouth.

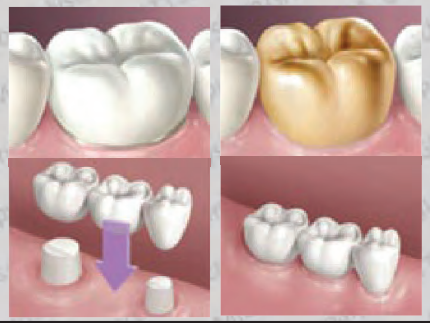

Experimental Materials

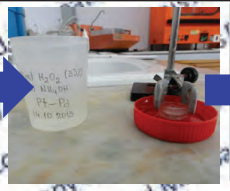

Surface preparing

Microscopy images

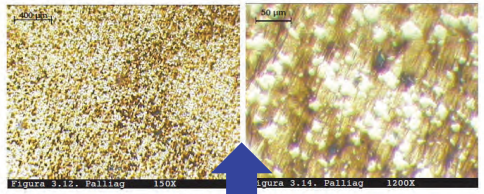

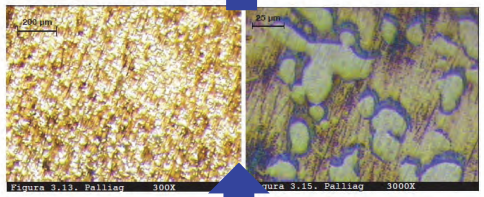

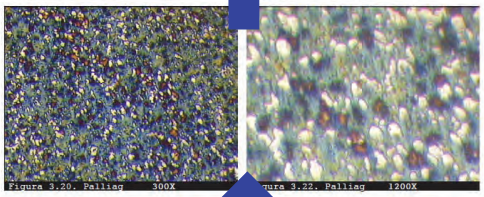

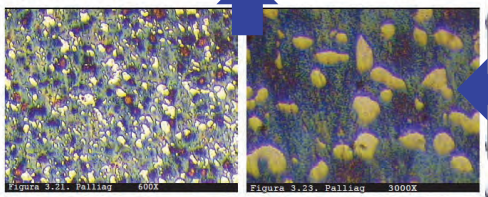

Conclusions

According to the results obtained during the corrosion potential tests during 30 minutes and 24 hours at room temperature at 40 °C.

After immersion in Ringer solution, the potential value of the sample studied decreases until it reaches equilibrium, when it stabilizes and remains constant.

It is concluded that the chemical and mechanical properties are acceptable when compared with reference dental alloys

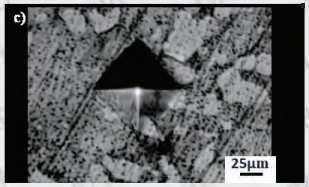

Metallography and SEM

UNIVERSIDAD DE LAS PALMAS DE GRAN CANARIA

PITTSBURGH

M&M 2021 MICROSCOPY & MICROANALYSIS August 1-5, 2021 - Pittsburgh, PA

M&M 2021 MICROSCOPY & MICROANALYSIS VIRTUAL MEETING AUGUST 1-5

MICROSTRUCTURE AND ADJUSTMENT IN TENSILE STRENGTH OF Al0.8CoCrFeNi FIBERS

Néstor R. Florido Suárez[1*], Pedro P. Socoro-Perdomo [1], Ionelia Voiculescu[2] Julia C. Mirza Rosca[1]

*[1]Mechanical Engineering Department, University of Las Palmas de Gran Canaria, Canary Islan, Spain, *e-mail:nestor.florido@ulpgc.es*

[2] LAMET, Politehnica University of Bucharest.

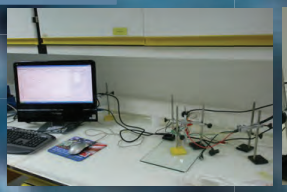

ALLOY COMPOSITION

Wt.% Al0.8CrFeCoNI [Al0.8]				
Al	Cr	Fe	Co	Ni
8.72	21.00	22.61	23.82	23.85

PRECISION CUTING MACHINE PRESS AND METALLOGRAPHIC POLISHER

MICROSCOPY ANALISYS

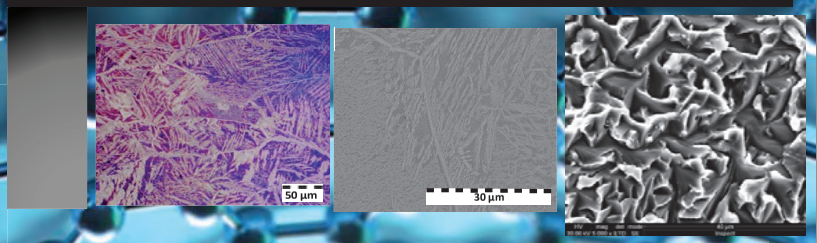

ELECTROCHEMICAL IMPEDANCE SPECTROSCOPY TEST

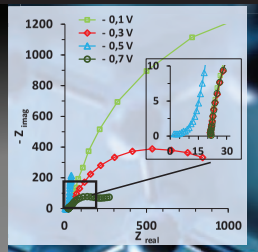

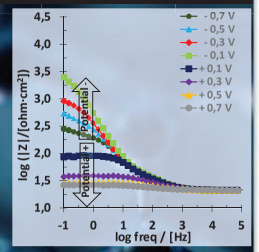

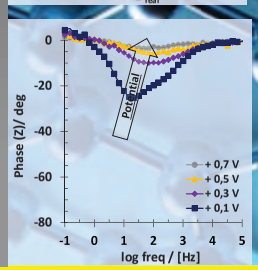

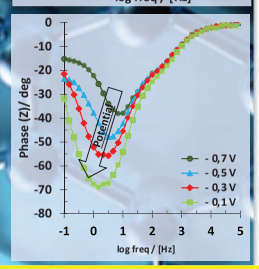

CONCLUSIONS

Tensile samples annealed at 1100 °C exhibit significant ductility, i.e., >15%, and higher tensile strength values. These outcomes indicate that the mechanical performance of HEA fibers can be customized to particular class of properties with an adequate selection of the high-entropy alloy and annealing temperature.

The improved ductility of high-entropy alloy fibers may be caused by the reduction of casting defects, the "curing" of small casting imperfections and the reduction of residual stress by annealing treatment and subsequent cutting process. These characteristics clearly demonstrate that the high-entropy alloys fibers can be recommended for low-dimensional products as wires, that require good strength, excelent thermal stability and high ductility.

EFFECT OF HEAT TREATMENT ON THE MICROSTRUCTURE AND CORROSIÓN RESISTANCE OF ALCOCRFENI HIGH-ENTROPY ALLOY

Nestor Florido-Suarez[1], Pedro Socorro-Perdomo[1], Victor Geanta[2], Julia Mirza-Rosca[1*]
[1]University of Las Palmas de Gran Canaria, Canary Island, Spain, *e-mail: julia.mirza@ulpgc.es
[2]Politehnica University of Bucharest, Romania

MICROSCOPY & MICROANALYSIS M&M2021

UNIVERSIDAD DE LAS PALMAS DE GRAN CANARIA

Introduction

AlCoCrFeNi is one of the most studied alloy systems from the area of high entropy alloys (HEA) due to it's attractive microstructure and mechanical properties. AlCoCrFeNi alloys are mainly prepared by vacuum arc remelting (VAR), which is based on the remelting of the raw elemental metals by means of the arc generated between the electrode and the metallic powder to be melted. However, arc remelting method requires high energy and the phase composition is not uniform, which is prejudicial to the mechanical properties of the alloy. It is often necessary to homogenize at high temperature and continue hot or cold working, followed by annealing treatment, to disintegrate the microstructure of the melt and thus obtain homogeneous materials with a fine-grained structure.

Experimental Materials

Element	NiCoCrAlFe	
	No Heat T.	Heat Treatment
Al, at%	12.00	9.89
wt%	6.33	5.14
Co, at%	6.59	8.48
wt%	7.58	9.62
Cr, at%	28.72	26.98
wt%	29.17	27.01
Fe, at%	26.56	26.40
wt%	28.98	28.38
Ni, at%	23.28	24.99
wt%	26.58	28.24
O, at%	2.38	2.46
wt%	0.74	0.76

Surface preparing

Metallography and SEM

Results CP

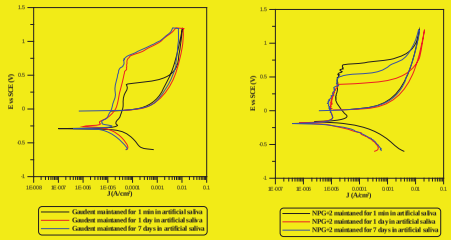

Results

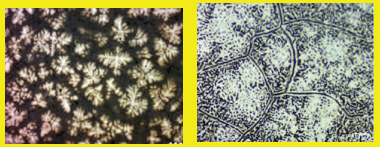

Results EIS

(a) after immersion for 1 min in saline solution

(b) after immersion for 7 days in saline solution

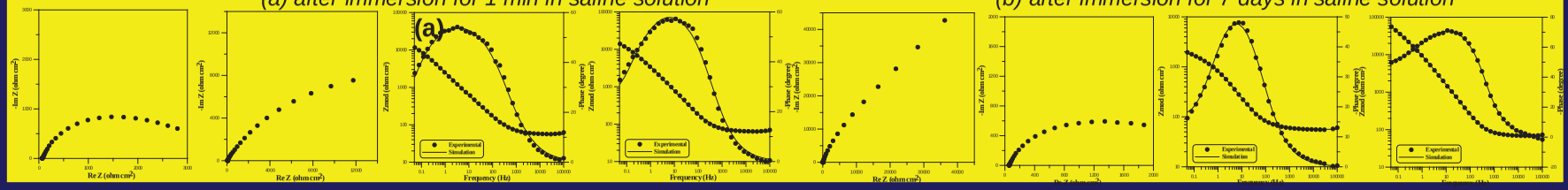

Conclusions

The heat treatment has a significant influence on the microstructure and the behavior of the alloys in simulated body fluid. With the heat treatment, the solidified microstructure varies from equiaxed dendritic grain to a wall-shaped structure with nanoprecipitates. The very high resistance of the heat treated alloy implies a high corrosion resistance which can be assigned to the formation of the protective chromium oxide layer. The obtained results demonstrate that the heat treatment alloy fulfill the prerequisites for its use as new material for nuclear applications.

MICROSCOPY & MICROANALYSIS MM2021

August, 1-5 • Pittburgh, PA

STATIC TESTING AND FATIGUE BEHAVIOR OF THREE HIGH-ENTROPY ALLOYS

N.Florido-Suarez[1], P.Socorro-Perdomo[1], V.Geanta[2], J.Mirza-Rosca[1*]

[1] University of Las Palmas de Gran Canaria, Spain, *julia.mirza@ulpgc.es

[2] Politehnica University of Bucharest, Romania

UNIVERSIDAD DE LAS PALMAS DE GRAN CANARIA

Fabrication

MRF ABJ 900 Vacuum Arc Remelting (VAR)

Composition (wt%)	$Al_{1.0}CrFeCoNi$	$Al_{0.8}CrFeCoNi$	$Al_{0.6}CrFeCoNi$
Al	10,67	8,72	6,68
Cr	20,55	21,00	21,47
Fe	22,13	22,61	23,12
Co	23,32	23,82	24,36
Ni	23,33	23,85	24,36

Preparation

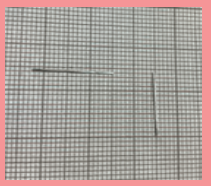

Bose Electro Force 3100

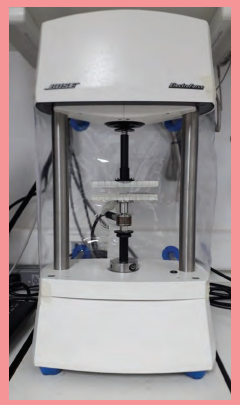

Testing

ASTM E466

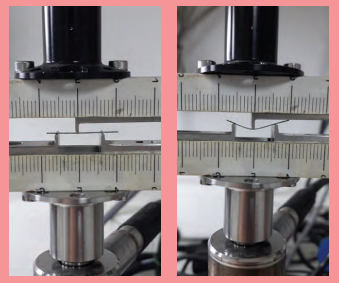

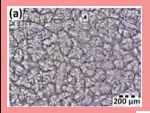

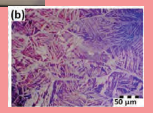

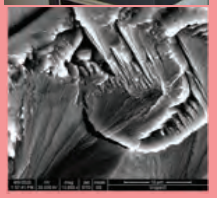

Conclusions

The mechanical properties obtained from static testing and fatigue behavior of high-entropy alloys were correlated with other mechanical parameters (hardness and rugosity). From the comparison of the fatigue resistance grade of AlCrFeCoNi HEA with other metallic materials, it is clear that the fatigue resistance of the investigated materials is significantly higher than that of other tested materials.

UNIVERSIDAD DE LAS PALMAS DE GRAN CANARIA

PITTSBURGH

M&M 2021 MICROSCOPY & MICROANALYSIS August 1-5, 2021 • Pittsburgh, PA

M&M 2021 MICROSCOPY & MICROANALYSIS VIRTUAL MEETING AUGUST 1-5

BIOCOMPATIBILITY OF NEW HIGH-ENTROPY ALLOYS WITH NON-CYTOTOXIC ELEMENTS

Pedro P. Socorro-Perdomo [1], Néstor R. Florido-Suárez [1], Ionelia Voiculescu[2], Julia C. Mirza Rosca[1]

[1] *University of Las Palmas de Gran Canaria, Canary Island, Spain, email: nestor.florido@ulpgc.es*

[2] *LAMET, Politehnica University of Bucharest, Rumania*

Two new experimental alloys (with the composition presented were obtained by Vacuum Arc Remelting from high purity chemical elements (99.5%)

	Wt.%					
	Mo	Ta	Ti	Zr	Nb	Fe
HEA 1	20.45	32.45	12.67	18.97		15.46
HEA 2	17.32	38.95	13.21	17.45	13.07	

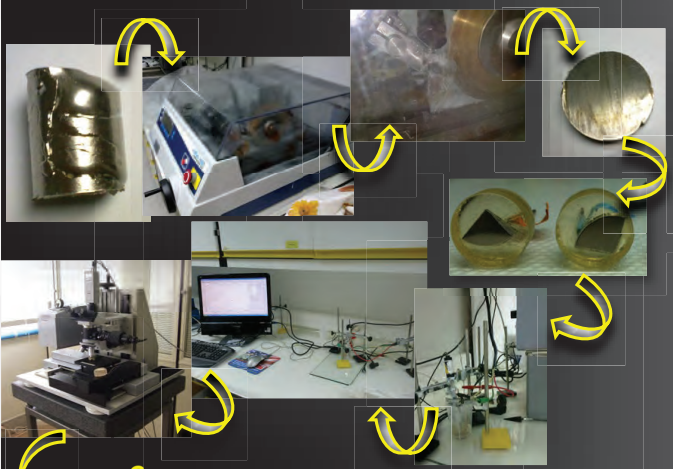

CHEMICAL ATTACK AND METALLOGRAPHIC ANALYSIS

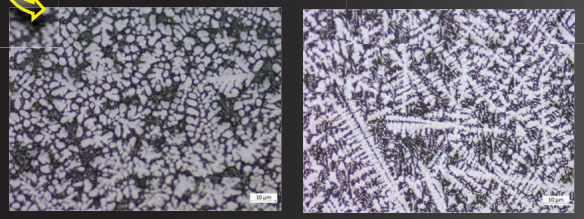

RESULTS AND DISCUSSION

Both HEA 1 and HEA 2 have an apparently homogeneous structure and the presence of dendrites due to the rapid cooling of these in the copper base where they have been manufactured can be clearly observed.

From the electrochemical tests we can say that HEA 1 has a lower corrosion potential than HEA 2, which means that HEA 1 is more susceptible to corrosion than HEA 2.

ELECTROCHEMICAL IMPEDANCE SPECTROSCOPY TEST

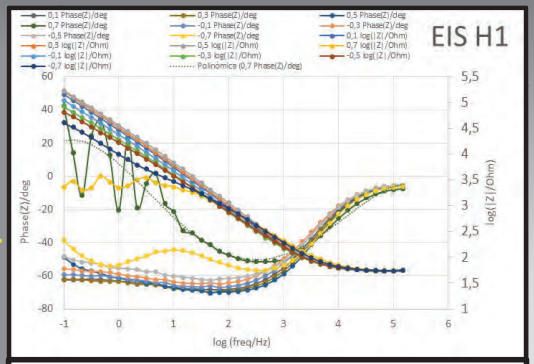

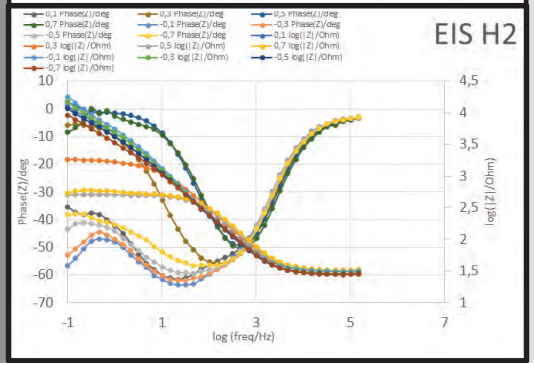

CONCLUSIONS

Both alloys exhibit spontaneous passivation with a low passive current density, low corrosion rate and high electrochemical impedance in Ringer solution, indicating a better bio-corrosion resistance than Ti6Al4V used nowadays. The good biocompatibility of the two alloys in simulated body fluid can be mainly attributed to the non-cytotoxic surface film and to the high corrosion resistance of the studied alloys. The surface film is non-cytotoxic because is consisted of oxides of high biocompatible elements as Nb, Ta and Ti. The high corrosion resistance leads to a less release of corrosion products during service life. Therefore, all the results further demonstrated the potential of the analyzed high-entropy alloys for biomedical applications.

2021 International Conference on Materials: Advanced and Emerging Materials

Part of the **International Conference on Materials- CN** series

22–24 Nov 2021

Materials, Characterization, Nanotechnology

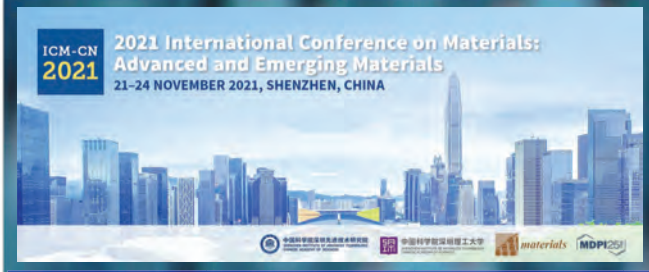

UNIVERSIDAD DE LAS PALMAS DE GRAN CANARIA

POLITEHNICA UNIVERSITATEA DIN BUCUREȘTI UPB 1818

NEW HIGH ENTROPY ALLOYS (HEA) WITH SMALL ADDITIONS FOR POSSIBLE USE AS BIOMATERIALS

Pedro P. Socoro-Perdomo [1], Néstor R. Florido Suárez[1], Ionelia Voiculescu[2] Julia C. Mirza Rosca[1]*

[1]*Mechanical Engineering Department, University of Las Palmas de Gran Canaria, Canary Islan, Spain, *e-mail: julia.mirza@ulpgc.es*

[2] *LAMET, Politehnica University of Bucharest.*

New class of materials has been developing in the last years and the materials from this class have unique structural properties that open up a wide range of possibilities for the creation and development of novel materials for specific applications. In the medical field, HEAs have been developed for metallic medical devices, in various alloy systems, where biocompatibility and mechanical properties are essential conditions. First, a base alloy was designed, a high entropy equiatomic multicomponent alloy with pure elements (99.95%) as Cr, Co, Fe, Mo and Ni (named LAS1) and from this alloy two other alloys are obtained by adding another alloying component. In one alloy, Ti is added (LAS2) and in the other Zr is added (LAS3) in order to study the mechanical behavior that allows us to consider its use as a biomaterial

Alloy Composition

Wt.%]							
Alloys	Cr	Fe	Mo	Co	Ni	P	Zr
LAS 1	19.61	20.57	17.15	21.24	20.62	0.21	-
LAS 2	19.33	19.52	20.85	20.44	19.50	-	-
LAS 3	19.80	20.23	19.18	20.34	19.74	-	0.71

Precision Cuting Machine Press and Metallographic Polisher

Electrochemical Impedance Spectroscopy Test

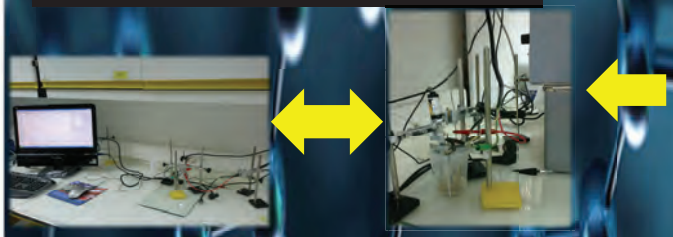

Microscopy Analisys

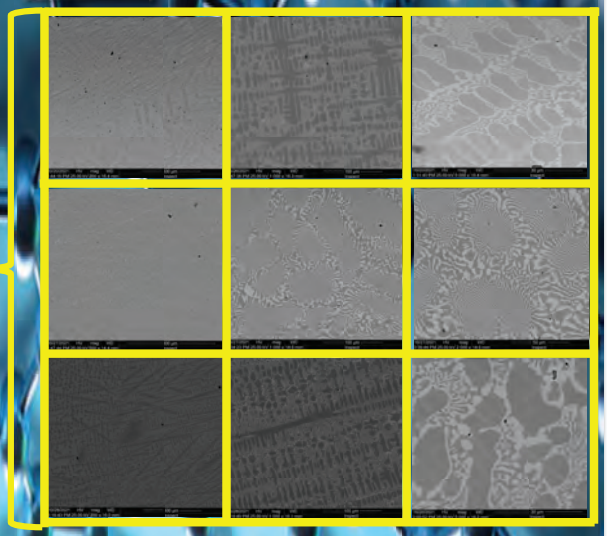

An ingot of each of these alloys is fabricated by vacuum arc melting in an inert argon atmosphere and six remeltings are carried out to ensure their homogeneity. By means of a three-point bending test, the modulus of elasticity E is calculated. The fatigue experiments were carried out. For this purpose, filaments are cut and tested in an Electroforce_3100 machine that applies a maximum load of 22 Newton. At least 10 tests are performed with each of the designed alloys and the mean

Scanning Electron Microscope

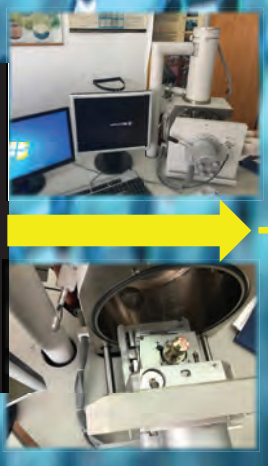

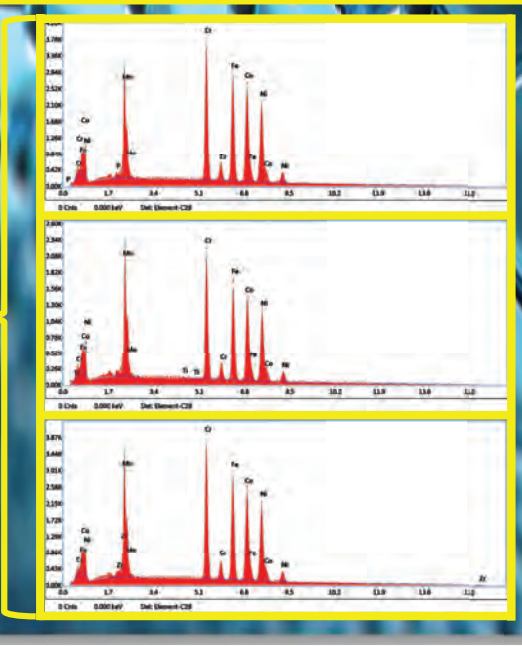

The effect of Tungsten addition on the Co-Cr dental alloys

Néstor R. Florido Suárez[1], Tomás Gil López[2], J.C.Mirza[1], Adriana Saceleanu[3]
[1]*Mechanical Engineering Department, University of Las Palmas de Gran Canaria, Spain* [julia.mirza@ulpgc.es]
[2]*Mechanical Engineering Department, Polytechnic University of Madrid*
[3] *Lucian Blaga University of Sibiu, Romania*

The variety of alloys for prosthetic restorations has increased rapidly over the last twenty-five years, which makes their selection for a given clinical situation very difficult. A series of properties - such as elastic modulus, microstructural phases, grain size, corrosion resistance, coefficient of thermal expansion, oxide and color, strength, hardness, - are of relevance when it comes to the correct selection of an alloy. The most important factor in such a choice is patient biosafety. The alloy selection decision has profound financial, legal, technical, practitioner satisfaction, and patient health consequences. The analyzed dental materials are Co-Cr alloys used for the fabrication of ceramic or composite coated crowns and bridges. Due to their coefficients of thermal expansion they are suitable for the most common metal veneering ceramics on the market

SAMPLE

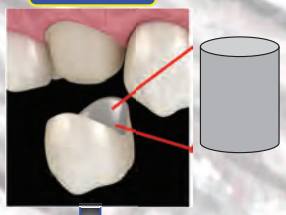

CHEMICAL COMPOSITION

	Wt.%						
Co-Cr 1	Co	Cr	W	Na	V	Nb	Mn
	56.31	24.72	9.16	3.17	1.99	1.54	0.93
Co-Cr 2	Co	Cr	Mo	Mn	Rb	Tc	Si
	61.17	30.10	4.17	1.62	1.06	0.58	0.24
Co-Cr 3	Co	Cr	Mo	Si	Mn	-	-
	57.66	32.32	4.96	2.06	1.34	-	-

EQUIPMENTS

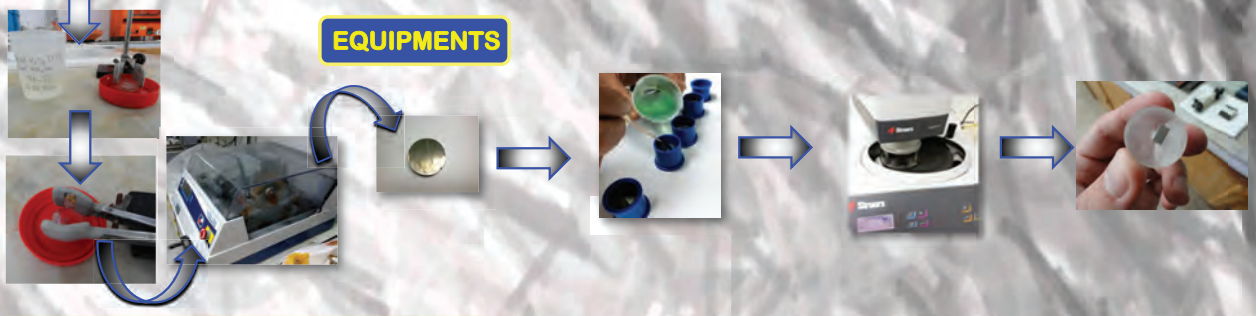

ELECTROCHEMICAL IMPEDANCE SPECTROSCOPY TEST

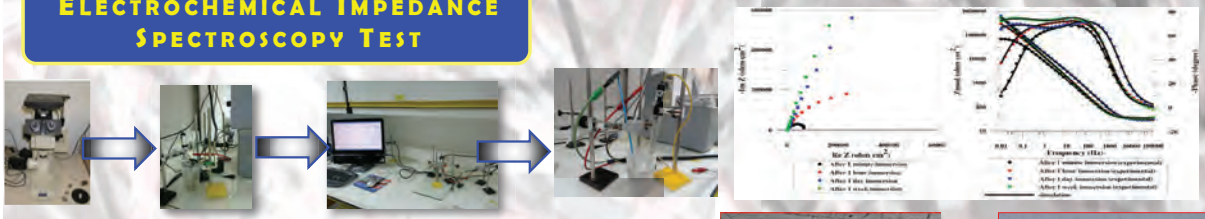

MICROSCOPY ANALISYS

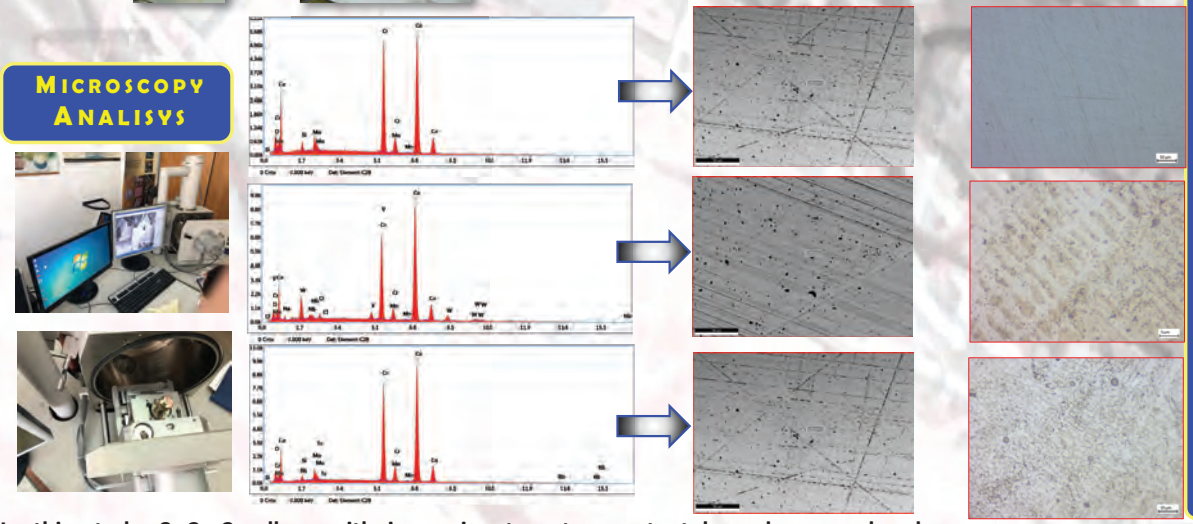

RESULTS

In this study, 3 Co-Cr alloys with increasing tungsten content have been analyzed. Corrosion potential, corrosion rate and pitting potential measurements have been carried out. The behavior under service conditions has been evaluated by means of electrochemical impedance spectroscopy whose spectra have been fitted to an equivalent circuit which has allowed to determine the characteristic parameters of the taking place process. The composition of the corrosion products has been analyzed by scanning electron microscopy and EDS. As the tungsten content increases, the properties of the alloy improve: it acquires optimum casting qualities and an extra fine molecular structure resulting in smooth and compact surfaces for easy and simple processing

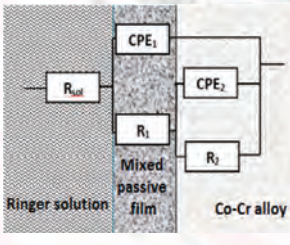

Conference motto:

-- STOPPING WARS AND MAKING PEACE --

BRAMAT 2022
12th INTERNATIONAL CONFERENCE ON MATERIALS SCIENCE & ENGINEERING

9-12 MARCH 2022
BRASOV, ROMANIA

ORGANIZED BY
TRANSILVANIA UNIVERSITY OF BRASOV

BRAMAT 2022
12TH INTERNATIONAL CONFERENCE ON MATERIALS SCIENCE & ENGINEERING
Transilvania University of Brasov - Romania
Materials Science and Engineering Faculty

Pedro P. Socorro-Perdomo[1], Néstor R. Florido-Suárez[1], Julia C. Mirza-Rosca[1], Adriana Saceleanu[2]
1 University of Las Palmas de Gran Canaria, Mechanical Engineering Dept.,
University Campus of Tafira, Engineering Building, 35017 Las Palmas de Gran Canaria, Spain, e-mail: nestor.florido@ulpgc.es
2"Lucian Blaga"University of Sibiu, Medicine Faculty, 550024 Sibiu, Romania, email: adriana.saceleanu@ulbsibiu.ro

CORROSION BEHAVIOR OF SOME NI-CR AND CO-CR DENTAL ALLOYS

The use of dental alloys as a material for bridges, crowns and prostheses is currently being investigated, taking into account their biocompatibility, as the material must be non-toxic and not cause allergies, inflammation or other reactions affecting the body.

In this field, Co-Cr and Ni-Cr based alloys are often used, as they have good corrosion resistance and high wear resistance due to the crystalline nature of cobalt and nickel. In addition, Ni-Cr and Co-Cr alloys have been used in the field of dentistry for porcelain or porcelain-fused-to-metal crowns due to their good biocompatibility, wear resistance, long service life, good mechanical properties and superior corrosion.

Experimental Materials


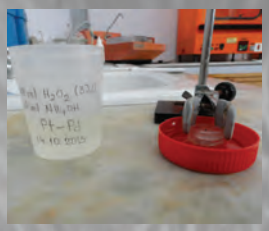


Surface Preparing



Metallography Analysis




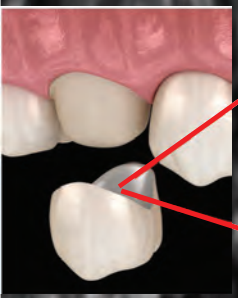

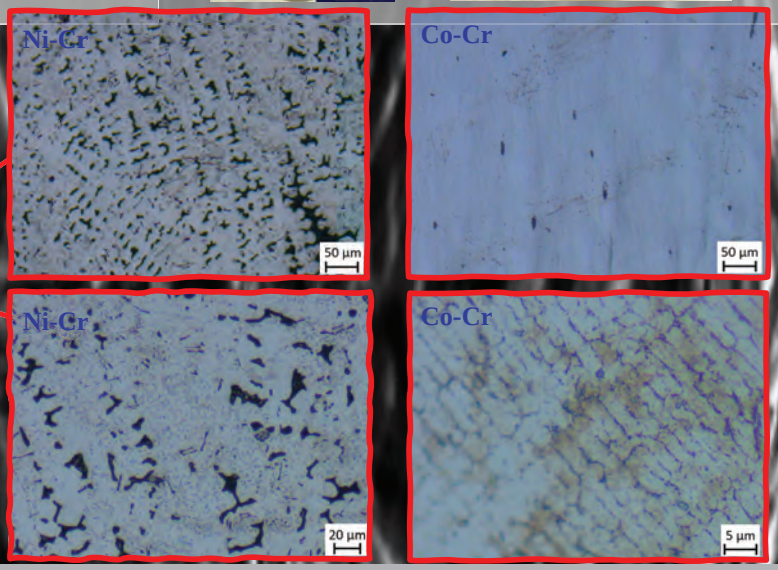

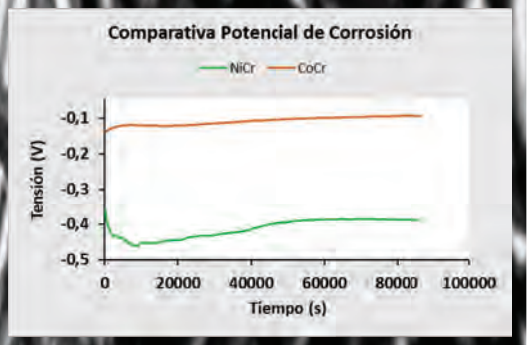

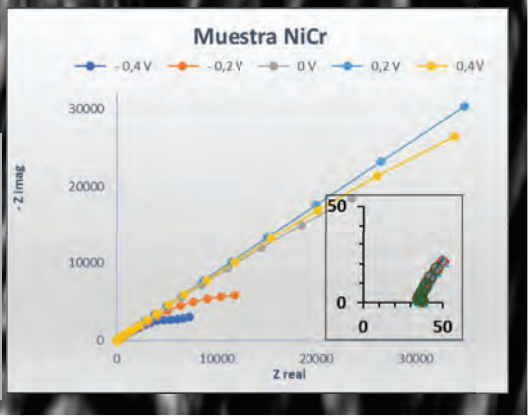

After electrochemical etching, the metallographic test is carried out by taking images with the metallographic microscope and by electrochemical test consisting in inserting a specimen into an electrochemical cell together with Saturated Calomel Electrode (SCE) as reference and Pt electrode as counter electrode. Corrosion potential (Ecorr) was determined and Electrochemical Impedance Spectroscopy (EIS) was applie

BRAMAT 2022
12TH INTERNATIONAL CONFERENCE ON MATERIALS SCIENCE & ENGINEERING
Transilvania University of Brasov - Romania
Materials Science and Engineering Faculty

UNIVERSIDAD DE LAS PALMAS DE GRAN CANARIA

Néstor R. Florido-Suárez[1], Pedro P. Socorro-Perdomo[1], Alexandru Pascu[2], Julia C. Mirza-Rosca[1]

[1] University of Las Palmas de Gran Canaria, Mechanical Engineering Dept., University Campus of Tafira, EngineeriEngineering Building, 35017, Las Palmas de Gran Canaria, Spain, e-mail: nestor.florido@ulpgc.es

[2] Transilvania University of Brasov, Materials Engineering and Welding Department, 29 Eroilor Blvd., 500036, Brasov, Romania, e-mail: alexandru.pascu@unitbv.ro

INTERNATIONAL TEACHING AND PRACTICE FOR ENGINEERING STUDENTS

The concept of teaching and practice has been developing for many years [1], intimately linked to the concept of "teaching and practice", as Jos Arets says in his work, "If you're not at the table, you're on the menu". One of the major drawbacks of new engineers is their lack of experience in the working world, with this "on-site" practical training programme, the new engineer will be able to develop their full creative potential directly [3] and provide students with a hands-on experience that adds specific practical value compared to the distance or classroom-based theory of specialised courses in intelligent building maintenance engineering

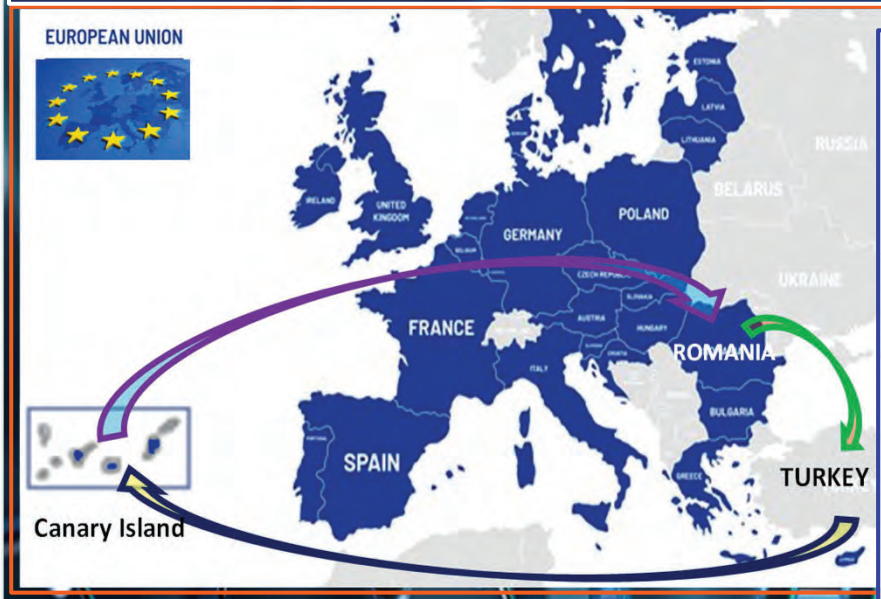

The teaching resources on technologies will be based on current applied research addressing healthcare smart public buildings. This provides students with a broad overview of the most advanced technologies, Internet of Things (IoT), and the latest technologies. [4], from devices (sensors, actuators, monitors, control facilities, etc.), connectivity, control, automation and data analysis. There will be a collaboration between 3 universities and 3 hospitals from 3 different countries (Spain, Turkey and Romania), each of which will benefit from the experience of the others, transferring the know-how available from all to all.

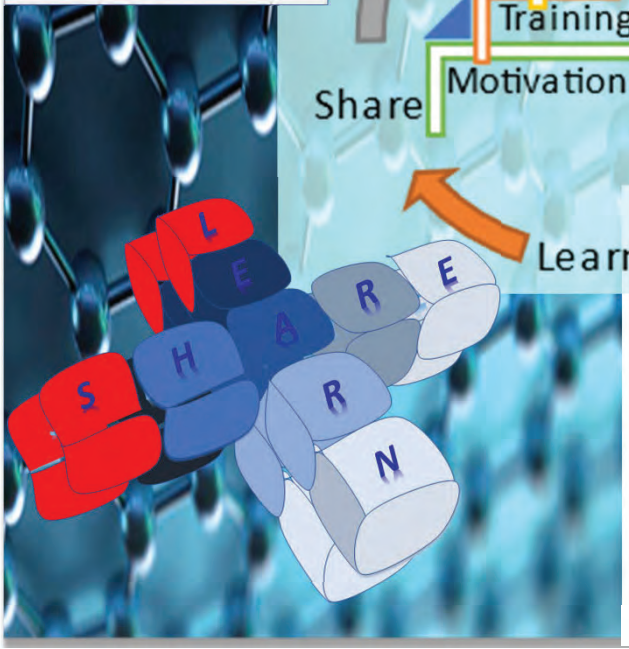

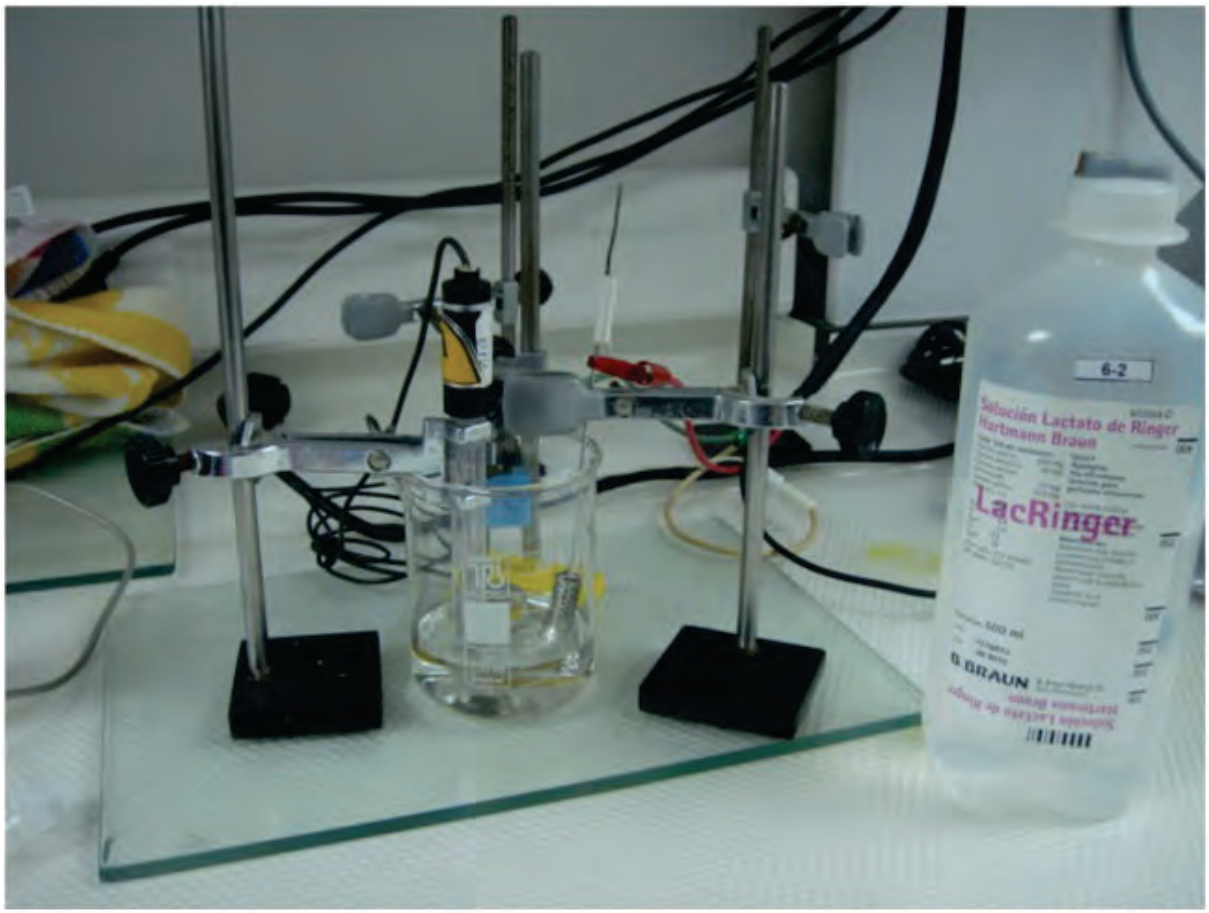

Conclusiones

7

7. Conclusiones

En este capítulo se resumen las principales conclusiones derivadas de la investigación y que se encuentran recogidas en las publicaciones científicas.

Las conclusiones son las siguientes:

- La Espectroscopia de Impedancia Electroquímica es una técnica muy potente para estudiar el comportamiento de la corrosión de las aleaciones de alta entropía en un entorno corporal humano simulado. Los resultados obtenidos fueron confirmados por las otras técnicas que se emplearon en este estudio. Los circuitos compuestos por una y dos constantes de tiempo, además de la resistencia óhmica del electrolito, se proponen como circuitos equivalentes para ajustarse al comportamiento de corrosión de las HEA. La resistencia de transferencia de carga en paralelo con la capacitancia de la doble capa está representada por la constante de tiempo de baja frecuencia, mientras que la de media frecuencia está relacionada con las reacciones de los constituyentes de la aleación en la superficie del metal. A través de esta técnica, se obtuvo información sobre los cambios de la capacidad protectora de las capas pasivas, según la composición de la aleación y el potencial de exposición, lo que demuestra que las aleaciones analizadas cumplen con los prerrequisitos para su uso como nuevos materiales para la fabricación de instrumentos médicos.
- La variación del contenido de aluminio en el sistema AlxCrFeCoNi tiene una influencia significativa en la microestructura y el comportamiento de las aleaciones en el fluido corporal simulado.

- A medida que disminuye el contenido de aluminio, la microestructura solidificada varía de grano dendrítico equiaxado a grano no dendrítico equiaxado y luego a estructura dendrítica columnar. En la estructura de grano equiaxado no dendrítico se observan placas laterales de Widmanstätten. La disminución del contenido de aluminio aumenta el límite de solubilidad de la fase sólida para el Ni y el Co, lo disminuye para el Cr y, el Fe casi no se ve afectado.
- El titanio y las aleaciones de titanio sufren una pasivación espontánea debido a la película de óxido que se forma en su superficie en la solución ácida reductora.
- El rango de potencial pasivo es muy amplio para los materiales estudiados en HCl 20% (superando los 2,0 V).
- A medida que aumenta el potencial, aumenta el grosor de la película pasiva y tiene una respuesta capacitiva (buena estabilidad) en un amplio rango de frecuencias.
- Se presentaron dos modelos de circuitos equivalentes que describen la pasivación espontánea del Ti, Ti-15Mo y Ti-15Mo-5Al en HCl 20%. En Ecorr se utiliza un simple circuito de Randles mientras que en el rango de potencial pasivo se utilizó un circuito equivalente con 2 constantes de tiempo para ajustar los datos experimentales. También se empleó un elemento constante de fase CPE en lugar del elemento capacitivo.
- Para todos los materiales analizados no hay iones liberados en la solución durante el rango de potencial pasivo.
- La adición de Mo y Al genera la formación de una capa pasiva con mayor capacidad de protección contra la corrosión que la del titanio.

- En una solución de HCl al 20%, la película de óxido sobre el Ti y las aleaciones estudiadas de Ti fabricadas mediante fusión por rayo láser presenta una alta resistencia a la corrosión y una estabilidad a largo plazo, lo que recomienda su uso para la fabricación de piezas metálicas empleadas en entornos industriales agresivos.
- Las gráficas de Nyquist para todas las aleaciones de Ti-Ta muestran los mismos semicírculos incompletos con diámetros grandes que aumentan con el potencial (hasta un valor crítico para cada aleación) debido a la mejora de las propiedades protectoras de la película pasiva formada en la superficie de la aleación.
- Para todas las aleaciones de Ti-Ta, los gráficos de fase de Bode mostraron un ángulo de fase, típico de una capa pasiva de barrera capacitiva formada en la superficie de una aleación.
- Los espectros de impedancia se ajustan con un circuito equivalente constante de una sola vez, común para una capa de óxido compacta, para todas las aleaciones de Ti-Ta en fluidos extracelulares. Tras un largo periodo de inmersión en el fluido corporal simulado, la película pasiva es más gruesa y desarrolla una estructura bicapa: una capa exterior porosa y una capa interior compacta. La adición de tántalo aumenta la estabilidad de la película pasiva debido al desarrollo de TaO25.
- De las aleaciones de Ti-Ta, la Ti-25Ta demuestra unas excelentes propiedades de resistencia a la corrosión y de capa pasiva, por lo que parece ser un producto prometedor para los dispositivos médicos metálicos.